NITRATE ISOTOPE ANOMALY AS A TRACER OF BIOGEOCHEMICAL PROCESSES

by

Laura Campisi

Thesis presented in part-fulfilment of the degree of Master of Science in accordance with the regulations of the University of East Anglia

School of Environmental Sciences
University of East Anglia
University Plain
Norwich
NR4 7TJ

June 2012

© 2012 Laura Campisi

The copy of the dissertation has been supplied on the condition that anyone who consults it is understood to recognise that its copyright rests with the author and that no quotation from the dissertation, nor any information derived there from, may be published without the author's prior consent. Moreover, it is supplied on the understanding that it represents an internal University document and that neither the University nor the author are responsible for the factual or interpretative correction of the dissertation.

Abstract

The general aim of the thesis is testing the potential of the nitrate MIF (mass-independent fractionation) signature as a tracer of biogeochemical processes.
Nitrate $\delta^{15}N$, $\delta^{17}O$ and $\delta^{18}O$ of water samples collected at the Marano lagoon (Italy) have been analysed, by combining the denitrifier method with the N_2O thermal decomposition in a gold furnace. No clear correlation between the magnitude of the capital delta ($\Delta^{17}O=\delta^{17}O+0.5*\delta^{18}O$) and the local atmospheric deposition has been found. Moreover, sewage treatments with ozone might be responsible for some high $\Delta^{17}O$ values associated to sampling points close to populated areas. Overall, the signal is low (0.6‰ on average, which would correspond to roughly 2% of atmospheric nitrate in sample water) and the error associated to the measure is no less than 75%.
To test the assumption that the atmosphere is the only source of a MIF signature, a set of nitrate minerals of different origin was analysed. The capital delta in a specimen of buttgenbachite (with formula $Cu_{36}(NO_3)_2Cl_8(OH)_{62}*4-10H_2O$) from Likasi mine (Congo, 4‰±1) and in a sample of nitromagnesite ($Mg(NO_3)_2*6H_2O$) collected at Pozalagua Cave (Spain, 10.3‰±0.4) would indicate the possibility that a significant isotope anomaly could be generated due to geochemical processes.
So far the MIF in atmospheric nitrate has been interpreted as the result of chemical reactions only, but it could be demonstrated that a series of mass dependent processes might generate an apparent $\Delta^{17}O$.
The study of the MIF is a relatively new field and the present work underlined some limits of this novel tracer. Further work should be focused on identifying the systems and the conditions for what the nitrate MIF can be considered as a conservative tracer. Particularly, attention should be paid to the effects of biological processes involved in the nitrogen cycle, such as nitrification and denitrification, and transport processes.

Content

1. Introduction

1.1. Aims and objectives of this research

The general aim of the present work is testing the use of the nitrate MIF (mass independent fractionation) signature as a tracer of biogeochemical processes.
It is important to point out that there are quite a few potential research lines that could be chosen to reach some objectives in this case, at least for two reasons.
Firstly, the nitrogen cycle is extremely complex and, particularly, nitrate can be a source or a sink associated to several enzymatic reactions. Thus, the assessment that the nitrate isotope anomaly behaves as a conservative tracer in some systems does not imply that it will be in others. Furthermore, since the study of the nitrate MIF is a recent field, there are still a number of assumptions that should be tested.
It is not possible to understand the choice of the objectives to reach for this project without considering the initial stage of the literature review, when I identified which answers I wanted to find in previously published works. Overall, the most important questions that I was focused on could be grouped in three categories:

1. Why does the nitrate recycling deserve attention and how many processes I should expect to consider in order to describe realistically the systems of interest through my data sets?
2. Why is a mass independent fractionation an anomalous process? How it was discovered and which explanation has been given to justify this apparently new phenomenon?
3. What is the origin of the MIF signature in atmospheric nitrate? What type of systems has been considered for testing the novel tracer? How did it work?

Thus, before indicating some feasible goals to reach in this project, a summary of this preliminary work is shown.

Nitrogen is an essential element for life, as it is a constituent of all the 21 aminoacids, the building blocks of proteins. Nitrogen containing species like ammonium and nitrate are therefore indispensable nutrients for photoautotrophs, the organisms representing the lowest trophic level that support the food web of any ecological community. The element is mainly present as molecular nitrogen (constituting the 78% of dry air), a form that is not readily available for organisms. Only lightning, volcanic and hydrothermal activities and some bacteria can fix the molecular nitrogen. Volatilization of dinitrogen gas from the earth's crust is thought to be the source of atmospheric nitrogen (Rayleigh, 1939)(Hutchinson, 1944). It has been calculated that, of a total N_2 reservoir of $1.8x10^{20}$ mol, $1.38x10^{20}$ mol of N is present in the atmosphere and the remaining is distributed between crustal and sedimentary rocks (Zhang and Zindler, 1993). There is a growing interest on the role of nitrogen bedrock on the global N cycle and several recent studies have shed some light on the interaction between the litosphere and the biosphere (Holloway and Dahlgren, 2002 and reference therein).
Several scientists tried to produce ammonia from atmospheric nitrogen in the early XX century. The first successful experiment dates back to 1909 and is due to Haber and Rossignol. The method became an industrial process with the aid of Bosch.
Nowadays the Haber-Bosh process, the nitrogen fixation reaction between N_2 and H_2 for generating NH_3 with the aid of an iron catalyst, allows the production of an

important precursor for both organic and inorganic compounds. It represents a necessary step in industry to create polymers for making fibers, plastics and resins, as well as for producing inorganic products like fertilizers and explosives. The importance of such a process has been emphasized in the title of a recent paper (Erisman et al., 2008 "How a century of ammonia synthesis changed the world").
As a result, anthropogenic activities increased the emission of reactive species containing nitrogen, which fact is currently causing a change in the global nitrogen cycle (Galloway et al., 2008).
The transformation of the nitrogen cycle due to the growing demand of nitrogen for agricultural and industrial activities resulted in negative effects on the environment, such as eutrophication and global acidification (Gruber and Galloway, 2008). Furthermore, nowadays the nitrogen cycle has been suggested to cause human health problems. For instance, several studies related cancer mortality with high levels of nitrate in drinking water (Jensen, 1982)(Barrett et al., 1998)(Sandor et al., 2001)(Coss et al. 2004). However, it is important to point out that there are other studies that failed to find any such connection (Beresford, 1985; Forman, 1989; Joossens et al., 1996).
Thus, there is an increasing interest in quantifying the contribution of anthropogenic activities to the change of the global N cycle. According to Rodhe et al. (2002), natural NO_x emissions rates from soils and lightning amount to 9 Tg. N/year, whereas man-made emissions have been estimated as 35Tg. N/year (of which 28Tg. N/year from industrial sources and the remainder from biomass burning). Lamarque et al. (2005) estimated that 35-50 Tg. N/year have been emitted during 2000. In the worst scenario, the same authors predicted that the emission of 98—131 Tg. N/year is expected by 2100. The author calculated that N emissions would grow by a factor of four by 2100 in China. Enhalt et al., (2001) calculated that tropical regions are expected to at least double or triple their present day emissions.
Fig. 1.1 illustrates the links of the nitrogen cycle with the carbon and the phosphorus cycle, the scale of human perturbation of the cycle and its complexity.

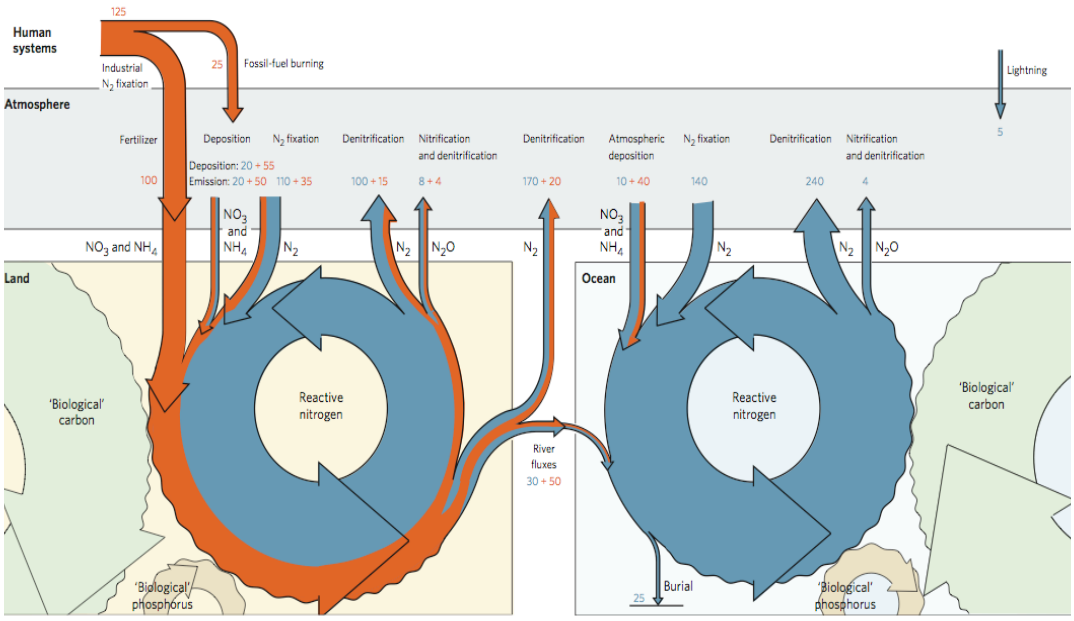

Fig. 1.1. *Depiction of the global N Cycle and the links with the global C and P cycles. Blue fluxes indicate natural fluxes, whereas red fluxes are due to anthropogenic activities (from Gruber and Galloway, 2008).*

Great attention is currently being paid to refining the knowledge of the N cycle because its understanding could be important for predicting the future climate change. This is because oceans can be important sinks for atmospheric CO_2, since nitrogen is a nutrient fueling the ocean productivity and, in turns, the carbon dioxide uptake.
In an early paper, Paerl (1988) suggested that the more acidic the rain, the higher the inorganic N inputs and the associated phytoplankton blooms. Globally, it is has been estimated that about 60-75% of oceanic surface waters are potentially seasonally N-limited (Duce, 2008). However, the atmospheric nitrogen inputs are regarded as small compared to the internal ocean nitrogen fluxes and so are unlikely to cause large-scale changes in phytoplankton activity. However, such changes are locally possible under special circumstances, like seasonal nutrient depletion. As an example, Spokes et al. (2000) calculated that inputs of air masses from polluted areas of the UK to Irish coasts could contribute up to 30% of the new marine production in that area. Nevertheless, in most cases even high nitrogen load will not enhance the oceanic productivity, because many areas will be still P-limited (Jickells, 2006).
Regarding the link between the N cycle and the future climate change, Duce (2008) pointed out that N_2O emissions (1,6 Tg N_2O/year, according to the same author), which are related to the nitrogen loading, can offset the beneficial effect of sequestering atmospheric CO_2 on the climate change, owing the great efficiency of nitrous oxide as a green-house gas.
It is important to draw attention on that fact that, in spite of the recognized importance of the nitrogen cycle, the uncertainties in the flux estimates are still rather large, with only few being better than ±20% and several others with uncertainties of ±50% and larger (Gruber and Galloway, 2008). To underline the magnitude of the uncertainties in the role of the atmosphere to redistribute the excess of reactive nitrogen produced by anthropogenic activities, a summary of different estimates of the atmospheric deposition of reactive nitrogen (Nr) is reported below.
According to Duce et al. (2008), the global atmospheric deposition of reactive nitrogen is 67 Tg. N/year, which is more than three times higher than during the pre-industrial era (20 Tg N/year). One third of the fixed nitrogen in the atmosphere is regarded as of anthropogenic origin, so that 32% of external source of Nr in the upper oceans is due to human activities, (but 3% of the total only if also upwelling is included). Dentener et al. (2006) estimated that 36-51% of all NO_y, NH_x and SO_x is deposited over the oceans. The authors claim that oceans receive 22,6 Tg N/year of NO_y (3,7 Tg N/year when considering the coastal shelves only), which has been calculated to be 7,5% of the total NO_x emissions. By contrast, Lamarque et al., (2005), using a set of six models, found that only 30% of NO_y is deposited over the oceans. Doney et al. (2007) found that one third of anthropogenic NO_x emissions (about 2 Tmol N/year) are deposited over the oceans. The deposition of nitrogen due to the combination of fossil fuel combustion and agriculture was estimated as a flux of 2,7 T mol N/year. The estimate by Luo et al. (2007) of a deposition rate equal to 39,6 Tg N/year is in good agreement with the one made by Galloway et al. in 2004 (39 Tg N/year). Krishnamurthy et al. (2010) has recently estimated that the atmospheric N deposition sustains the 5,1% of oceanic sinking PON (particulate organic nitrogen) export, with significant regional differences, since nitrogen inputs can support locally up to 50% of export production.
The study of the atmospheric nitrogen input in the North Sea along a coastal ecosystem revealed large spatial and temporal variability but a significant reduction to background levels over a distance of only 200 Km. from the coast (De Leuw, 2001). Nevertheless, according to the North Sea Task Force (report published in 1993), the

atmospheric contribution can be estimated as about 30% of the total nitrogen in the North Sea.
In certain systems the use of the isotopic measurements of nitrogen containing species provides additional information, which is useful for confirming the magnitude of such fluxes. For instance, isotopic studies have been successfully undertaken for understanding the nitrogen marine cycle, which is represented in fig. 1.2 (from Gruber, 2008).

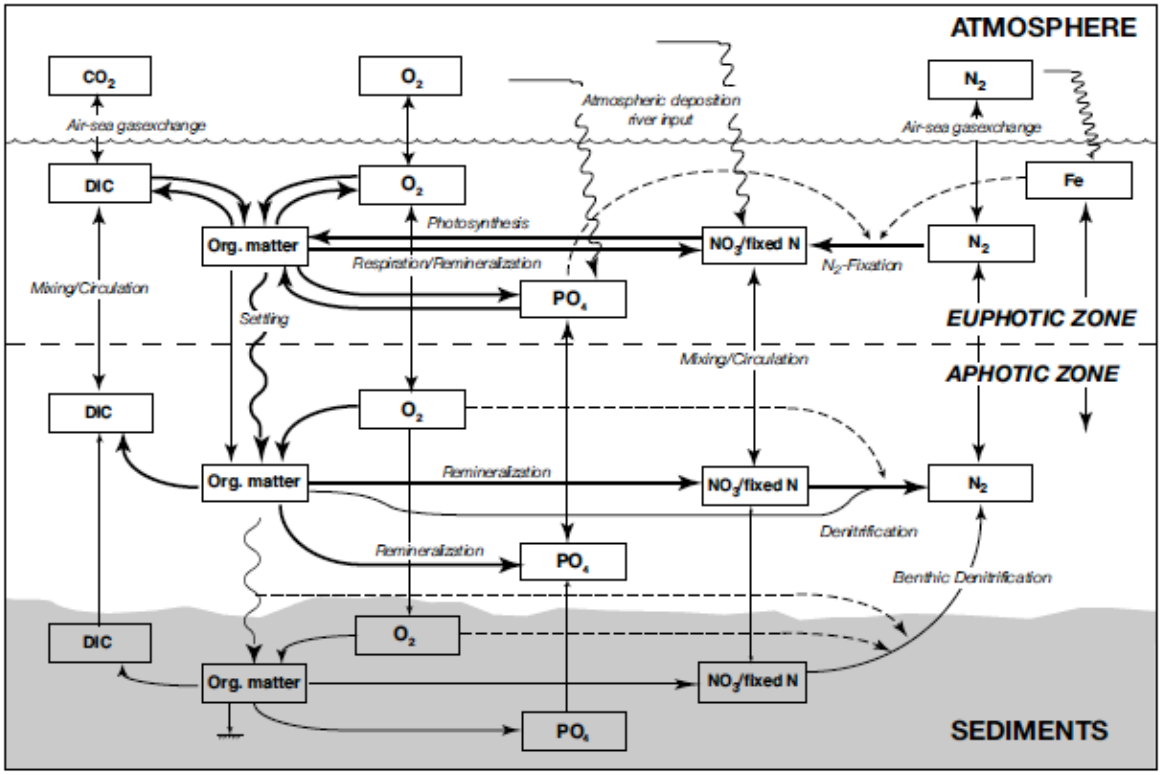

Fig. 1.2. *Representation of the marine N cycle and the main processes involved in it (from Gruber, 2008).*

Fig. 1.3 illustrates the isotopic enrichments associated to the most important biological processes of the marine N cycle.

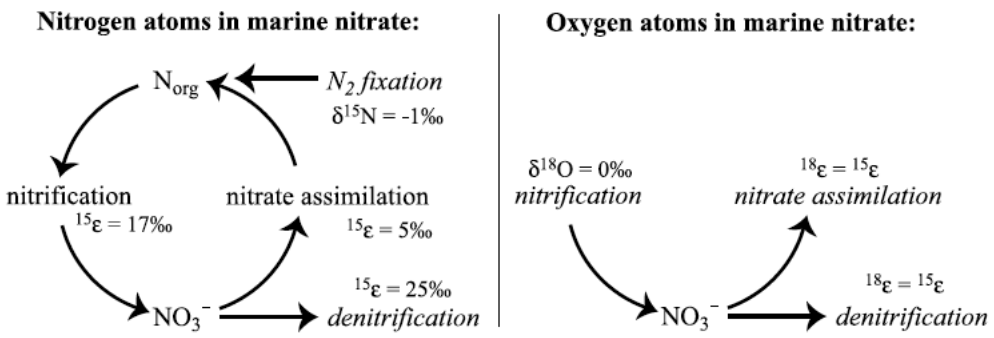

Fig. 1.3. *Scheme of the isotopic signatures associated with the most important biological processes involved in the marine nitrate cycle (from Sigman et al., 2005).*

Coupling the study of the nitrate dual isotope (i.e. $\delta^{15}N‰$ and $\delta^{18}O‰$) with profiles of nitrogen concentration and N* (excess nitrogen, defined as $N^*=[NO_3^-]-16[PO_4^{3-}]+2.9$, which can be used as an indicator of areas of N_2 fixation and denitrification, according to Deutsch et al., 2001) allows determination of the relative importance of the major biogeochemical processes involved in the local N marine cycle (Sigman et al., 2005)(Sigman et al. 2009a)(Sigman et al., 2009b). According to Hansell et al. (2007), it was calculated that in the North Atlantic 38% of N* is due to atmospheric deposition, 28% to mixing processes and only 33% to N fixation. However, Krishnamurthy et al. (2010) pointed out that, since N/P can be also offset by denitrification, the role of the atmosphere estimated by Hansell et al. might be overestimated. Furthermore, Baker et al. (2007) mentioned that the assessment of nitrogen fixation using nitrogen isotope-based methods could be overestimated up to a factor of 2, if atmospheric nitrate inputs are not taken into account.

Thus, for several reasons, it would be important developing alternative methods to confirm our knowledge of atmospheric N inputs, in order to be able to reduce the overall uncertainty on the global N cycle. The analyses of the nitrate mass independent fractionation (MIF, a deviation from a classical mass dependent fractionation, which can be defined with the acronym MDF), which seems to be a signature of atmospheric nitrate, could help to trace the atmospheric nitrate deposition. The possibility of a mass dependent fractionation was first postulated by Craig (1957), based on the theoretical calculations of the isotope partitioning under equilibrium and kinetic conditions (Urey, 1947; Bigeleisen and Mayer, 1947; Bigeleisen, 1949).

A mass dependent fractionation can be detected in elements with three or more isotopes, as it is defined as a relationship between two distinct pairs of fractionated isotopes of the same element (for instance between the pair [isotope1+isotope2] and the pair [isotope1+isotope3], or between the pair [isotope1+isotope2] and the pair [isotope3+isotope4] etc.).

This relationship is a function of only the masses of the isotopes of the two pairs. The mass dependent fractionation in nitrate refers exclusively to oxygen isotopes, since nitrogen is an element with only two isotopes.

The mass dependent fractionation of any three isotopes 1, 2 and 3 of the same element implies that the isotope partitioning between two phases a and b follows the condition expressed in eq. 1.1.

$$\alpha_{2/1}^{a-b} = \left(\alpha_{3/1}^{a-b}\right)^{\beta} \qquad \text{Eq. 1.1}$$

According to eq. 1.2, the isotope fractionation constant $\alpha_{2/1}^{a-b}$ can be calculated by considering the mole fractions X of the isotopes 1 and 2 in the phases a and b.

$$\text{where } \alpha_{2/1}^{a-b} = \frac{\left(\frac{X_2}{X_1}\right)_a}{\left(\frac{X_2}{X_1}\right)_b} \qquad \text{Eq. 1.2}$$

An analogous equation defines the isotope fractionation constant $\alpha_{3/1}^{a-b}$, when considering the mole fractions X of the isotopes 1 and 3 in the phases a and b.

The value of the exponent of the right side of eq. 1.1 can be theoretically calculated for any element, based on the mass m_1, m_2 and m_3 of the three isotopes involved in the fractionation between the phases a and b (Matsuhisa et al., 1978)(eq. 1.3).

$$\beta = \frac{\left(\frac{1}{m_1} - \frac{1}{m_2}\right)}{\left(\frac{1}{m_1} - \frac{1}{m_3}\right)} \qquad \text{Eq. 1.3}$$

It is beyond of the scope of this section illustrating thoroughly how the parameter β is derived, as it involves the calculation of the partition function of the isotopologues (which are molecules differing only in the isotopic composition), which can be found in Urey, 1947.
Briefly, according to Urey's theory, the partition function (which is the normalizing factor ensuring that the sum of the probabilities of a certain energy state of a species is one) of the isotopologues can be split into two terms, a quantum mechanical part f and a classical mechanical part, the latter term being cancelled out when equilibrium conditions are reached. When the temperature is sufficiently high, f can be simplified to eq. 1.4.

$$f = 1 + \frac{1}{24}\left(\frac{h}{k_b T}\right)^2 \sum_j \left(\nu_{j,1}^2 - \nu_{j,2}^2\right) \qquad \text{Eq. 1.4}$$

The term k_b is the Boltzmann's constant, h is the Planck's constant, T is the temperature and ν_{j1} defines the independent j-th vibrational mode of the isotope 1 (in a linear molecule with N atoms, there are 3N-5 independent vibrational modes, whereas there are 3N-6 modes in non linear molecules).
Assuming that atoms behave as harmonic oscillators, the natural frequency of the oscillator in hertz can be expressed by considering the force constant K (which can be inferred from the Hooke's Law) and the mass m of the oscillator (eq. 1.5).

$$\nu = \frac{1}{2\pi}\sqrt{\frac{K}{m}} \qquad \text{Eq. 1.5}$$

Based on Urey's theory, assuming that the force constant is the same for any isotope of an element in a phase, it can be demonstrated that the logarithm of any isotope fractionation constant $\alpha^{a\text{-}b}$ equals the difference of ln(f) in the two phases a and b where the partitioning occurs (Young, 2002)(eq. 1.6).

$$\ln \alpha^{a-b} = \ln f_a - \ln f_b = 1 + \frac{1}{24}\left(\frac{h}{k_b T}\right)^2 \left(\frac{1}{m_1} - \frac{1}{m_2}\right) \sum_j \left(\frac{K_{j,a}}{4\pi^2} - \frac{K_{j,b}}{4\pi^2}\right) \qquad \text{Eq 1. 6}$$

$K_{j,\,a}$ and $K_{j\,b}$ are the force constants of the independent vibrational mode j-th in the phase a and b, respectively.
The ratio of the two mass fractionation constants $\alpha_{2/1}^{a-b}$ and $\alpha_{3/1}^{a-b}$ defines the parameter β (eq. 1.5).

$$\frac{\ln \alpha_{2/1}^{a-b}}{\ln \alpha_{3/1}^{a-b}} = \frac{\frac{1}{24}\left(\frac{h}{k_b T}\right)^2 \left(\frac{1}{m_1} - \frac{1}{m_2}\right) \sum_j \left(\frac{K_{j,a}}{4\pi^2} - \frac{K_{j,b}}{4\pi^2}\right)}{\frac{1}{24}\left(\frac{h}{k_b T}\right)^2 \left(\frac{1}{m_1} - \frac{1}{m_3}\right) \sum_j \left(\frac{K_{j,a}}{4\pi^2} - \frac{K_{j,b}}{4\pi^2}\right)} = \frac{\left(\frac{1}{m_1} - \frac{1}{m_2}\right)}{\left(\frac{1}{m_1} - \frac{1}{m_3}\right)} \qquad \text{Eq. 1.7}$$

When eliminating the logarithms of the left-hand side of eq. 1.7, the result in eq.1.1 is therefore obtained.
It is important to point out that eq. 1.6 is valid only when equilibrium is obtained and therefore, based on this approach, any deviation from the mass dependent fractionation should occur in case of irreversible processes, for which the classical mechanical part of the isotopologue partition function cannot be cancelled out.
It is worth drawing attention on the character of universality of equation 1.7. To do that, eq. 1.7 is written as eq. 1.8 by using the definition of eq. 1.2.

$$\frac{\ln\left(\frac{\left(\frac{X_2}{X_1}\right)_a}{\left(\frac{X_2}{X_1}\right)_b}\right)}{\ln\left(\frac{\left(\frac{X_3}{X_1}\right)_a}{\left(\frac{X_3}{X_1}\right)_b}\right)} = \frac{\ln\left(\frac{{}^2R_a}{{}^2R_b}\right)}{\ln\left(\frac{{}^3R_a}{{}^3R_b}\right)} = \frac{\left(\frac{1}{m_1} - \frac{1}{m_2}\right)}{\left(\frac{1}{m_1} - \frac{1}{m_3}\right)} \qquad \text{Eq. 1.8}$$

The fractionation constant α describes the abundance ratio of any two isotopes and it strictly depends (see eq. 1.6) on the temperature and the phases a and b between which the fractionation occurred (through the parameters $K_{j,a}$ and K_{jb}). By contrast, based on eq. 1.8, when observing the three isotopes of the fractionating element altogether, it can be shown that, no matter what the temperature and the phases a and b are, the overall distribution of the three isotopes in two phases will be depending only on the masses of the isotopes considered.
In other words, if we consider that the relative abundance of two isotopes like ^{16}O and ^{18}O are variable parameters depending on the temperature of formation and the phases a and b, the relative abundance of the isotope ^{17}O in the two phases can be always determined without the necessity of measuring it, provided that equilibrium conditions were reached.
It is worth remembering that eq. 1.8 is possible due to the approximation at reasonably high temperatures (eq. 1.4). Urey (1947) calculated the temperature dependence of $\ln\alpha_{2/1}/ \ln\alpha_{3/1}$. He showed that for $T \rightarrow 0K$ such ratio approaches the ratio of the zero-point energy differences of the various isotopic species, whilst for $T \rightarrow \infty$ the fractionation of all isotope ratios tend to the same number, regardless of the chemical element considered.
The overall partitioning of three or more isotopes is usually considered temperature independent because the range of the parameter β is rather limited (see fig. 1.4, showing some calculations for water and carbon dioxide, from Urey, 1947)

Table A1. Theoretical $^{17}O/^{16}O$ and $^{18}O/^{16}O$ fractionations* for CO_2–H_2O

T(°K)	CO_2			H_2O			CO_2 - H_2O		
	Q^{17}/Q^{16}	Q^{18}/Q^{16}	Ratio	Q^{17}/Q^{16}	Q^{18}/Q^{16}	Ratio	Δ_{17}	Δ_{18}	Ratio
273.16	.065 561	.124 299	.5275	.037 528	.070 724	.5306	.028 033	.053 575	.5233
298.16	.058 133	.110 176	.5276	.033 924	.063 933	.5306	.024 209	.046 243	.5235
500.	.026 920	.050 905	.5288	.018 107	.034 116	.5307	.008 813	.016 789	.5249
1000.	.008 175	.015 427	.5299	.006 879	.012 959	.5308	.001 296	.002 468	.5251

Fig. 1.4. *Urey's theoretical calculations (1947) of the temperature dependence of the fractionation constant of $^{17}O/^{16}O$ and $^{18}O/^{16}O$ in the system CO_2-H_2O (from Matsuhisa et al. 1978).*

It is useful rearranging eq. 1.8 in terms of delta values (defined in eq. 1.9), since all published data are reported in delta notation.

$$\delta_a^i = \frac{{}^iR_a}{{}^iR_S} - 1 \qquad \text{Eq. 1.9}$$

Substituting in eq. 1.8 the isotopic ratio R_b in the phase b with the isotopic ratio R_S in a reference material S (with the condition that S has also been generated by a mass dependent fractionation, see Miller, 2002), allows rewriting eq. 1.8 as eq. 1.10.

$$\ln^2 R_a - \ln^2 R_S = \beta(\ln^3 R_a - \ln^3 R_S) \qquad \text{Eq. 1.10}$$

The term ^2R_a is expressed in eq. 1.11, after rearranging eq. 1.9.

$${}^2R_a = {}^2R_S(\delta_a^2 + 1) \qquad \text{Eq. 1.11}$$

Eq. 1.12 defines the natural logarithm of ^2R_a, based on eq. 1.11.

$$\ln^2 R_a = \ln\left({}^2R_S(\delta_a^2 + 1)\right) = \ln^2 R_S + \ln(\delta_a^2 + 1) \qquad \text{Eq. 1.12}$$

Similarly, $\ln^3 R_a$ can be defined in eq. 1.13

$$\ln^3 R_a = \ln\left({}^3R_S(\delta_a^3 + 1)\right) = \ln^3 R_S + \ln(\delta_a^3 + 1) \qquad \text{Eq. 1.13}$$

Substituting eq. 1.12 and eq. 1.3 in eq. 1.10 gives eq. 1.14.

$$\ln(\delta_a^2 + 1) = \beta \ln(\delta_a^3 + 1) \qquad \text{Eq. 1.14}$$

It is worth mentioning that there are currently at least other two ways to define the isotope delta values, which fact unfortunately causes some confusion. First, several authors include the factor 1000 in the definition of the delta value (eq. 1.9). As a result, eq. 1.14 becomes eq. 1.15.

$$1000\ln\left(\frac{\delta_a^2}{1000}+1\right)=\beta 1000\ln\left(\frac{\delta_a^3}{1000}+1\right) \qquad \text{Eq. 1.15}$$

Hulston and Thode (1965) proposed to define the delta values as $\delta^2 = \ln({}^2R_a/{}^2R_S)$. This definition is currently not too popular among authors, apart from some scientists using a kinetic $\beta=\ln(m_1/m_2)/\ln(m_1/m_3)$ (Matsuhisa et al., 1978)(Young et al., 2002)(Wombacher and Rehkamper, 2003).

The isotopic measurements can be shown in a three isotopes plot, which is a plot where the ordinate is $\ln(1+\delta^{17}O)$ (or $1000\ln(1+\delta^{17}O/1000)$, depending on how the delta value is defined) and the abscissa is $\ln(1+\delta^{17}O)$ (or $1000\ln(1+\delta^{18}O/1000)$). When a mass dependent fractionation has occurred, measurements are found along a line passing through the origin called the TFL (the terrestrial fractionation line), whose slope equals β.

A value of β of 0.528 for the oxygen isotopes is widely accepted, being an average of experimental values (fig. 1.5, the letter λ instead of β is used, from Rumble et al., 2007). This value fits well with the theoretical β defined in eq. 1.3 (0.529 when considering the masses of the oxygen stable isotopes). If β is defined as $\ln(m_1/m_2)/\ln(m_1/m_3)$ (a definition used in case of kinetic processes), β for the oxygen isotopes should be 0.515 (note in fig. 1.5 that a slope of the mass fractionation line close to 0.515 has been found when measuring the oxygen isotopic composition of leaf and stem water).

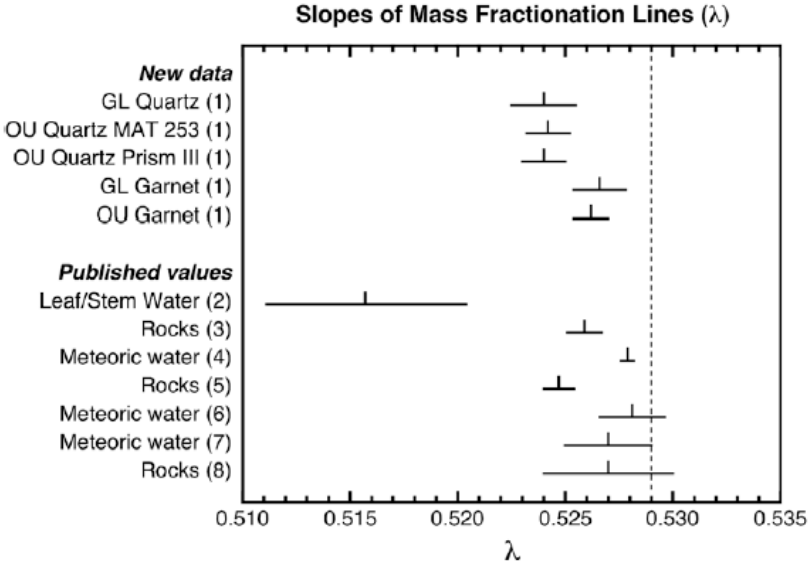

Fig. 1.5. *Published values of λ. Mean values are marked by vertical ticks; horizontal bars indicate the corresponding 95% confidence intervals (from Rumble et al., 2007 and reference therein).*

Any measurements deviating from the TFL are regarded as anomalous, and mass independent fractionations are evoked as responsible for the isotope anomaly. The magnitude of the mass independent fractionation (also defined with the acronym MIF, to be opposed to MDF, which means mass dependent fractionation), measured in capital delta ($\Delta^{17}O$) can be therefore quantified by considering the deviation from the TFL in a three isotopes plot (fig. 1.6, from Thiemens. 2006).

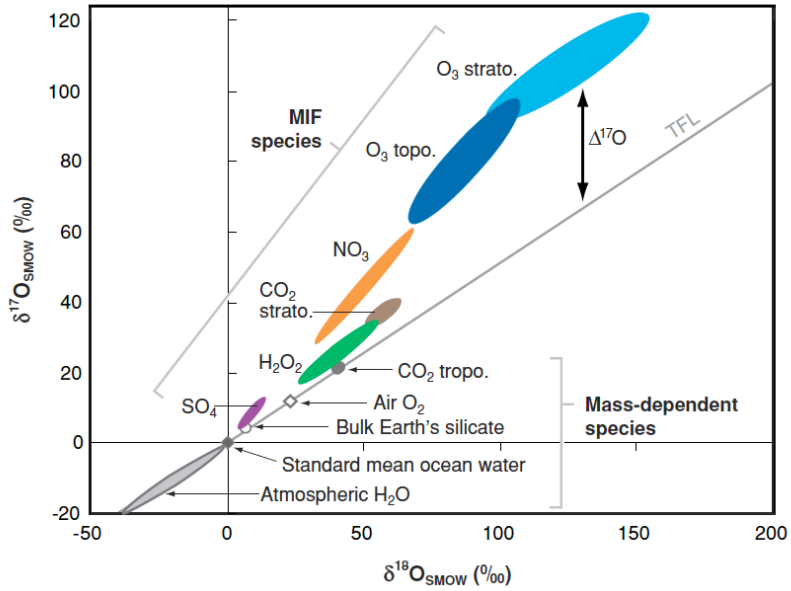

Fig. 1.6. *Oxygen isotope anomaly of atmospheric species (from Thiemens, 2006).*

As it can be seen in fig. 1.6, $\delta^{17}O‰$ and $\delta^{18}O‰$ can be used instead of $\ln(1+\delta^{17}O)$ and $\ln(1+\delta^{18}O)$ as the ordinate and the abscissa of the three isotopes plot. This is due to the approximation $\ln(1+x) \approx x$ (if $x<<1$).
However, it has been calculated that such commonly used approximation would result in an isotope anomaly being depending on the magnitude of $\delta^{18}O$ (Miller, 2002)(see also section 2.3). As an example, in fig. 1.7 the TFL (obtained by plotting $\ln(1+\delta^{17}O)‰$ vs. $\ln(1+\delta^{18}O)‰$) and its approximation (when plotting $\delta^{17}O‰$ vs. $\delta^{18}O)‰$) are shown.

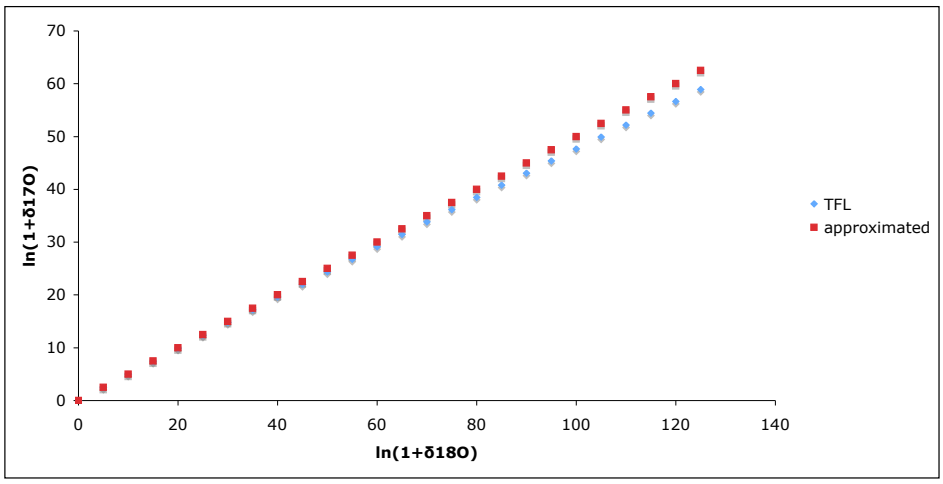

Fig. 1.7. *Difference in the slope of $\ln(1+\delta^{17}O)‰$ vs. $\ln(1+\delta^{18}O)‰$ and in the slope of $\delta^{17}O‰$ vs. $\delta^{18}O‰$.*

Thus, in a three isotopes plot, any data points from samples formed during a mass dependent process should lie in the same line. This means that measuring the isotopic composition of the phase b (R_b of eq. 1.8) is not necessary to understand whether the

isotopic composition found in the phase a was due to a mass dependent process or not, since it is sufficient that the isotopic ratio in the phase a is compared with the isotopic ratio of any reference material S that was generated by a mass dependent process. This observation justifies the change of the phase b with the reference material S in eq. 1.8.

The first measurements deviating from the TFL were found in CAIs (calcium aluminium inclusions in chondrites, the usual main component of meteorites) by Clayton et al. (1973), possibly reflecting the oxygen isotopic heterogeneity of the early solar system (Clayton et al., 1976)(Clayton, 1993).

An anomalous isotope fractionation in a terrestrial environment was first measured in atmospheric ozone (Thiemens and Heidenreich, 1983). There are currently two different positions on the origin of the isotope anomaly in ozone, one stressing the importance of the symmetry of isotopomers (also called isotopic isomers, which are species with the same number of each isotope of each element but differing in their position, for instance two isotopomers of propane are the species CH_3CHDCH_3 and $CH_3CH_2CDH_2$) and the other underlying the kinetic origin of the process.

The former is based on the observation that symmetric molecules like $^{17}O^{17}O^{17}O$ and $^{18}O^{18}O^{18}O$ are less abundant that what should be statistically expected. This observation has been related to the finding that no zero point energy change occurs between the formation and the dissociation of these two types of molecule (Heidenreich III and Thiemens, 1986). Therefore, according to the authors, thermodynamics would explain the anomalous enrichment of ^{17}O in ozone, which is the highest isotope anomaly that has ever found so far (fig. 1.6).

Thereafter, a full quantum treatment of the process has been developed and the theory is currently known as the RRKM (Rice, Ramsperger, Kassel, Marcus) theory (Marcus and Rice, 1951)(Marcus, 1952), which has been recently modified by Gao and Marcus (2001)(2002)(2007).

The second approach is based on the observation that six rate coefficients of ozone formation would contradict the role of molecular symmetry (Mauersberger et al., 1999). This could be due to the fact that fast isotope exchange reactions between O and O_2 would rapidly recycle the atoms before ozone is produced. Thus, "the large variability of the rate coefficients of ozone formation $O+O_2 \Rightarrow O_3$ of about 50% characterizes the ozone isotope effect and demonstrates its kinetic origin" (Janssen et al., 2001)

Atmospheric nitrate is the second species with the highest isotope anomaly (fig. 1.6), owing to the ozone oxidation of nitrate precursors. The reactions leading to "atmospheric nitrate" (a term referring to both gaseous HNO_3 and particulate nitrate in aerosol) in the troposphere are important loss processes for major oxidants producing ozone, as discussed below.

There are two main reactions leading to HNO_3. The first one is the third-body reaction between OH radical and NO_2, which is a major loss for NO_x during daytime (R.1).

$$NO_2 + OH + M \Rightarrow M + HNO_3 \qquad \text{R.1}$$

The second pathway leading to nitrate is the reversible third-body reaction between NO_2 and the radical NO_3, whose product is N_2O_5 (R.2). The dinitrogen pentoxide can be hydrolyzed to nitric acid more efficiently at nighttime (R.3).

$$NO_2 + NO_3 + M \Rightarrow M + N_2O_5 \qquad \text{R.2}$$

$N_2O_5 + H_2O \Rightarrow 2*HNO_3$ R.3

The general scheme is presented in fig. 1.8 (from Atkinson, 2000).

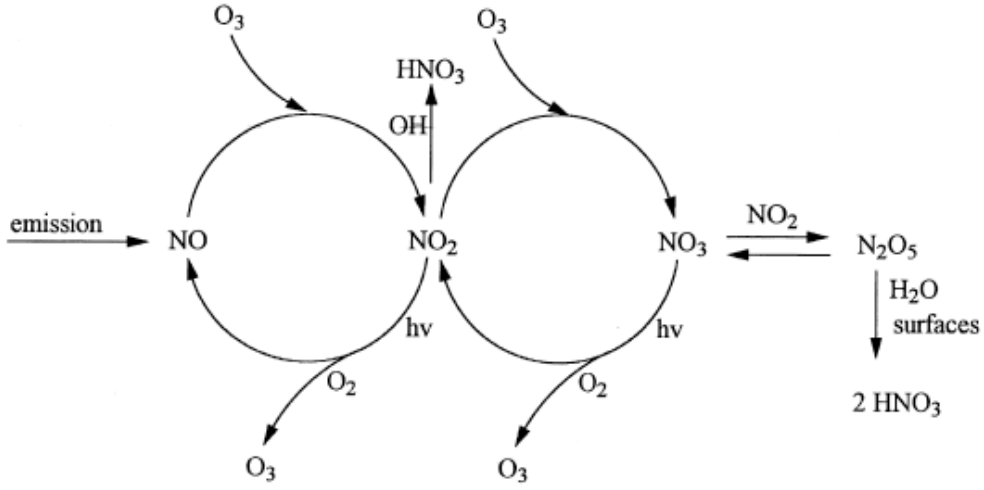

Fig. 1.8. *Scheme of HNO_3 production due to ozone oxidation of nitrogen oxides (from Atkinson, 2000).*

No evidence of the possibility of a homogeneous gas-phase reaction between N_2O_5 and water vapor has been found (Atkinson et al., 1997), but the reaction can quickly proceed in hydrated aerosol (DeMore et al., 1997).
Heterogeneous reactions between nitrogen oxides and chlorine and bromine reservoir species on the surface of polar stratospheric clouds over Antarctica leading to the production of nitric acid (see R.4-R.7) play a central role for the occurrence of the Antarctic ozone hole (Tolbert and Middlebrook, 1990)(Alexander et al., 2009).

$ClONO_2 + H_2O \Rightarrow HOCl + HNO_3$ R.4

$ClONO_2 + HCl \Rightarrow Cl_2 + HNO_3$ R.5

$N_2O_5 + HCl \Rightarrow ClNO_2 + HNO_3$ R.6

$BrONO_2 + H_2O \Rightarrow HOBr + HNO_3$ R.7

Another reaction leading to HNO_3 and HNO_2 is the heterogeneous hydrolysis of NO_2. Zhang and Tao (2010) have recently demonstrated that the homogeneous reaction of hydrolysis of NO_2 in the gas phase is also possible (see R.8).

$2NO_{2(g)} + H_2O_{(g)} \Rightarrow HONO_{(g)} + HNO_{3\,(g)}$ R.8

However, reaction R8 could become important only in the presence of ammonia, which would remove the product HNO_3 by forming ammonium nitrate, the most common nitrate species in aerosol. This is due to the fact that clusters of complexes HNO_3-NH_3 are strongly favorable and that a four-units cluster would already resemble to the ammonium nitrate crystal structure (Zhang and Tao, 2010).

Starting from nitric acid and ammonia, two potential mechanisms can lead to ammonium nitrate formation (Brost et al., 1988) (Tang 1980). The first one involves the production of gaseous NH_4NO_3 that rapidly nucleates to yield particles, as pointed out by Zhang and Tao (2010). The second possibility is that reaction takes place on the surface of existing particles, with the role of a third body. It is usually believed that heterogeneous chemistry on existing particles is the more important mechanism in ammonium nitrate formation.

Due to its high Henry's law constant, atmospheric nitrate partitions preferably in the aqueous phase in cloud as well as in non-cloud aqueous aerosol rather than in the gaseous phase, provided excess base is available (DeMore et al., 1997) and it is then deposited to the ground via wet and dry deposition mainly as particulate nitrate.

Nitric acid is efficiently scavenged and undergoes reactions mainly when the surface to volume ratio of particles is high or, in coarse mode aerosol, when the chlorine and carbonate content is high (Pakkanen et al., 1996). Consequently, the presence of soil dust as well as sea spray aerosol would enhance the formation of particulate nitrate as $Ca(NO_3)_2$ or $NaNO_3$, respectively.

Time scales necessary to achieve equilibrium concentrations between gaseous HNO_3 and particulate nitrate may differ by orders of magnitude with a change of pH, being shorter in more acidic conditions for most common reactions involving HNO_3 (Meng and Seinfeld, 1996).

The presence of nitrate in aerosol in a crystalline phase is possible, as studies on the mineralogical structure of nitrate in aerosol with the Raman, FTIR and the XRD would suggest (Sturges and Harrison, 1989; Esteve et al., 1997; Davis, 1984; Harpale et al., 2006; Fung and Tang, 1992; Maria et al., 2002). Furthermore, the phases diagrams of most common nitrate solid phases in aerosol have been determined (Martin, 2000)(Martin et al., 2003) and recent studies would suggest that identifying the polymorphic phase of ammonium nitrate in aerosol samples could give an indication of the temperature of formation (Wu et al., 2007)(Wu and Chan, 2007). It would be interesting to test whether there is a relationship between the magnitude of the nitrate isotope anomaly and the temperature of formation of ammonium nitrate in aerosol.

A global model of $\Delta^{17}O$ in atmospheric nitrate has been developed (Alexander et al., 2009, see fig. 1.9), to suggest that the relative importance of the night-time and day-time chemistry and the Antarctic stratospheric inputs of nitrate in the troposphere causes both seasonal trends and changes in the atmospheric nitrate MIF signal as a function of latitude.

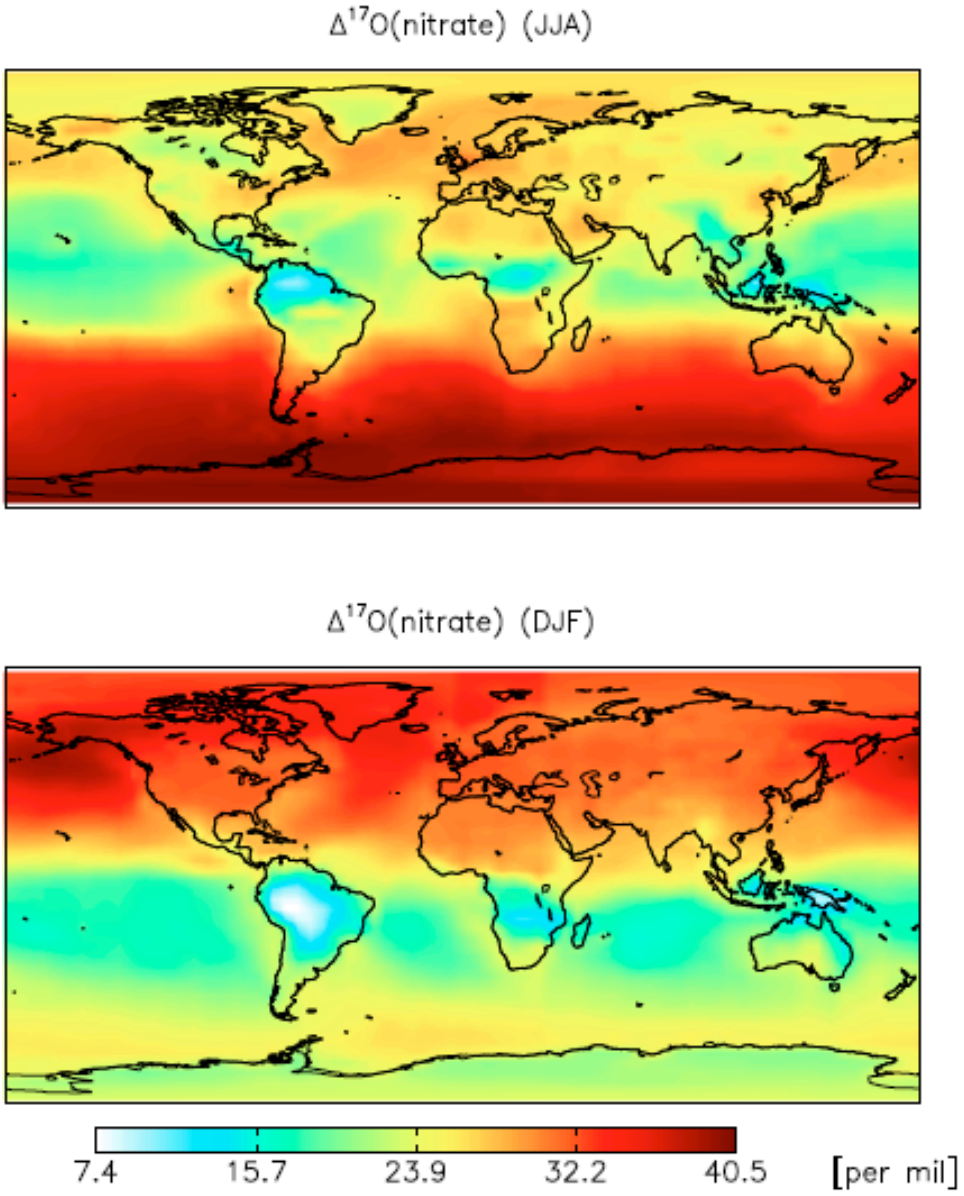

Fig. 1.9. *June-July-August (top) and December-January-February (bottom) average nitrate* $\boldsymbol{\Delta}^{17}O$ *(‰) values 0–200m above the surface (from Alexander et al., 2009).*

It is important to point out that, to the best of our knowledge, no measurements of the mass independent fractionation of atmospheric HNO_3 has been made, probably due to the difficulty of trapping HNO_3 without generating artifacts (see Nie et al. 2010 and reference therein).

As a result, when dry deposition is an important nitrate load mechanism, it could be difficult quantifying the uncertainty on the effective range of the isotope anomaly of atmospheric nitrate deposited to the ground, due to the uncertainty on the isotope anomaly of precursor HNO_3.

Because the atmosphere is regarded as being the only source of a nitrate isotope anomaly, it has been suggested that the MIF signature could be used as a tracer to

understand the importance of atmospheric nitrate inputs on watershed systems (Kendall et al., 2007, see fig. 1.10).

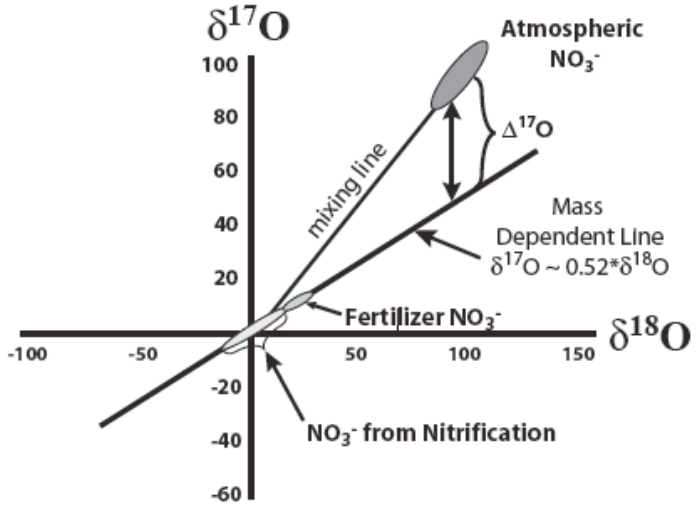

Fig. 1.10. *Schematic relationship between $\delta^{17}O$ and $\delta^{18}O$ in nitrate of different origin (from Kendall et al., 2007).*

The tracer has been already used to understand the origin of the most important nitrate ore deposits of the world (Michalski et al., 2004)(Li et al., 2010) and the presence of a nitrate isotope anomaly proved that the nitrate minerals at Atacama Desert (Chile) and in the Turpan-Hami basin (China) were derived from long-term atmospheric deposition. Measurements of the isotope anomaly in lakes (Michalski and Thiemens, 2006)(Tsunogai et al. 2011) allowed considerations on the dynamics of nitrate recycling in the water column. Analyses of the nitrate isotope anomaly in surface water samples from the Pacific Ocean have also been undertaken (Tsunogai, 2007, see section 3.2 and fig. 3.33).

Thus, we are currently at the first stage of the assessment of the ability of the nitrate MIF signature to trace atmospheric nitrate deposition. The use of the nitrate isotope anomaly in future studies will be successful only if it will be possible to prove that the MIF signature is a conservative tracer in natural systems and that the atmosphere is effectively the only source of a nitrate isotope anomaly. Demonstrating that both hypotheses, which are usually regarded as assumptions (Thiemens. 2006)(Kendall et al., 2007)(Morin et al., 2009), are correct will be the major objective of the present thesis. Furthermore, a second objective will be identifying the current precision of the method, in order to assess what is the threshold above which the detection of a nitrate isotope anomaly is certainly related to the content of atmospheric nitrate in sample water.

Reaching these objectives should help to recognize the conditions that could limit the use of the tracer and it would allow identifying the systems where the nitrate MIF signature has the greatest potential.

1.2. Structure of the thesis

The content of the present thesis reflects the compromise between the goals that I wanted to pursue and what I could effectively undertake.
Producing data sets of good quality still represents the greatest difficult when working with the nitrate MIF and the extension of chapter 2, dedicated to the method, reflects this difficulty. In fact, most of my works was focused on testing the precision and the accuracy of the method. I believe that the assessment of the accuracy of the method currently represents the major issue. This is mainly because of a trend in the oxygen delta values (possibly depending on unwanted reactions in the gold furnace) that is difficult to take into account. This problem would strongly limit the use of measured $\delta^{17}O$ and $\delta^{18}O$. However, what is generating the trend seems to be a mass dependent process and the capital delta can still be determined. Further tests were designed to identify the chance of an artifact due to sample size, sample volume and degree of salinity. Some kinetic tests have been undertaken to verify that an incomplete denitrification by *Pseudomonas aureofaciens* would not change any sample capital delta value. The presence of high copper concentration in nitrate solutions has been found to influence *Pseudomonas aureofaciens* conversion to nitrous oxide, suggesting that there is the possibility that some biological processes could be responsible for the production of an isotope anomaly when certain pollutants at high concentration are present.
The choice of analysing the samples collected at Marano lagoon (chapter 3) didn't really come after a careful selection of which type of system should be investigated. Yet, using this data set gave me the advantage of comparing the results obtained with the method described in chapter 2 with the analyses of major nutrients concentration. A further advantage was the literature dedicated on the biological community in the lagoon, which gives an indication of major biological processes involved in the local nitrogen cycle. The analysis of this data set has a first subchapter dedicated to the nitrogen delta values and a second one focused on discussing the measured capital delta values.
Measuring some nitrate minerals of different origin (chapter 4) gave me the opportunity to test the chance that the atmosphere is not the only source of a MIF signal. Some laboratory tests on evaporation and partial melt of nitrate solutions complement the discussion on the possibility that geochemical processes could generate measurable capital delta values.
In some cases I couldn't make use of my data to reach satisfactorily the objectives that I chose and I tried to find an answer indirectly, by combining the results of other authors with some calculations (chapter 5). This chapter has been written to reach two goals. Firstly, I wanted to reconcile some unexpected results from both the lagoon samples and the minerals. This could be possible by demonstrating that the statement that a mass dependent process cannot change the magnitude of an isotope anomaly is not always correct. Thus, in this chapter it is shown that, when considering hypothetical "real" cases (i.e. when dealing with absolute isotope concentrations), it is not always possible to distribute any initial number of isotopes among phases so that an observer would find that only mass dependent fractionations have occurred. Another question still remained after reading the work of the most important papers mentioned in the literature review. What is really new and anomalous in the MIF? The possibility that the discovery of the MIF might reflect the fact that the theory explaining the mass dependent fractionation is incomplete is discussed before drawing some final conclusions and recommending some future work (chapter 6).

2. Method development

2.1 The denitrifier method

The nitrate isotopic measurements discussed in Chapter 3 and 4 are obtained by using the denitrifier method.
The denitrifier method (Sigman et al., 2001) is currently the only method that allows the isotopic measurements of the nitrogen and oxygen isotopic composition of samples with a nitrate concentration of 2μM. This is due to its high sensitivity (the samples size required is two orders of magnitude smaller than that for previous methods) (Revesz et al., 1997) (Silva et al., 2000), a reasonably good precision (standard deviation of measured delta values of 0.3‰ on average) and a blank size less than 10% of the signal size from 20nmol of sample (Sigman et al., 2001).
The method is based on using denitrifying bacteria, which can reduce nitrate and nitrite to N_2O but which cannot reduce the N_2O further.
Denitrifies normally reduce the nitrate to N_2O, following the sequence S. 2.1.

$$NO_3^- \rightarrow NO_2^- \rightarrow NO \rightarrow N_2O \qquad \text{(S. 2.1)}$$

Any denitrifying bacteria lacking the enzyme N_2O-reductase might be suitable for the method. The nitrous oxide produced by the bacteria is then extracted and purified for IRMS measurements.
Since nitrous oxide formation requires two atoms of nitrogen, two molecules of nitrate are necessary to generate a molecule of N_2O. As a result, only 1 of 6 nitrate oxygen atoms is preserved in the final product, the nitrous oxide.
Furthermore, the sample's pristine isotopic signature is not entirely preserved due to an oxygen isotope exchange with water during bacterial conversion (see section 2.3).
The denitrifying bacteria species *Pseudomonas aureofaciens* is usually the preferred strain for the method, owing to the smaller oxygen isotope exchange (5% on average) with water during nitrate conversion, compared to *Pseudomonas chlororaphis* (Casciotti et al., 2002).
Pseudomonas aureofaciens culturing protocol used at the SIL UEA laboratory has been adapted from Frank Yi Wang, (2006), which is based on Sigman's teamwork at Princeton University and Matt McIlvin personal communication, with some additional information from the UEA SIL experience.
The stock of bacteria for the denitrifier method at the SIL UEA derives from bacterial colonies cultured at Princeton University.
The culture stock is suspended in a aqueous mixture containing glycerol (that would prevent the frozen cells being damaged by water expansion during solidification) and stored in 2.5 ml eppendorfs at -76°C in the dark.
To revive the culture from the stock, a small amount of frozen cells is removed from the 2.5 ml eppendorf with a sterile 100μL pipette tip and dropped in an agar plate (that will be named as P1, where the number is indicating the bacterial generation in respect to the culture stock).
The agar plate P1 is immediately streaked with a sterile loop, starting from the drop of frozen cells. This process allows the separation of bacteria that will be therefore in condition to generate distinct bacterial colonies. After placing the lid on P1, parafilm is used to seal the agar plate, in order to prevent the chance of contamination.

Every inoculated agar plate is stored at room temperature in the dark for 3-10 days, or until the single colonies become too large to be distinguished from each other. After 10 days from bacteria inoculation, plates are regarded as old and discarded.
A single colony is transferred from the agar plate P1 to a second agar plate P2 with a sterile loop. Streaking is immediately carried out on plate P2, in the same ways as for the streaking on plate P1. This would allow the formation of single colonies that can be used for inoculating other agar plates, similarly to the inoculation of the agar plate P2. This process can be repeated several times using cultures from P1 to produce successively up to four more plates (P2-P5).
To prepare a batch of samples for nitrate IRMS measurements, a single bacterial colony of *Pseudomonas aureofaciens* is transferred from a freshly grown colony on an agar plate with ID P2-P5 to a sterile 15ml centrifuge tube containing 9ml of media for bacterial culturing.
Therefore only bacterial colonies from the 2^{nd} to the 5^{th} generation (with respect to the culture stock) are used for the nitrate isotopic measurements with the denitrifier method. This strategy has been chosen to find a compromise between the necessity of avoiding the chance of genetic mutations in late generations with the opportunity of postponing the use of the culture stock, in order to delay its consumption.
The media for bacterial culturing is prepared with 1.8g KNO_3, 0.45g $(NH_4)_2SO_4$, 11.7g K_2HPO_4, and 54g Triptych Soy broth granules added to 1800ml MQ. The dissolved mixture is transferred in 450ml glass bottles and 15ml centrifuge tubes and autoclaved for 90 minutes. Sterilized stoppers are placed into bottles immediately after media sterilization and seals are crimped. Similarly, centrifuge tubes are tightened with sterilized lids.
Media bottle and media tubes can be stored in the dark at room temperature for up to one year. If any bottles or tubes become cloudy at any time during storage, they will be discarded, to avoid the chance of undesired contamination.
The tube is then incubated at room temperature overnight on a shaker table. This first step is necessary to ensure that the colony was successfully inoculated. This can be done by inspection of the cloudiness of the media, since uncontaminated media is perfectly clear.
An aliquot of 2.7 ml of the incubated media is transferred into 450ml bottle (4 bottles in total can be inoculated per tube) containing the same media by injecting through seals. After bacteria inoculation, the bottles are incubated in the dark on a shaker table for 6-10 days.
After the incubation period, the culture from a 450ml media bottle is evenly divided between 250ml centrifuge bottles and centrifuged for 10 minutes at 4950 rpm. The liquid above cells is poured off gently, to leave the cells at the bottom of the bottle. A pink or yellowish layer of concentrated bacteria will be visible at the bottom of each centrifuge bottle.
An appropriate volume of NFM (nitrate free media) is added to the first centrifuge bottle (approximately 0.15 ml NFM per 1 ml of original medium).
The NFM (nitrate free media) is prepared adding 0.5g $(NH_4)_2SO_4$, 13g K_2HPO_4, and 60g Triptych Soy broth granules to 2000ml MQ.
The content of the centrifuge bottle is then transferred to a second bottle and mixed to resuspend the centrifuged bacteria. The step is repeated until all cells are resuspended in one centrifuge bottle.
An amount of 2 ml of the cell concentrate is pipetted in to 18ml vials. No more than 45 vials can be prepared from one 450ml media bottle inoculated with the bacteria.

Stoppers are placed into vials and seals are crimped before purging the vials with helium.
Undesired nitrous oxide, coming from both the atmosphere and from any bacterial conversion before sample injections, would increase the blank size and lower the precision of the method. In order to remove as much nitrous oxide as possible and to ensure anaerobic conditions, vials are purged through venting needles with helium at a flow of 60-70 ml/min for approximately 45 minutes. Vials are removed from the purge system and placed sideways on a shaker table overnight. A second purge with helium for 45 minutes is made before sample injections to remove any residual nitrous oxide.
The samples can now be added to the vial. To avoid any contamination with the previous samples, the syringe used for sample injections is always rinsed 10 times with MQ and then 3 times with a small aliquot of sample water. If sample injection volume is greater than 1ml, a venting needle is inserted through the butyl stopper so that the vial does not become pressurized, as high pressure would favor gas leakage.
After each sample injection, vials are placed in the tray in inverted position to prevent any gas leakage, and incubated overnight. The following morning 0.1-0.2 ml of 6M NaOH is injected into each vial and shaked to lyses instantaneously the bacteria. It is assumed that 100nmol of sample is converted in few hours.
In a normal batch of samples, blanks and standards (4mM nitrate solutions in MQ) were carried through the bacterial procedure alongside samples.
The N_2O is usually analyzed as a batch with the IRMS (Isotope Ratio Mass spectrometry) within the next few days. A batch of samples would be discarded if storage before IRMS measurements lasted for more than one month.

2.2 The IRMS N_2O analysis system

The isotopic measurements of nitrate can be further improved by coupling the denitrifier method with a fully automated N_2O extraction-purification-isotope analyses system (Casciotti et al., 2002).
Kaiser et al. (2007) successfully tested an online N_2O conversion to N_2 and O_2 in a gold furnace at 800°C followed by GC separation.
Such a thermal decomposition in a gold tube allows measurements of the $\Delta^{17}O$ with a sensitivity of two-three orders of magnitude higher than previous offline thermal decomposition methods (sample size thereby reduced to 50nmol of nitrate) and a precision for the isotope anomaly of in the range 0.3-0.5‰ (Kaiser et al., 2007). All our samples have been analyzed using the system described by these authors and the reader is referred to the article for a detailed description of the extraction line.
The nitrous oxide due to bacterial nitrate conversion is extracted from the 18ml vials with a Gilson auto-sampler and transferred into a vacuum line, a nitrous oxide extraction line connected with an IRMS (Isotope Ratio Mass Spectrometry).
Gross water is removed with a Nafion dryer. A second trap made with magnesium perchlorate on top and carbosorb at the bottom removes residual water and CO_2. VOC (Volatile organic compounds) are extracted from the sample with a second trap, which immediately follows the first one. The third trap is a type "F" Trap (OV®-1 /Tenax®/Silica Gel Traps, manufactured by Teledyne Tekmar).
A cryogenic trap is used to separate the nitrous oxide from molecular nitrogen and oxygen. Thus, a loop is temporarily immersed in liquid nitrogen so that the nitrous oxide is kept frozen in the loop, while nitrogen and oxygen are vented out.

Once the entire sample is collected in the trap, the loop is lifted from the liquid nitrogen container, to be warmed up to room temperature and turned again into a gas, while a second cryogenic trap is immersed in liquid nitrogen. The second loop has a smaller inner diameter and is meant for sample concentration.
After concentration, the sample is lifted from the container and warmed up again. The nitrous oxide is then separated from any other residual organic compound in a GC precolumn. Once the nitrous oxide has reached the end of the GC column, whatever is following is backflushed and vented out through the automated switching of a valve (previous tests had been undertaken to asses the time window after which the nitrous oxide has passed the GC column).
The N_2O is then passed through a gold furnace at a temperature in the range 700-900°C which converts the purified nitrous oxide to O_2 and N_2. A second GC column separates the oxygen from the nitrogen, allowing the IRMS measurements of both molecules. The oxygen sample peak is eluted first, whilst the nitrogen sample peak usually follows after 2-3 minutes.
The IRMS is a Europa GEO 20-20 mass-spectrometer on-line with a TGII prep system. An oxygen reference gas and a nitrogen reference gas are directly injected from the cylinders to the IRMS through the switching of a valve.
This strategy of analyzing pulses of oxygen and nitrogen reference gas before any measurements of samples coming from the extraction line allows the correction of the sample delta values for the drift of the IRMS source.
There could be several reasons why the reference gas delta values drift during the run. Assuming that no isotope fractionation occurs in the short pathway from the reference gas cylinder to the IRMS ionization chamber, a possible explanation is a change in the sensitivity of the instrument during the run.
Moreover, it was found (data not shown) that the drift in the oxygen reference gas delta values can be minimized if the IRMS ionization chamber is conditioned with pulses of the same gas for about half an hour prior to the start of the run. This finding might suggest a sort of a memory effect in the IRMS ionization chamber.
Fig. 2.1 shows the chromatograph of a measurement lasting 720 seconds (12 minutes). The measurements of samples whose results are discussed in Chapter 3 and 4 last 15 minutes per sample. The difference is due to the fact that a higher purging time compared to the measurement described in fig. 2.1 is used, which improves the nitrous oxide extraction efficiency from the vial.

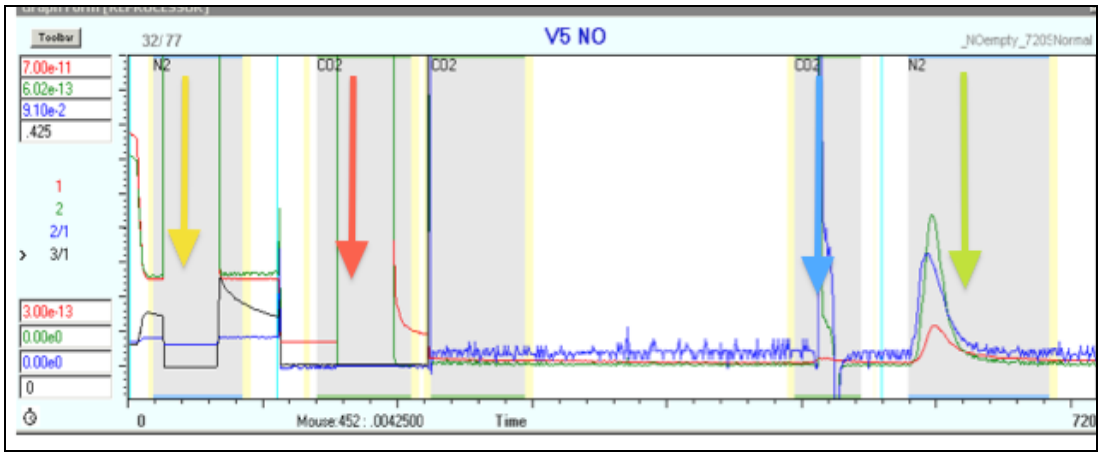

Fig. 2.1. *Example of chromatograph at the end of a measurement of decomposed nitrous oxide with the IRMS.*

The grey areas of the chromatograph (Fig 2.2) correspond to the integration window selected to calculate the reference gasses and the samples isotopic ratio.
The yellow borders of the grey areas define the integration window for quantifying the level of background, which will be automatically subtracted to the reference gasses and samples total beam areas by the software running the IRMS.
The yellow arrow corresponds to the area for integrating the pulse of N_2 reference gas, whilst the red arrow indicate the area where the oxygen reference gas is expected.
In this particular event file, there is the option of analyzing a second pulse of oxygen reference gas, immediately after the first one (third grey area from the left in the chromatograph of fig. 2.1).
The strategy of having more than one oxygen reference gas pulse to measure has been tested to rule out the chance that the drift in the oxygen reference gas delta values was due to effects similar to those affecting samples oxygen delta values (see section 2.3).
There are some evidence (data not shown) revealing that the drift in the reference oxygen delta values can be slightly minimized when considering the second pulse of oxygen reference gas that immediately follows the first one (third grey area in fig. 2.1 from the left).
This would suggest that some of the problems affecting the sample delta values could partially derive from processes occurring in the IRMS ionization chamber.
The blue and the green arrow in fig. 2.1 indicate the integration window of the sample oxygen peak and the sample nitrogen peak, respectively.
During the run, the beam intensity detected by the three isotope detection cups of the IRMS and the ratio between signals can be displayed in each chromatograph.
The number 1 on the left of the chromatograph in fig. 2.1 indicates the first cup, the one with the lowest sensitivity, which is dedicated to analyze the beam intensity of the most abundant species, like ^{16}O and ^{14}N.
The ratio 2/1, shown as a blue line in the chromatograph of fig 2.1, indicates the isotopic ratios $^{18}O/^{16}O$ and $^{15}N/^{14}N$, whilst the ratio 3/1 (the black line in fig. 2.1) refers to the isotopic ratio $^{17}O/^{16}O$.
The results of a run are automatically stored as text files and can be exported as Excel files for the measurements analysis.

2.3 Data processing

All isotopic measurements have to be reported in delta value notation, which is defined in Eq. 2.1.

$$\delta = (R_i/R_s - 1) \qquad \text{(Eq. 2.1)}$$

For nitrate measurements, R represents the isotopic ratios $^{17}O/^{16}O$, $^{18}O/^{16}O$ and $^{15}N/^{14}N$ in the sample *i*-eth and in a reference *s*. Nitrate isotopic measurements are therefore discussed in terms of $\delta^{17}O$, $\delta^{18}O$ and $\delta^{15}N$, depending on the elemental ratio considered.
The reference *s* for the oxygen delta values is VSMOW, whilst nitrogen delta values are reported against the reference AIR.
VSMOW (Vienna Standard Mean Ocean Water) is a water standard for oxygen and hydrogen isotopic measurements. It is a recalibration of the older water standard SMOW, which has be undertaken in 1967 by Harmon Craig.
AIR is a standard for the nitrogen isotopic measurements and corresponds to the average isotopic composition of N_2 in air.

Recent measurements of the nitrate standards USGS34 and USGS35 (Bohlke et al., 2003) allow the nitrate $\delta^{17}O$ and $\delta^{18}O$ to be reported in the VSMOW scale and the nitrate $\delta^{15}N$ to be reported in the AIR scale.
In fact, there is not wide consensus on whether to include the per mille sign (‰) in the delta notation or not (compare for example the delta definition in Young et al., 2002 with the one in Morin et al., 2009). The choice of not including the ‰ sign in the delta value notation has been made for the samples discussed in the chapters 2-4.
The IRMS described in section 2.2 gives the isotopic measurements both in terms of raw delta values and by showing the three elemental $^{a}X/^{b}X$ ratios of the sample.
Raw delta values indicate the sample delta values when the reference *s* is the first measurement of the run. In our case, the first measurement of any run is always a gaseous mixture, a 20ppm N_2O in N_2, which is therefore set by default with raw delta values of zero (i.e. the first sample has the same isotopic composition as the reference *s*). The gaseous mixture, that will be named "20ppm", is usually transferred from a tank to 18ml glass vials for 15 minutes, while air in the sealed vials is vented out through a needle.
The comparison of the delta values of the 20ppm gas standard with the nitrate standards USGS34 and USGS35 allows distinguish any isotope fractionation occurring in the extraction line from the isotope effects associated with bacterial conversion.
The first step for data reduction is the correction of sample and standard raw delta values for the drift of the IRMS source. To do that, it is necessary to consider the deviation from the first measurement of the oxygen and the nitrogen reference gas delta values (set by default as equal to zero) from the following measurements of the same gas. As explained in section 2.2, both reference gasses do not come from the extraction line but are directly injected to the IRMS.
All the measurements of the oxygen and the nitrogen reference gas raw delta values are reported against the first measurements of the same gas. Ideally, with no drift of the source, the oxygen reference gas raw delta values and the nitrogen reference gas raw delta values should be therefore always close to zero. In fact, the last measurements of the oxygen reference gas have been observed to have raw delta values up to 10‰ higher or lower then zero, whereas the nitrogen reference gas raw delta values are usually close to zero.
The deviation of the sample and standard raw delta values due to any drift of the source is corrected, assuming linear drift between samples, by using Eq.2.2.

$$^{a}\delta_{raw\text{-}z} = (^{a}Y_z / {}^{a}Y_1 \,/\mathrm{AVERAGE}(^{a}W_z, {}^{a}W_{z+1})/\mathrm{AVERAGE}(^{a}W_1, {}^{a}W_2))-1)\ ‰ \qquad \text{(Eq.2.2)}$$

for z=1, 2,….n

$^{a}\delta_{raw\text{-}z}$ is one of the three sample raw delta values of the z-eth measurement; $^{a}Y_z$ is the isotopic $^{a}Y/^{b}Y$ ratio of the z-eth measurement (with Y=O, N, and b being the most abundant isotope of Y). $^{a}W_z$ is the z-th measurement of the reference gas elemental isotopic ratio (W=O, N and b being the most abundant isotope of W).
$^{a}Y_1$ is the elemental $^{a}O/^{b}O$ ratio of the first sample coming from the extraction line, which is the 20ppm N_2O in N_2, against which all the other samples raw delta values are calculated.
The second step for data reduction is the calculation of the parameters *m* and *q* of the calibration curve, which is necessary to report the sample isotopic measurements versus the international standards VSMOW and AIR.

The parameters *m* and *q* are the slope and the intercept respectively of the linear regression obtained by plotting standard raw delta values versus standard 'true' delta values (in the VSMOW and AIR scales). Sample calculated delta values in the VSMOW and AIR scale are obtained by using Eq. 2.3.

$$^{a}\delta_{calculated} = m\ ^{a}\delta_{raw} + q \qquad \text{(Eq.2.3)}$$

The parameter *m* is related to the compression factor of raw delta values. The compression factor of raw delta values is a measure of the difference between the delta units in the 20ppm scale with the delta units in the VSMOW and AIR scales.
Sample delta values depend on the isotopic composition of the reference chosen (through the term R_s in Eq. 2.1). Thus, the difference among samples raw delta values certainly depends on the isotopic composition of the reference 20ppm.
In addition, the pristine isotopic composition of both the sample and the reference 20ppm could have been altered due to any process occurring before the IRMS analyses. This will also affect the sample raw delta values (through any change in the terms R_i and R_s of Eq. 2.1)
Such processes would include any isotope fractionation during bacterial conversion (vials prepared with the denitrifier method) and during the nitrous oxide extraction, purification and thermal decomposition (both the 20ppm and the vials prepared with the denitrifier method).
As an example, the difference between the standards USGS34 and USGS35 in 'true' $\delta^{17}O$ (vs. VSMOW), based on internationally agreed values (Bohlke et al., 2003) is 66.3‰. Yet, the first raw delta values of the same standards (vs. 20ppm) in Table 2.1 differ by about 46‰.
Calculating the slope *m* and the intercept *q* of Eq.2.3 by considering two or more standards whose isotopic composition is known would allow taking into account the changes in the delta units when passing to a different scale, without the necessity of identifying the isotopic composition of the 20ppm and the processes that could alter the isotopic composition of any sample reaching the IRMS.
Usually the slope *m* calculated for the oxygen delta values of samples whose results are discussed in Chapter 3 and 4 is in the range 1.3-1.7, resulting in a 30-70% compression factor.
An ideal slope *m* of 1 (compression factor equal to zero) is always found in the nitrogen delta values. Therefore, some processes due to the denitrifier method or occurring during the sample passage in the extraction line and/or the IRMS ionization chamber would fractionate the sample oxygen delta values only.
The oxygen delta values are calculated from raw delta values in the following manner: when the overall uncertainty in both standards $\delta^{17}O$ and $\delta^{18}O$ after drift correction is below 2‰, the calibration curve will be obtained by using all the standards raw delta values of a run.
If the precision in at least one oxygen delta value is worse than 2‰, the sample delta values will be calculated based on the calibration curve obtained with the standard data sets that are closer in the sequence to the sample and whose uncertainty is not greater than 2‰. Usually two calibration curves are sufficient to calculate all the samples of a batch, but sometimes it was necessary to group the standards measurements in three data sets.
As an example, Table 2.1 reports an extract of the raw $\delta^{17}O$ values from a batch. Standards delta values are written in bold.

Measurement	Sample name	Raw $\delta^{17}O$ ‰ (vs. 20ppm)	True $\delta^{17}O$ ‰ (vs. VSMOW)	Calculated $\delta^{17}O$ ‰ (vs. VSMOW)	True $\delta^{17}O$ - calculated $\delta^{17}O$
1	20 ppm N2O	0.00		-0.62	
14	**USGS35**	**37.07**	**51.46**	**51.46**	
15	35T 1H	32.44		44.80	
16	35T 1H	31.77		43.85	
17	45T 3D	33.71		46.64	
20	35T 3D	33.23		45.94	
21	35B 3D	31.22		43.06	
22	35B 3D	31.57		43.56	
25	**USGS34**	**-9.07**	**-14.8**	**-14.80**	
slope	**1.4**				
intercept	**-1.8**				
35	**USGS35**	**33.90**		**52.40**	
36	CRY60	15.21		23.17	
43	**USGS34**	**-9.39**	**-14.8**	**-15.31**	**-0.5**
46	**USGS35**	**33.62**	**51.46**	**51.96**	**-0.5**
47	35B 24H	33.98		52.53	
48	35B 24H	34.33		53.07	
49	35T 24H	31.18		48.14	
50	35T 24H	30.83		47.60	
63	**USGS35**	**32.34**	**51.46**	**49.96**	**1.5**
slope	**1.6**				
intercept	**-0.6**			**stdev**	1

Table 2.1. *Extract from a data set as an example of data reduction with the calculation of* $\delta^{17}O$ *(vs. VSMOW) starting from raw* $\delta^{17}O$ *(vs. 20ppm).*

After 35 measurements (Table 2.1), there is a change in the USGS35 raw $\delta^{17}O$ values of about 10%, which gives a standard deviation, and therefore an overall uncertainty, in the raw $\delta^{17}O$ values of 2.3‰. When considering all four measurements of USGS35 in Table 2.1, the precision drops to 2.4‰.

By contrast, the standard USGS34 has constant raw $\delta^{17}O$ values (compare the 14^{th} measurement with the 46^{th} measurement of the run shown in Table 2.1), and the associated standard deviation is 0.2‰.

The samples and standards in Table 2.1 are therefore separated in two groups: the elements of the first group are displayed in Table 2.1 in orange cells, whilst blue is the color for the second group. Each sample calculated delta value is obtained by using the slope and the intercept of its group.

The disadvantage of the method is the assumption of a step change in the parameters used for calibrating the measured delta values. Yet, without this strategy, the precision in the oxygen delta values of samples measured during long runs could be two or three times worse.
As a result, the slope *m* of the calibration curve changes from 1.4 to 1.6, whereas the intercept *q* changes from -1.8 to -0.6 (Table 2.1). The problem of the daily shift in the delta values (and consequently the change of the slope *m* and the intercept *q* of the calibration curve over time) will be further discussed in the present section.
There are two different ways to calculate the oxygen isotope anomaly starting from sample calculated $\delta^{17}O$ and $\delta^{18}O$ (Miller, 2002).
A mass dependent process is a process that would generate an oxygen isotope partitioning between the phases *a* and *b* that is governed by Eq. 2.4.

$$^{17}R_a/^{17}R_b = (^{18}R_a/^{18}R_b)^{0.528} \quad \text{(Eq. 2.4)}$$

$^{a}R_i$ indicates the isotopic ratio $^{a}O/^{16}O$ in the phase i. The value 0.528 in Eq. 2.4 is the parameter β defined in Eq. 2.5 (see chapter 1) when the element considered is the oxygen (Young et al., 2002).

$$\beta = \frac{\frac{1}{m_1} - \frac{1}{m_2}}{\frac{1}{m_1} - \frac{1}{m_3}} \quad \text{(Eq. 2.5)}$$

In the usual notation the parameter m_1 in Eq.2.5 is the lightest isotope of the element (^{16}O in our measurements), whilst m_3 is the heaviest.
The deviation from a mass dependent process can be evaluated with a parameter $k_{a,b}$.
This can be done by considering the oxygen isotopic signature in the phase *a* compared to the oxygen isotopic signature of a standard material *b* lying on the TFL (terrestrial fractionation line). The TFL is the line upon which data points from samples that are fractionated by mass-dependent processes lie in a three-oxygen isotopes plot (see chapter 1).
A deviation from the TFL is measured using Eq. 2.6.

$$^{17}R_a/^{17}R_b = (1+k_{a,b})(^{17}R_a/^{17}R_b)^{0.528} \quad \text{(Eq. 2.6)}$$

The same deviation can be reported also in delta values, instead of in absolute ratios (Eq. 2.7).

$$1 + \frac{\delta^{17}O}{1000} = (1 + k_{a,b})(1 + \frac{\delta^{18}O}{1000})^{0.528} \quad \text{(Eq. 2.7)}$$

The most common standard material for the oxygen isotopic measurements is VSMOW. After isolating the term $(1+k_{a,b})$ from Eq. 2.7 and considering the logarithms of both sides, the deviation from the isotopic signature of a mass dependent process can be evaluated in terms of the capital delta (Eq. 2.8).

$$\Delta^{17}O = 1000k_{a,b} \approx 1000\ln(1 + k_{a,b}) = 1000\ln\left(1 + \frac{\delta^{17}O}{1000}\right) - 0.528 * 1000\ln(1 + \frac{\delta^{18}O}{1000})$$

(Eq. 2.8)

Eq. 2.8 made use of an approximation (Eq. 2.9) of the logarithm of (1+x).

$$\ln(1+x) = x + x^2/2 + x^3/3 + \ldots + x^n/n \qquad \text{for } x \ll 1 \qquad \text{(Eq. 2.9)}$$

The isotope anomaly can be calculated according to Eq.2.8 when assuming $x = k_{a,b}$ and neglecting all the terms of the series in Eq. 2.9 after the first one (Miller, 2002).
The same approximation of the function ln(1+x) in Eq. 2.9 is used for eliminating the two logarithms of the right-hand side of Eq 2.8 (Eq. 2.10).

$$\Delta^{17}O = 1000k_{a,b} \approx 1000\ln(1+k_{a,b}) \approx \delta^{17}O - 0.528\,\delta^{18}O \qquad \text{(Eq. 2.10)}$$

The second definition of the isotope anomaly (Eq. 2.10) is the most commonly used to represent the data in a three isotope plot.
Yet, when sample $\delta^{17}O$ and $\delta^{18}O$ have high absolute values, the calculation of the capital delta according to Eq. 2.10 would deviate from the isotope anomaly defined in Eq.2.8. because the condition in Eq.2.9 that $x \ll 1$ (with $x = \delta^{17}O$ and/or $x = \delta^{18}O$) is not met.
Consequently, the notation of $\Delta^{17}O$ using the logarithms will be preferred in this thesis for the calculation of the isotope anomaly.
Similarly to the oxygen raw delta values, the isotope anomaly from raw delta values is smaller by about the 20% compared to the isotope anomaly from calculated delta values (vs. VSMOW). Therefore, all the capital delta values relative to the tests discussed in the present chapter, which are reported as raw delta values, have to be increased by about the 20%, if the effects that are investigated have to be reported in the VSMOW scale.
There are at least two different ways to calculate the precision of the isotopic measurements.
The first one is the residual method: standard calculated values are compared with standard true values (last column in Table 2.1). The resulting standard deviation of the difference reported in the last column in Table 2.1 will indicate the precision of the isotopic measurements. When all the standards raw delta values of a run are considered, the calculated precision will include the effect of the daily shift.
The precision calculated with the second method is the average of all the standard deviations obtained from the calculated delta values of replicates. When using the second method, it is possible to take into account the precision of the isotopic measurements in the short term.
After comparing the results from both methods, the worst precision will be indicated, to show the uncertainties of that day of measurements.
In order to appreciate the quality of the data, it is necessary to draw attention to some potential artifact effects due to either the IRMS or the extraction line that could have an influence on the results. The strategy to tackle the various problems will be also indicated.
The memory effect is the most important problem. It affects the oxygen delta values only and occurs when samples measured during a run differ greatly in their isotopic composition. In a sequence that constitutes of two samples alternated in groups of 3-4 replicates, this effect is recognizable when the first one or two replicates of a sample show an isotopic composition that is closer to the previous sample. The reason of the effect on the oxygen delta values is not clear.

In fig. 2.2 the memory effect is shown by alternating measurements of 20ppm N_2O in N_2, with N_2O generated from nitrate with an electric discharge (to have a gas with a negative anomaly).

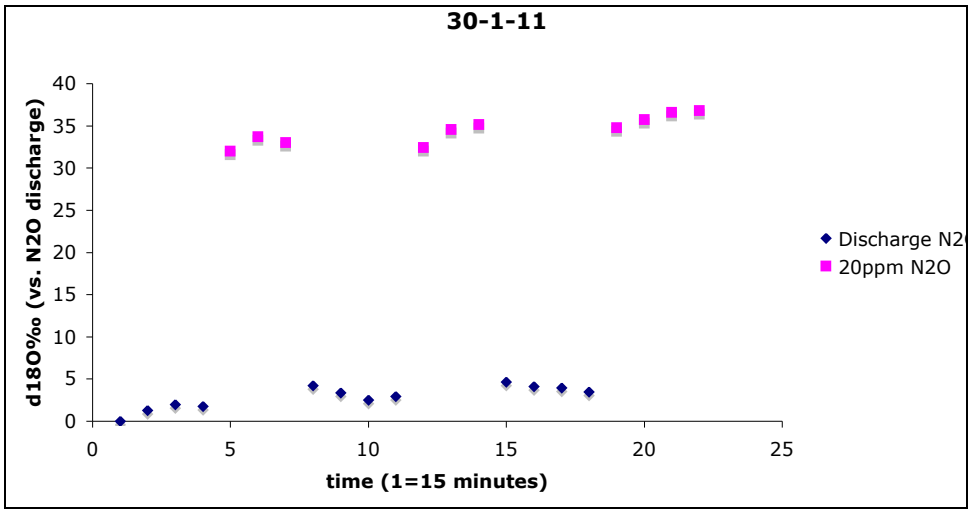

Fig. 2.2. *Illustration of the memory effect in $\delta^{18}O$ (vs. N_2O discharge) in N_2O discharge and 20ppm N_2O in N_2 run on 30/01/11.*

In fig. 2.2 the first one or two measurements of the 20ppm grouped in triplicates are more depleted in ^{18}O, similarly to the previously analyzed samples of N_2O discharge. On the other hand, the first one or two measurements of the N_2O discharge grouped in triplicates are more enriched in ^{18}O, similarly to the previously analyzed samples of 20 ppm.
The memory effect is usually of the order of 1-2‰ and would therefore affect the precision of measured oxygen delta values, if the data from all replicates are considered.
Consequently, to prevent artifacts due to the memory effect, all the samples whose results are discussed in Chapter 3 and 4 are measured in duplicates or triplicates and the data from the first replicate is discarded (standards are always measured in groups of triplicates and the average values is calculated by considering the last two measurements).
It has been found that increasing the sample size decreases the memory effect (data not shown). On the other hand, an increased sample size makes the peak separation between O_2 and N_2 worse, with the drawback that the choice of the timing of the integration window could affect the raw delta values (if the tale of the sample oxygen peak has to be cut, to be able to detect the sample nitrogen peak).
Unlike measured $\delta^{18}O$ and $\delta^{17}O$, the capital delta is a relatively stable signal that is not affected by the memory effect when the sample size is higher than 100 nanomoles.
Therefore, depending on sample availability and GC column performance, a range of 100-200 nmol nitrate has been found to be the most suitable for the samples whose results are discussed in Chapter 3 and 4.
Once the raw data have been corrected for the drift of the source, it is possible to identify that there is still a shift in the oxygen raw delta values. As an example, in

Table 2.1 the USGS35 raw $\delta^{17}O$ is 37.1‰ (vs. 20ppm) during the first measurement and 32.3‰ (vs. 20ppm) at the end of the run.
It is not clear whether the daily shift in the oxygen delta values is connected to the memory effect or not.
Some results (data not shown) might suggest that the shift in the oxygen delta values could be less important when the samples of a batch do not greatly differ each other for the isotopic composition. This would imply that the daily shift in the oxygen delta values might be a sort of a memory effect in the long term.
Generally the shift in the oxygen delta values is usually greater at the beginning of the run. As a result, to minimize the effect on the samples, a dozen vials of 20ppm N_2O are placed at the start of the run. During runs lasting more than 10 hours, the shift can become worse towards the end.
Sometimes this problem seems to be correlated with a ratio of N_2/O_2 that is variable during the run. The ratio N_2/O_2 is dependent upon the sample size, as is clear when comparing 20ppm N_2O (around 40nmol) with samples (100-200 nmol)(fig. 2.3 and fig. 2.4). A theoretical N_2/O_2 ratio of 2 is never reached. One suggested reason is that the IRMS ionization efficiency of molecular nitrogen is higher compared to molecular oxygen. This would result in a ratio N_2/O_2 that is higher than two.
However, this ratio is not always above the theoretical value (compare fig. 2.3 and fig. 2.4).

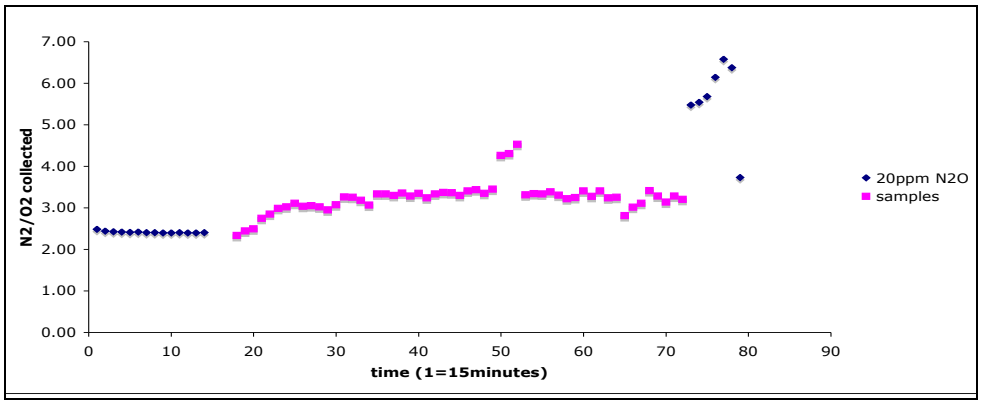

Fig. 2.3. *Sample ratio N_2/O_2 on 2/12/09.*

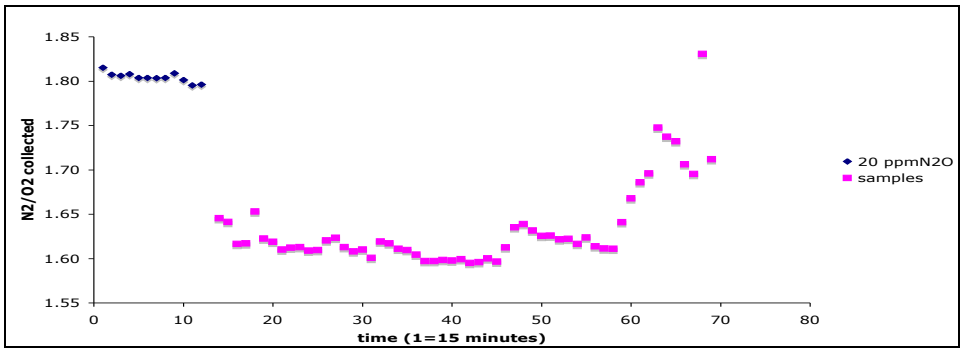

Fig. 2.4. *Sample ratio N_2/O_2 on 19/04/11.*

This finding might suggest that the ratio N_2/O_2 does not depends on the ionization efficiency only. Hence, there could be some unknown processes occurring during the passage of samples in the extraction line that would cause a change in the size of the nitrogen and/or the oxygen collected during a run. The partial loss of sample might generate an oxygen isotope fractionation that could be responsible for the oxygen daily shift.
Since the MIF signal in the standards is usually stable during the run (data not shown), it can be inferred that there are unknown processes during the online N_2O extraction and conversion causing a mass dependent fractionation.
The daily shift is probably dependent on unknown processes occurring in the furnace, since measurements of $\delta^{18}O$ and $\delta^{15}N$ with the same extraction line and IRMS are stable during the run.
It is possible that the problem depends on some conditions in the furnace that are not constant during the run. For instance, the temperature might change over time or there could be a species acting as a catalyst for a side reaction concerning the nitrous oxide decomposition whose concentration is increasing or decreasing during the run.
Tests on the sample total beam areas as a function of the temperature in the furnace and the carrier gas flow rate suggest that the nitrous oxide conversion is never complete (data not shown). The chance of an isotope fractionation changing with the degree of nitrous oxide thermal decomposition cannot be excluded a priori.
There is more than one possible reaction for the nitrous oxide decomposition at high temperature (Yang and Blasiak, 2005):

$$N_2O + O \Rightarrow N_2 + O_2 \quad \text{(R1)}$$

$$N_2O + O \Rightarrow NO + NO \quad \text{(R2)}$$

$$N_2O + H \Rightarrow NO + NH \quad \text{(R3)}$$

$$N_2O + H \Rightarrow N_2 + OH \quad \text{(R4)}$$

Experiments on the Arrehnius kinetic coefficients k, which is defined as:

$$k=Aexp(-E/RT)$$

gave a pre-exponential constant A of $1.4e^{12}$ and $2.9e^{13}$ and an activation energy E of 10.8 and 23.15 cal for R1 and R2, respectively (Yang and Blasiak, 2005). Therefore reaction R1 and R2 would have comparable reaction rates at a temperature of 800°C.
The nitric oxide produced during reaction R2 can be easily converted to N_2 and O_2 with the aid of the Au from the wall of the furnace as a catalyst (Kapteijn et al., 1996). Yet, it is possible that the degree of such a conversion might change over time and that this variation could impart a variable isotope effect on standards oxygen raw delta values (Table 2.1).
The presence of H in the furnace (which would support reactions R3 and R4) can be due to dissociated residual water coming from the extraction line or from the dissociated water that is the oxidation product of organic compounds. For instance any molecule of methane reaching the furnace can be oxidized to carbon monoxide, generating two molecules of water (R5):

$$CH_4 + 1.5O_2 \Rightarrow CO + 2H_2O \quad \text{(R5)}$$

The example of reaction R5 emphasizes the importance of having a good purification before sample decomposition. This is because reaction R5 can affect the quality of the measurements of samples oxygen delta values, due to the potential loss of the oxygen coming from the nitrous oxide decomposition.
The species OH can also be involved in nitrous oxide thermal decomposition (R6):

$$N_2O + OH \Rightarrow N_2 + HO_2 \qquad (R6)$$

$$NO + HO_2 \Rightarrow NO_2 + OH \qquad (R7)$$

Reaction R6 would again affect the samples oxygen delta values only. The reagent OH in reaction R6 can be regenerated with reaction R7, whose occurrence will be depending on reactions R2 and R3.
The presence of unreacted nitrous oxide and nitric oxide during the run has been detected (fig. 2.5 and fig. 2.6). However, because both species have a high retention time in the GC column that follows the furnace (see section 2.2 for the extraction line description), they tend to be concentrated in the capillary, reaching the IRMS about 12-16 hours after the start of the run.
Consequently, the signal of unreacted nitrous oxide will be detected as broad oscillations (fig 2.5).

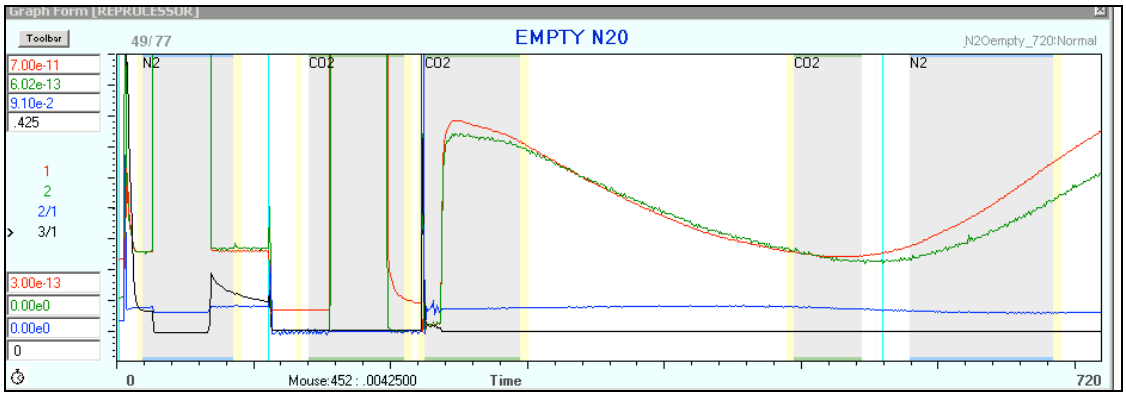

Fig. 2.5. *N_2O background after 49 measurements (12 hours after the start of the run).*

Nitric oxide is a molecule that easily breaks in the IRMS ionization chamber: a noisy signal will be seen few hours after the appearance of the nitrous oxide oscillations (fig 2.6).

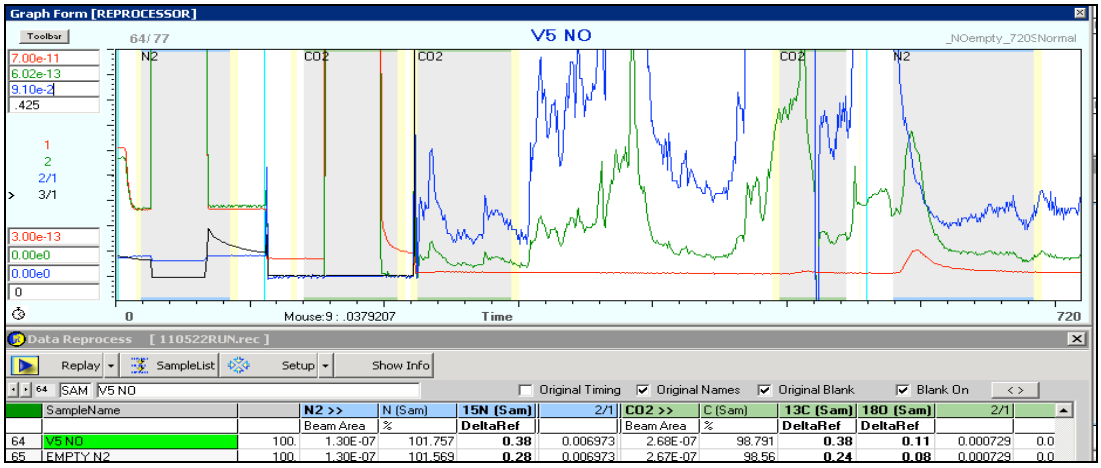

Fig. 2.6. *NO background after 64 measurements (16 hours after the start of the run).*

Thus, due to high retention time in the GC column, it is not possible to measure the change over time of N_2O and NO after each sample measurement (if there is any), in order to correlate it with the shift in the samples oxygen delta values.
Several other reactions can occur in the furnace, depending on the type of trace species not removed in the extraction line. Further studies should be carried out to understand which reaction could affect the nitrous oxide conversion to N_2 and O_2 and the possibility that a correlated change over time would generate an isotope effect in the oxygen formed by the nitrous oxide thermal decomposition.
As it was shown in Table 2.1, the daily shift generates a change in both the intercept and the slope of the calibration curve.
In theory it would be possible to take into account the change over time of the calibration curve by finding the functions $m(t)$ and $q(t)$, representing the change over time of the slope and the intercept of the calibration curve (Eq. 2.3).
Once $m(t)$ and $q(t)$ are known, the sample delta value measured at the time t_i will be calculated using $m(t_i)$ and $q(t_i)$ instead of the fixed parameter m and q of Eq. 2.3. This strategy sometimes improves the precision of the $\delta^{17}O$ and $\delta^{18}O$ data by up to 100%.
The daily shift in the oxygen delta values can be rather variable, lowering the precision of sample $\delta^{18}O$ and $\delta^{17}O$ to 2-4‰ (vs. VSMOW). In samples not highly fractionated, like the samples from the Marano Lagoon (Chapter 3), this variability would strongly affect the interpretations.
Unfortunately the assumptions of a linear or a logarithmic temporal trend with no inversion are not met at all times, and the precision when considering explicitly the oxygen daily shift is not always enough of an improvement to justify the strategy.
Consequently, due to the oxygen daily shift on measured delta values, no discussion of sample $\delta^{18}O$ and $\delta^{17}O$ will be undertaken and samples $\Delta^{17}O$ and $\delta^{15}N$ only will be considered.
Another issue to consider in assessing the data quality is the blank and the effect of the water oxygen exchange during nitrate bacterial conversion. Both effects are indirectly considered when calculating the calibration curve with the raw delta values of the standards.

It is theoretically possible to calculate the shift in the delta values due to both factors, if the magnitude and the isotopic composition of the blanks are known and we have knowledge of the water oxygen isotopic composition.
However, if some of the assumptions are not met, there is the chance of introducing an artifact. As a result, there is no general consensus on whether blanks and the water exchange has to be considered directly or not and data reduction protocols might differ among laboratories.
The strategy of correcting indirectly the sample delta values for the blanks and for the water oxygen exchange has been chosen for a number of reasons.
As explained in section 2.6, the sample size concerning the measurements discussed in Chapter 3 and Chapter 4 are 100 and 200 nanomoles respectively, apart from the case of few rare copper nitrate minerals.
The blank size is always below 5% of a 100nmol nitrate sample and usually it is less than 1%. Thus, making a blank correction does not change significantly the sample delta values.
Moreover, the size and the delta values of the blanks in a batch can be extremely variable so that defining an averaged size and an averaged isotopic composition might be meaningless for the purposes of data reduction.
As an example, in Table 2.2 the size of one blank is 5 times greater than the other two blanks of the same batch, with a difference in the capital delta of about 700‰ (vs. 20ppm).

	Size (μg of N)	**$\Delta^{17}O$ ‰ (vs. 20ppm)**	**$\delta^{15}N$ ‰ (vs. 20ppm)**
Blank	0.002	532	45
Blank	0.002	1260	81
Blank	0.102	497	32

Table 2.2. *Example of the size and the isotopic composition of the blanks of a batch*

This variation can be due to either a real blank variability, the effect of the background in the extraction line and/or the IRMS ionization chamber and it could also depend on the choice of the integration window of the signal. Moreover, it might be that the sample size (discussed in section 2.6) and the memory effect are significant for the capital delta if the sample size is smaller than 20nmol.
Before discussing further sample correction for the blank, it is important to point out how the size of blanks and samples measured with the IRMS will be reported and why it is meaningless to present the data concerning the total beam area detected by the IRMS in terms of nanomoles.
Firstly, not all the sample converted with the denitrifier method will reach the IRMS ionization chamber. Several tests (data not shown, see section 2.6 on the sample size effect) confirmed that there is a partial loss of sample in the extraction line.
The total beam area of the reference 20ppm is usually in the range $3x10^{-8}$-$6x10^{-08}$mA. The range of measured total beam area (in mA) will be variable not only due to the effective sample size, but also depending on the daily sensitivity of the IRMS.
It is assumed that the 20ppm vials contain around 40 nanomoles of N_2O because the total beam areas are usually the 35-45% of the total beam area of 100nmol of sample.

The total beam area of the reference 20ppm is also shown by default as 8μg of N. Consequently, the size of the following samples can be presented as total beam area (in mA), or as μg of N.
The sample size shown as μg of N will never be an accurate value, as it is calculated by the software that runs the IRMS by taking into account that the first signal in mA, from the reference 20ppm, is set equal to 8 μg of N, no matter what the effective size of the reference 20ppm is.
On the other hand, also the measurements of the sample size in mA are not accurate, being depending on the daily sensitivity of the IRMS and the variable loss of sample in the extraction line.
Because neither the total beam areas in mA nor the sample size in μg of N are accurate values of the number of sample nanomoles measured by the IRMS, the second option has been chosen (size in μg of N), to avoid making comparisons between small figures.
Even when the size is similar in each blank, the isotopic composition might be still variable. For instance, the data from the eight blanks of a batch (using bacteria from the same colony and grown in the same media bottle) are reported in Table 2.3.

	Size (μg of N)	**$\delta^{17}O$ ‰ (vs. 20ppm)**	**$\delta^{18}O$ ‰ (vs. 20ppm)**	**$\Delta^{17}O$ ‰ (vs. 20ppm)**	**$\delta^{15}N$ ‰ (vs. 20ppm)**
Blank	0.8	-12.6	-15.5	-4.4	-4.1
Blank	0.8	-8.3	-23.1	4.0	-3.4
Blank	0.7	-4.8	-22.6	7.3	-4.6
Blank	0.7	0.6	-26.8	15.1	-8.1
Blank	0.8	-18.9	-16.1	-10.4	-0.7
Blank	0.7	-23.8	-21.3	-12.6	-6.7
Blank	0.6	3.7	-24.5	17.0	-7.7
Blank	0.6	-10.3	-21.4	1.1	-5.0
stdev	**0.1**	**9.3**	**3.9**	**10.9**	**2.4**

Table 2.3. *Example of the size and the isotopic composition of the blanks of a batch*

The variability in blanks isotopic composition will limit the opportunity of correcting the sample delta values for the blank. This is because the calculation of sample delta values corrected for the blank requires the blank isotopic composition and the relative importance of the blank size compared to the sample size (the parameters δ_{blank} and b of Eq. 2.11, respectively).

$$\delta_{sample\ corr} = a\delta_{sample} + b\delta_{blank} \quad \text{(Eq.2.11)}$$

The parameters a and b in Eq. 2.11 meet the following conditions:

b=(blank size/sample size); a= (1-b).

Eq. 2.11 implies that corrections for blanks with an isotope composition similar to the sample isotopic composition will be minimal even if the blank size is higher than 5% the sample size. Yet, if the standard deviation of blanks delta values is too high, the samples correction for the blanks become meaningless.
Blanks are therefore analysed mainly to ensure that the size is below the 5% of the sample size. If it is not, another batch of the same group of samples will be prepared with the denitrifier method and analyzed, until a blank lower than 5% of the sample size is obtained.
During bacterial nitrate conversion, an isotope exchange between water and the intermediates of denitrification causes an isotope fractionation in the nitrous oxide (Casciotti. 2002). *Pseudomonas aureofaciences* is usually preferred to *Pseudomonas chlorofaciens* for the denitrifier method due to the lower magnitude of the effect.
It could be possible to calculate the shift in sample measured oxygen delta values due to the water isotope exchange, provided that the water isotope composition is known.
The isotopic composition of local water used for preparing the NFM (nitrate free media) is known. However, the 2ml of NFM with resuspended bacteria can be from almost 100% to 16% of the water in a vial prepared for the isotopic measurements with the denitrifier method, depending on sample injection volume. This is because the maximum sample volume injection allowed is 10 ml.
In this circumstance the sample water, whose isotopic composition is usually unknown, will be the 84% of total water in the vial (12 ml, of which 2ml of NFM).
Furthermore, calculating the water exchange implies that the fractionation factor associated with the isotope exchange is known.
Because the lack of genetic mutation within the fifth generation from the stock colonies (that are stored at -76°C) can never be guaranteed, it is safer not to make any assumption on the magnitude of the water exchange and the relative isotope effect on converted nitrate, as they might change due to the occurrence of a genetic mutation.
There is some evidence that the fractionation during nitrate conversion might be colony-dependent. On 15/3/11, the standards USGS34 and USGS35 were converted to nitrous oxide by using bacteria from two different colonies of the same agar plate (Table 2.4).

Colony ID	**Standard**	**$\delta^{15}N$ ‰ (vs. 20ppm N_2O)**
1	USGS34	-1.1
1	USGS34	-1.1
1	USGS34	-1.1
2	USGS34	-3.4
2	USGS34	-3.5
2	USGS34	-3.5
1	USGS35	4.0
1	USGS35	3.9
1	USGS35	3.8
2	USGS35	1.0
2	USGS35	0.9
2	USGS35	1.0

Table 2.4. *Standards nitrogen isotope composition measured with the denitrifier method and using two different colonies from the same agar plate*

The results shown in Table 2.4 would suggest that there is an isotope effect in the nitrogen delta values that could be colony-dependent. Interestingly, the relative difference between the two standards nitrogen delta values is roughly the same in both colonies.
As a final comparison, Table 2.5 shows the difference in the calculated delta values of samples from the Marano lagoon, when the correction for the blank and the water isotope exchange is made directly or indirectly.

Sample ID	**$\Delta^{17}O$ ‰ (vs. VSMOW) shift (dir-indir)**	**$\delta^{15}N$‰ (vs. AIR) shift (dir-indir)**	**Date analyses**
42	0.2	-0.1	2/7/10
43	0.1	-0.1	2/7/10
45	0.1	-0.1	2/7/10
46	0.5	0.0	2/7/10
47	0.1	-2.9	2/7/10
48	0.1	0.0	2/7/10
49	0.1	-0.1	2/7/10
50	0.2	-0.1	2/7/10
51	0.1	-2.4	2/7/10
52	0.2	-1.5	2/7/10
average	**0.2**	**-0.7**	
stdev	**0.1**	**1.1**	
69	-0.2	-0.4	30/7/10
71	-0.2	-0.6	30/7/10
81	-0.2	-0.6	30/7/10
82	-0.1	-0.6	30/7/10
83	-0.2	-0.6	30/7/10
85	0.1	-0.6	30/7/10
86	-0.2	-0.6	30/7/10
87	-1.0	-0.6	30/7/10
88	-0.2	-0.5	30/7/10
91	-0.1	-0.5	30/7/10
93	-0.3	-0.5	30/7/10
95	-0.2	-0.5	30/7/10
96	-0.2	-0.5	30/7/10
97	-0.2	-0.5	30/7/10
99	-0.2	-0.6	30/7/10
100	-0.1	-0.6	30/7/10
average	**-0.2**	**-0.5**	
stdev	**0.2**	**0.1**	

Table 2.5. *Sample calculated delta values difference when correction for the blanks and the water isotope exchange is directly or indirectly considered.*

The results in Table 2.5 would suggest that a direct correction for the blanks and the water isotope exchange generates a small shift (0.2‰ vs. VSMOW on average) in sample oxygen calculated delta values compared to when both effects are indirectly taken into account through the calculation of the calibration curve.
The difference in the nitrogen delta values after direct blank correction with the delta values that do not explicitly take into account the size and the isotopic composition of measured blanks is more relevant (Table 2.5) and comparable with the least overall uncertainty in sample $\delta^{15}N$ (which is 0.3‰ vs. AIR, as it is calculated after results in Table 2.6).
It is important to point out that the sample size effects (discussed in section 2.6) on sample delta values is more important when the total beam area is small. This problem could therefore generate an artifact in the blank isotopic composition, but not in sample delta values. Furthermore, the memory effect will strongly affect the oxygen isotopic composition of blanks, because the effect is more important with decreasing size. For this reason, the indirect correction for the blanks by calculating the slope *m* and the intercept *q* of the calibration curve is chosen before reporting the measurements discussed in Chapter 3 and 4.
Based on the comparison of samples measured on different days, the variability among days has been calculated. Table 2.6 shows the capital delta and the nitrogen delta values of four samples from the laboratory tests on the nitrate MIF change during the liquid-gas transition (Chapter 4) that have been analyzed in three or four batches (always in duplicates).

Sample ID	**$\Delta^{17}O$ ‰ (vs. VSMOW)**	**Stdev**	**$\delta^{15}N$ ‰ (vs. AIR)**	**Stdev**	**Date**
35T 3D	17.5	0.2	1.0	0.2	21/3/11
35T 3D	17.2	0.8	1.1	0.1	24/3/11
35T 3D	17.2	0.6	0.9	0.2	19/4/11
35B 3D	16.5	0.2	1.1	0.2	21/3/11
35B 3D	17.4	0.8	1.0	0.1	24/3/11
35B 3D	17.1	0.5	0.2	0.1	16/4/11
35B 3D	17.5	0.6	0.8	0.2	19/4/11
45T 24H	18.2	0.2	1.2	0.2	21/3/11
45T 24H	17.2	0.5	-0.4	0.1	16/4/11
45T 24H	17.5	0.6	1.4	0.2	19/4/11
45P 24H	17.1	0.8	0.9	0.1	24/3/11
45P 24H	17.3	0.5	0.8	0.1	16/4/11
45P 24H	17.0	0.6	1.0	0.2	19/4/11

Table 2.6. *Comparison of sample calculated delta values from different batches.*

The oxygen delta values in Table 2.6 seem less precise, but more accurate that the nitrogen delta values, since the samples $\delta^{15}N$ that have been analyzed on the 16/4/11 are lower than expected by about 1(vs. AIR) in most cases.
When considering a wider data set consisting of 14 different samples that have been analyzed in two, three or four different batches (50 measurements in total), and after discarding two data, the precision of the capital delta considering the measurements variability among days is 0.35‰ (vs. VSMOW).
After rejecting the nitrogen delta values that have been analyzed on the 16/4/11, the overall precision of $\delta^{15}N$ is 0.3‰ (vs. AIR) (if those measurements are taken into account, the averaged standard deviation is doubled).
It might be possible that on the 16/04/11 an unusual effect shifted the nitrogen delta values by about 1‰. Therefore, to take into account the variability among days of measurements, the precision for the measurements of $\Delta^{17}O$ and $\delta^{15}N$ will never be below 0.4‰ and 0.3‰ respectively.

2.4 Salinity

The effect of salinity during bacterial nitrate conversion has been tested, to verify that the isotopic measurements of saline, brackish and freshwater samples from the Marano lagoon (discussed in Chapter 3) are effectively comparable when using the denitrifier method.
To mimic the ionic strength of seawater and to assess at the same time that no interference during bacterial conversion occurs owing to the presence of the two major ions in saline waters, Cl^- and Na^+, NaCl solutions were prepared and added to vials before sample injections.
The two ions contribute for more than the 85% salinity of average seawater. Taking into account that the sodium chloride content in average seawater is 35g/L, the effect of salinity on the isotopic measurements with the denitrifier method when the NaCl concentration range spans from 17.5 to 70g/L has been tested.
Several NaCl solutions have been prepared and added to the 2ml NFM (nitrate free media) containing bacteria, in order to obtain different salinities within the same volume of 3ml (2ml of NFM+1ml of appropriate NaCl solution). This precaution has been taken to avoid the chance of interferences due to any volume effect. Moreover, all NaCl solutions have been added to blanks in triplicates, to check that the blank size is not increasing with the salinity.
Because commercial sodium chloride always contains some nitrate content, the NaCl solutions have been added to the 2ml bacteria suspended in NFM after the first purge with helium. Therefore the nitrate in commercial NaCl is assumed to be converted to nitrous oxide and removed by the end of the second purge with helium. The nitrate standards USGS34 and USGS35 injected amount to 150nmol (Table 2.7).

Standard	1ml NaCl (g/L)	Sample size (nmol)	$\delta^{15}N$ ‰ (vs. 20ppm)	$\Delta^{17}O$ ‰ (vs. 20ppm)
USGS34	//	150	-1.9	-3.8
USGS35	//	150	3.1	15.2
USGS34	70	150	-1.8	-3.6
USGS34	70	150	-1.6	-3.5
USGS35	70	150	3.0	15.4
USGS35	70	150	2.9	15.7
USGS34	35	150	-1.7	-3.7
USGS34	35	150	2.9	15.1
USGS35	35	150	3.0	
USGS34	17.5	150	-1.9	-3.7
USGS34	17.5	150	-1.8	
USGS35	17.5	150	2.5	15.4
USGS35	17.5	150	2.7	15.0

Table 2.7. *Nitrate standards delta values (vs. 20ppm) in water with a salinity ranging from 0-70g/L NaCl*

The difference between delta values among all samples is within the range of the uncertainties due to IRMS measurements for both nitrogen and oxygen.
Furthermore, all blanks are similar in size and the variability of their isotopic composition is high regardless the salinity (Table 2.8).

Salinity (g/L NaCl)	Size (µg of N)	$\Delta^{17}O$ ‰ (vs. 20ppm)	$\delta^{15}N$ ‰ (vs. 20ppm)
//	0.01	-55.52	17.9
//	0.06	-31.37	9.6
//	0.02	-284.55	9.3
70	0.01	103.87	60.1
70	0.01	-250.61	69.2
70	0.01	-356.07	61.8
35	0.03	65.39	38.7
35	0.03	170.69	40.1
35	0.00	140.29	54.9
17.5	0.03	-188.86	42.3
17.5	0.02	-424.92	48.0
17.5	0.01	-169.30	53.6

Table 2.8. *Size and isotopic composition of blanks in water with a salinity ranging from 0-70g/L NaCl.*

An increasing trend can be found in the blank nitrogen delta values as a function of salinity (fig. 2.7).

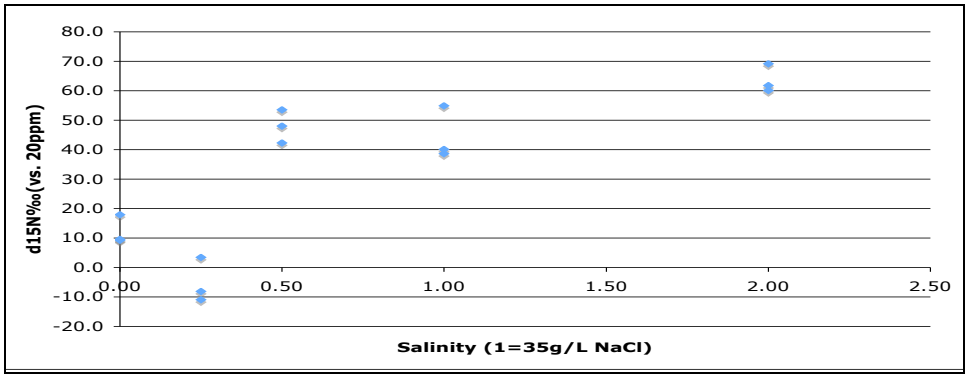

Fig. 2.7. *Blank δ^{15}N‰(vs. 20ppm) in water with a salinity ranging from 0-70g/L NaCl.*

However, because the blank size is usually below 1% of the signal of a sample with a size of 100nmol nitrate, such a trend has a very small effect on sample nitrogen delta values.
A second short experiment has been carried out using the standard USGS34 only with a size of 20nmol, to test that salinity causes no effect also at a lower sample size.
When the sample size is below 50nmol, the precision of the method that includes the N_2O conversion in the gold furnace is rather low. Consequently, no thermal decomposition in the gold furnace has been carried out and nitrous oxide $\delta^{18}O$ and $\delta^{15}N$ only have been measured.
The second experiment confirmed that there is no effect of salinity on the nitrate isotopic measurements with the denitrifier method, even when using the lowest sample size possible (Table 2.9).

Standard	**NaCl (g/L)**	**Sample size (nmol)**	**δ^{15}N ‰ (vs. 20ppm)**	**δ^{18}O ‰ (vs. 20ppm)**
USGS34	//	20	-4.5	-27.5
USGS34	70	20	-4.1	-27.8
USGS34	17.5	20	-4.3	-27.8

Table 2.9. *Size and isotopic composition of the nitrate standard USGS34 in water with a salinity ranging from 0-70g/L NaCl.*

Thus, there is no effect of salinity on the precision of both oxygen and nitrogen isotope measurements when using the denitrifier method. Moreover, there is no systematic effect on accuracy, which makes possible the comparison of the isotopic measurements of saline, brackish and freshwater samples of the Marano lagoon.

2.5 Volume effect

It is known that there is an effect of vials headspace on the nitrate isotope measurements with the denitrifier method (Sigman et al., 2001).
The occurrence of a headspace effect has to take into account when measuring a group of samples with different nitrate concentrations in the same batch. For this

reason, the data coming from the Marano lagoon, discussed in Chapter 3, might be particularly affected.
It is important to mention that there is certainly a volume effect because of the water isotope exchange during microbial conversion. The species *Pseudomonas aureofaciens* is usually preferred to *Pseudomonas chlorofaciens* owing to the lower isotope exchange effect (Granger et al., 2008).
As it was pointed out when discussing the data reduction issues, theoretically the isotope water exchange can be calculated, provided the oxygen isotope composition of water samples is known. Unfortunately, we don't have any data for the Marano lagoon oxygen water samples.
Thus, when sample volume injections are comparable or higher than the 2ml resuspended bacteria in NFM, the contribution of water samples could become important.
Another potential volume effect can occur due to the nitrous oxide extraction efficiency of the Gilson auto-sampler.
It is widely accepted that there is an N_2O partitioning between the liquid and the gas phase (Weiss and Price, 1980). This partitioning will generate an isotope fractionation that is depending on the volumes of each phase.
Ideally, if all the nitrous oxide is extracted from vials, such a partitioning will not affect the measurements. The needle of the Gilson auto-sampler has been designed to collect the nitrous oxide of both phases but a higher efficiency is expected for the sample in the gas phase, because of the higher mobility of species in such a physical state.
High helium flow rates are necessary to stir well the liquid phase and to increase the N_2O mobility in water. Long purging time could also help to minimize the amount of nitrous oxide left in the vial. However, if the purging time lasts for too long, most of the extracted nitrous oxide would stay in the liquid nitrogen trap for a longer time (see section 2.2), and the chance of a temperature gradient changing over time will cause an isotope fractionation that varies over time. This occurrence will lower the benefits of an improved nitrous oxide extraction from the vials.
If extraction efficiency is the main reason of the volume effect in our data sets, a solution can be easily found: it would be sufficient to add the appropriate aliquot of MQ to vials before sample injection, in order to get the same volume and the same sample size in each vial of a batch. If this is the chosen strategy, it is important to verify first that the nitrate content in MQ is effectively below the IRMS detection limit.
It is therefore necessary to assess what is the magnitude of the effect of vials headspace on the nitrate isotopic measurements and trying to understand its main reason.
The effect of the addition of MQ in the range 0.1-10ml to the 2ml bacteria suspended in NFM before injection of nitrate standards has been tested. Blanks with added MQ (from 0.1 to 10ml) have also been prepared and analyzed in triplicates.
The water was added immediately before the 100nmol injections of the standards USGS34 and USGS35, as it is assumed that MQ would contain nitrate below the detection limit. However, if the nitrate content in MQ is above the IRMS detection limit, the size and the delta values of blanks will be affected by the addition of MQ, and the uncertainties due to dilution with MQ can be assessed and compared with the volume effect.
Because MQ is used for preparing both the NFM and the nitrate standard solutions, no change in the measured delta values due to the water isotope exchange is expected.

An increasing trend with the addition of MQ has been found in the standards nitrogen delta values only (fig. 2.8).

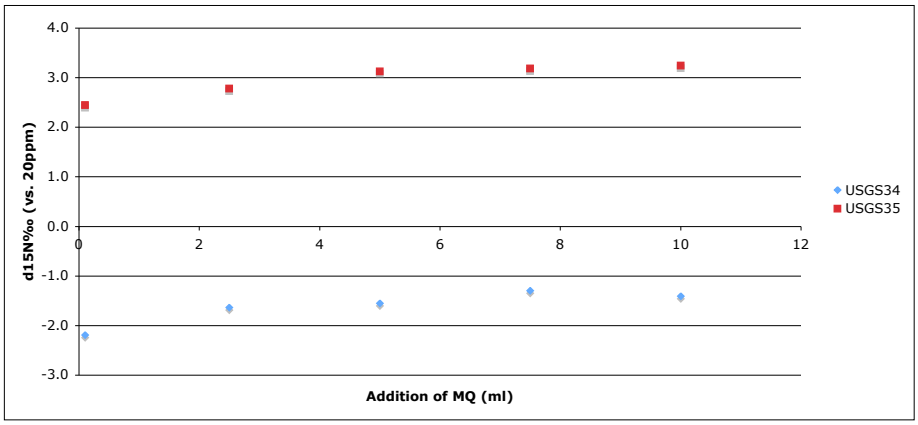

Fig. 2.8. *$\delta^{15}N$‰(vs. 20ppm) in the standards USGS34 and USGS35 in vials where MQ addition ranged from 0.1-10 ml.*

Every data point in fig. 2.8 represents the average delta values obtained from triplicates. The volume effect in the range 0.1-10ml addition of MQ for the nitrogen delta values proved to be below 1‰ for both standards.
During this test, no clear dependence of the addition of MQ on the standards total beam area has been found (fig. 2.9).

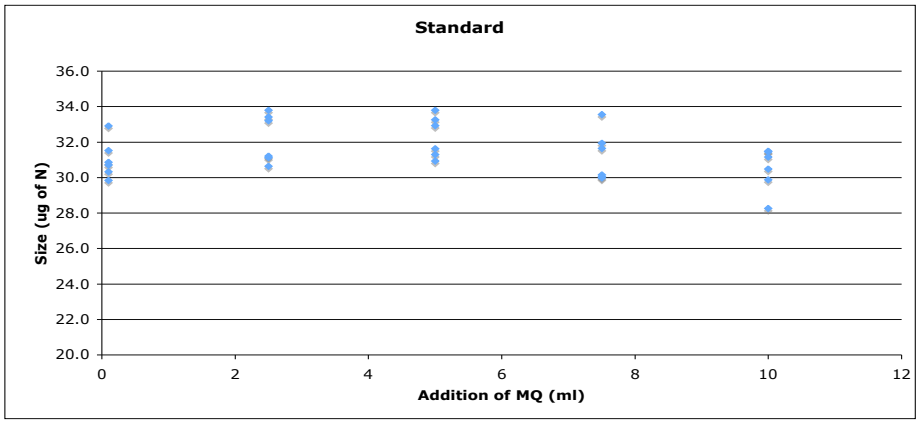

Fig. 2.9. *Standards size (μg of N) in vials where MQ addition ranged from 0.1-10 ml.*

A comparison of the results in fig. 2.8 and fig. 2.9 would suggest that the needle extraction efficiency cannot be responsible for the trend in sample nitrogen delta values. This is because the difference in the total beam area of samples with 0.1ml and 10ml of added MQ is minimal, whilst the difference in their nitrogen delta values is the greatest. Thus, the volume effect should not be related to the nitrous oxide partitioning between the two phases in the vials.
The dilution with MQ has been found to have an effect on the size of blanks (fig. 2.10).

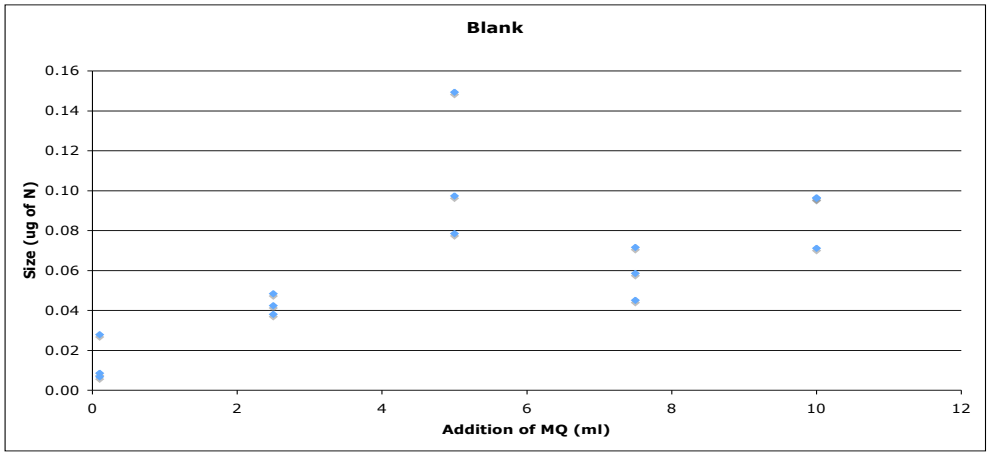

Fig. 2.10. *Blank size (μg of N) in vials where MQ addition ranged from 0.1-10 ml.*

When rejecting the data concerning the 5ml addition of MQ in blanks (fig. 2.10), a trend in the blank size with a high Pearson coefficient of 0.82 is found. Such a trend would suggest that the nitrate content in MQ is not below the detection limit of the IRMS.
Eq. 2.12 indicates the measured linear trend in blank total beam areas associated with the volume effect (excluding the data points of 5ml addition of MQ).

Blank total beam area= 0.0065*(ml of MQ) +0.018 (Eq. 2.12)

The intercept of the linear trend would indicate the blank size when no MQ is added. The slope of the linear trend would suggest that the blank size increases by 36% per each ml of MQ added to vials.
In this particular batch, the blank size when no MQ is added is the 0.05% of 100nmol of nitrate standard with no addition of MQ (always considering averaged values from the analyzed triplicates). According to the results shown in fig. 2.10, when 10ml of MQ is added to vials, the blank size becomes the 0.18% of 100nmol of nitrate that has an addition of 10ml of MQ.
This blank contribution on samples size is still very small and it is plausible to assume that it will not have a measurable effect on sample delta values. Therefore, the nitrate content due to the addition of MQ should not be responsible for the trend in samples nitrogen delta values.
It is possible that another nitrogen containing species present in the MQ added to vials might be responsible for a nitrogen isotope exchange during the nitrate bacterial conversion. However, blank nitrogen delta values show a dependence on the addition of MQ only above 5ml (fig. 2.11).

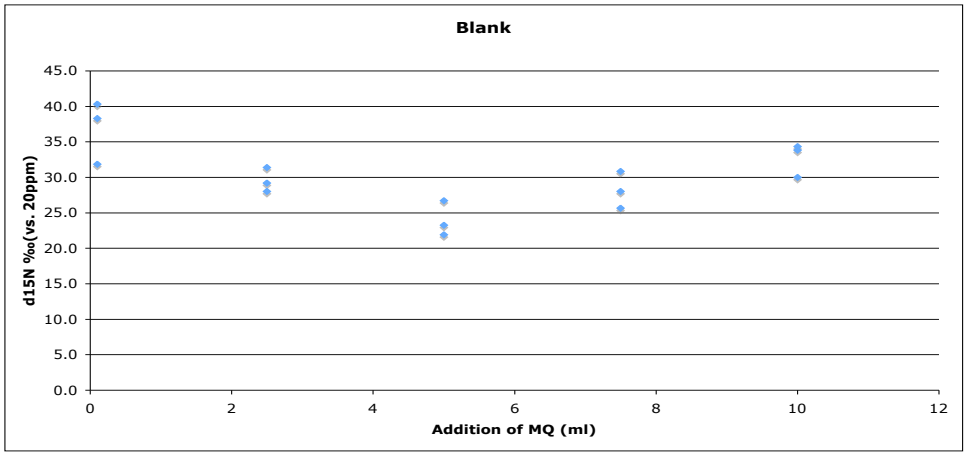

Fig. 2.11. *Blank δ^{15}N‰(vs. 20ppm) in vials where MQ addition ranged from 0.1-10 ml.*

Results in fig. 2.11 would neither confirm nor reject the hypothesis of a nitrogen containing species in MQ affecting samples nitrogen delta values.
To confirm the results presented so far, another test on the volume effect followed. The standard USGS34 only with a size of 50nmol has been used, to minimize any memory effect (section 2.2) and to verify that decreasing the sample size will not increase the magnitude of the effect on the nitrogen delta values.
To remove any interference due to daily shifts (section 2.2), the samples with the highest difference (addition of 0.1 and 10ml MQ) were placed at the start of the run.
The second test confirmed that there is a volume effect in the nitrogen delta values only. The shift is reasonably low in the range 0.1-5ml and below 0.2‰ in the range 5-10ml of addition of MQ (fig. 2.12).

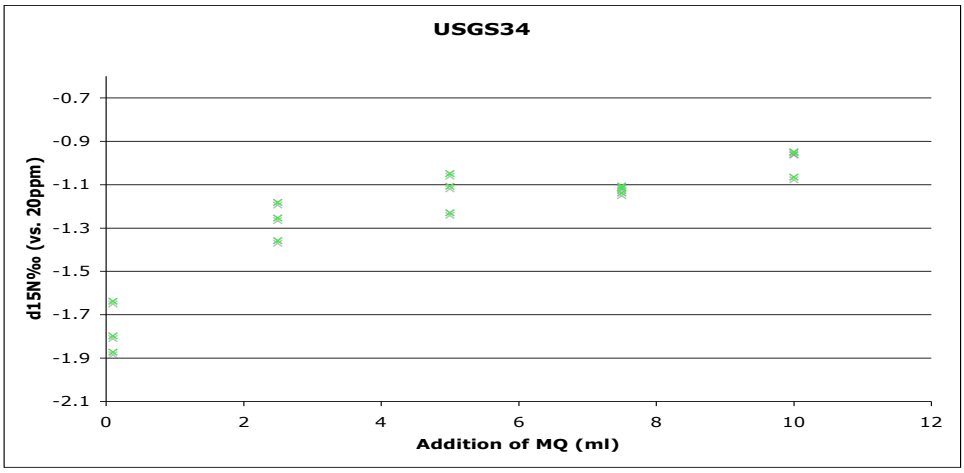

Fig. 2.12. *USGS34 δ^{15}N‰(vs. 20ppm) in vials where MQ addition ranged from 0.1-10 ml*

By contrast to the finding from the previous test (fig. 2.9), the nitrous oxide extraction efficiency clearly seems to decrease with the addition of MQ (fig. 2.13).

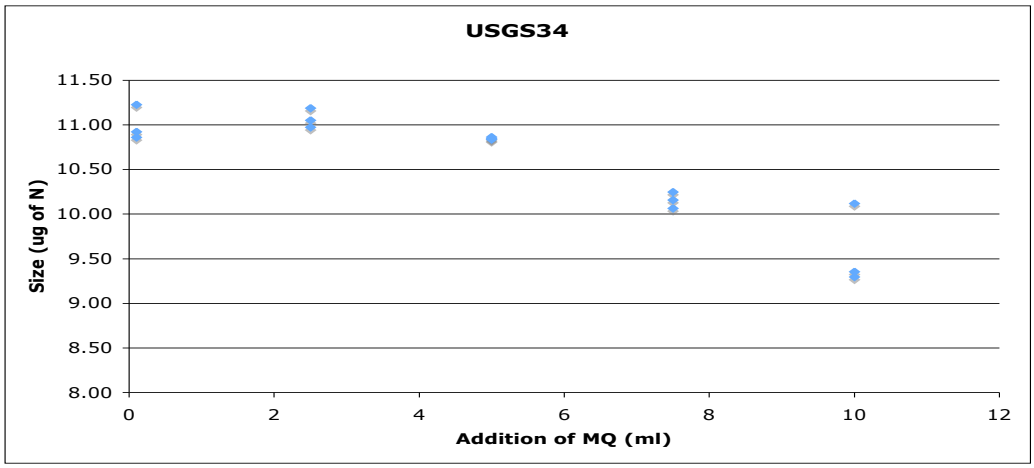

Fig. 2.13. *USGS34 size (µg of N) in vials where MQ addition ranged from 0.1-10 ml.*

However, the trend in the nitrogen delta values due to the addition of MQ is higher when the trend in the standard total beam areas due to the addition of MQ is minimal (compare fig. 2.12 and fig. 2.13). Thus, the results from both charts would suggest that no significant isotope fractionation is coupled with problems related to the needle extraction efficiency.
Another difference with the first test on the volume effect is that the size of blanks does not seem to be affected by the addition of MQ (fig. 2.14), suggesting no presence of nitrate or nitrite in MQ.
Therefore blanks in this test mainly derive from the expulsion of nitrous oxide from bacterial cells after NaOH injections (Casciotti et al., 2002).

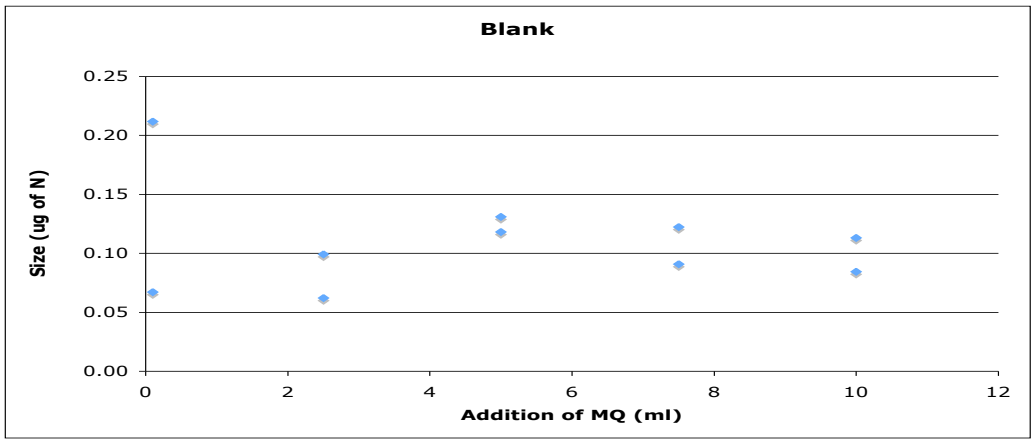

Fig. 2.14. *Blanks size (µg of N) in vials where MQ addition ranged from 0.1-10 ml.*

Unlike sample nitrogen delta values, blanks nitrogen delta values show again no trend with the increasing addition of MQ (data not shown).
The volume effect in blanks was discussed in the first article on the denitrifier method (Sigman et al., 2001) (fig. 2.15), when the blank size as a function of the addition of

nitrate free water was tested for two different types of water (deionized water and Sargasso Sea water).

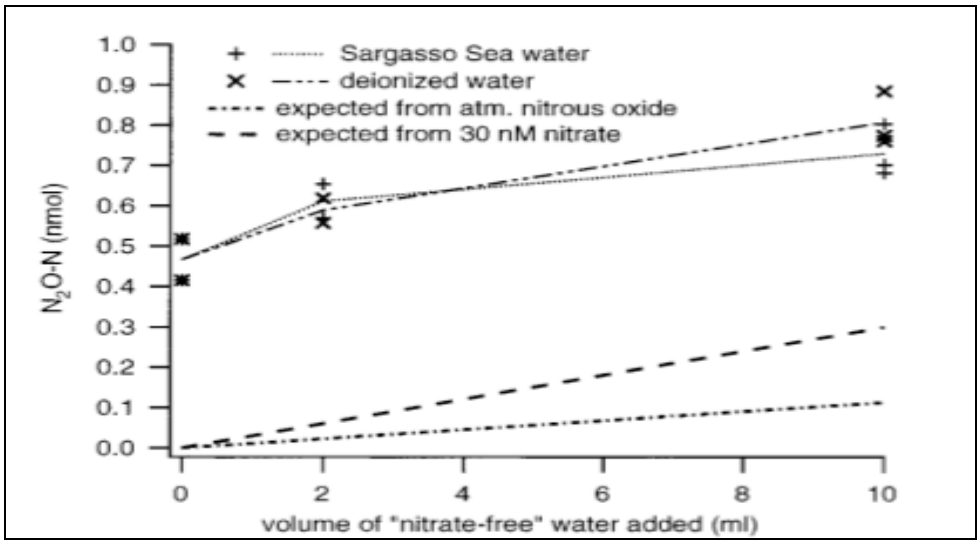

Fig. 2.15. *Blank size (nmol) as a function of the volume of nitrate-free water added (ml), from Sigman et al., 2001.*

No mention of an isotope effect in the measured delta values has been made by the authors.
To sum up, both the presence of some nitrate or nitrite in MQ and a worse needle extraction efficiency have been found only once during the two tests on the volume effects. However, both factors would not explain the volume effect that has been found in both tests. Thus, the reason of a shift in the sample nitrogen delta values due to MQ addition is still unclear.
Overall, the volume effect on the nitrogen delta values as it is measured during both tests is not so important compared to other effects like the sample size, beings about 0.8‰ in the volume range 0.1-10ml addition of MQ.
In order to minimize any artifacts on the nitrogen delta values due to differences in the sample volume injections, samples will be grouped in batches that have the smallest nitrate concentration range. Sample will be therefore measured without the need for dilutions with MQ.

2.6 Sample size

The total beam areas of the samples of a batch with the same concentrations often differ from each other by 10% or more (see fig. 2.9). One reason is the difficulty of injecting small volumes of sample (when the nitrate concentration of a sample is particularly high) or if the reported nitrate concentrations are not accurate enough compared to the resolution of the sample size measurements with the IRMS.
Some tests have been undertaken to study the chance of a sample size effect on both the isotope anomaly and the nitrogen delta values by considering the range 40-200 nmol of nitrate injected.

It was found that there is a large increasing trend in both $\delta^{18}O$ (fig. 2.16) and $\delta^{17}O$ (data not shown) with the increasing size in all the standards considered.

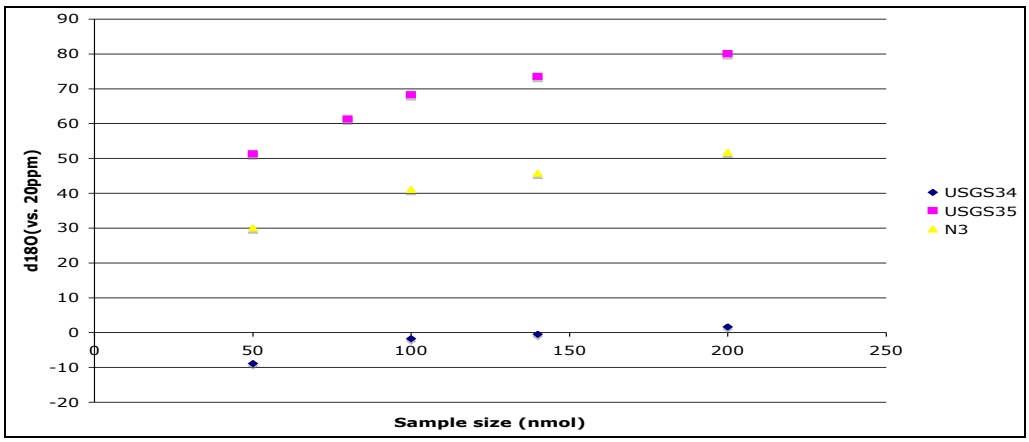

Fig. 2.16. *Standards $\delta^{18}O$‰(vs. 20ppm) as a function of a sample size ranging from 50 to 200 nmol.*

Yet, no change in the capital delta with the sample size has been found in both the standards USGS34 and N3, whereas there is an increasing trend in the isotope anomaly of the standard USGS35 (fig. 2.17).

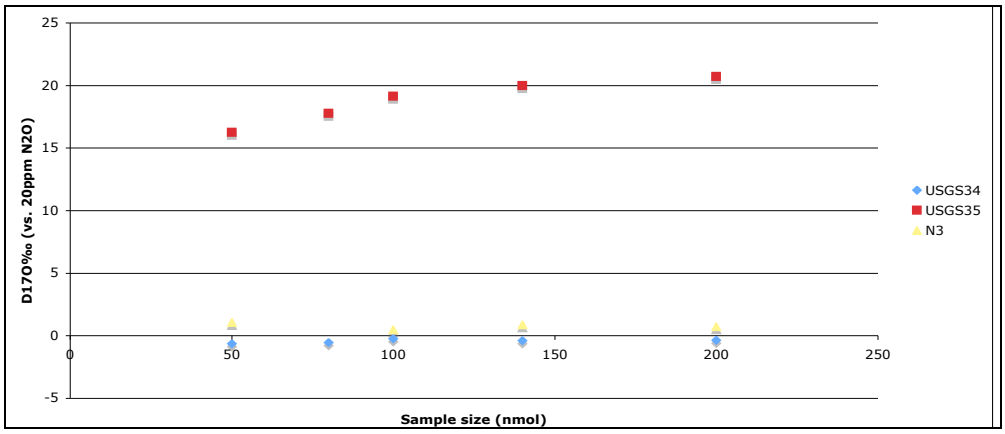

Fig. 2.17. *Standards $\Delta^{17}O$‰(vs. 20ppm) as a function of a size ranging from 50 to 200 nmol.*

It is worth noting that the standards USGS34 and N3 are both potassium nitrate salts that have an isotope anomaly of zero. The former is prepared by equilibrating reagent-grade HNO_3 with Antarctic snow-melt water (Bholke et al., 2003), whereas the IAEA-N3 is a dried salt prepared by A. Mariotti between 1983 and 1985. The standard USGS35 is made from chilean nitratine ($NaNO_3$) and has a MIF signature of 21.1‰ versus VSMOW (Bohlke et al., 2003). Therefore the effect of the sample size on the MIF signature depends on the sample isotopic composition.
When the sample size is larger then 100 nmol, the increasing trend of the isotope anomaly with the sample size becomes small. Over a threshold of 200 nmol, the standard USGS35 has a capital delta value of 21‰ (versus 20ppm), which

approximates to the true reported delta value against the standard VSMOW (Bohlke et al, 2003).
Consequently, in case of a sample size of more than 200 nanomoles, there might be no compression of the scale of the capital delta (which is usually around the 20%, as it was discussed in the section 2.3) and the calibration curve has the ideal slope of 1.
By contrast to the oxygen delta values, the sample size effect generates a decreasing trend in the $\delta^{15}N$ of all the standards, with the largest effect being observed in the standard USGS34 (fig. 2.18) when the sample size is larger than 100nmol.

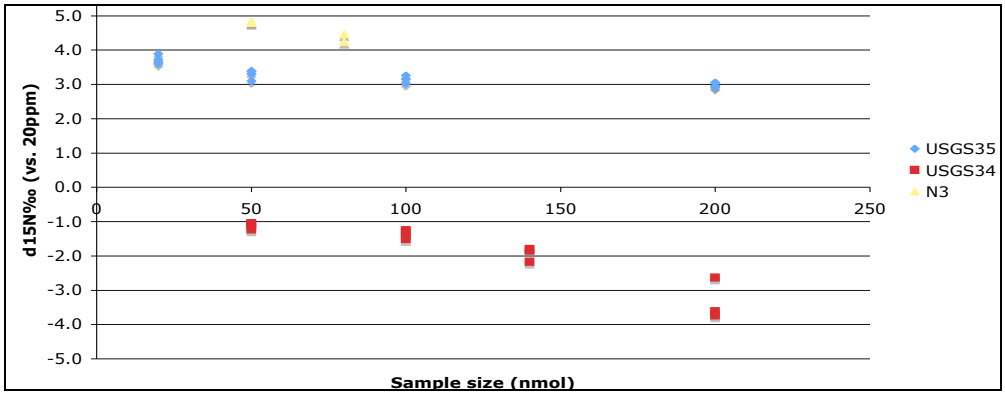

Fig. 2.18. *Standards $\delta^{15}N$‰(vs. 20ppm) as a function of a size, ranging from 50 to 200 nmol.*

It is likely that there is not a single factor causing the sample size effect. This is because it has been found that the magnitude of the sample size effect is variable, depending on days of measurements.
It is known that the ionization efficiency of the IRMS is higher for the nitrogen than for the oxygen, resulting in a ratio N_2/O_2 that is higher the theoretical value of two (section 2.3). The ratio N_2/O_2 depends on the sample size (fig. 2.19).

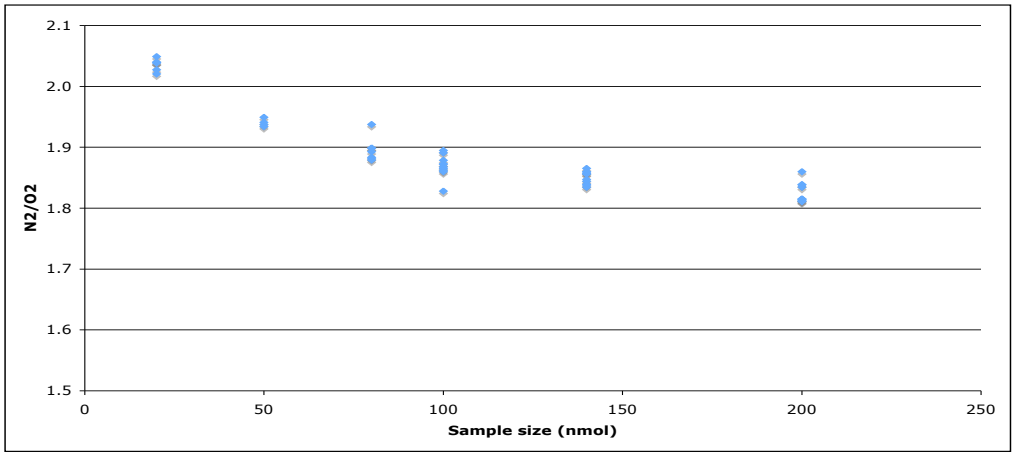

Fig. 2.19. *Standard ratio N_2/O_2 when the size is ranging from 50 to 200 nmol.*

As discussed in section 2.2, the sample ratio N_2/O_2 analyzed by the mass spectrometer can be below or above the theoretical value of two, depending on days of run (fig. 2.2

and fig. 2.3). Consequently, the deviation from the theoretical value cannot always be attributed only to the ionization efficiency in the IRMS.
Another potential explanation for the measured effect of the sample size on the isotopic measurements is that any partial loss of sample in the extraction line that causes an isotope fractionation is likely to be a process that is size-dependent.
This is due to the fact that, if there is any isotope effect in the extraction line, because there is likely not enough time for the fractionating sample to reach the condition of equilibrium, the isotopic fractionation will probably follow the Rayleigh equation.
The isotopic ratio R of a species with an initial isotopic ratio R_0 that is fractionated in an open system can be calculated at any time by using the Rayleigh equation (Eq. 2.13)(Ono et al., 2006).

$$1000*\ln(R/R_0)= \varepsilon_{Rayleigh} \ln(f) \qquad \text{(Eq. 2.13)}$$

The parameter $\varepsilon_{Rayleigh}$ is the isotope enrichment, whereas f is the fraction of species left in the system ($f=C/C_0$ where C and C_0 are the final and the initial concentration).
Consequently, depending on the time lapse after which an isotope fractionation is interrupted (for instance due to the switching of a valve or for a sudden change in the temperature), there will be a distinctive isotopic composition in both the fraction of species trapped and the one removed from the system.
The concentration of the species removed from the system will be depending on the carrier gas flow rate and the length of the pathway in the extraction line where the isotopic fractionation occurs. As a result, C is a function of C_0.
There are several parts of the extraction line where an isotope fractionation might be possible. As an example, tests on the N_2O conversion efficiency of the furnace revealed that increasing the temperature and lowering the carrier gas flow rate in the furnace would increase the degree of nitrous oxide conversion to N_2 and O_2 (data not shown).
There are several reasons why the maximum efficiency (100% nitrous oxide decomposition) is not possible to reach. First, the melting point of gold (the material of the furnace that acts as a catalyst), which is 1064°C, is never achieved (for precautions the maximum temperature reached in the furnace is 900°C).
Furthermore, increasing the temperature will increase also the Arrhenius coefficient constants of unwanted reactions like reactions R3 and R6.
Moreover, decreasing the carrier gas flow rates means that the oxygen from decomposed N_2O will stay for longer intervals of time in the furnace. This will increase the chance of oxidation reactions with volatile organic compounds, like in reaction R5 (section 2.3), which would affect the oxygen delta values.
This would imply that the sample conversion in the furnace is always partially incomplete. Consequently, an isotope fractionating process following the Rayleigh equation cannot be excluded a priori.
Some isotope effects have been found to occur in the first loop used for the liquid nitrogen trap: changing the helium flow rates inside the loop or changing the interval of time after which the trap is immersed again in liquid nitrogen proved to have an effect on the measured delta values (data not shown). Also this isotopic effect might be size-dependent.
The easiest way to tackle the problem is ensuring the least variation in the total beam area of samples and standards of a batch.

Thus, when the total beam area of a sample differs by more than 10% from the averaged total beam area of the standards used for calculating the calibration curve, the data concerning the sample is rejected.
Rejecting standard measured delta values when the total beam area differs too much from the averaged value is particularly important, since the size effect in the standard delta values would influence all the calculated sample delta values through the calibration curve.
Hence, all standards whose total beam area differs more than 5% from the averaged standard total beam area are excluded from the data set for the calculation of the calibration curve.
Due to the low nitrate concentration in some samples from the Marano lagoon, the sample size chosen for this group of samples is 100 nmol. Regarding the nitrate mineral specimens, whose isotopic measurements are discussed in Chapter 4, the sample size is never less than 200 nmol, apart from few rare copper nitrate minerals, for which a sample size of 50 nmol had to be used. Hence, when the sample availability for potential further measurements is not an issue, the sample size chosen will be large enough to minimize any size effect on measured delta values.

2.7 Kinetic effect

The atmosphere is not the sole source of a nitrate isotope anomaly. The possibility of generating an isotope anomaly during geochemical processes has been discussed in Young et al., 2001. The authors calculated that a cyclical removal of oxygen from a system caused by a process associated with a high isotope fractionation, in the range 35-40‰ (vs. VSMOW), would generate an isotope anomaly of 0.9 ‰ (vs. VSMOW). The nitrate MIF signature can be regarded as a tracer because the magnitude of the signal due to geochemical processes should be small compared to the one generated in the atmosphere.
To the best of our knowledge, the magnitude of a nitrate isotope anomaly due to biological processes has not been studied yet. The chance of an artifact in measured capital delta values due to an incomplete bacterial conversion in vials prepared for the nitrate isotopic measurements with the denitrifier method has been investigated.
To evaluate any kinetic effects, after injection of the standards USGS34 and USGS35, the bacteria are killed after fixed periods of time, ranging from 30 seconds to 3 minutes, to stop the nitrate microbial conversion to nitrous oxide. This time range was first chosen since, according to Sigman et al. (2001), most nitrate should be converted in 10 minutes.
To increase the chance of an immediate death, the volume of the 6M NaOH solution injected has been tripled.
The degree of nitrate conversion is calculated taking into account the total beam area of standards that have been completely converted. A complete conversion is assumed to occur if bacteria are killed with 0.2ml 6M NaOH after twelve hours since sample injections.
The fig. 2.20 shows the data of the first test, when 100 nmol of standards were injected.

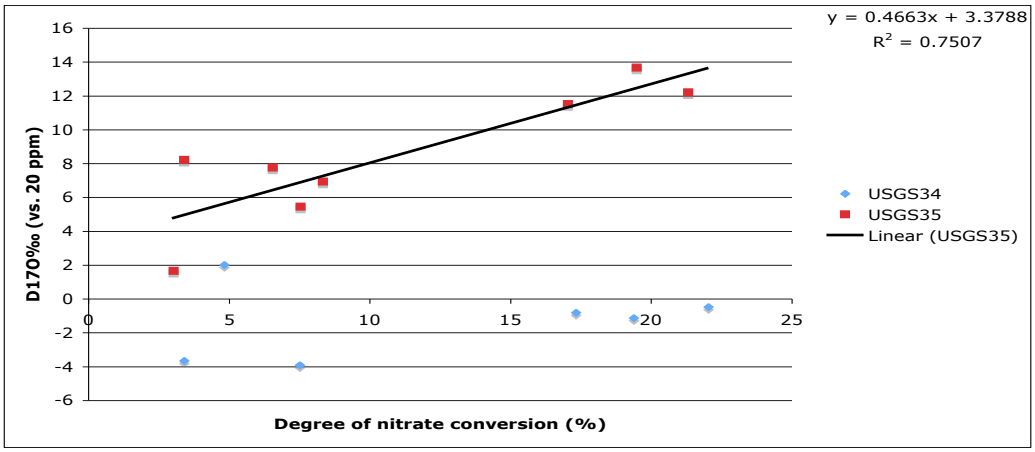

Fig. 2.20. *Standards $\Delta^{17}O$‰(vs. 20ppm) as a function of nitrate conversion.*

The sample size can generate an artifact in the isotope anomaly of the standard USGS35 (fig. 2.17). Furthermore, the sample size effect is not always of the same magnitude, as it was discussed in section 2.6. Consequently, no attempts have been made to correct the oxygen delta values of the standard USGS35 for the sample size effect.

Therefore the following tests have been undertaken by using the standard USGS34 only, due to the lack of a sample size effect when 50nmol or more of standard is analyzed (fig. 2.17).

It is important to point out that, when the degree of nitrate conversion is low, the isotopic composition of blanks contributes more to the isotopic measurements of the standard USGS34. The blanks of the first test showed the usual variability (Table 2.10, compare with Table 2.2) in the isotopic composition.

	Size (µg of N)	**$\Delta^{17}O$ ‰ (vs. 20ppm)**
blank	0.08	-25.5
blank	0.06	-38.6
blank	0.07	67.8

Table 2.10. *Size and isotopic composition of blanks during the first kinetic test*

When the degree of conversion of 100nmol of the standards USGS34 is around 5%, the blank size would contribute to the delta values by 10%. Therefore the blank isotopic composition will give an important contribution to standards oxygen delta values.

Because of the high variability in the blanks isotope anomaly (Table 2.10), it makes no sense to define an average blank isotope anomaly, in order to correct the USGS34 delta values for the blank (see also section 2.3 on data reduction), but it is possible to test the possible magnitude of the blank effect.

When considering that the MIF signal measured in the standard USGS34 might have a 10% with an isotope anomaly of 60‰ (vs. VSMOW) due to blanks (a values which is close to the highest reported in that batch, see Table 2.10), the effective isotope

anomaly of the standard USGS34 that shows a capital delta of -4‰ vs. VSMOW (data point from fig. 2.20) becomes higher than 6‰ vs. VSMOW.
As a consequence, when the degree of nitrate conversion is low, the results of the test are strongly affected by blanks.
A blank with a size of 0.1% of the sample size and an isotope anomaly of 60‰ (vs. VSMOW) will shift the sample anomaly by only 0.06‰ (vs. VSMOW). Further tests show that the capital delta values of the standard USGS34 might deviate from the expected value when the fraction of nitrate converted is below the 20%.
It is therefore necessary to increase the size of the nitrate converted, to decrease the effect of blanks on measured delta values, without increasing the degree of nitrate conversion. Hence, more tests using higher sample sizes and waiting longer intervals before NaOH injections have been undertaken.
The results from a test where the standard USGS34 injected amount to 500 nmol are discusssed. The 20% of sample conversion when the sample size is 500nmol proved to correspond to an interval of roughly seven minutes between a sample and the 0.6ml 6M NaOH injection.
The choice of a sample size of 500nmol is to make a compromise between the need of a good separation of the nitrogen and oxygen sample peaks in the GC column after the furnace (see section 2.2 for the description of the system) and the requirement of analyzing the capital delta of samples with a conversion less than 20% of total nitrate but with no strong interference of blank.
Taking into account the average blank size and the total beam area of the control standards (100% conversion of 500nmol of standard), when the bacterial conversion reaches the 5% of total nitrate, the blanks would contribute to the 0.1% of the measured isotope anomaly shown in fig. 2.21. As a result, the blank contribution to measured capital delta values can be regarded as negligible if more than 5% of nitrate has been converted to nitrous oxide.

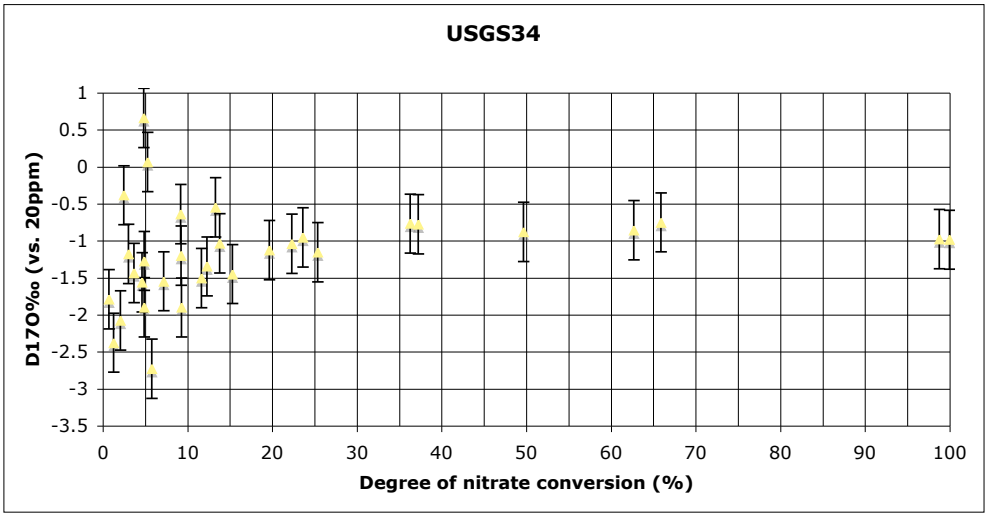

Fig. 2.21. *USGS34 $\Delta^{17}O$‰(vs. 20ppm) as a function of nitrate*

Error bars in fig. 2.21 represent the minimum uncertainty in the isotope anomaly measurements due to the variability among different days of run (see section 2.3 on data reduction).

Overall, there is a tendency towards more negative isotope anomalies in the range 5-15% of nitrate converted. However, data in that range of nitrate conversion (%) are rather scattered and no indubitable conclusions can be drawn. It was confirmed that no deviation from the expected isotope anomaly is found after the 20% of nitrate conversion (fig. 2.21).
It is important to point out that if a negative isotope anomaly in the nitrous oxide could be generated during bacterial conversion, the nitrate in the remaining pool will acquire a positive $\Delta^{17}O$.
The fig. 2.22 shows all the raw delta values of the test, including the nitrogen delta values. The results reveal that the isotope effects due to an incomplete nitrate conversion by *Pseudomonas aureofaciens* lead to a logarithmic trend for the oxygen delta values and to a linear trend for the nitrogen delta values.
The two data points circled in red in fig. 2.22 proved to be outliers, being outside the range $x=Q_3+h$, (with $h=1.5(Q_3-Q_1)$, Q_3 and Q_1 are the third and the first quartile respectively of the data points related to a degree of nitrate conversion equal or below 20%).
When excluding the outliers (fig. 2.22, the Pearson coefficient R^2 for a linear trend in the nitrogen delta value is 0.97, whereas R^2 is slightly higher than 0.9 in both oxygen isotope logarithmic trends with the degree of nitrate conversion (R^2 is below 0.75 when assuming a linear trend of the oxygen delta values).

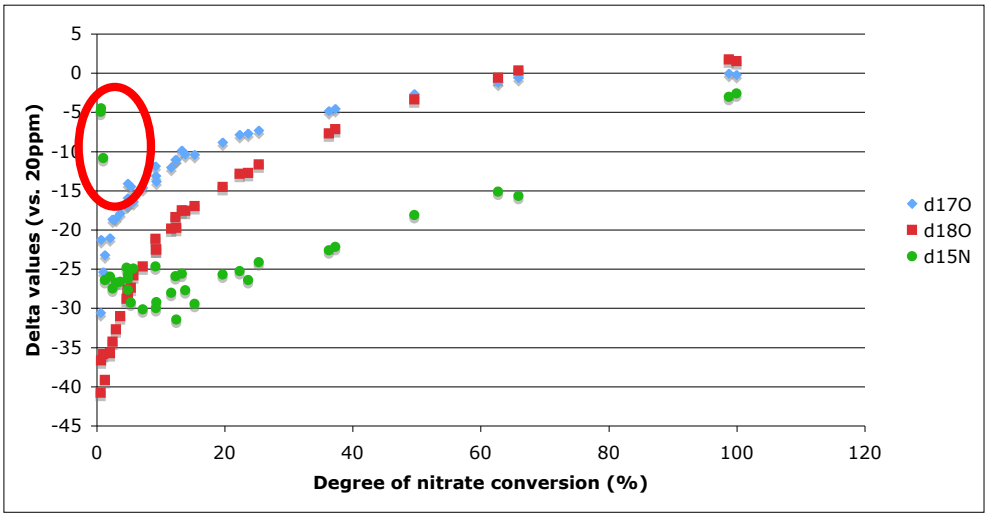

Fig. 2.22. *USGS34 raw delta values as a function of nitrate conversion*

The slope of the trends in fig. 2.22 would suggest that *Pseudomonas aureofaciens* selects at first the nitrate molecules according to the oxygen isotopes, with a slight preference for ^{18}O containing molecules, compared to ^{17}O containing molecules. This preference would be responsible for the tendency towards negative isotope anomalies.
Later on, once the 10-15% of nitrate conversion occurred, bacteria would select the nitrate molecules based on the presence of either lighter nitrogen or oxygen isotopes in a similar way (note in fig. 2.22 that the slope of the trends in the range 15-65% nitrate conversion is similar for ^{18}O and ^{15}N).
In the range 65-100% nitrate conversion, the oxygen delta values become stable, whilst a linear trend is still observed in the nitrogen delta values.

Bacterial enzymatic reactions determine the preference of nitrate molecules containing lighter isotopes for denitrification. Theoretically, it is possible to consider the biological advantage of such selection in term of thermodynamic properties and calculate the resulting isotope fractionation at each stage of the nitrate conversion (Casciotti, 2009).
In fact, several factors can influence the resulting N_2O isotopic composition (transport of nitrate to cell, diffusion to the enzyme active site, fractionation associated with the enzyme/substrate dissociation) (Casciotti, 2009) and no attempts to calculate the enzymatic reaction rates based on the differences in the molecular vibration frequencies due to the presence of lighter isotopes have been undertaken.
The tests on kinetic processes confirmed that bacteria would convert rapidly any sample with a size in the range 50-500nmol. After 15minutes, the 60% of 500nmol of nitrate is converted. Therefore it is safe to assume that a sample with a size in the range 50-200 nmol should be completely converted in 10hours, as it is assumed in the protocol described in section 2.1.
It could be useful to carry out further tests using the standard USGS35 (that has an isotope anomaly of 21‰ vs. VSMOW), to be able to distinguish between the sample size effect and the kinetic effect due to partial nitrate conversion to nitrous oxide, to prove that a MIF signal cannot be consumed during denitrification.

2.8 Copper test

Copper is an essential transition element for *Pseudomonas aureofaciens* because of the copper-type enzyme nitrite reductase, which is responsible for the nitrite conversion to N_2O (Zumft, 2005) and other copper proteins involved in the bacterial metabolism (Matsubara and Zumft, 1982). Yet, the element is known to be toxic for most organisms when the concentration is above a certain threshold. To the best of our knowledge, there is no study on the assessment of such a threshold in *Pseudomonas aureofaciens.*
It has been proved that the bacterial behavior in "copper-shock" cultures and "copper-adapted" culture of *Pseudomonas aeruginosa* proved to be different (Teitzel et al., 2006). *Pseudomonas aureofaciens* has the same copper-type enzyme for nitrite reduction, and might have a similar tolerance to high copper concentration.
Pseudomonas aureofaciens nitrate conversion when copper is present at different concentrations was tested, in order to assess whether the isotopic composition of copper nitrate minerals can be analyzed with the denitrifier method without generating artifacts.
The samples from the copper nitrate minerals discussed in Chapter 4 would contain both nitrate and copper ions with a ratio Cu/NO_3 ranging from 2 to 18, depending on the stoichiometry of the mineralogic phase.
However, because nitrate copper minerals are rare phases associated with more abundant copper sulphates and oxides, it is believed that the ratio Cu/NO_3 in samples dissolved in MQ will be much higher than the theoretical value.
However, no copper concentration in solution were measured before analyzing the isotopic composition of the nitrate copper minerals. Thus, the ability of *Pseudomonas aureofaciens* to convert nitrate in the wide range of 10-1000 Cu/NO_3 has been tested.
Due to the fact that the antimicrobial properties of copper might be a problem for the nitrate conversion by *Pseudomonas aureofaciens*, the copper removal by inducing a precipitation of $Cu_3(PO_4)_2$, $Cu(OH)_2$ and $CuCO_3$ has also been evaluated.

This has been carried out with the addition of dissolved KH_2PO_4, NaOH and Na_2CO_3 in solutions of 0.1M $CuSO_4$, 10mM $CuSO_4$ and 1mM $CuSO_4$.
Due to the low dissociation constant of the salts $Cu_3(PO_4)_2$, $Cu(OH)_2$ and $CuCO_3$, all the considered reactions are thermodynamically favorable. At room temperature the number of collisions between reactants is high enough to easily overcome the energy barrier. As a consequence, the copper precipitate should form instantaneously.
Before any reaction, dilutions have been carried out so that 5 ml of copper solution will be mixed with 5ml of solution with an appropriate reagent concentration (Table 2.11).

Reaction ID	**0.1 M $CuSO_4$ (ml)**	**MQ added to 0.1 M $CuSO_4$ (ml)**	**MQ added to the reagent (ml)**	**Reagent**	**Cu/reagent**
1	5	//	4	1ml 0.5M KH_2PO_4	Cu/PO_4=1
2	0.5	4.5	4.9	0.1ml 0.5M KH_2PO_4	Cu/PO_4=1
3	5	//	//	5ml 0.5M KH_2PO_4	Cu/PO_4=1/5
4	0.5	4.5	4.5	0.5ml 0.5M KH_2PO_4	Cu/PO_4=1/5
5	5	//	4	1ml 0.5M NaOH	Cu/OH=1
6	0.5	4.5	4.9	0.1ml 0.5M NaOH	Cu/OH=1
7	5	//	//	5ml 0.5M NaOH	Cu/OH=1/5
8	0.5	4.5	4.5	0.5ml 0.5M NaOH	Cu/OH=1/5
9	5		4.5	0.5ml 1M Na_2CO_3	Cu/CO_3=1
10	0.5	4.5	4.95	0.05ml 1M Na_2CO_3	Cu/CO_3=1
11	5	//	2.5	2.5ml 1M Na_2CO_3	Cu/CO_3=1/5
12	0.5	4.5	4.75	0.25ml 1M Na_2CO_3	Cu/CO_3=1/5
13	5	//	//	5ml N1M Na_2CO_3	Cu/CO_3=1/10

Table 2.11. *Description of reactions with number ID 1-13, tested for copper removal*

To improve the separation between the copper precipitate and the remaining solution, samples are centrifuged for 30 minutes at 4000 rpm in two steps (15 minutes each).
An aliquot of 6ml of supernatants is transferred to 15ml centrifuge tubes and the pH of the solutions is measured. The original 0.1M $CuSO_4$ solution, that will be used

undiluted for testing the applicability of the denitrifier method when the ratio Cu/NO_3 is 1000, has a pH of 3.5.
Table 2.12 shows the initial ratio Cu/NO_3 and the ratio Cu/reagent, and also the pH and the color of transferred supernatants.

Reaction ID	**Cu/NO_3**	**Cu/reagent**	**Final pH**	**Color of surnatant**
1	1000	Cu/PO_4=1	3.2	pale green
2	100	Cu/PO_4=1	4.35	clear
3	1000	Cu/PO_4=1/5	7.6	clear
4	100	Cu/PO_4=1/5	7.5	clear
5	1000	Cu/OH=1	4.46	same colour as 1
6	100	Cu/OH=1	5.01	clear
7	1000	Cu/OH=1/5	12.7	clear
8	100	Cu/OH=1/5	12.1	clear
9	1000	Cu/CO_3=1	5.6	clear
10	100	Cu/CO_3=1	6.1	clear
11	1000	Cu/CO_3=1/5	10.4	pale blue
12	100	Cu/CO_3=1/5	10.48	clear
13	1000	Cu/CO_3=1/10	10.8	blue

Table 2.12. *Color and final pH in solutions 1-13 after mixing copper solutions with the reagent.*

Because the reactions number 3 and 4 gave the most satisfactory results in terms of final pH (the one closest to neutral condition) and lack of color (since the color is given by the copper present in solution), they have been repeated, to verify their reproducibility. Also, based on the results concerning the reactions with the other reagents, new reactions with different ratios Cu/reagent have been tested, in order to obtain the best compromise between the need of obtaining a solution copper free at a final neutral pH (Table 2.13).

Reaction ID	**Cu/NO_3**	**Cu/reagent**	**Final pH**	**Color of surnatant**
14 (same as reaction 3)	1000	Cu/PO_4=1/5	7.5	clear
15 (same as reaction 4)	100	Cu/PO_4=1/5	7.5	clear
16	1000	Cu/PO_4=1/4	7.36	clear
17	100	Cu/PO_4=1/4	7.3	clear
18	1000	Cu/OH=1/2	9.3	clear
19	100	Cu/OH=1/2	6.9	clear
20	1000	Cu/CO_3=2	9.3	clear
21	100	Cu/CO_3=2	8.8	clear

Table 2.13. *Color and final pH in solutions with ID 14-21 after mixing copper solutions with the reagent.*

The solutions shown in Table 2.13 have been prepared by mixing 5ml of an appropriate copper solution with 5ml of an appropriate reagent solution, similarly to the reactions described in Table 2.11.
Based on the final pH and the color of the final solutions, reactions with the number ID 3, 4, 5, 6, 9, 10, 16 and 17 have been selected as a potential preliminary step to remove copper before measuring the isotope anomaly with the denitrifier method.
Therefore the transferred surnatants after the reactions with number ID 3, 4, 5, 6, 9, 10, 16 and 17 have been added to vials containing 2ml of suspended bacteria in NFM for the isotopic analyses of the standards USGS34 and USGS35.
To verify the effect of residual copper in solutions, the measured delta values were compared with the delta values of control standards USGS34 and USGS35 from vials where no copper is present.
Since the nitrate content in commercial $CuSO_4$ has not been measured, the copper solutions and the transferred surnatants are added to the 2ml of suspended bacteria in NFM before purging with helium, to let the bacteria convert any nitrate to nitrous oxide when the gas can be removed.
However, because of the concern that bacteria might not survive for a long time, due to the presence of copper in solution, all vials have been purged only once for a longer time (1.5 hour) at a helium flow rate that is the double the rate required in the protocol described in section 2.1.
This choice has been made because in the first published protocol for the denitrifier method (Sigman et al., 2001), two hours of purge with helium at 10-20ml/min is required, to have blanks with a size equal to the 10% of a 20nmol nitrate sample. After purging with helium, samples have been immediately injected into vials. Therefore no more than two hours occurred between the copper solutions injections and samples injection in each vial.
The opportunity that bacteria can survive when copper ions are present in the nitrate solutions has been tested by adding to some vials with 2ml bacteria in NFM an aliquot of 0.5ml of 0.1M $CuSO_4$, 10mM $CuSO_4$ or 1mM$CuSO_4$.
To minimize the volume effect, an aliquot of MQ was previously added so that the final volume in each vial is always 3ml (2ml of which from bacteria suspended in NFM) (Table 2.14). Thus, the copper solutions injected are diluted into the vials 4.5 times.

Sample ID	**Standard**	**Cu/NO_3**	**Copper solution treated/untreated**	**Cu/reagent**	**MQ (ml)**
1	USGS34	//	0	//	1
2	USGS34	//	0	//	1
3	USGS35	//	0	//	1
4	USGS35	//	0	//	1
5	USGS34	1000	0.5ml of 0.1M Cu	//	0.5
6	USGS34	1000	0.5ml of 0.1M Cu	//	0.5
7	USGS35	1000	0.5ml of 0.1M Cu	//	0.5
8	USGS35	1000	0.5ml of 0.1M Cu	//	0.5
9	USGS34	100	0.5ml 10 mM Cu	//	0.5
10	USGS34	100	0.5ml 10 mM Cu	//	0.5
11	USGS35	100	0.5ml 10 mM Cu	//	0.5
12	USGS35	100	0.5ml 10 mM Cu	//	0.5
13	USGS34	10	0.5ml 1 mM Cu	//	0.5
14	USGS34	10	0.5ml 1 mM Cu	//	0.5

15	USGS35	10	0.5ml 1 mM Cu	//	0.5
16	USGS35	10	0.5ml 1 mM Cu	//	0.5
17	USGS35	1000	1ml of 0.1M Cu	Cu/PO_4=1/5	//
18	USGS35	1000	1ml of 0.1M Cu	Cu/PO_4=1/5	//
19	USGS35	100	1ml of 10mM Cu	Cu/PO_4=1/5	//
20	USGS35	100	1ml of 10mM Cu	Cu/PO_4=1/5	//
21	USGS34	1000	1ml of 0.1M Cu	Cu/PO_4=1/5	//
22	USGS34	1000	1ml of 0.1M Cu	Cu/PO_4=1/5	//
23	USGS34	100	1ml of 10mM Cu	Cu/PO_4=1/5	//
24	USGS34	100	1ml of 10mM Cu	Cu/PO_4=1/5	//
25	USGS35	1000	1ml of 0.1M Cu	Cu/PO_4=1/4	//
26	USGS35	1000	1ml of 0.1M Cu	Cu/PO_4=1/4	//
27	USGS35	100	1ml of 10mM Cu	Cu/PO_4=1/4	//
28	USGS35	100	1ml of 10mM Cu	Cu/PO_4=1/4	//
29	USGS35	1000	1ml of 0.1M Cu	Cu/OH=1	//
30	USGS35	1000	1ml of 0.1M Cu	Cu/OH=1	//
31	USGS35	100	1ml of 10mM Cu	Cu/OH=1	//
32	USGS35	100	1ml of 10mM Cu	Cu/OH=1	//
33	USGS35	1000	1ml of 0.1M Cu	Cu/CO_3=1	//
34	USGS35	1000	1ml of 0.1M Cu	Cu/CO_3=1	//
35	USGS35	100	1ml of 10mM Cu	Cu/CO_3=1	//
36	USGS35	100	1ml of 10mM Cu	Cu/CO_3=1	//
37	USGS34	1000	1ml of 0.1M Cu	Cu/CO_3=1	//
38	USGS34	1000	1ml of 0.1M Cu	Cu/CO_3=1	//
39	blank	//	//	//	1
double amount of bacteria					
40	USGS34	//	//	//	1
41	USGS34	//	//	//	1
42	USGS35	//	//	//	1
43	USGS35	//	//	//	1
44	USGS34	1000	0.5ml 0.1M Cu	//	0.5
45	USGS34	1000	0.5ml 0.1M Cu	//	0.5
46	USGS35	1000	0.5ml 0.1M Cu	//	0.5
47	USGS35	1000	0.5ml 0.1M Cu	//	0.5
48	USGS34	100	0.5ml 10 mM Cu	//	0.5
49	USGS34	100	0.5ml 10 mM Cu	//	0.5
50	USGS35	100	0.5ml 10 mM Cu	//	0.5
51	USGS35	100	0.5ml 10 mM Cu	//	0.5
52	USGS34	10	0.5ml 1 mM Cu	//	0.5
53	USGS34	10	0.5ml 1 mM Cu	//	0.5
54	USGS35	10	0.5ml 1 mM Cu	//	0.5
55	USGS35	10	0.5ml 1 mM Cu	//	0.5
56	USGS35	1000	1ml of 0.1M Cu	Cu/PO_4=1/5	//
57	USGS35	1000	1ml of 0.1M Cu	Cu/PO_4=1/5	//
58	USGS35	100	1ml of 10mM Cu	Cu/PO_4=1/5	//

59	USGS35	100	1ml of 10mM Cu	Cu/PO_4=1/5	//
60	blank	//	//	//	1ml

Table 2.14. *Sample volume injections for IRMS measurements concerning the first test for copper removal.*

Furthermore, a test was carried out to determine if a higher number of bacteria per vial might improve the chance of a total conversion of nitrate. To test that, the bacteria from two centrifuge bottles (see section 2.1 on the protocol of the denitrifier method) were suspended in 45ml of NFM, to fill 20 vials with 2ml per vial (sample ID 40-60) (Table 2.14).
The bacteria from another two centrifuge bottles were suspended in 90ml of NFM (following the protocol described in section 2.1), to fill 40 vials with number IDs 1-39 (Table 2.14).
In this way, the vials with a number ID in the range 40-60 should have roughly double the amount of bacteria, compared to the vials with an ID in the range 1-39.
A standard size of 50nmol has been injected in each vial for $\delta^{15}N$ and $\delta^{18}O$ analyses. Since the 50nmol standard comes from a 0.1ml 0.5mM standard solution, the dilution of copper in the vials due to the addition of 0.1ml of a nitrate solution is considered negligible.
The decision not to use the gold furnace in the first test was to avoid the memory effect and the daily shift on the delta values (see section 2.2) and to test the chance that bacteria could convert at least half of the samp section le size that is usually required for the analyses of the isotope anomaly.
Unfortunately, due to the short purge time, the blank size was exceptionally high. Also, there was a problem in the extraction line during the run and, after about thirty measurements, there was an increasing loss of sample. Thus, only some speculations can be made after this first test.
Table 2.15 shows the size of some of the samples described in Table 2.14 that were placed at the start of the run (and that probably did not experience any loss of sample).
The size of the blank with the double amount of bacteria is roughly the 50% of the control standards (Table 2.15, compare sample 60 with samples 40 and 42). Because the measurements of this test are strongly affected by blank, the standard delta values will not be presented.

Sample ID	Standard	Cu/NO_3	Cu/Reagent	Size (μg of N)
1	USGS34	//	//	133.2
5	USGS34	1000	//	60.2
6	USGS34	1000	//	59.9
15	USGS35	10	//	64.6
16	USGS35	10	//	85.5
17	USGS35	1000	Cu/PO_4=1/5	79.0
18	USGS35	1000	Cu/PO_4=1/5	69.5
19	USGS35	100	Cu/PO_4=1/5	84.1
20	USGS35	100	Cu/PO_4=1/5	90.3
40 (double bacteria)	USGS34	//	//	210.0
42 (double bacteria)	USGS35	//	//	189.1
56 (double bacteria)	USGS35	1000	Cu/PO_4=1/5	123.2
57 (double bacteria)	USGS35	1000	Cu/PO_4=1/5	133.8
58 (double bacteria)	USGS35	100	Cu/PO_4=1/5	136.1
59 (double bacteria)	USGS35	100	Cu/PO_4=1/5	128.8
60 (double bacteria)	blank	//	//	111.3

Table 2.15. *Measured size of some samples from the first test for copper removal.*

Interestingly, the control standard with sample ID 1, which had been converted with a usual amount of bacteria, was around 60% the size of the control standard converted with the double amount of bacteria (sample ID 40 and 42 in Table 2.15).
Usually 50nmol of nitrate should be in the range 8-10 μg of N, a size that is below the one that has been measured in the control standard with sample ID 1 (Table 2.15). Therefore most of the nitrous oxide should come from the bacterial conversion of some other nitrogen containing species that could not be removed from the vials due to the short purge time.
The dependence of the nitrous oxide size on the number of bacteria might suggest that an incomplete process is generating the effect: the converted species was not entirely consumed.
Denitrifying bacteria like *Pseudomonas aureofaciens* can generate nitrite under aerobic conditions from organic nitrogen. It is likely that the aerobic conditions in the vials ceased after a similar lapse of time in both the vials with a usual and the double number of bacteria. Considering the high helium flow rate used for the helium purge and that the vials volume is 18ml only, bacteria presumably stayed at aerobic conditions in NFM for a relatively short time.
The results shown in Table 2.15 might therefore suggest that *Pseudomonas aureofaciens* heterotrophic nitrification of organic nitrogen to nitrite could be the process responsible for the unusual size of all the samples. The organic nitrate is present in the sealed vials as Tryptic soy broth dissolved in nitrate free media.
In the first article on the denitrifier method (Sigman et al., 2001), it was explained that the Tryptic soy broth is used by *Pseudomonas aureofaciens* for assimilation only. Yet, it is possible that a relevant amount of nitrite can be produced from the organic nitrogen in Tryptic soy broth and that, by the end of the second purge with helium, nitrite is converted as nitrous oxide and removed from the vials through the needle.

Another observation concerning the results in Table 2.15 is that the sample size decreases by roughly 50% when copper was present in solution, regardless of the ratio Cu/NO_3 (compare samples with ID 5 and 6 with samples with ID 15 and 16). This might suggest that a threshold in the copper concentration not higher than 0.2mM could significantly slow down the bacterial metabolism.
The treatment with a phosphate reagent slightly increases the nitrous oxide size from 50% to the 60% control standard (in both the groups of vials with the usual and the double amount of bacteria) suggesting this reagent can remove some of the copper, or at least detoxify it.
The most important finding from the results in Table 2.15 is that *Pseudomonas auerofaciens* seems to be able to survive when copper is present in solution at a concentration up to 22mM. This confirms some results that have been recently published (Tedesco and Jacinthe, 2009)(Magalhaes et al., 2007)(Twinning et al., 2007) on the connection between decreased denitrification rates and elevated copper concentrations.
The results of the first test guided to the choice of how to design a second test. The main goal was investigating that there is no formation of a MIF signal during *Pseudomonas aureofaciens* nitrate conversion related to the presence of copper in solution.
All vials were purged twice for 45 minutes following the ordinary protocol. An aliquot of 100 nanomoles of standard USGS34 (from a 4mM standard solution) is injected in each vial after the second purge with helium.
Addition of 1ml MQ before sample injections has been made in the control standards (samples with ID 1-3 in Table 2.16, similarly to samples in Table 2.14 with ID 1 and 2), to avoid the interference of any volume effect (section 2.5).
A volume of 0.5ml of $0.1MCuSO_4$ untreated (in samples with ID 4-6 in Table 2.16) and 1 ml of transferred supernatant from 5ml of $0.1MCuSO_4$ that had been treated with the reagent KH_2PO_4 diluted in 5ml (samples with ID 7-9) was injected just before the second purge with helium.
The calculated ratio Cu/NO_3 in samples with ID 4-6 is 1000, and the copper concentration of the 3ml solution in vials (of which 2ml from bacteria suspended in NFM, 0.5ml from MQ and 0.5ml from $0.1MCuSO_4$) is calculated to be 22.2mM (the contribution of USGS34 volume injection is neglected).
The samples in Table 2.16 with ID 7-9 correspond to samples with ID 21 and 22 in Table 2.14, with the only difference that the reagent concentration in the 5ml solution to be mixed with the copper solution is doubled, to get a ratio Cu/PO_4 of 1/10.
All samples have been analyzed for the isotopic measurements with the gold furnace.

Sample ID	Description	Size (μg of N)	$\Delta^{17}O$ ‰ (vs. 20ppm)	$\delta^{15}N$ ‰ (vs. 20ppm)
1	USGS34	25.7	-0.07	-0.8
2	USGS34	25.8	0.10	-1.1
3	USGS34	26.8	0.08	0.2
4	USGS34+0.5ml 0.1M$CuSO_4$	11.6	1.63	-19.8
5	USGS34+0.5ml 0.1M$CuSO_4$	11.8	1.35	-19.6
6	USGS34+0.5ml 0.1M$CuSO_4$	11.5	1.31	-8.3
7	USGS34 + Cu/PO_4 =1/10	24.4	0.14	0.6
8	USGS34 + Cu/PO_4 =1/10	25.5	-0.05	0.7
9	USGS34 + Cu/PO_4 =1/10	26.3	0.09	0.4

Table 2.16. *Size and isotopic composition of the nitrate standard USGS34 after the second test for copper removal.*

It was confirmed that the treatment with the reagent KH_2PO_4 removed enough copper to allow the bacteria to completely convert the nitrate to nitrous oxide in 12 hours. This is because the size of the standard USGS34 in vials with ID 7-9 is comparable with the control standard with ID 1-3 (Table 2.16).
The sample size of the nitrate standard USGS34 with ID 4-6 (Table 2.16) is the 45% of the control standard size. This finding would suggest that the microbial conversion to nitrous oxide has been slowed down by the high copper concentration in solution.
Residual copper, or the reagent left in solution, caused a shift in the nitrogen delta values only of about 1‰ (vs. 20ppm), whilst the isotope anomaly in samples where the copper solution has been treated with the reagent is the same as the control standard (Table 2.16).

Blanks ID	0.1M$CuSO_4$	Addition of MQ (ml)	Size (μg of N)	$\Delta^{17}O$ (vs. 20ppm)	$\delta^{15}N$ (vs. 20ppm)
1	//	1	0.024	-269	-152
2	//	1	0.001	-371	-197
3	1ml treated with PO_4	//	0.03	13.14	88.4
4	1ml treated with PO_4	//	0.04	-154.42	64.1
5	0.5ml	0.5	0.58	-0.57	17.5
6	0.5ml	0.5	0.36	16.04	29.0

Table 2.17. *Size and isotopic composition of blanks after the second test for copper removal*

It was verified that copper in solution would increase the blank size more than an order of magnitude (compare the size of blanks with ID 1 and 2 in Table 2.17 with blanks with ID 5 and 6). However, the blank size in 5 and 6 will be still unimportant, being roughly 2% of a 100nmol nitrate sample.
Furthermore, blanks with ID 3 and 4 (concerning vials where 1ml of solution comes from supernatants transferred from copper solution treated with the reagent) have a similar size of blanks where no copper is present (Table 2.17). This might suggest that there is no copper in the transferred supernatant or the copper concentration is below the threshold that generates stress in *Pseudomonas aureofaciens* cultures.
When analyzing the copper nitrate minerals, because the effective copper concentration after sample dissolution in MQ will not be measured, the following strategy will be chosen: assuming a copper concentration of 0.1mM, an aliquot of KH_2PO_4 will be added to have a ratio Cu/PO_4 of 1/10. After centrifugation, if the precipitate is visible, after transferring the supernatant in another 15ml centrifuge tube, the same amount of reagent will be added again. The procedure will be repeated until there is no precipitate after centrifugation.
Remarkably, the presence of copper in solution caused an isotope anomaly in the standard USGS34 (sample ID 4-6 in Table 2.16). Because there is usually a 20% compression scale in the isotope anomaly calculated from raw delta values (see section 2.3 on data reduction), the true isotope anomaly in the VSMOW scale will be in the range 1.5-1.9‰.
This isotope anomaly is certainly not due either to a sample size effect (which does not occur below 50nmol of USGS34, see fig. 2.17) or to kinetic effects, since we tested that the partial conversion of more than 20% of nitrate wouldn't generate any anomaly in the standard USGS34 (fig. 2.21).
To sum up, results shown in Table 2.16 might suggest that bacteria might generate an isotope anomaly at high level of stress. This would question the assumption that the atmosphere is the only source of a MIF signal.
The copper concentration used for the tests discussed in the present section is reasonably not occurring in a natural system. The effect of low copper concentration on the denitrifier method has not been further investigated, since the main purpose of the experiments was testing the suitability of the denitrifier method for the isotopic analyses of copper nitrate minerals.
Because of the measured shift in the nitrogen delta values (Table 2.13), the analyses of copper nitrate minerals, discussed in Chapter 4, will be focused on the capital delta values only, for which no effects due to the presence of any residual copper has been found.
Further experiments should be carried out to assess the chance that copper adapted cultures for the denitrifier method could allow precise measurements of nitrogen delta values in samples where the copper content is high or moderate.
Magalhaes et al. (2007) found that pollutants like copper, cadmium, zinc, lead and chromium affect denitrification rates in estuarine sediments. If unusual denitrification rates due to pollutant concentrations result in unexpected isotope fractionations, the isotopic studies aiming at understanding the assessment of the relative importance of denitrification over other processes should take into account such effects.
Moreover, the chance that *Pseudomonas aureofaciens* conversion to nitrous oxide in samples with heavy elements concentrations above a certain threshold might interfere with the nitrate and nitrite isotopic measurements should also be investigated.

2.9. Summary

Table 2.18 shows a summary of the uncertainties in the isotopic measurements and the strategy to tackle the problems, if there is any.

	Uncertainties in δO‰	**Uncertainties in Δ17O‰**	**Uncertainties in δ15N‰**	**Solution**
Memory effect	±1-4 (vs. VSMOW)	±0.4-0.7 (vs. VSMOW) for sample size ≤100nmol	//	Samples are analyzed in groups of duplicates or triplicates and the oxygen delta values from the first replicate are always discarded
Daily shift	±1-4 (vs. VSMOW)	±0.3-0.6 (vs. VSMOW)	//	Two or more calibration curves are considered when the overall uncertainties in the oxygen delta value is higher than 2‰
Blank+water isotope exchange	not considered	±0.2 (vs. VSMOW)	±0.6 (vs. AIR)	
Variability among different days of run	not considered	±0.4 (vs. VSMOW)	±0.3 (vs. AIR)	
Salinity	//	//	//	//
Volume	//	//	0.8-1 (vs. 20ppm) in the range 0-10ml of added MQ	Samples are grouped in batches according to their injection volumes
Sample size	Depending on sample isotope composition. Higher in USGS35	Depending on sample isotope composition. Higher in USGS35	Depending on sample isotope composition. Higher in USGS34	The sample size is 100 nanomoles or higher and any replicate whose total beam area is differing more than 10% from the others will be discarded
Kinetic effect	Depending on sample isotope composition	Depending on sample isotope composition	Depending on sample isotope composition	Injections of 6MNaOH 10 hours after sample injections

Copper in solution (treated with KH_2PO_4)	//	//	1 (vs. 20ppm)	The capital delta values of copper nitrate minerals only are discussed

Table 2.18. *Summary of the influence of various effects on the overall precision of the isotopic measurements discussed in Chapters 3 and 4.*

To sum up, it is possible to find a solution for most of the problems that can affect the sample isotopic measurements. The oxygen delta values will be mainly influenced by the daily shift. If the precision due to the daily shift is lower than the uncertainty of 0.4‰ (vs. VSMOW) due to variability among days of run, the latter uncertainty will be used.
The nitrogen delta values will have a minimum uncertainty of 0.3‰(vs. AIR) for the same reason.

3. FONIMAR, a monitoring program of pollution sources at the Marano Lagoon (Italy).

The monitoring programme FONIMAR (Individuazione e caratterizzazione delle potenziali **FO**nti dei **NI**trati nella Laguna di **MAR**ano - Identification and characterization of potential nitrate sources at the Marano Lagoon) was set up in February 2009 in a region designated as a nitrate vulnerable zone (NVZ).
The primary goal of the program is the identification and differentiation of the main anthropogenic nitrogen sources in the Marano Lagoon and its catchment area. A novel approach has been chosen, which combines the study of the stable isotopes of nitrate ($\delta^{15}N$, $\delta^{18}O$ and $\Delta^{17}O$) with co-tracers like $\delta^{11}B$, the stable isotopes of water ($\delta^{2}H$ and $\delta^{18}O$) and the stable isotopes of sulphate ($\delta^{34}S$ and $\delta^{18}O$). The details of the results can be found in Saccon et al. (2011), which is presented in Appendix 2. A second paper on the monitoring program FONIMAR has been recently submitted by the same authors.
The discussion in the present chapter will be limited to the analyses of the data of the nitrate isotopic anomaly and $\delta^{15}N$ only. The major goal is the identification of the contribution of the atmosphere as a nitrate source to the lagoon.
Usually the uncertainties in the estimates of the nitrate atmospheric inputs by using the isotope anomaly consider the uncertainties of the isotopic measurements only (Tsunogai et al., 2011)(Michalski and Thiemens, 2006). Section 3.3 will be dedicated on assessing the least magnitude of the MIF signature that can be considered significant, when evaluating in addition the uncertainties due to some necessary assumptions regarding the atmospheric nitrate deposition and its MIF signature.
The Marano lagoon is located in the Northern Adriatic Sea (Northeast Italy) and it is entirely included in the Province of Udine of the Friuli-Venezia Giulia region. The lagoon has a surface of about 77 km^2, with a length of nearly 14 km and an average width of 5.5 km. A detailed bathymetry chart of the lagoon has been presented in October 2011 and can be found in Appendix 1.
The Friuli-Venezia Giulia is the region of Italy with the highest annual rainfall. The long-term average precipitation rate is shown in fig. 3.1 (Friuli-Venezia Giulia is circled in red).

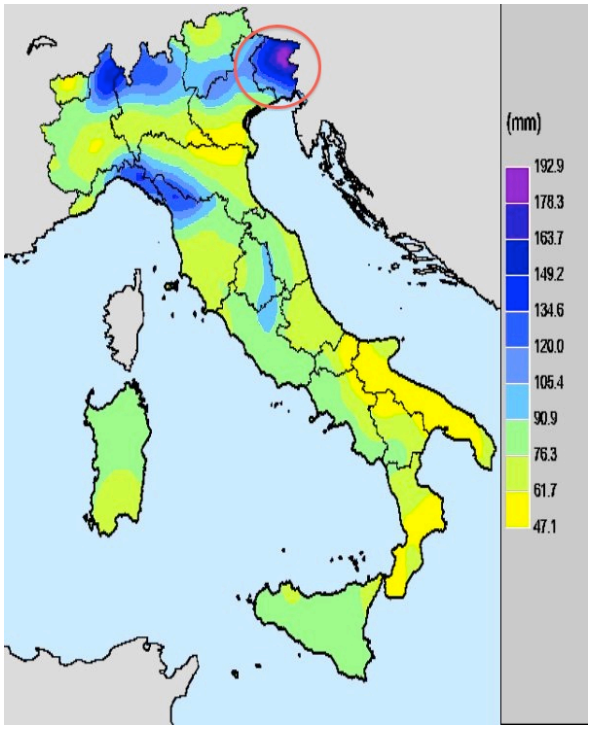

Fig 3.1. *Average annual precipitation (mm of rain/yr) for the period 1969-1990. from http://www.scia.sinanet.apat.it.*

In addition, the North of Italy is considered to be among the most polluted regions in Europe, with the highest tropospheric NO_2 concentration (see fig. 3.2), which is the most important nitrate precursor in the atmosphere, as it was underlined in chapter 1.

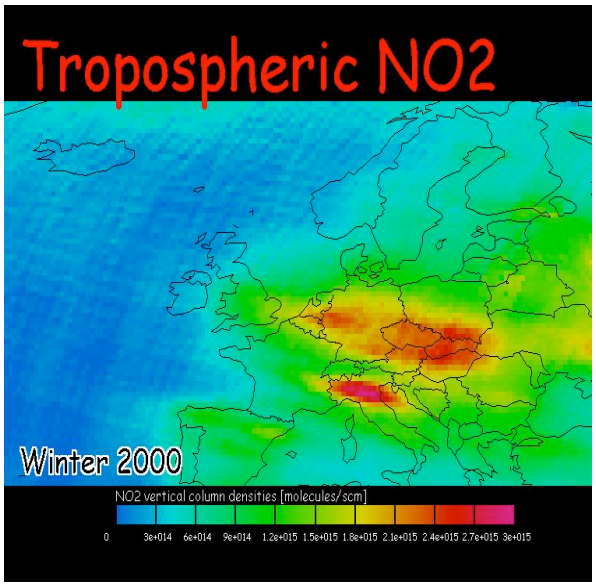

Fig 3.2. *GOME measurements of tropospheric NO_2 from http://troposat.iup.uni-heidelberg.de/TROPOSAT-1/ar_2001/ar-over_2001.htm.*

Because the atmospheric nitrate can be easily transferred to the Marano lagoon via wet deposition, the nitrate atmospheric input in the study area is expected to be significant.
The water samples from the lagoon, its tributary rivers, the area known as "linea delle risorgive" (the groundwater upwelling line), groundwater, sewer pipe and open sea were collected and analyzed on a quarterly interval from 2009 to 2010. In order to identify the origin of nitrate at the Marano lagoon, a total number of 47 sampling points is chosen, to include a grid of sampling stations across the lagoon and a set of sampling stations in areas that can act as potential nitrate sources.
The sampling locations were distributed as follows: 16 sampling points along the lagoon's navigation channels, 11 sampling points in shallow water areas of the lagoon, 3 sampling points in the lagoon inlets to the Adriatic Sea, 1 sampling point in the open sea, 14 sampling points along the main tributary rivers of the lagoon, 6 sampling points along the groundwater up-welling line and 4 groundwater sampling points.
A description of the sampling sites and a map of the whole sampling area are presented in Appendix 1.
Of the total number of 188 samples (47 for each sampling campaign), 53 were analyzed for their $\delta^{15}N$ and $\Delta^{17}O$ nitrate composition using the method described in Chapter 2, 24 of which come from the water samples collected in May 2009, 14 in September 2009, 4 in November 2009 and 11 in February 2010. A larger subset of samples was analysed for the $\delta^{15}N$ and $\delta^{18}O$ values by other participants (see Appendix 2).
The complete data set is presented in Appendix 1 along with other key data such as nitrate concentration and salinity.
The water sampling depth in the lagoon has been fixed at mid-water depth, to avoid overestimating the contributions of rainfall in the upper layers of the water column and the microbiological processes linked to the lagoon bottom. Most channels have a depth of about 3m, whereas shallow water areas are mainly in the range 0.2-0.8m depth (fig. 3.3).

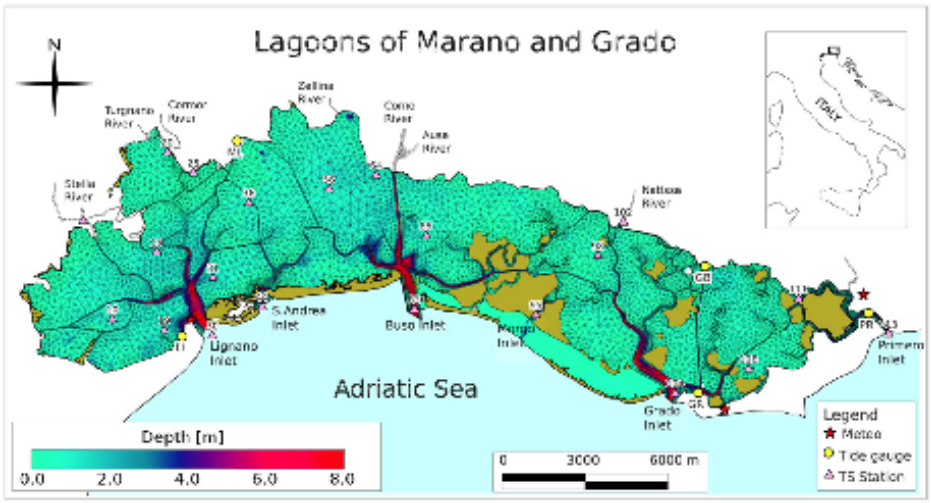

Fig. 3.3. *Bathymetry of Marano and Grado Lagoons, from Ferrarin et al., (2010).*

The measurements of nitrate, nitrite, and ammonium concentration have been undertaken in-situ by other members of the research team using a portable spectrophotometer "WTW FC photoFlex/Turb 430 LED".

3.1.The analysis of nitrate $\delta^{15}N$ and $\Delta^{17}O$ from the Marano Lagoon.

In the present section, the isotopic composition of the 53 measurements obtained with the method described in chapter 2 are presented and discussed, with a focus on the nitrogen isotopes. The assessment of the relative importance of atmospheric nitrate in sample water, based on measured $\Delta^{17}O$, will be the main subject of section 3.2.
There is no clear difference in the nitrogen isotopic composition of samples from the lagoon in any of the surveys. For instance, in fig. 3.4 the results concerning the sampling campaign in May show that the nitrogen delta values from different categories of sampling sites overlap.

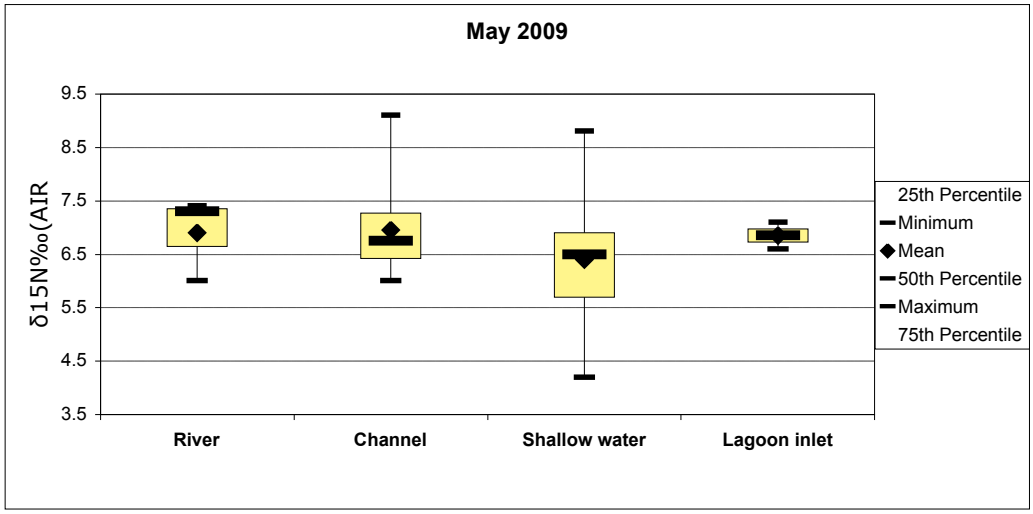

Fig. 3.4. *$\delta^{15}N$‰(AIR) at location with sample ID x in May2009.*

The average nitrogen delta value of the entire data set presented in fig. 3.4 is 6.7‰. By using the 2-mean t-test, it was confirmed that there is no statistical difference among all categories, since the null hypothesis (any data set of two groups are part of the same population) is accepted with 95% of confidence.
The category "river" consists of three samples from the river Ausa. It is important to point out that only one of the three samples measured from the river have a salinity below 2.5ps (with a measured $\delta^{15}N$‰ of 6.0), whilst the other two are in the region of the river mouth and have a salinity of about 22 psu, which fact would suggest the occurrence of mixing with seawater.
Another observation is that no temporal trends were observed in the nitrogen delta values across all categories. As an example, in fig. 3.5 the data subset referring to the samples from shallow water areas is presented. The nitrogen delta values of the sampling sites with ID 8, 13, 14, 15 and 24 do not show any significant change when different sampling campaigns are considered.

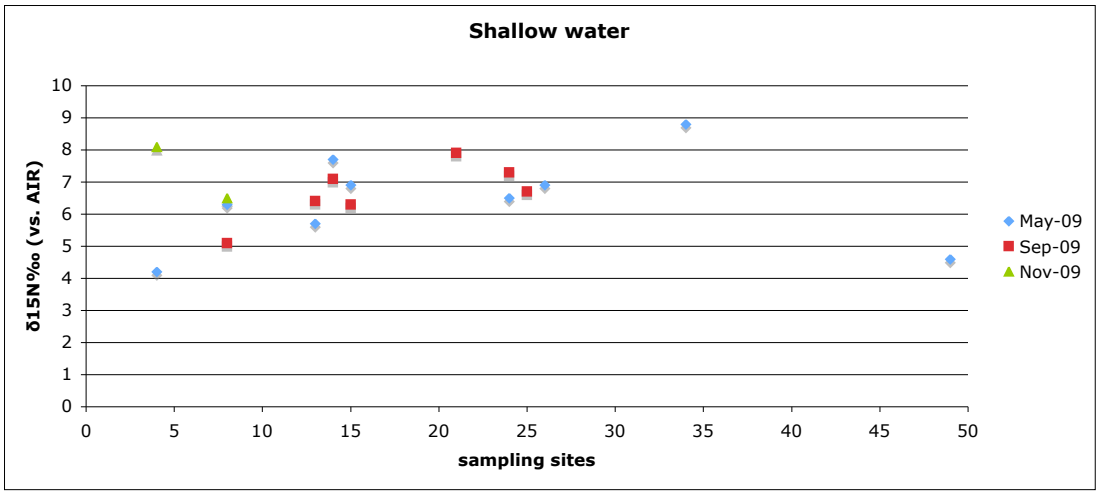

Fig. 3.5. *δ^{15}N‰ (AIR) in shallow water at location with sample ID x in May, September and November (2009).*

Table 3.1 (which is also fig. 3 of Appendix 2) shows the nitrogen delta values of the most common fertilizers in the region.

δ^{15}N ‰	Organic and synthetic fertilizers
4.79	Manure (bovine) from Marianis farm
3.77	Liquid manure (bovine) from Marianis farm
8.52	Liquid manure (pigs)
0.59	Urea
0.30	Ammonium nitrate

Table 3.1. *δ^{15}N‰(AIR) of the main organic and synthetic fertilizers typically used in Friuli Venezia-Giulia (from Fig.3 in Appendix 2).*

The use of co-tracers is necessary to distinguish the effect of mixing of different nitrate sources with distinctive isotopic signatures from the isotope fractionation due to local biogeochemical processes. The conclusion after the investigation of co-tracers (the reader is referred to Chapter 6 of Appendix 2) is that most nitrate in the Marano lagoon is related to the use of manure, both liquid and solid.
The most interesting result from the analyses of the 53 sample measurements is the observation for both the nitrogen and the oxygen isotopes that there is an increased variability when the nitrate content is low (fig. 3.6 and fig. 3.7) (the detection limit of the nitrate measurements is 0.44mg NO_3/L).

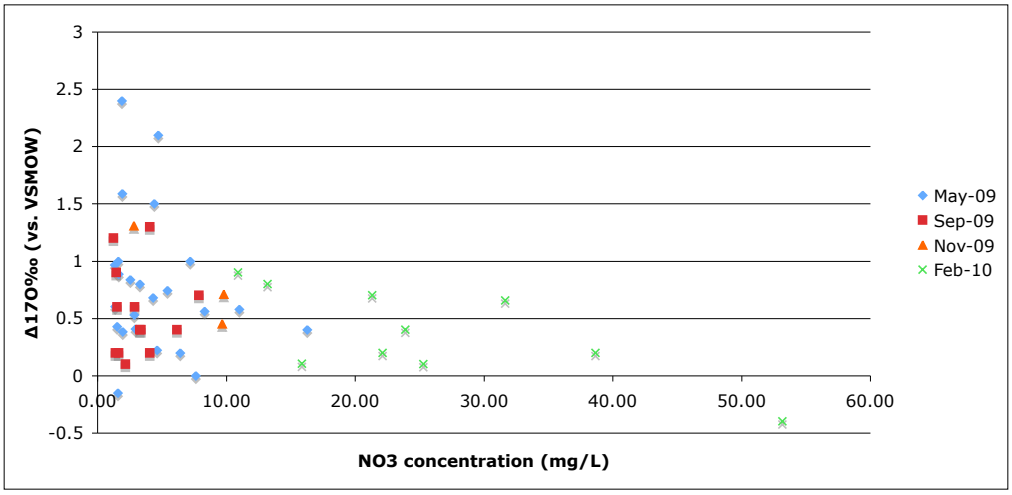

Fig. 3.6. *$\Delta^{17}O$‰ (VSMOW) as a function of the nitrate concentration (mg NO_3/L).*

As discussed in chapter 4 and chapter 5, there are some evidences that changes in the isotope anomaly due to mass dependent processes could be possible when the nitrate concentration is low, which fact would limit the use of the tracer. Some explicit calculations of the shift in the capital delta as a function of the magnitude of a mass dependent process acting as a nitrate sink and the initial nitrate concentration are presented in chapter 5.

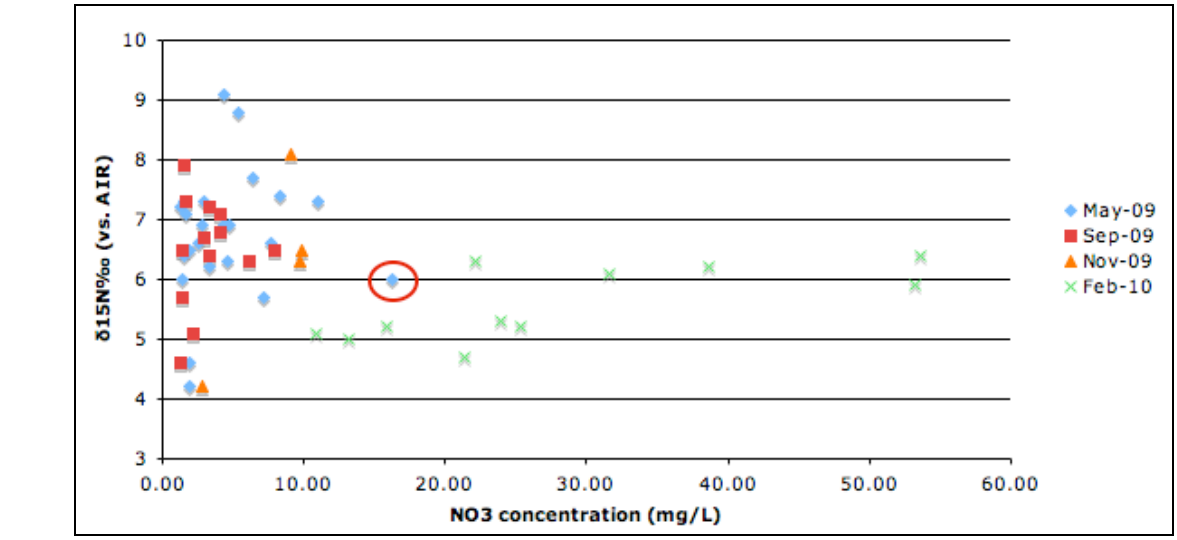

Fig. 3.7. *$\delta^{15}N$‰(AIR) as a function of the nitrate concentration (mg NO_3/L).*

Of the samples collected in February 2010, those analyzed with the method discussed in chapter 2 were freshwater samples from rivers and from the groundwater upwelling line, the latter category being the sample group with the highest nitrate concentration. The choice of plotting the nitrogen delta values from freshwater and saline water samples altogether in fig. 3.7 as a function of the nitrate concentration is to underline

the homogeneity in the isotopic composition of the former group (with high nitrate concentrations), compared to the heterogeneity of the latter. A two-mean t test indicates that the results from freshwater samples of fig 3.7 are statistically different from the group comprising the other data points of fig. 3.7.
Unfortunately, by considering the data set of the 53 samples only, it is impossible to rule out the chance that the greater homogeneity of the freshwater samples is depending on a greater homogeneity of the nitrogen delta values in the whole area during the winter sampling campaign. However, results in fig. 3.5 showed no temporal trend in nitrate $\delta^{15}N$(vs. AIR) from the shallow water samples for the period May-November 2009 (a similar result was found in samples from the lagoon channels, data not shown).
In addition, the only brackish water sample (psu below 2.5) that has been analyzed in May 2009 (a blue diamond emphasized with a red circle in fig. 3.7) fits well with the other data points corresponding to freshwater samples (green crosses in fig. 3.7). These observations might indicate that the freshwater samples do not show significant temporal variability in their isotopic signature, although this conclusion does require further sample analysis to confirm it.
These remarks would suggest that the lack of temporal trends in samples $\delta^{15}N$ could indicate that the higher heterogeneity in nitrate $\delta^{15}N$ from the sampling stations of the lagoon area reflects biogeochemical processes in the lagoon.
The nitrate concentration is also relatively constant over the entire year of sampling in most of the stations (fig. 3.8), although it varies greatly between sites.

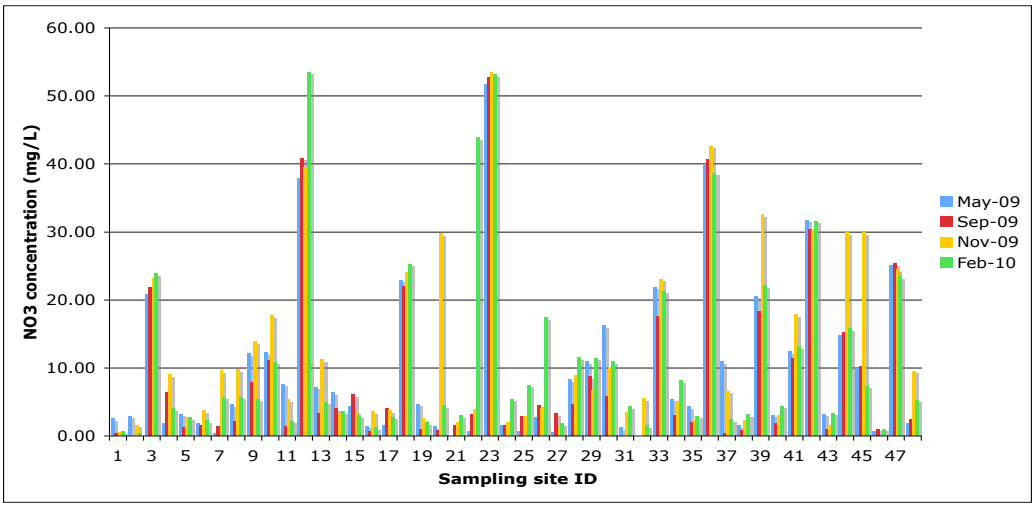

Fig. 3.8. *Nitrate concentration (mg NO_3/L) per sampling site after each sampling campaign.*

After splitting the nitrate concentration data set concerning the spring campaign in two groups, one for the restricted area of the lagoon (consisting of the data from the lagoon inlets to the Adriatic Sea, the shallow water and the channels) and the other for its surroundings (samples from a sewer pipe, from the rivers and along the groundwater upwelling line), it has been found that the nitrate content in the sampling sites of the lagoon is on average five times less compared to the areas dedicated to agricultural activities (fig. 3.9).

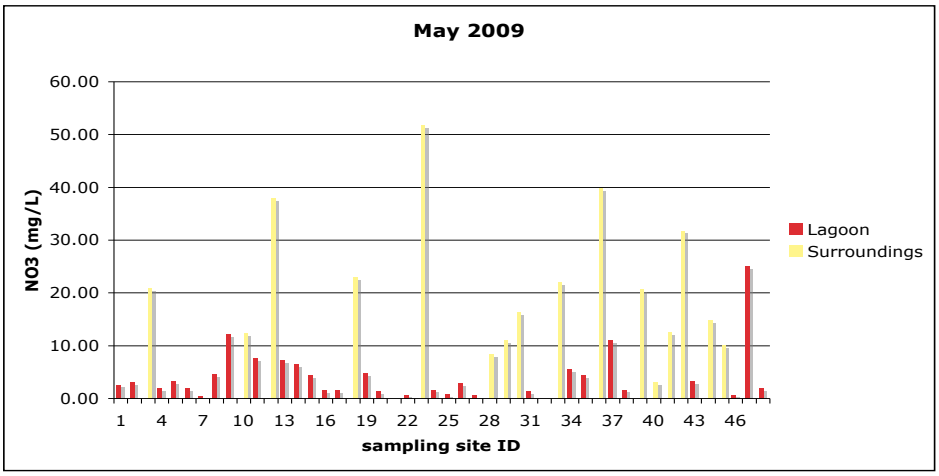

Fig. 3.9. *Nitrate concentration (mg NO_3/L) in the lagoon and its surroundings during the spring sampling campaign.*

The riverine inputs into the lagoon can be traced by measurements of salinity.

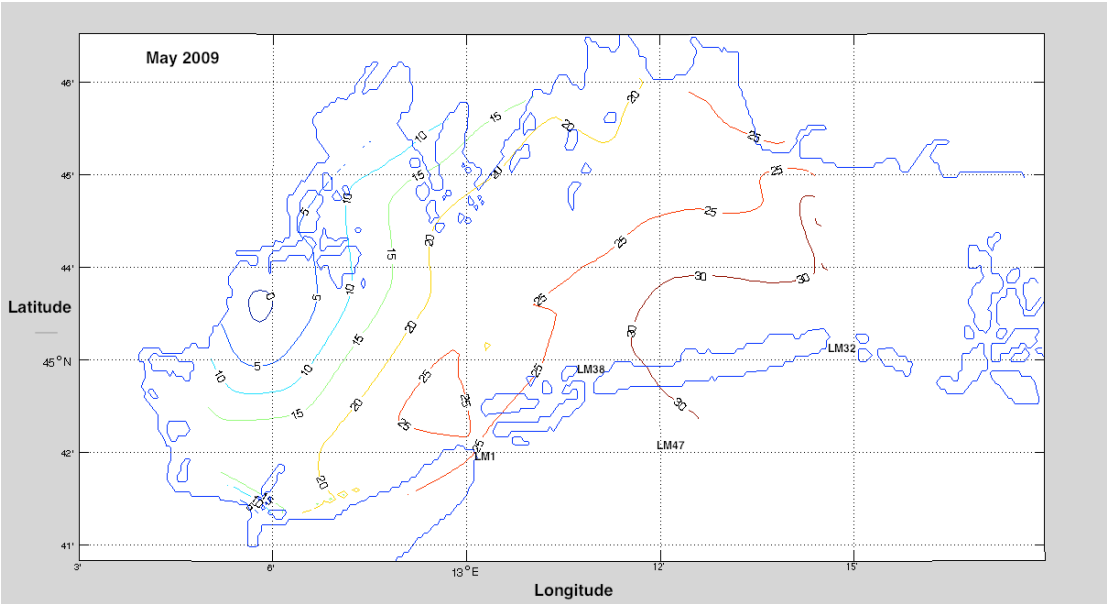

Fig 3.10. *Salinity (in PSU) during the spring sampling campaign.*

In the lagoon area the salinity is increasing with the distance from the river mouths (fig. 3.10). It is worth noting that the western part of the lagoon shows a lower salinity compared to the eastern side, due to the input of the rivers Stella, Turgnano and Cormor but also due to water circulation in northern Adriatic Sea (flowing east to west, according to Frascari et al., 1988).
Such observation is confirmed by the recent study of Ferrarin et al. (2010), who found that the coastal seawater would enter into the Marano lagoon through the Buso inlet (site LM32, which is indicated in fig. 3.10) and leave the lagoon through the S. Andrea inlet (site LM38, see fig. 3.10) and the Lignano inlet (site LM1). According to the authors, the limited water depth causes the lagoon to be strongly influenced by

both the action of the local NE wind called Bora and tidal forcing. The reader is referred to Map 3 in Appendix 1 for the modeling of water circulation in the Marano lagoon, which shows the residual currents of the area (from Ferrarin et al., 2010).
The mean nitrate distribution in the lagoon over the year (fig. 3.11, from Saccon et al., 2011) is similar to the salinity gradient shown in fig. 3.10, suggesting that the major nitrate source in the lagoon derives from riverine inputs.

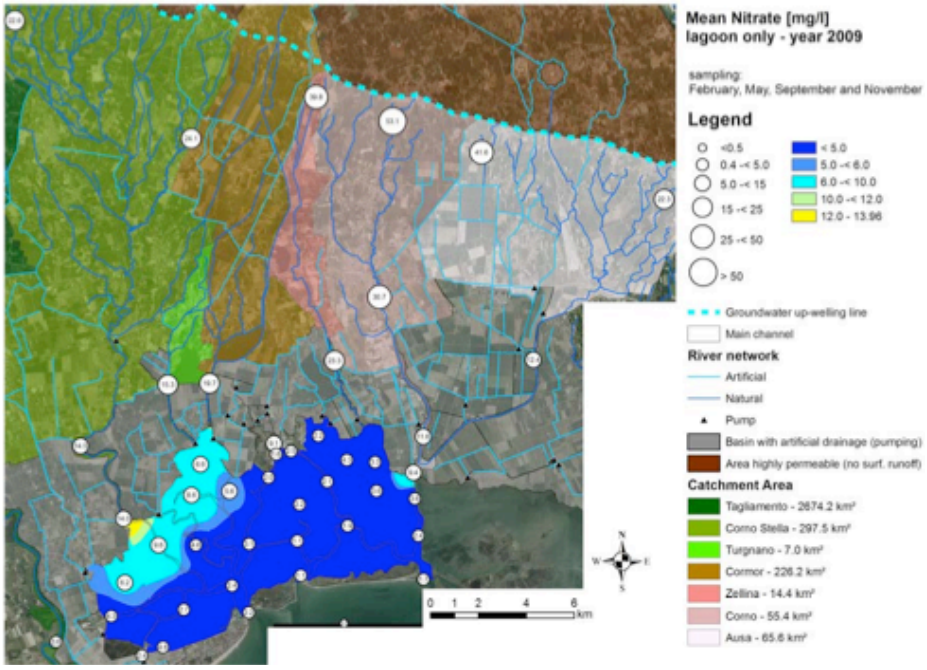

Fig. 3.11. *Mean nitrate concentration considering the period February 2009-November 2009.*

As a first approximation, the nitrate atmospheric input to the lagoon will be excluded in the present discussion and the hypothesis of a simple mixing of two nitrate sources (one due to riverine inputs and the other from coastal seawater) will be evaluated. The assessment of the relative importance of atmospheric nitrate over the other external inputs, based on the analyses of the nitrate isotope anomaly, will be the main topic of section 3.2.
The nitrate $\delta^{15}N$ measurements from the catchments area samples (green crosses in fig. 3.7) would indicate that there is a high degree of homogeneity. This observation would suggest the presence of a major nitrate source in the lagoon with a distinctive $\delta^{15}N$ of 5.6‰ associated with the riverine input, which is about 1‰ lower than the average nitrogen delta value that has been found in the lagoon.
To identify the isotopic composition of the potential nitrate source from coastal seawater, the data points concerning the sampling sites where salinity is closer to open sea (sampling site 47) are taken into account.

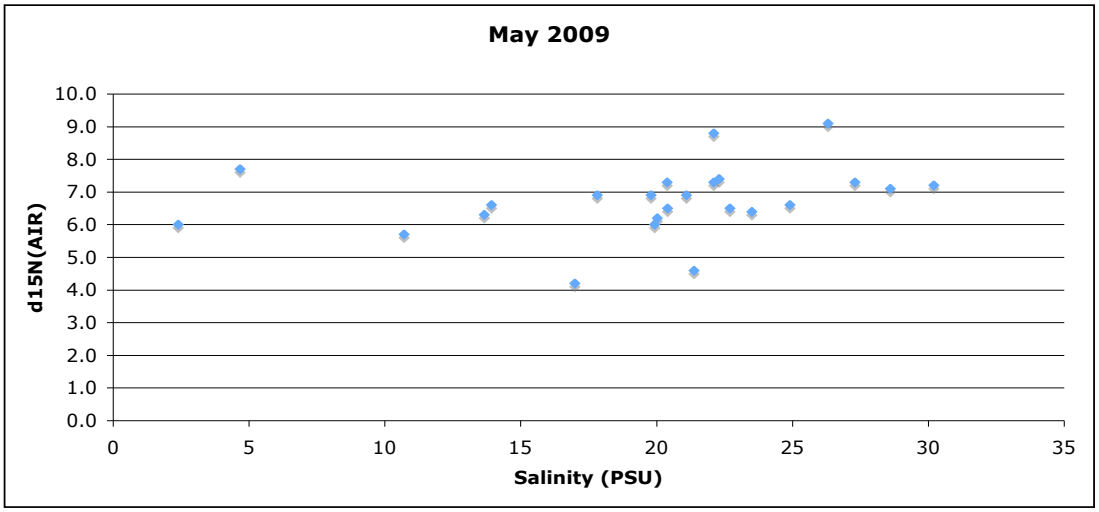

Fig. 3.12. *$\delta^{15}N$‰ (AIR) after the spring campaign as a function of salinity.*

The three data points corresponding to the measured samples with the highest salinity within the lagoon subset have a distinctive $\delta^{15}N$(AIR) of 7‰ (fig. 3.12). As discussed in Chapter 2, the analytical uncertainties on the nitrogen delta values are 0.3‰.
If we assumed that the nitrogen delta values in the lagoon are mainly due to mixing of two nitrate sources only, because of the small difference in the averaged isotopic composition of the two end-members (5.6‰ vs. 7‰), a higher homogeneity and a clearer increasing trend with salinity should be expected in the $\delta^{15}N$ presented in fig. 3.12.
Consequently, the nitrogen delta values in fig. 3.7 might suggest that the lagoon area can be regarded as a heterogeneous system with some nitrate sinks and/or sources due to local processes that are not affected by seasonal variations (fig. 3.5) but which do modify the isotopic signature.
This observation is confirmed when showing the nitrate concentration as a function of salinity (fig. 3.13).

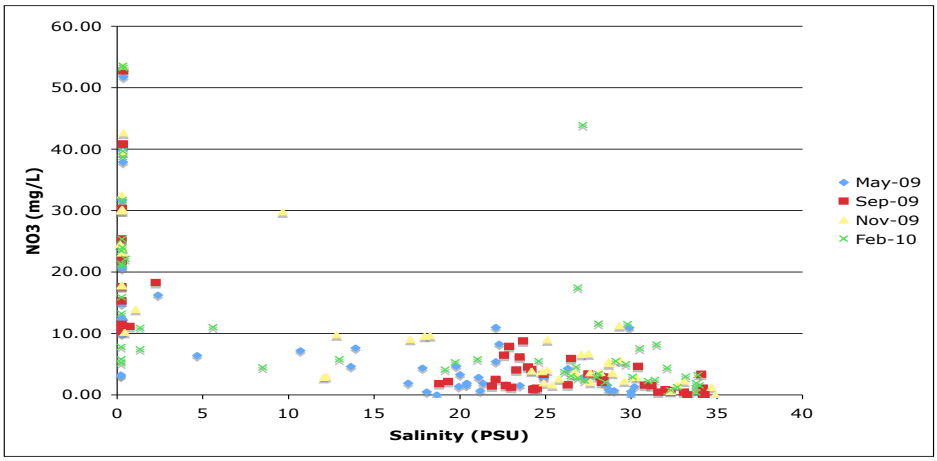

Fig. 3.13. *The nitrate concentration in the whole area as a function of salinity during the entire sampling campaign.*

Excluding the data concerning the groundwater samples (the freshwater samples with the highest nitrate concentration range), results in fig. 3.13 indicate that there is still no linear relationship between the nitrate concentration and salinity and that nitrate within the lagoon is kept in the range 1-11mg NO_3/L, regardless of salinity.
The nitrate concentration at the sampling site with ID 47 (see fig. 3.10), in the open sea area, has been found to be always lower than 1.1mg NO_3/L. Comparison of fig.3.13 with the mapped data on salinity in May 2009 (fig. 3.10) would suggest that there could be local sinks in the vicinity of river mouths, but also some nitrate sources where the salinity is comparable with the open sea.
Fig. 3.14 shows the nitrate N isotopic composition at the Marano lagoon in May 2009.

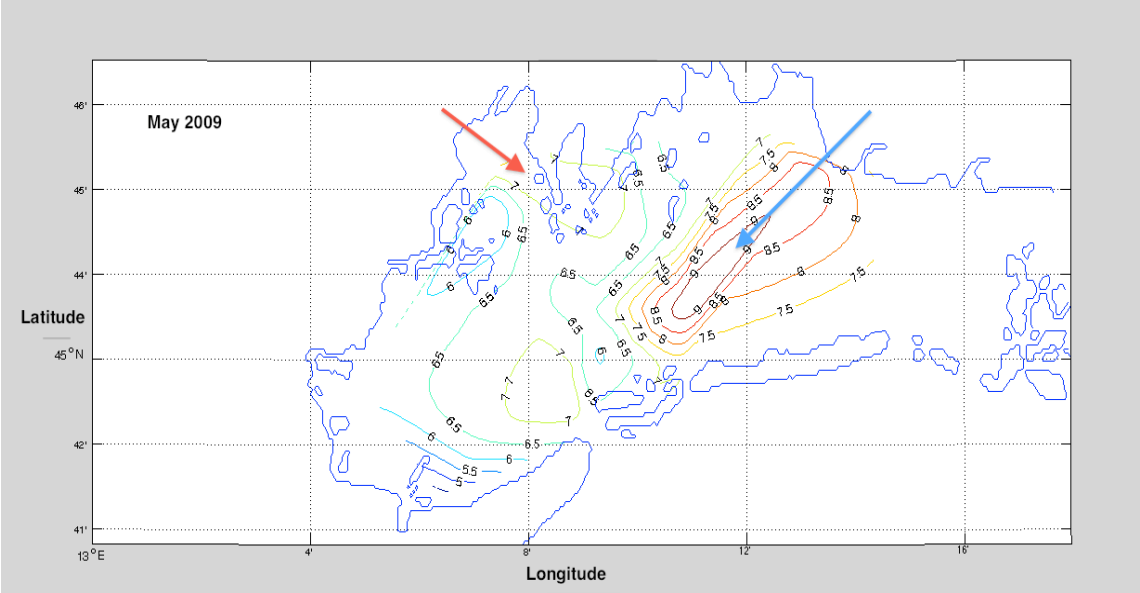

Fig. 3.14. *$\delta^{15}N$‰(AIR) distribution at the Marano lagoon in May 2009*

Assimilation and denitrification are potential local processes occurring in the lagoon and acting as a nitrate sink.
Assimilation of nitrate can be traced with the isotopic composition of both nitrate N and O, due to the tendency of fractionating in a similar way (i.e. $^{15}\varepsilon/^{18}\varepsilon=1$), regardless of the magnitude of the isotope enrichment ε (Granger et al., 2004).
The enrichment factor ε corresponding to the isotopic fractionation α between two phases is expressed in Eq. 3.1.

$$\varepsilon = 1000(\alpha-1) \qquad \text{(Eq.3.1)}$$

It is assumed that in natural environments the nitrate isotopic composition during assimilation follows the `Rayleigh equation (Eq.2.13).
Unfortunately, as discussed in chapter 2, the method used to measure the sample isotope anomaly does not have a good precision in measured $\delta^{18}O$. Thus, only $\delta^{15}N$ and $\Delta^{17}O$ data can be used.
As a consequence, it is not possible to evaluate the chance of assimilation within the lagoon based on the N isotopic measurements only. This is because the nitrate N

isotopic enrichment due to assimilation is rather variable, ranging from 5.6 to 20.4‰ (Granger et al., 2004).
A study showing the cells distribution and the overall biomass in the lagoon has been recently published (Facca and Sfriso, 2009) (see the biomass distribution at the Marano and Grado lagoon, which is presented in fig. 3.15). Phytoplankton distribution was estimated as cell abundance using the Utermöhl's method and the carbon content (biomass) was evaluated as a function of cell sizes by using the inverted light microscope, according to the Edler's formulation.

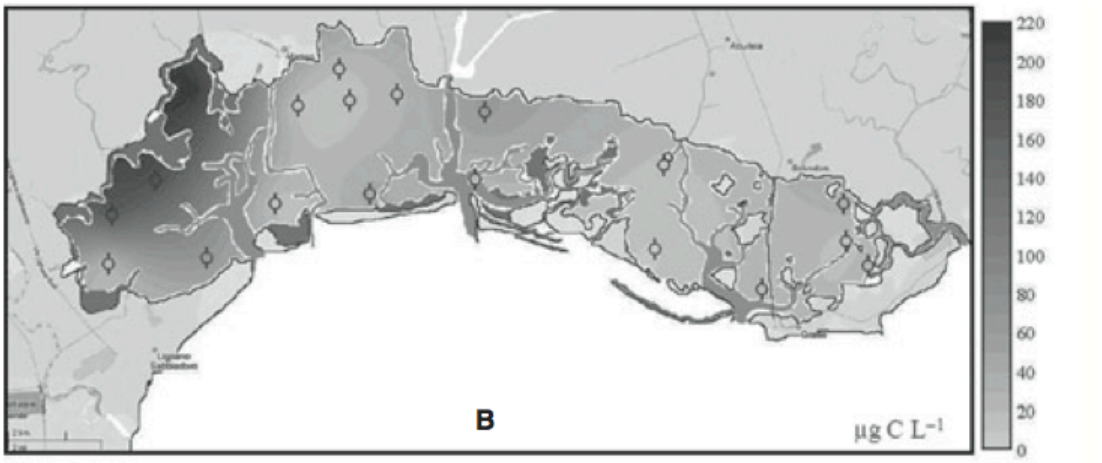

Fig. 3.15. *Biomass distribution at the Marano and Grado lagoons (µg C/ L) (from Facca and Sfriso, 2009).*

At the Marano and Grado Lagoon, cell abundances vary between 0.6 and $2.2 \cdot 10^6$ cells/L. Blooms up to $18 \cdot 10^6$ cells/L were only recorded close to the main river outflows. The blooming species were diatoms (*C. Closterium* and, to a minor extent, *N. Frustulum)*.
Photosynthesis rates are expected to be higher where more nutrients are available for biomass growth. Light should not be a limiting factor, owing to the moderate water depth in the whole lagoon area. The P gradient is similar to the nitrate distribution, suggesting that rivers are also the main source of phosphorus in the lagoon (compare fig.3.16 with fig. 3.11).

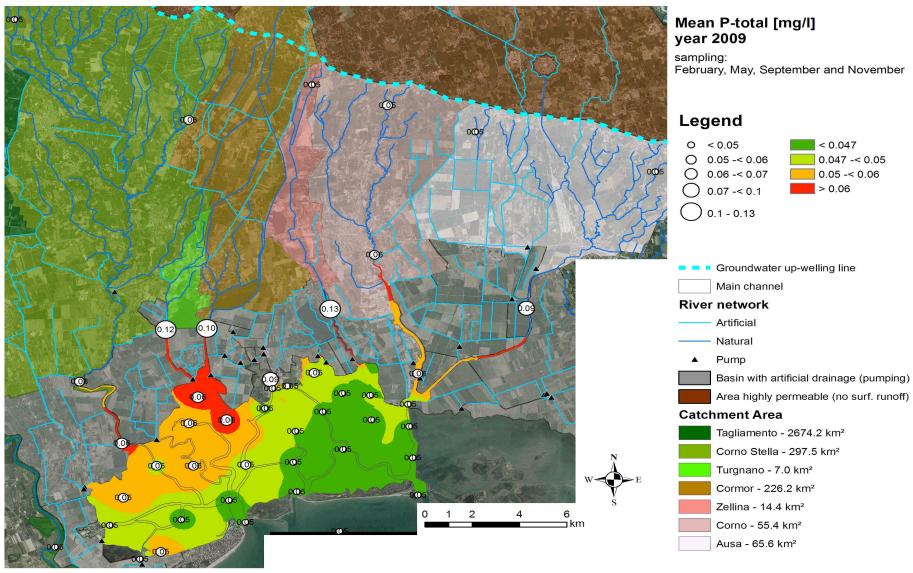

Fig. 3.16. *Mean total phosphorus at the Marano lagoon in 2009 (from Saccon et al., 2011).*

The region emphasized with a red arrow in fig. 3.14 could be a region of photosynthetic assimilation due to it being the vicinity of nutrients inputs (N and P) from two rivers, high cell density and local low residual currents (see Map 3 in Appendix 1), which increases the nutrients resident time and cell dispersion.
In fact, the ratio N/P in the mouths of the rivers Turgnano and Stella is one order of magnitude higher than the Redfield ratio (the molecular ratio N:P in plankton, which is an indicator of which nutrient is a limiting factor for assimilation).
Therefore, due to the limited availability of phosphorus, only low assimilation rates are possible, which fact could explain the small difference of 1‰ between average nitrate $\delta^{15}N$ in freshwater and the measured $\delta^{15}N$ nearby the mouth of Turgnano and Cormor rivers.
Overall, because of the limited gradient in P concentrations within the lagoon and given that P is more likely to be limiting than nitrate, it seems that photosynthetic nitrate uptake is unlikely to be the dominant nitrate removal mechanism in the lagoon.
Thus, other sink processes must occur to take into account the drop of the nitrate concentration from 8mg/L at the rivers mouth to the 2 mg/L in the center of the lagoon.
Denitrification in the water column is excluded due to the oxygen levels in the lagoon (Saccon, personal communication). In addition, high denitrification rates would result in high nitrogen delta values, which have not been found in the whole lagoonal area. However, denitrification in the lagoon might occur in the sediments.
Denitrification in the sediments (benthic denitrification) of the Seine River results in lower isotope enrichment of the remaining nitrate pool compared to denitrification in the water column (riparian denitrification)(fig. 3.17, from Sebilo et al., 2002).

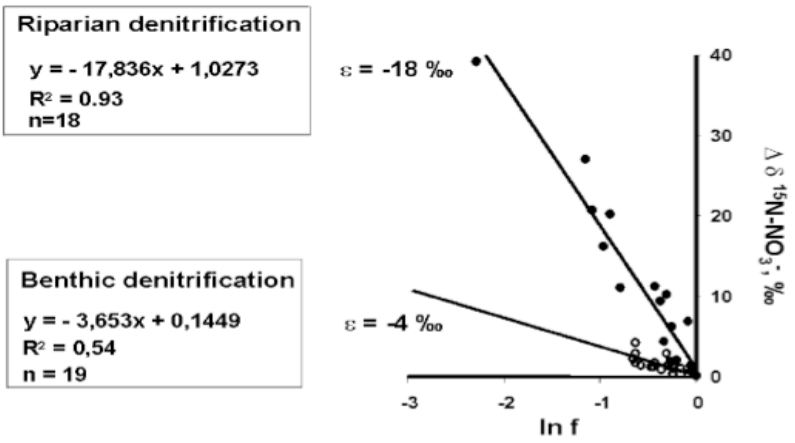

Fig. 3.17. *Isotopic enrichment factor of $\delta^{15}NO_3$−-N (ε‰) during riparian and benthic denitrification (from Sebilo et al., 2002).*

This is due to the low nitrate availability in the sediments, which causes diffusion being the limiting step of the nitrate uptake (Sigman et al., 2003)(Sebilo et al., 2002). A similar difference has also been found in the seawater of the Santa Barbara Basin, Caifornia (Sigman et al., 2003). The authors suggested that almost no nitrate fractionation would occur due to denitrification within the seabed.

Therefore, it is expected that any denitrification in the sediments at the Marano lagoon would generate from null to moderate changes in $\delta^{15}N$, which is consistent with the small range observed in the measured nitrogen delta values.

It is important to underline that pollution at the Marano lagoon is particularly elevated. According to Covelli et al. (2009), an amount of 186.000 kg of Hg was deliberately discharged into the main drainage system (the Ausa–Corno River, whose mouth is sampling site LM27) from 1940s to 1984 by a chlor-alkali plant.

Also, the lagoon has experienced a secondary long-term Hg input, originated from mining activity for cinnabar extraction (HgS) in Idrija (Slovenia). As a result, exceptionally high Hg concentration is found in sediments (Covelli et al., 2009).

Mercury within the lagoon is mainly present as cinnabar (HgS) and as bioavailable MeHg (methylmercury). A work that comprised the Grado Lagoon suggested that sulphate-reducing bacteria caused the methylation of mercury in anoxic conditions. Most of the bacterial methylation should be generated within the sediments (Emili et al., 2011). The change in Hg speciation has increased the level of toxicity of the pollutant.

In Map 4 and Map 5 of Appendix 1, the lagoonal distribution of Hg, Cd, Cr, Pb, Cu, and Ni are shown, from a report presented in 2007 from the Regional Agency for the Environment Protection of Friuli Venezia Giulia. The effect of arsenic (especially nearby the Lignano inlet) on metabolic processes has been recently investigated in a PhD thesis (De Pol, 2009).

Denitrification rates should be affected by the presence of heavy metals, resulting in either an increase or a decrease of N_2O production, depending on the type of pollutant (Tedesco and Jacinthe, 2009)(Twining et al., 2007)(Magalhaes et al., 2007).

The tests described in section 2.8 underlined that copper at extremely high concentration could generate a distinctive nitrate isotope fractionation and an isotope anomaly during denitrification by *Pseudomonas aureofaciens*. Further laboratory tests should clarify how heavy metals would affect the isotopic signature of most

biological processes concerning the nitrogen cycle and what is the threshold in the pollutant concentration after which a deviation from expected nitrate N and O delta values is possible.
Moreover, other inputs, including organic matter (fig. 3.15), may well stimulate reducing conditions in the sediments and thereby encourage denitrification.
The nitrate distribution in the lagoon during the spring sampling campaign is presented in fig. 3.18.

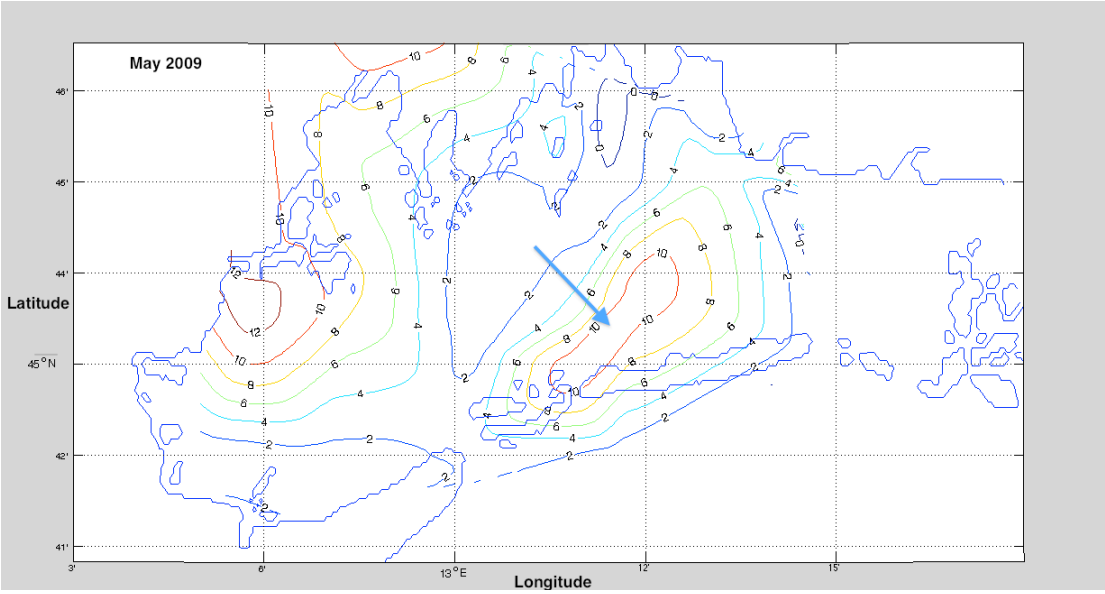

Fig. 3.18. *Nitrate distribution in the lagoonal area in May 2009.*

The highest nitrate concentration in the lagoon is nearby the river mouth of Corno Stella. The results in fig. 3.18 can be compared with the mapped data on salinity in fig. 3.10, showing that the river Corno Stella is the most important source of nitrate from freshwater.
The second peak in the nitrate concentrations (blue arrow in fig. 3.18) corresponds to the area with the highest nitrate N delta values (blue arrow in fig. 3.14).
According to the bathymetry chart (see Appendix 1), the local region of high nitrate concentration is along the second most important channel of the lagoon.
Nitrification and remineralization of degraded organic matter, which is present as particulate organic matter (POM) and dissolved organic matter (DON), are the potential processes that could generate this local nitrate source.
Remineralization is assumed to yield nitrate with the $\delta^{15}N$ of sinking organic matter (Sigman et al., 2009). The phytoplankton in an estuarine environment could have a nitrogen isotope composition ranging from +6 to +11‰ (Peterson and Howarth, 1987). The range is similar to the isotopic composition of marine phytoplankton (Cloern et al., 2002). Nakatsuka et al. (1992) calculated that POM during a phytoplankton bloom in Saanich Inlet (British Columbia), when the nitrate assimilated has a nitrogen isotopic composition of 5‰, should have nitrogen delta values varying from 6 to 9‰. Thus, the local nitrate source at the Marano lagoon could be due to remineralization of phytoplankton.
High nitrification rates might be shown by the nitrite and ammonium distribution in the lagoon (fig. 3.19 and fig. 3.20, both from Saccon et al., 2011).

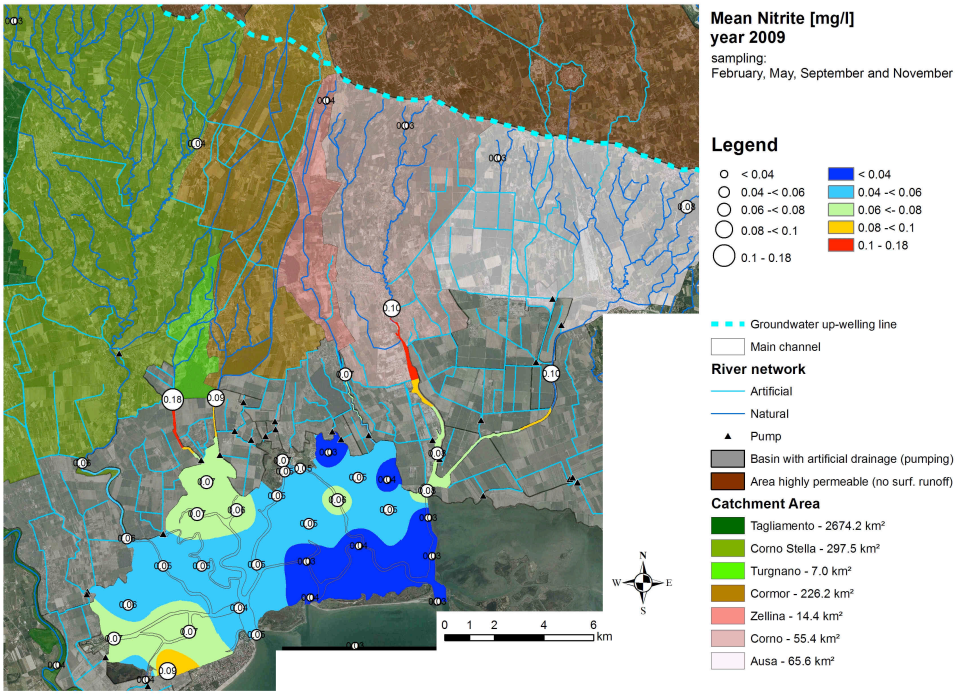

Fig. 3.19. *Mean nitrite distribution at the Marano lagoon in 2009 (from Saccon et al. 2011).*

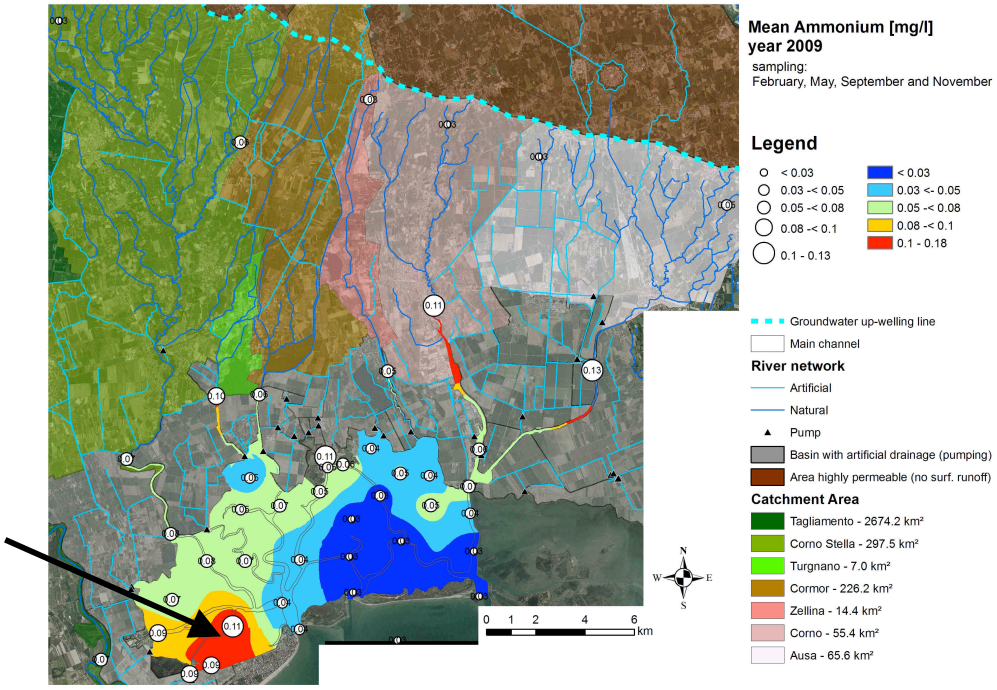

Fig. 3.20. *Mean ammonium distribution at the Marano lagoon in 2009 (from Saccon et al. 2011).*

The lagoon area close to the town Lignano Sabbiadoro, which marked with a black arrow in fig. 3.20, has a high ammonium concentration, suggesting the chance of nitrification.
This nitrate peak is partially produced locally, either due to biological processes or associated to waste treatments in the populated area of Lignano Sabbiadoro, since the concentrations of the species are higher compared to local freshwater from the Tagliamento River (sampling site LM40)
Ammonium might derive from the sewage of the populated area of Lignano Sabbiadoro. It is known that there is the chance of nitrite and nitrate build-up in activated sludges (Turk and Mavinic, 1989)(Randall and Buth, 1984)(Corredor and Morell, 1994). However, nitrite is also an intermediate species during both nitrification and denitrification. Denitrification in the water column of that area is excluded, due to aerobic conditions (Saccon, personal communication).
Nitrification in a shallow coastal environment (Ise Bay, Japan) produces a nitrogen isotope enrichment of -24.5‰ in the nitrate (Sugimoto et al., 2008). Unfortunately, no measurements of ammonium $\delta^{15}N$ at the Marano lagoon have been undertaken. Thus, it is no possible to identify the chance of local nitrification based on the difference in the isotopic composition of nitrate and its potential substrate.
It is important to point out that measured nitrate $\delta^{15}N$ nearby Lignano Sabbiadoro are in the range of nitrate from sewage (Rogers, 2003)(Tucker et al., 1999)(Cifuentes et al., 1988). Hence, there is the possibility that ammonium, nitrite and nitrate nearby Lignano Sabbiadoro are all byproducts of local sewage treatments.
The results concerning the summer campaign are now discussed and compared with the data related to the spring campaign.
Before the summer sampling campaign, which lasted from the 1st to the 4th of September, the weather was particularly dry, due to the lack of rainfall and because of exceptionally high temperatures (the local meteorological conditions are explained in details in section 3.2).
In August 2009 the monthly highest temperature for the period 1999-2011 was reported. Furthermore, for 16 days the temperature was above 30ºC, which is higher than the average period of 9 days (from 1999 to 2011).
The dry conditions caused high evaporation rates, evidenced by an overall increase of salinity within the lagoon (fig. 3.21).

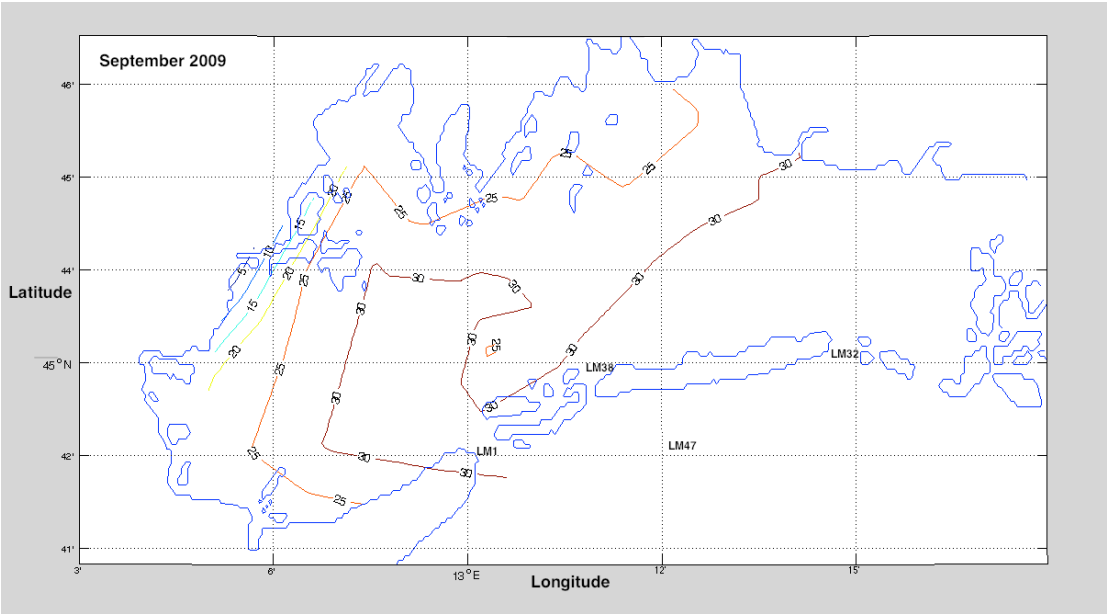

Fig. 3.21. *Salinity (in PSU) during the summer sampling campaign.*

The nitrate concentration in the Adriatic Sea (sampling site LM47, see fig. 3.21) in September has been found to be 1mg/L. The area corresponding to 1mg NO_3/L (green arrow in fig.3.22) perfectly matches the water with a salinity of 30psu, suggesting a change in the water circulation with a novel input of coastal seawater from Lignano inlet (site LM1) and, possibly, from S. Andrea inlet (site LM38).

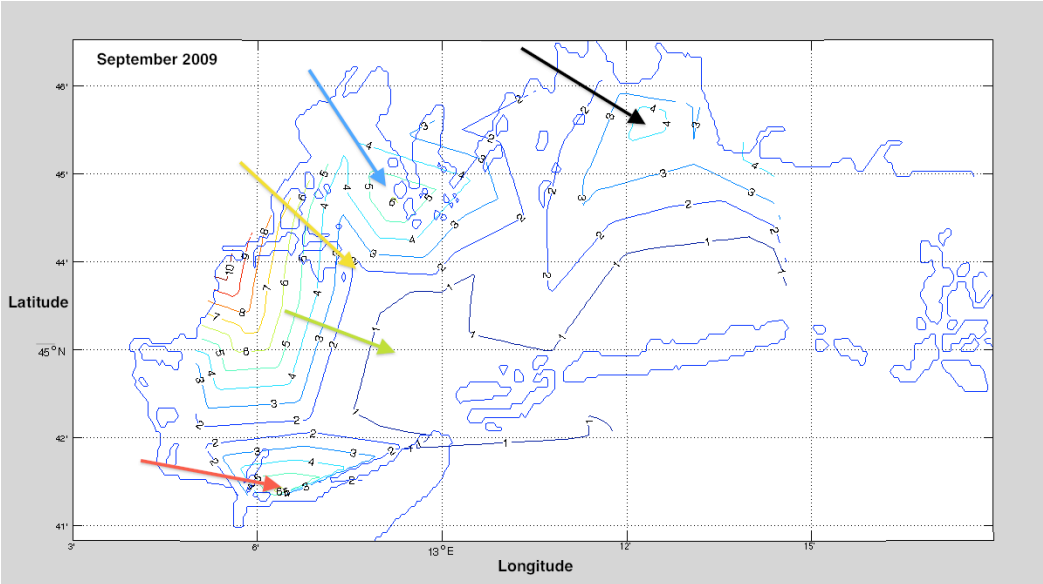

Fig. 3.22. *Nitrate distribution in the lagoonal area in September 2009.*

The local nitrate source along the second channel disappeared, but two spots of high nitrate concentration, emphasized with a black and a blue arrow in fig. 3.22, are found where residual currents are usually minimal (Ferrarin et al., 2010, see Appendix 1). This could be due to the change of direction of water masses.

Moreover, the yellow arrow in fig. 3.22 indicates that the entrance of saline water split in two distinct regions the nitrate input from the rivers (compare the nitrate distribution in the region with the salinity gradient in fig. 3.21).
The spot of high nitrate marked with a black arrow in Fig. 3.22 might be some residual nitrate from the second channel, possibly dislocated by seawater input from the western lagoon inlets.
Interestingly, along the populated area of Lignano Sabbiadoro (red arrow in fig. 3.22) the local nitrate concentration is significantly higher in the lagoon than in the Tagliamento River (which is 1.8mg NO_3/L, sampling site LM40).
Furthermore, the nitrate N isotope fractionation has not changed (fig. 3.23), consistent with the suggestion that the local nitrate source has an isotopic signature that can be related to sewage treatments.

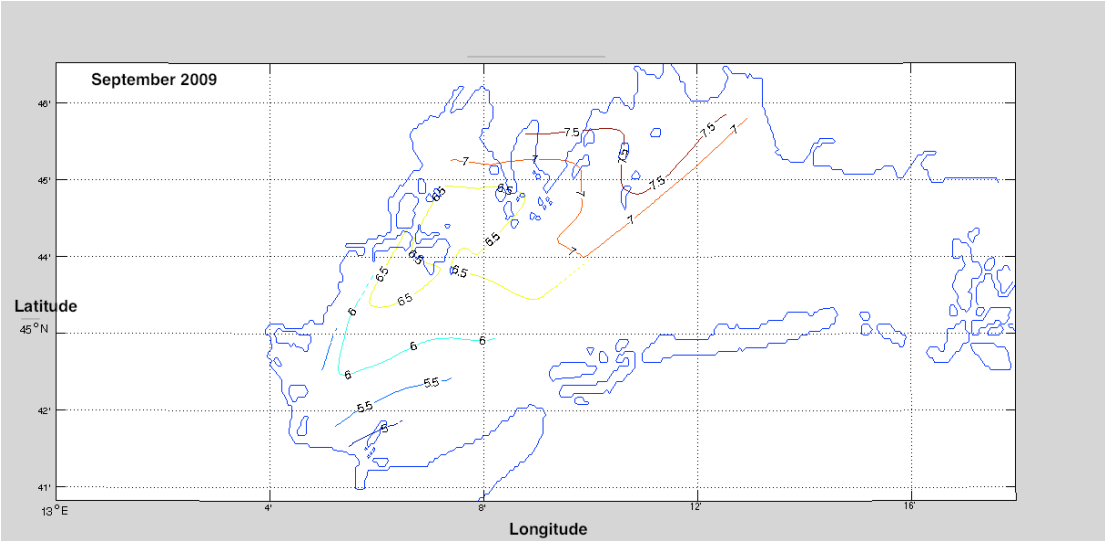

Fig 3.23. *δ^{15}N‰(AIR) distribution at the Marano lagoon in September 2009*

The region where the nitrate N delta values are roughly 1-1.5‰ higher compared to measurements from the lagoonal area affected by riverine inputs corresponds to a zone with a peak in the nitrate concentrations (see black arrow in fig. 3.22).
Similarly to the findings concerning the second channel of the lagoon (blue arrow in fig. 3.18), the correlation between ^{15}N enrichment and nitrate concentration might be due to partial remineralization of organic matter.
To sum up, a combination of assimilation and denitrification in the sediments are necessary to take into account the biomass distribution and the similar gradient of nitrate and phosphorus in the lagoon over the year, associated with no substantial nitrate N isotope fractionation. Denitrification is probably enhanced due to both the presence of organic matter and the exceptional level of pollutants in the sediments.
In May, a local nitrate source with the isotopic signature of phytoplankton has been found in the second most important channel of the lagoon, probably due to remineralization of degraded organic matter. Another local nitrate source, nearby Lignano Sabbiadoro, and associated with the highest peaks of ammonium and nitrite in the lagoon, could be a byproduct of local sewage treatments.
In September higher evaporation rates caused the entrance of seawater from the western inlet, which redistributed the nitrate in the lagoon.

Overall, the gradient of nitrate N delta values in the lagoon is very small, suggesting that the system is rather complex and that, more likely, a combination of factors influences the local nitrate cycling of the area.
The results presented so far show the necessity of combining different approaches. Ideally, the nitrate isotopic measurements should be coupled not only with chemical analyses, but also with the study of the food chain of the system, to be able to identify the isotope fractionation associated with local biological processes.
The remaining discussion will be focused on the use of the isotope anomaly, to evaluate the atmospheric nitrate content in sample water.

3.2 Assessing the contribution of the atmosphere as a nitrate source in the Marano lagoon with the nitrate MIF signature.

The nitrate isotope anomaly in the atmosphere is generated by ozone oxidation of NOx. There are several pathways leading to the formation of atmospheric nitrate, and their relative importance over the year would generate a seasonal trend in the MIF signature, as it has been discussed in chapter 1.
It is possible to calculate the relative importance of the atmospheric input in a nitrate containing pool by considering the potential sources of a nitrate isotope anomaly (Eq.3.1).

$$\Delta^{17}(O)_{sample} = a\,\Delta^{17}(O)_{atm} + b\,\Delta^{17}(O)_{ext} + c\,\Delta^{17}(O)_{int} \qquad \text{(Eq.3.1)}$$

The letters a, b and c of Eq. 3.1 follow the requirement a+b+c=1 and define the contribution of the MIF signal in the lagoon from the atmosphere, other external and internal nitrate sources, respectively. The nitrate isotope anomaly found in some nitrate minerals (see Chapter 4) and during the copper tests (see section 2.8) would indicate that b and c in Eq.3.1 might not be always null.
Assuming as a first approximation that the atmosphere is the only source of the tracer (i.e. b and c are equal to zero, a is equal to 1), the atmospheric contribution is easily calculated with Eq.3.2 (Michalski and Thiemens, 2006).

$$\text{Atmospheric nitrate (\%)} = \left(\frac{\Delta^{17}O_{sample}}{\Delta^{17}O_{atmosphere}} \right)\% \qquad \text{(Eq.3.2)}$$

The latitude influences the magnitude of seasonal variations, with the highest differences occurring at the poles. The aerosol measurements of the nitrate isotope anomaly from Michalski et al. (2003), from samples collected at La Jolla (33°N), were considered as a reference to represent the nitrate isotope anomaly of mid-latitude aerosol (fig. 3.24).

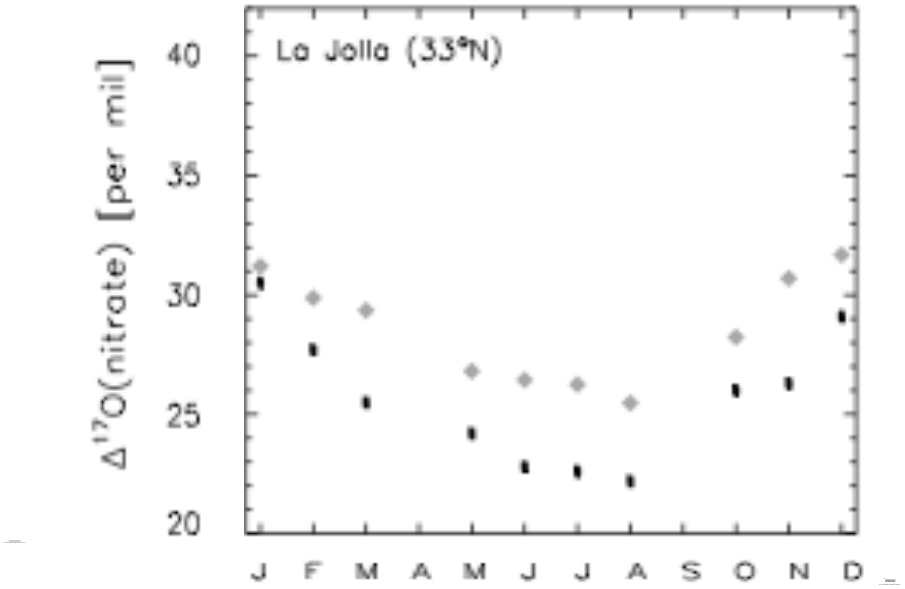

Fig. 3.24. *Chart from Alexander et al, 2009. The modeled values of the MIF signal in nitrate aerosol (grey diamonds) are compared with observations (black squares) at La Jolla (from Michalski et al., 2003).*

The evaluation of the atmospheric input in the lagoon, according to Eq. 3.1 and Eq.3.2, implies that internal sinks due to biological processes (like assimilation and denitrification) are assumed to be mass dependent.
It is generally believed that a mass dependent process fractionating a nitrate pool with a MIF signature cannot change the isotope anomaly (Tsunogai et al., 2011)(Morin et al., 2009)(Kendall et al., 2007)(Thiemens, 2006). Without this assumption, the potential of the nitrate MIF signature as a tracer will be seriously questioned.
In the following charts, the length of the error bars will represent the uncertainties in the assessment of the atmospheric input to the Marano lagoon, based on the uncertainties of the isotopic measurements of sample water only. Other sources of uncertainties will be discussed in section 3.3.
Sample measurements of the capital delta values will be discussed taking into account the meteorological conditions during the sampling campaigns.
Of the 53 data points considered, the data subset related to samples from shallow water, the lagoon inlets and the channels are discussed taking into account the data from the meteorological station in Lignano Sabbiadoro, which is close to the sampling site LM1.
The measurements concerning the winter campaign are from freshwater samples only and, due to the sampling site locations, the data from the meteorological station of Palazzolo Stella are chosen for the discussion of the atmospheric input via wet deposition. The station of Palazzolo Stella is close to the sampling site LM41.
Based on the sampling date, it is therefore possible to make a qualitative assessment of the potential of the nitrate MIF signal as a tracer of atmospheric nitrate deposition. This is because, assuming that the wet atmospheric deposition is the dominant nitrate load mechanism, it is expected that periods of dryness or nitrate inputs through rainfall should have an effect on the magnitude of the nitrate isotope anomaly in sample water.

The assumption of the relative importance of the nitrate load due to the dry deposition of HNO_3 at the Marano lagoon will influence the uncertainties in the calculation of the atmospheric nitrate content in sample water, as it will be explained in section 3.3. However, due to high precipitation rates in the region, at a first approximation the dry atmospheric deposition will be regarded as minimal. Thus, most of the nitrate deposited to the lagoon is assumed to be due to the scavenging of aerosol by rain events.

Another point to take into account is that the time over which the impact of atmospheric nitrate deposited will be seen in the mid depth water samples will depend on the occurrence of stratification or mixing in the water column. Overall, apart from the driest period in the summer, the absence of stratification and a fast vertical mixing is safely assumed, due to the moderate water depth of the lagoon (Ferrarin et al., 2010) (Saccon, personal communication).

The relationship between atmospheric nitrate deposited and precipitation rates is not easy to establish because of the lack of data on the nitrate content in rainfall. The nitrate load due to wet deposition is usually higher after a long period of dryness, because of the scavenging of aerosol that had time to accumulate nitrate from the atmospheric HNO_3 reservoir (i.e nitrate accumulation in sea-salt aerosol due to chlorine displacement) (Spokes and Jickells, 2005)(Pakkanen, 1996)(Brimblecombe and Cleggs, 1988).

Moreover, the atmosphere is not a static reservoir and abrupt changes in the gaseous nitrate concentration can often occur, depending on factors like the aerosol scavenging efficiency (which varies with the chemistry and the physical state of the atmospheric species) and air mass trajectories. Thus, when using the nitrate isotope anomaly as a tracer, ideally the analyses of the nitrate content in sample water should be coupled with the analyses of nitrate in rainwater.

As a consequence, no exact calculation will be undertaken to discuss the difference between expected and measured isotope anomaly in samples from the Marano lagoon area.

The samples from the spring campaign in 2009 were collected in the period 25^{th}-29^{th} May. It is expected that the lagoon samples collected on the 25^{th} and 26^{th} of May would have a lower anomaly. This is because rainfall during the period 10^{th} May – 26^{th} May was limited to 1mm (on the 15^{th} May). The first rain in the second part of the month occurred on the 27^{th} (17mm in 3 hours, starting from 9 am). Therefore, wet deposition could be able to increase the nitrate isotope anomaly in sample water from sites where the nitrate due to fertilizers is less important.

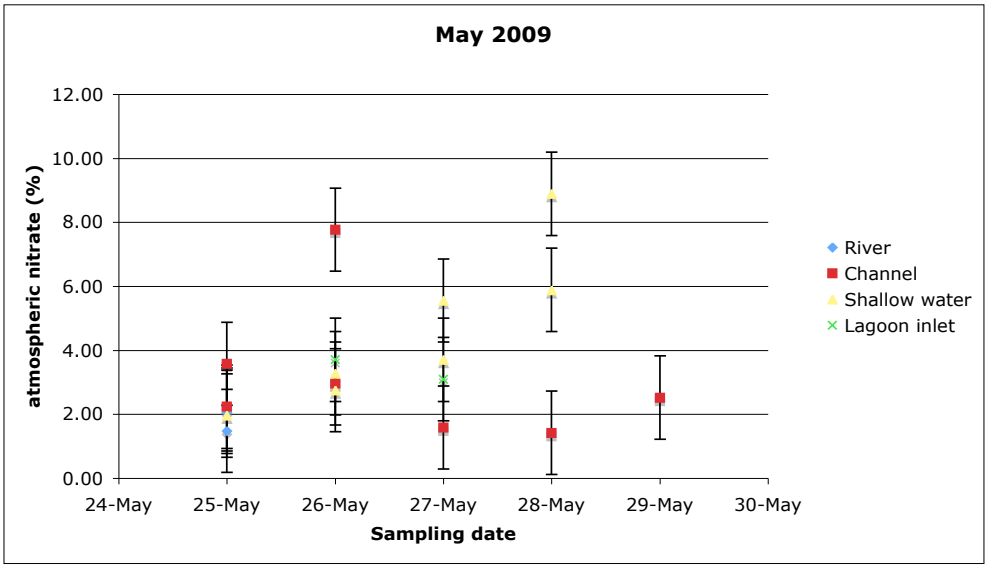

Fig. 3.25. *The atmospheric nitrate in sample water (%) grouped per sampling date during the spring sampling campaign.*

The samples from shallow water would suggest that the atmospheric input of nitrate to the Marano lagoon due to rain (calculated by using Eq.3.2) increased from roughly 3% (data points before the 27th May) to 7% (measurements after the 27th May) (fig. 3.25, the entire data set is presented in Appendix 1). On the other hand, the nitrate content along the channels does not seem to be immediately affected by meteorological conditions. This could be due to the fact that the moderate rainfall on the 27th May would contribute less on the nitrate budget within the deeper water column of the channels.

The samples from the summer campaign in 2009 were collected during the period 1st September- 4th September. Rainfall during the period 10th August – 10th September was restricted to 1mm (on the 13th August). As a result, the samples from this subset should have a lower anomaly, due to the small atmospheric inputs via wet deposition.

Interestingly, the magnitude of the isotope anomaly in the channels in September is comparable with the one that has been measured in shallow water in May (compare fig. 3.25 with fig. 3.26).

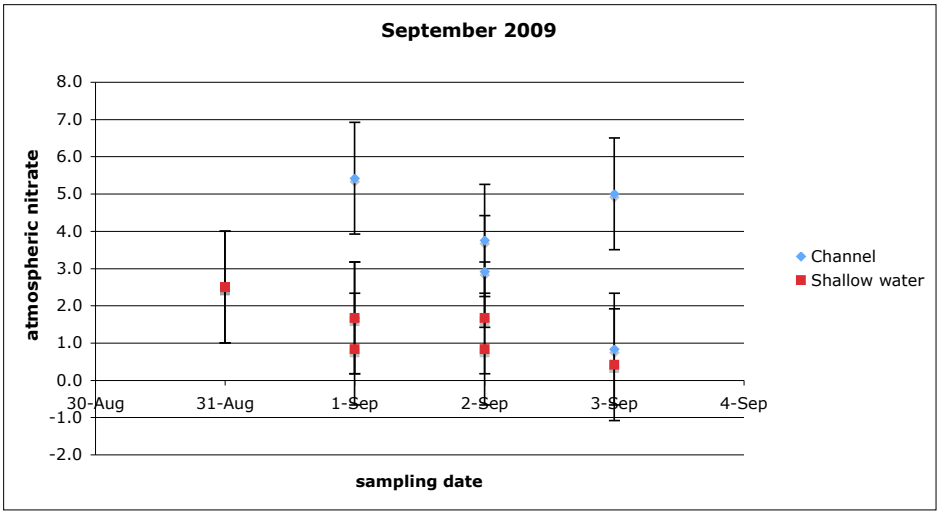

Fig 3.26. *The atmospheric in shallow water and in the channels (%) grouped per sampling date during the summer sampling campaign.*

Intuitively, if assuming that the surface water thickness is the same in the whole lagoon area, the mid depth water from the channels should be less influenced by atmospheric deposition compared to shallow water areas, due to the higher depth at which samples are collected.
However, as opposed to the expected results of the spring campaign, the samples from the channels collected during the summer campaign have a higher anomaly compared to shallow water samples.
A possible explanation is that during the summer a nitrate source or a local process seems to dilute the nitrate MIF signal in shallow water. Alternatively, a process occurring at the bottom lagoon might have generated a MIF signal that is detectable in the channels.
Nevertheless, it is important to point out that a linkage between isotope anomaly in sample water and local rainfall is not necessarily expected, unless precipitation rates are high.
The first ten days of November was the period with the highest total precipitation during 2009 with 162 mm of rain, 104 mm of which fell in 24 hours, starting from the 2nd November at 9 am.
Samples measured for the isotope anomaly were collected on the 5th of November. Therefore, due to the exceptional precipitation rates, a higher nitrate atmospheric contribution should be expected compared to the atmospheric nitrate found in the samples from the summer campaign.

	Sampling site ID	**NO_3 (mg/L)**	**Atmospheric nitrate (%)**	**Error**
Channel	LM 05	2.84	5.0	±1.4
Channel	LM 07	9.67	1.7	±1.4
Shallow water	LM 08	9.79	2.7	±1.4

Table 3.3. *The atmospheric nitrate in sample water (%) during the autumn sampling campaign.*

Again the results were contrary to expectations (see Table 3.3), since the MIF signal from the lagoon is not any higher (compare the atmospheric nitrate (%) of table 3.3 with the results referring to the dry period of the summer campaign in fig.3.26).
When comparing the results from fig. 3.25 and fig. 3.26 and table 3.3, the atmospheric nitrate in the lagoon appears to be a relatively stable parameter in the range 2-5%, regardless of the occurrence of nitrate load via wet deposition. This finding might suggest that some competitive processes could buffer the nitrate MIF signal immediately after precipitation.
This observation is more evident when comparing the data set concerning samples of the same category from different sampling campaigns in the same chart.
Because of the difference in the meteorological conditions during the summer and the autumn campaigns, it is striking that the data shows no difference (fig. 3.27) in the atmospheric contribution at sampling sites LM5 and LM8 (circled in red). Moreover, despite the dry conditions during September, the atmospheric nitrate is higher at this time of the year than in May (see sampling locations LM11 and LM17 in fig. 3.27, emphasized with blue diamonds).

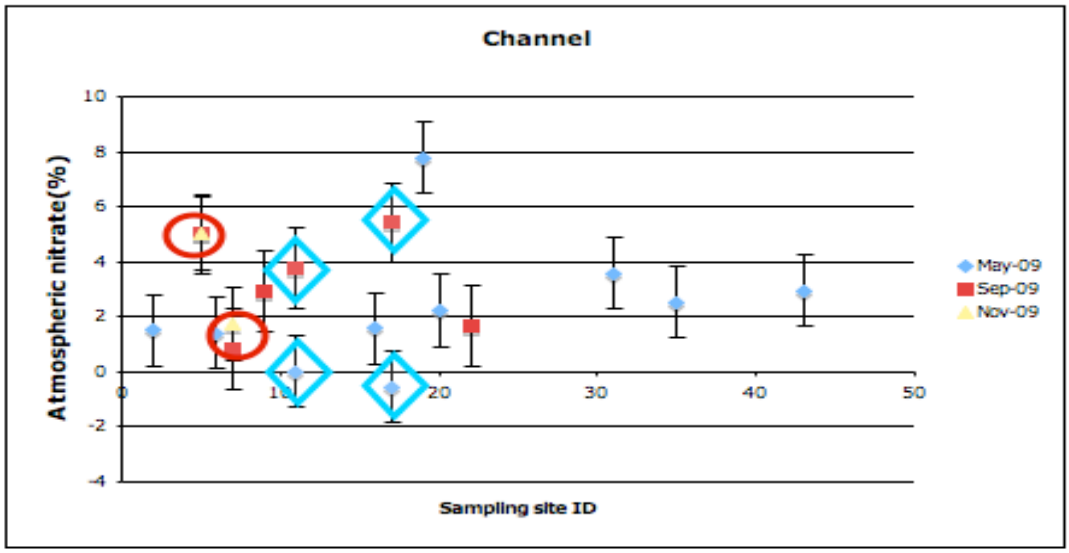

Fig. 3.27. *The atmospheric nitrate in the lagoon channels (%) during three different sampling campaigns.*

This result would question the potential of the tracer to constrain the nitrate atmospheric inputs, at least in coastal areas, where they are small compared to other nitrate inputs.
The samples from the winter campaign that were analyzed are freshwater samples only. The river samples have been collected on the 15-17th February, whilst the groundwater upwelling line samples have been sampled on the 18th February.
At the meteorological station of Palazzolo Stella, 98mm of rain fell in 72 hours, starting from 10 pm on the 17th February.
Surprisingly, a couple of samples from the groundwater upwelling line proved to have an isotope anomaly that is comparable with the one found in rivers (fig. 3.28).

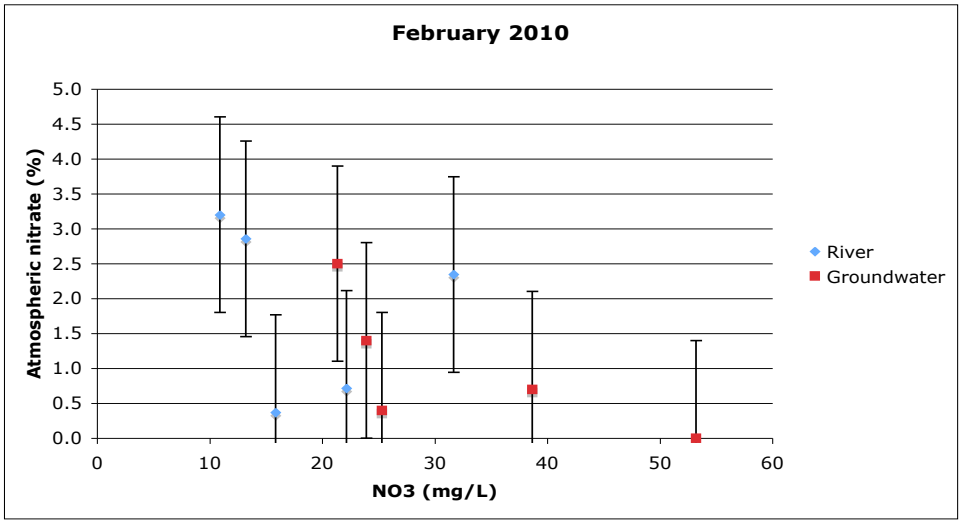

Fig. 3.28. *The atmospheric nitrate in sample in freshwater samples collected in February 2010.*

The nitrate isotope anomaly in groundwater is expected to be minimal, since nitrate should mainly derive from leaching after intense biological and chemical processes occurring in soils.

It is possible that the uncertainties on the calculation of the atmospheric nitrate (%) (according to Eq. 3.2) are affected not only by the uncertainties of the IRMS measurements of $\Delta^{17}O$ in sample water, but also on the necessary assumptions on the nitrate isotope anomaly in the atmosphere. Section 3.3 will be focused on this issue.

The salinity measurements might help to clarify some incongruence in the calculated values of the atmospheric nitrate content in sample water from the lagoon area. Because the nitrate atmospheric deposition is assumed to be the same in the whole sampling area, the magnitude of the MIF tracer is predicted to be less important in freshwater samples, where a major nitrate source due to local farming is present. Surprisingly, the expected trend is interrupted at an intermediate salinity (fig. 3.29), suggesting that either a process in the marine environment might dilute or consume the MIF signal or a local process is increasing the tracer in brackish water.

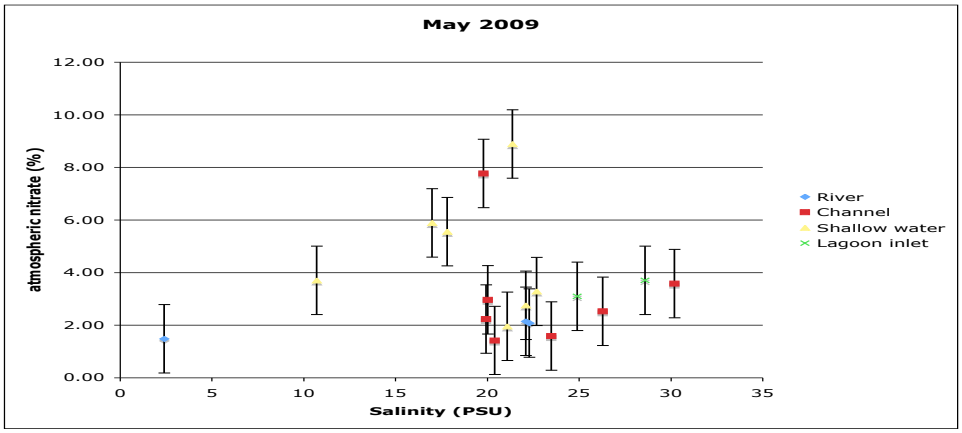

Fig. 3.29. *The atmospheric nitrate in sample water as a function of salinity (in psu).*

The nitrate isotope anomaly distribution in the lagoon exhibits three local peaks (fig. 3.30).

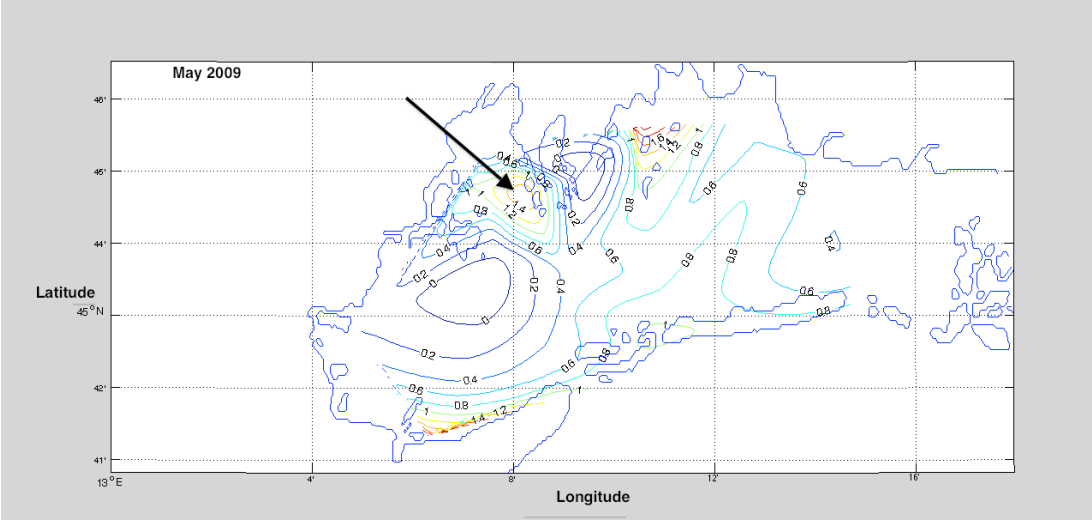

Fig. 3.30.*The nitrate isotope anomaly distribution in the lagoon in May 2009.*

The peak emphasized with a black arrow corresponds to a region with minimal currents and high cell density, where partial assimilation of nitrate and phosphorus is possible. However, because assimilation is a nitrate sink, the process shouldn't change the relative importance of atmospheric nitrate input.
It is important to point out that the highest MIF signal in a limited area is expected where the nitrate concentration has a minimum, because nitrate sinks are assumed not to change the magnitude of the tracer, whilst any nitrate source would dilute the signal.
Interestingly, the other two peaks in the isotope anomaly are in the vicinity of the towns Lignano Sabbiadoro and Marano Lagunare, the only populated areas of the lagoon.
When excluding the data points responsible for the three peaks in the nitrate isotope anomaly in the lagoonal area, which could be due to local processes associated with human activities in populated areas, the MIF signal becomes more clearly dependent on the relative importance of nitrate riverine inputs, since an increasing trend of atmospheric nitrate percentage in sample water with increasing salinity can be observed (fig. 3.31).

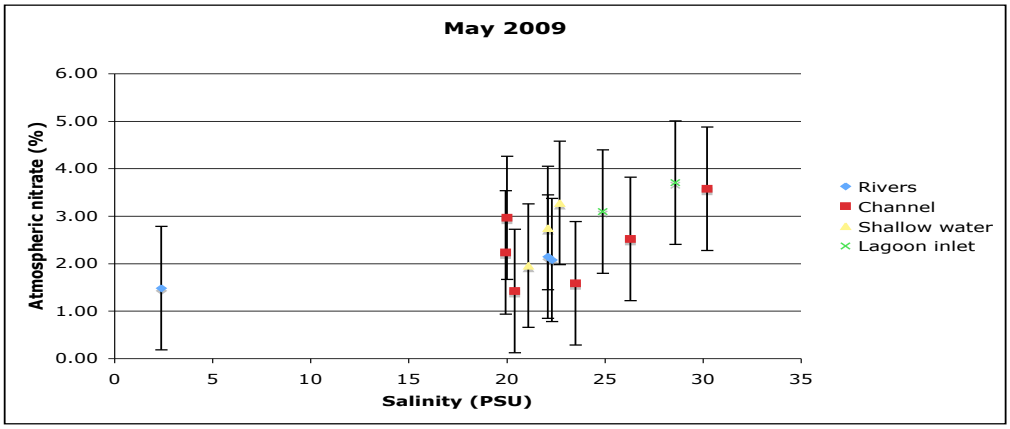

Fig. 3.31. *The atmospheric nitrate in sample water as a function of salinity (psu).*

However, the isotope anomaly increase with salinity in fig. 3.31 is rather small, probably due to the presence of a local nitrate source along the second channel (see section 3.1) diluting the MIF signal where the water is saline.
It is worth comparing the results from the spring campaign with the mapped data of the summer campaign (fig. 3.32).

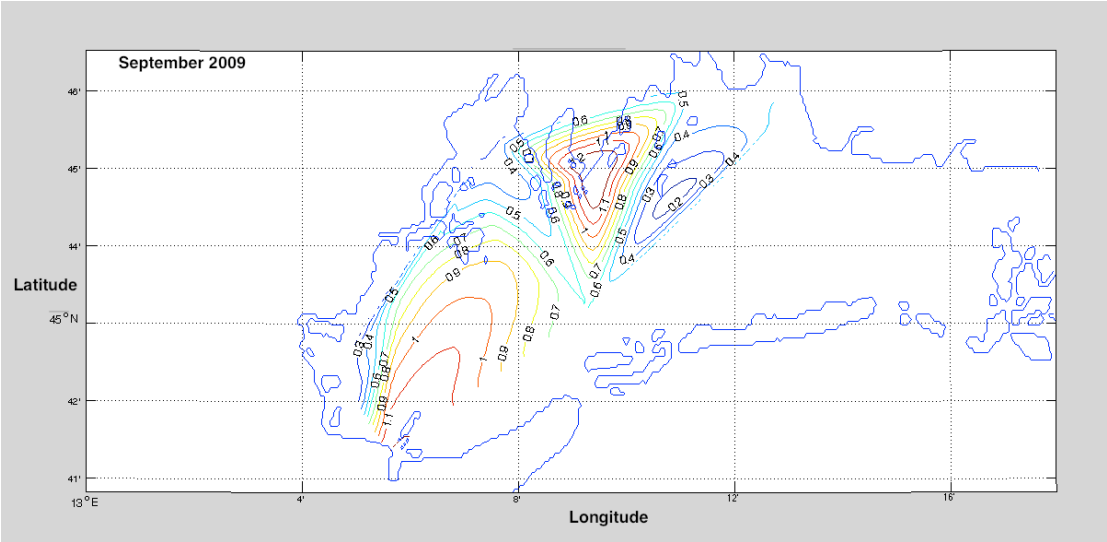

Fig. 3.32. *The nitrate isotope anomaly distribution in the lagoon in September 2009.*

During both sampling campaign, the highest isotope anomaly is found in the sites LM5, nearby the populated areas of Lignano Sabbiadoro. The region with an isotope anomaly higher than 1‰ became wider during the summer.
In this site a local source of nitrate, possibly a byproduct of local sewage treatments, was previously identified (see section 3.1). A potential explanation for the peak in the populated areas is that local sewage could have been treated with ozone and that it is possible that the ozone could generate a nitrate isotope anomaly in water.
Interestingly, a comparison with measurements (Tsunogai, 2007) in the Pacific Ocean would reveal that in the Tokyo Bay (the only orange circle of fig. 3.33) the surface

water during the summer 2006 had a higher anomaly compared to open ocean systems.

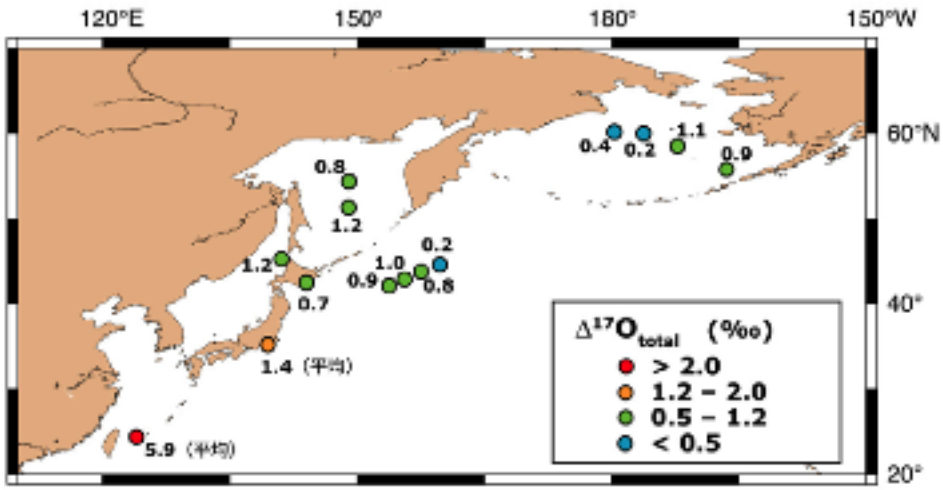

Fig. 3.33. *Nitrate MIF signal in the Pacific Ocean (Tsunogai, 2007)*

Comparison of fig. 3.32 and fig. 3.33 might indicate that the nitrate isotope anomaly in water could be associated to sewage treatments. In fact, it is surprising that the isotope anomaly in fig. 3.33 is lower when the distance from the coast increases.
The second peak of the isotope anomaly in the lagoon in September (fig. 3.32) lies in an intermediate region between the other two MIF peaks that were identified after the sampling in May (fig. 3.30).
Because only 13 samples have been measured from the subset collected in September, it is possible that the interpolation is affected by missing important points. For instance, unlike for the samples collected in May, only the site LM 17, in the western zone, is representative of the populated area of Marano lagunare. This would shift the MIF peak of the area to the western part. Thus, also the MIF peak in that region could derive from sewage treated with ozone, similarly to the site close to Lignano Sabbiadoro.
During the summer, in the area where assimilation is more likely to occur, the isotope anomaly has decreased since May from a maximum of 1.5‰ down to 0.4‰ (which is the magnitude of the uncertainties due to IRMS measurements), whilst the nitrate distribution of this restricted area has not significantly changed.
Owing to the entrance of seawater from the Lignano inlet, it is possible to hypothesize that the increase of salinity changed the nitrate O fractionation due to assimilation and/or denitrification in the sediments, affecting the local isotope anomaly.
It might be legitimate arguing that speculating on measurements at mid-water depth might not be appropriate when using the tracer, and that surface water samples should have been preferred. Because the main purpose of the project was identifying the major nitrate source in the lagoon, the contribution of atmospheric nitrate in surface water would have lead to an overestimate of the atmospheric input.
Moreover, measuring the isotope anomaly at mid-water depth would allow verifying that transport processes prevent the lagoon being a system organized in closed compartments.
As an example, it is worth comparing our results with two study cases on a lake (Michalski and Thiemens, 2006) (Tsunogai et al, 2011). In both works the nitrate

isotope anomaly has been found even in the bottom lake, which has been regarded as the proof of a good vertical mixing (fig. 3.34).

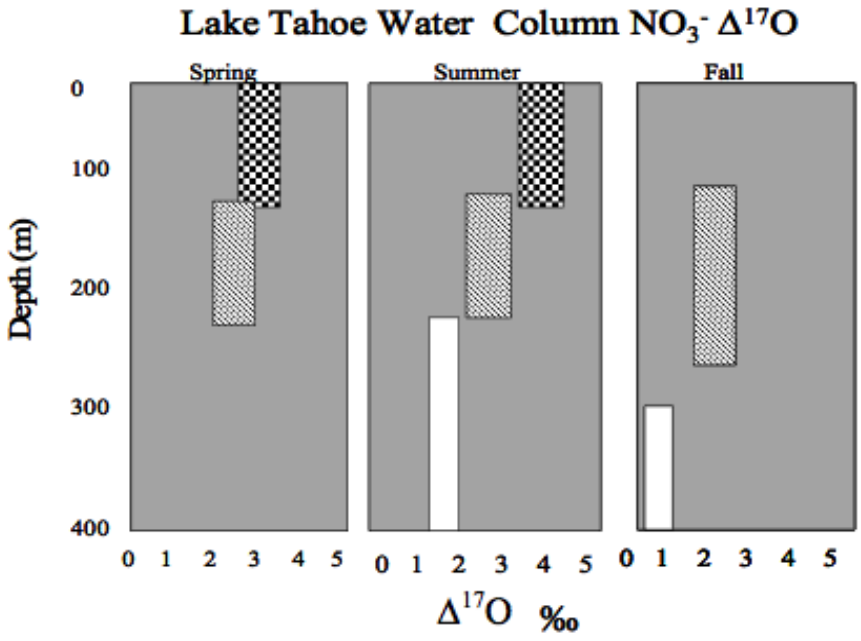

Fig. 3.34. *Vertical distribution of $\Delta^{17}O$‰ at Lake Tahoe from samples collected in 2005 (from Michalski and Thiemens, 2006). Average nitrate isotope anomaly in the water column is shown using different hatchings corresponding to three different levels (0-150m, 150-250m and 300-400m).*

Such findings would suggest that the MIF signal is a rather conservative tracer. In both studies the magnitude of the isotope anomaly at mid-water depth is comparable with the measurements discussed in the present chapter (fig. 3.34)(fig. 3.35).

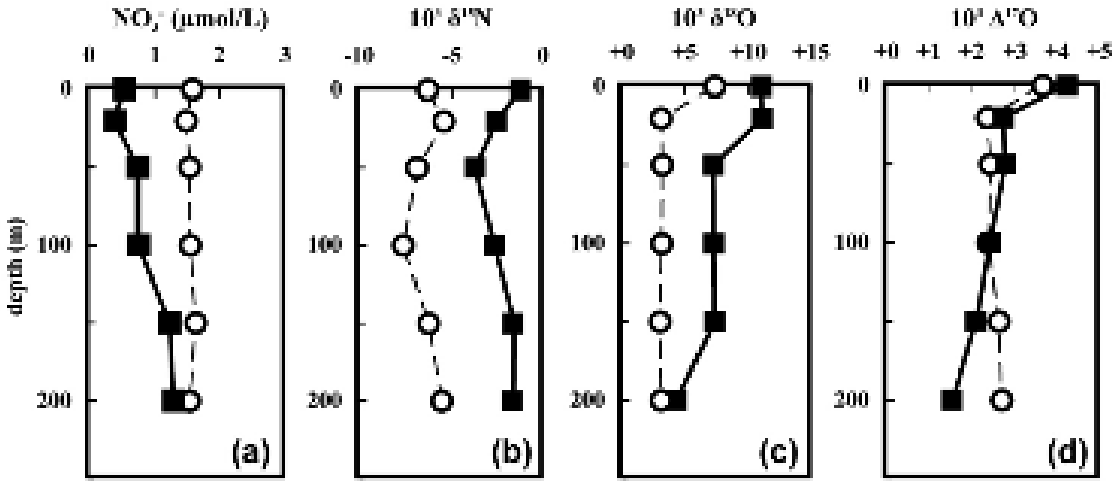

Fig. 3.35. *Vertical distribution of concentration **(a)**, $\delta^{15}N$‰ **(b)**, $\delta^{18}O$‰ **(c)**, and $\Delta^{17}O$‰ **(d)** of nitrate at Lake Mashu in June (white circle) and August (black square) 2007(from Tsunogai et al., 2011).*

The results from the bottom lake in fig. 3.35 are particularly interesting: after a period of well mixing at Lake Mashu in June 2007, the depth profiles changed in August 2007. The nitrate concentration in the water column decreased, which would suggest, according to the authors, the occurrence of a sink process that might be assimilation. This has been confirmed by considering measured nitrate N delta values.
Yet, at the bottom of the lagoon, there is almost no loss of nitrate and no fractionation of $\delta^{18}O$, whilst the capital delta dropped in two months time by more than 1‰, suggesting the chance of a process consuming molecules containing ^{17}O not in a mass-dependent way.
Denitrification has been excluded by the authors because nitrite concentration was below the detection limit. However nitrite is a reactive intermediate and, since the detection limit was a ratio NO_2/NO_3 of 10%, denitrification should not have been excluded a priori, especially because of the lack of data concerning ammonium in the water column.
Whatever the process at the bottom of Lake Mashu is, the profiles shown in fig. 3.35 would suggest that the isotope anomaly might be consumed. Alternatively, a negative anomaly could be produced in the colder months or a positive anomaly could be generated during the summer.
Similarly to the measurements of the Marano lagoon samples, at Lake Tahoe (fig. 3.34) the highest anomaly in surface and mid depth water was detected in August when, due to low precipitation rates, the main atmospheric nitrate load, via wet deposition, should be less important.
To sum up, the spatial distribution and the temporal trend of the MIF signal in the lagoon does not seem to be effectively correlated with the nitrate load via wet deposition. It could be expected that moderate rainfall would not generate a measurable increase of the isotope anomaly in sample water. Yet, because of the limited water depth of the lagoon, it is surprising that the MIF signal in November, when 10cm of rain fell in one day, is comparable with the MIF signal in the summer.
The nitrate isotope anomaly nearby Lignano Sabbiadoro and Marano Lagunare could derive from local sewage treatments with ozone. However, a third peak in the MIF signal in May, in a region of assimilation and/or denitrification in the sediments, enhanced by longer nutrients residence times, would indicate that nitrate sinks might be able to change the isotope anomaly.
In order to draw any conclusion on the quality of the data set from the Marano lagoon samples, the last section will be dedicated on the precision of the method, based on the overall uncertainties in assessing the atmospheric nitrate in sample water, and its accuracy.

3.3 Assessing the uncertainties related to the use of the nitrate MIF signature as a tracer of nitrate atmospheric deposition.

The goal of the present section is evaluating the potential of the nitrate MIF signature as a tracer of atmospheric nitrate, based on the precision and the accuracy of the method.
So far, error bars indicated the uncertainty due to IRMS measurements only, which is equal to 0.4‰(vs. VSMOW).
The atmospheric input calculated by using the nitrate isotope anomaly depends on the uncertainties of the denominator and numerator of Eq.3.2 (Michalski and Thiemens, 2006).

$$\text{Atmospheric nitrate (\%)} = \left(\frac{\Delta^{17}O_{sample}}{\Delta^{17}O_{atmosphere}} \right)\% \qquad \text{(Eq.3.2)}$$

According to the error analysis (Taylor, 1982), the relative error of the quotient q=x/y can be calculated by using Eq. 3.3.

$$\frac{\delta q}{|q|} \approx \frac{\delta x}{|x|} + \frac{\delta y}{|y|} \qquad \text{(Eq.3.3)}$$

The value of q, which includes its best representation (q_{best}) and the associated relative error ($\delta q/|q_{best}|$), is expressed in Eq.3.4.

$$q = q_{best}\left(1 \pm \frac{\delta q}{|q_{best}|}\right) \qquad \text{(Eq.3.4)}$$

where $q_{best}=x_{measured}/y_{measured}$

Eq.3.3 is valid only when the relative errors of x and y (i.e. δx and δy) are small numbers.
It is important to point out that the relative error of x (the isotope anomaly in sample water) in the data points concerning the Marano lagoon samples is not small.
This is because the uncertainty due to IRMS measurements is equal to 0.4‰(vs. VSMOW), whilst the measured anomaly at the Marano lagoon ranges between -0.4 and 2.4‰(vs. VSMOW), resulting in a relative error varying from 1 to 0.17.
Usually $\delta q/|q|$ is expressed as a percentage, which leads to a range of relative error from 100% to 17% of the measured anomaly in sample water from the lagoon. Thus, the uncertainties on measured MIF from the sample water discussed in section 3.2 are not irrelevant.
In the best case, the local $\Delta^{17}O_{atmosphere}$ is measured and also the uncertainty on y is related to IRMS measurements. This would result in an overall uncertainty of q that can be calculated with Eq.3.5.

$$\frac{\delta q}{|q|} \approx \left(\frac{\delta x}{|x|} + \frac{\delta x}{|y|} \right) \qquad \text{(Eq.3.5)}$$

A consequence of Eq.3.5 is that, the bigger the absolute values of the isotope anomaly in sample water and the atmosphere is, the lower the relative error connected to the use of the MIF signature as a tracer.
As a result, the relative error of q is minimal during the winter, owing to the highest nitrate isotope anomaly in aerosol in December and January.
If the isotope anomaly in local aerosol is not measured, several assumptions on its expected value have to be made. Firstly, the results in fig. 3.24 on the seasonal variations of the isotope anomaly (from Michalski et al., 2003) show that at mid latitudes the nitrate MIF in aerosol ranges from about 22 to 30‰(vs. VSMOW). When the MIF seasonal trend is not taken into account, average nitrate isotope anomaly would be 26‰. However, a large uncertainty of 4‰ should be associated with the assumed value.

When the seasonal trend is considered according to fig. 3.24, a step function is available, and the uncertainty associated with the aerosol nitrate isotope anomaly is related to the distance between data points.
When assuming that there is a linear change over time in the aerosol MIF signature, the decreasing trend from January to July can be calculated as (30‰-22‰)/6, which is equal to a change in the nitrate MIF in aerosol of 1.3‰ per month, an uncertainty three times smaller than when aerosol MIF seasonal trend is not taken into account.
The uncertainty related to fact that there is a seasonal trend is more than three times higher than when the nitrate isotope anomaly in aerosol is measured (usually 0.4‰ with the system described in section 2.2). Assuming an average uncertainty in the IRMS measurements of 0.4‰, the overall uncertainty in the calculation of the nitrate atmospheric input in sample water when the nitrate MIF signal is not measured is described by Eq.3.6.

$$\frac{\delta q}{|q|} \approx \frac{0.4}{|x|} + \frac{1.3}{|y|} \qquad \text{(Eq.3.6)}$$

Based on Eq.3.6, the relative error on the nitrate MIF in aerosol ranges from 4.3% in January to 5.9% in July.
In fact, fig. 3.24 would suggest that the seasonal trend is not linear with time and that the function fitting the seasonal trend of the capital delta values in atmospheric nitrate is a sinusoid.
The simplest sinusoid that meets the requirements of having a zero of 22 when the independent variable t is equal to 7 (where t would represents time in months) and a maximum of 30 when t is equal 1 is Eq. 3.7.

$$\Delta^{17}O(t) = 26+4\cos(t-1)\pi/6 \qquad \text{(Eq.3.7)}$$

Eq.3.7 fits reasonably well the data points from Michalski et al. (2003) (fig. 3.36).

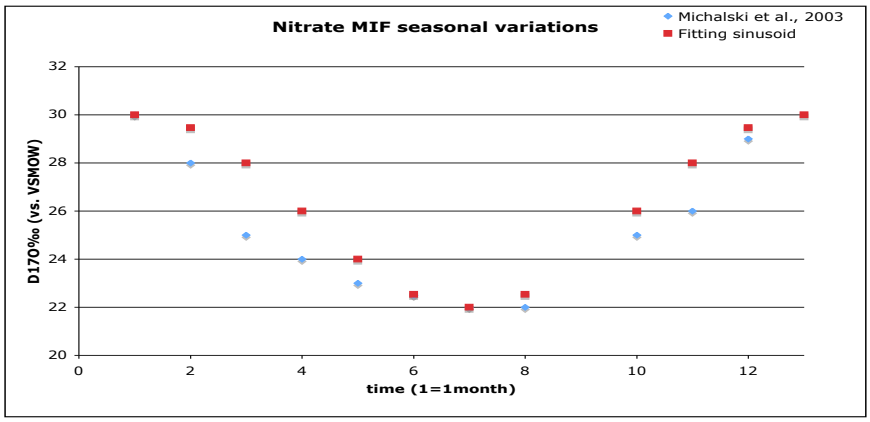

Fig. 3.36. *Comparison of calculated vs. observed (from Michalski et al., 2003) seasonal trend of the MIF signal in nitrate aerosol.*

A better fitting will be certainly found with a Fourier transform but the task would be beyond the scope of the present section, aiming at a gross evaluation of the uncertainty related to the MIF seasonal trend.

The variation of the MIF signature as a function of the time of the year can be approximated to the derivative of Eq. 3.7 (Eq.3.8).

$$\frac{d\Delta^{17}O}{dt} = -\frac{2\pi}{3}\sin(t-1)\frac{\pi}{6} \qquad \text{(Eq.3.8)}$$

Table 3.4 shows the change over time of the isotope anomaly (calculated with Eq. 3.7) and its differential $d\Delta^{17}O$ for each month of the year.

Month of the year	**$\Delta^{17}O$‰ (t) (Eq.3.7)**	**($d\Delta^{17}O$‰/dt) (Eq.3.8)**	**Abs($d\Delta^{17}O$‰/dt)**
1	30	0.0	0.0
2	29.5	-1.0	1.0
3	28	-1.8	1.8
4	26	-2.1	2.1
5	24	-1.8	1.8
6	22.5	-1.0	1.0
7	22	0.0	0.0
8	22.5	1.0	1.0
10	26	2.1	2.1
11	28	1.8	1.8
12	29.5	1.0	1.0
13	30	0.0	0.0
Average			**1.2**

Table 3.4 *Calculated seasonal trend of the MIF signal in nitrate aerosol and its change rate as a function of the time of the year.*

Results in Table 3.4 indicate that the average monthly uncertainty due to nitrate aerosol MIF seasonal variations is 1.2‰(vs. VSMOW), which is similar to the uncertainty indicated in Eq. 3.6.
However, in spring and in the autumn, the change of the isotope anomaly over time is faster, with a maximum rate of 2.1‰ per month in April and October, whilst a minimum is observed in January and July.
The overall uncertainty on the assessment of the nitrate atmospheric inputs that takes into account the seasonal trend of the nitrate MIF signal is described in Eq. 3.9.

$$\frac{\delta q}{|q|} \approx \frac{0.5}{|x|} + \frac{1}{|y|} * \left(\left| \frac{2\pi}{3}\sin(t-1)\frac{\pi}{6} \right| \right) \qquad \text{(Eq.3.9)}$$

Another source of uncertainty when the nitrate MIF in aerosol is not measured depends on the ratio fine/coarse mode of nitrate aerosol, which is an indicator of the ratio continental/marine aerosol. This is because the nitrate MIF signal is usually higher in coarse mode aerosol.
The difference in the nitrate MIF signal between fine and coarse mode (<1μ and >1μ, respectively) at Trinidad Head (coastal California) varied in a month from 0 to 4.5‰(vs. VSMOW)(fig. 3.37, from Patris et al., 2007).

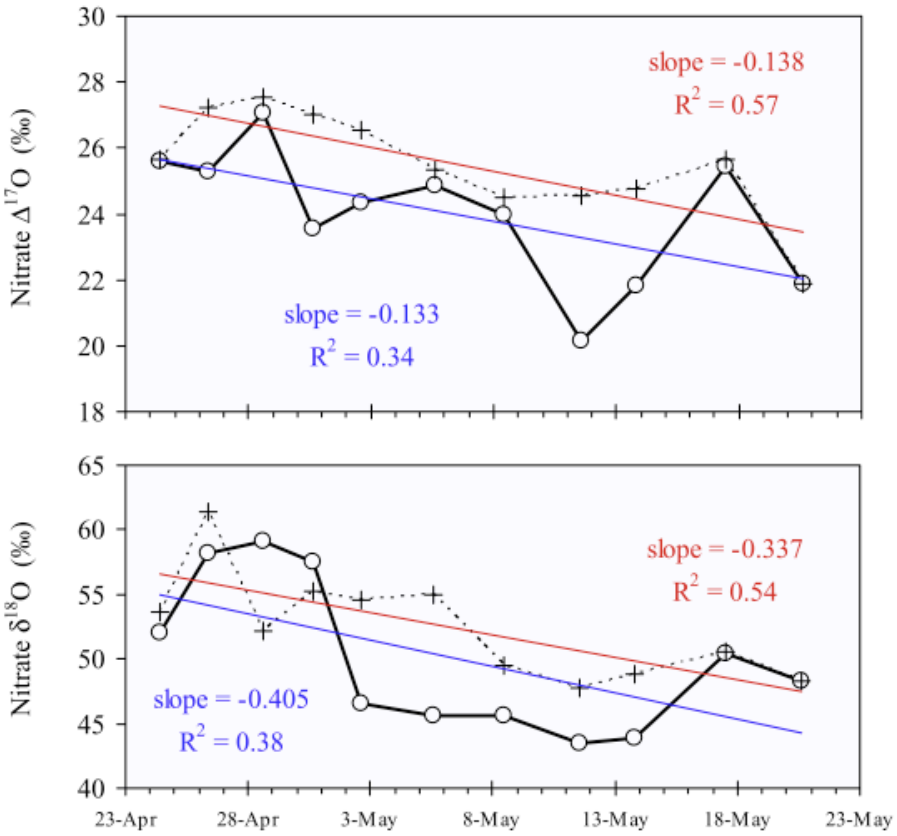

Fig. 3.37 *Capital delta value and $\delta^{18}O$‰ in submicron (thick solid lines) and supermicron (dashed lines) particles at Trinidad Head, coastal California (from Patris et al., 2007).*

A study in the Atlantic Ocean (Morin et al., 2009) showed a similar difference, with the nitrate isotope anomaly in fine mode aerosol (ranging from 0 to the 40% of total nitrate) differing roughly from 0 to 8‰ compared to coarse aerosol (fig. 3.38)

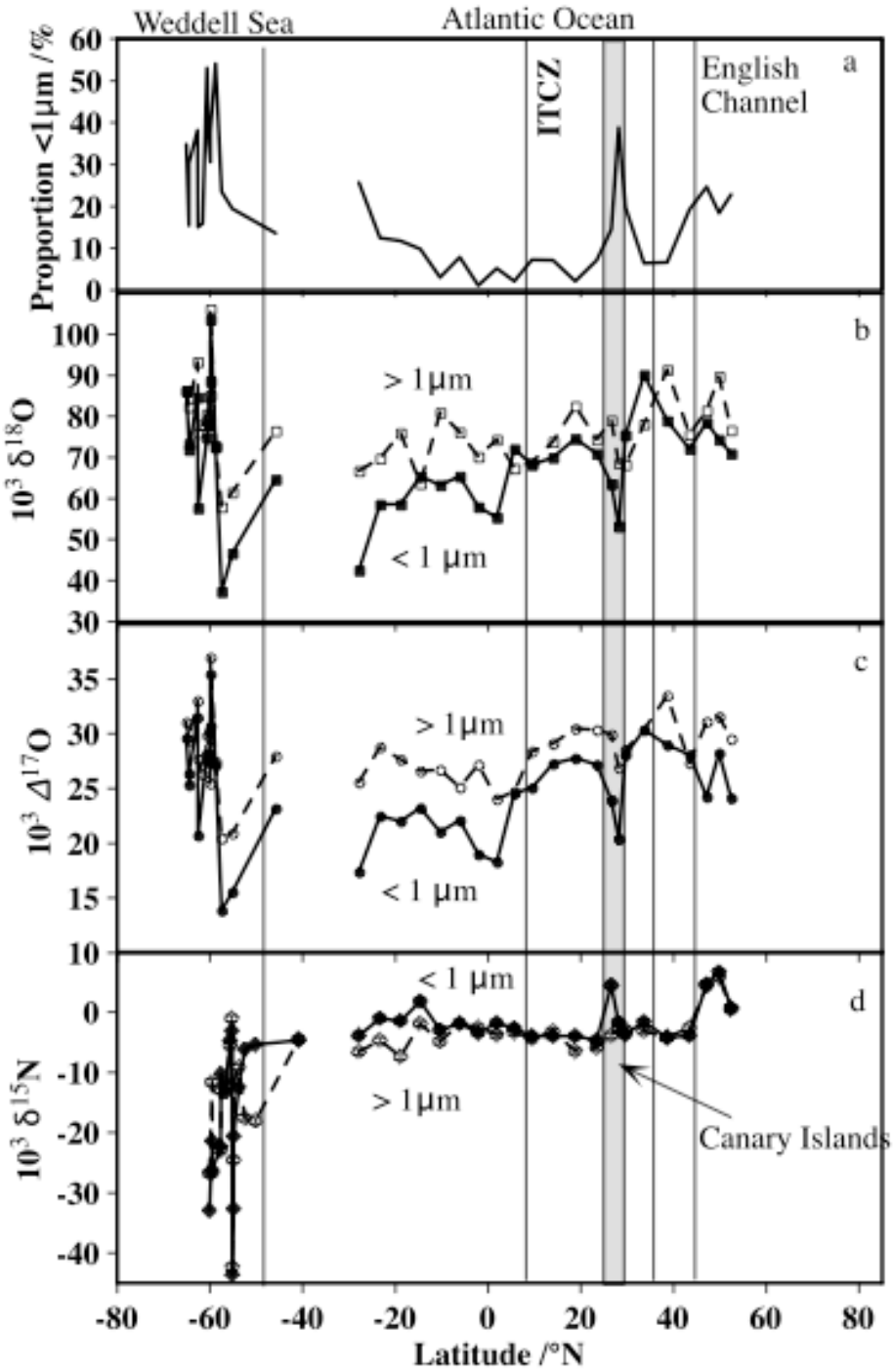

Fig. 3.38 *Latitudinal profiles of (a) the fraction of nitrate residing in the submicron mode and (b) $\delta^{18}O$‰, (c) $\Delta^{17}O$‰, and (d) $\delta^{15}N$‰. Supermicron (submicron) particles are indicated with open (solid) symbols (from Morin et al., 2009).*

Due to the geographical position of the Marano lagoon (a coastal environment close to the industrial area of Porto Marghera and the Po Valley), changes of air trajectories might cause the ratio fine/coarse mode to change.
Because of the fact that only few studies have been undertaken on this difference, it is difficult to quantify the uncertainty due to a variable ratio fine/coarse mode in nitrate aerosol.

Yet, the magnitude of the effect that has been measured so far seems to be remarkably high if the isotope anomaly in sample water is in the range 0-2.4‰(vs. VSMOW) and if Eq.3.3 is used to calculate the overall uncertainty.
Considering the data presented in fig. 3.37 and fig. 3.38, a relative error on expected MIF in nitrate aerosol of at least 1‰(vs. VSMOW) should be considered, due to changes of air mass trajectories.
Such an effect would generate an additional term in the relative error due to the assumption of the local nitrate MIF in the atmosphere (Eq.3.10).

$$\frac{\delta q}{|q|} \approx \frac{0.5}{|x|} + \frac{1}{|y|} * \left(1 + \left| \frac{2\pi}{3} \sin(t-1)\frac{\pi}{6} \right|\right) \qquad \text{(Eq.3.10)}$$

Finally, even when the nitrate isotope anomaly in aerosol is measured, the contribution of gaseous HNO_3 to the nitrate MIF signature will be still unknown.
It is important to point out that difficulties at evaluating the gaseous nitrate concentration, mainly due to artifacts of denuder systems (Nie et al., 2010)(Chang et al., 2002)(Appel et al., 1990)(Dasch et al., 1989), might be the main reason for what no measurements of the MIF signal in HNO_3 have been undertaken so far.
According to Michalski et al. (2003), the gaseous HNO_3 due to homogeneous hydrolysis of NO_2 at mid-latitude (model based on measurements at La Jolla, California) should have an isotope anomaly of 23.3‰(vs. VSMOW), whilst the nitrate in aerosol deriving from heterogeneous hydrolysis of N_2O_5 would have an anomaly of 29.2‰(vs. VSMOW).
However, this distinction has been made based on the nitrate precursor only. Yet, there is always an exchange between the atmospheric nitrate in the gas and the aqueous phase, which should lower the difference between the MIF in aerosol and in HNO_3.
Several factors contribute to the local partitioning of atmospheric nitrate and it is beyond the scope of the present section to take them into account in a rigorous way.
Intuitively, any change in the relative humidity could affect the partitioning of atmospheric nitrate. Moreover, the chemistry involved, and particularly the content of sulphate and ammonium in the atmosphere, has also an influence on the nitrate partitioning (Ansari and Pandis, 2000).
A study on the nitrate partitioning over Tokyo (Morino et al., 2006) might help to understand the nitrate partitioning at the Marano lagoon.
This is because of the geographical position of the Japanese city, which is along the coast but also subjected to inputs of nitrate of continental origin, due to both pollution (fine aerosol) and to Asian dust (Jickells et al., 2005)(Galloway et al., 2004) (the area of North Adriatic is affected by African dust events, according to Prodi et al., 2009).
As expected, during the winter the atmospheric nitrate resides mainly in aerosol, being on average 95% of total nitrate ($TN=NO_3+HNO_3$), whilst the HNO_3 is the prevalent nitrate species during the summer (82% of total nitrate on average)(Morino et al., 2006).
During a sampling campaign in May at Bresso (6 km north of the Milan city center), the HNO_3 was the 25% of total nitrate (Baltensperger et al., 2002). The same authors found that the gaseous nitrate in Verzago (35 km north of the Milan city center) during the same period was the 44%. During the sampling campaign in June, the ratio HNO_3/TN at both stations was not significantly different from the sampling campaign in May.

It is expected that continental air masses from the Po valley would reach the Marano lagoon. Thus, during the summer, when the overall uncertainty of the assessment of the atmospheric nitrate input to water is the lowest, there is an additional term in the relative error of measured (or expected) isotope anomaly in the atmosphere.
If the difference in the isotope anomaly of atmospheric nitrate between the aqueous and the gas phase is 6‰ and the 50% of atmospheric nitrate is in the gas phase, the MIF signal in atmospheric nitrate should be 3‰ lower than the isotope anomaly measured in nitrate aerosol.
As a consequence, even when the isotope anomaly in nitrate aerosol is measured, there should be an additional term due to the MIF signal in gaseous HNO_3 (Eq. 3.11, compare with Eq. 3.5).

$$\frac{\delta q}{|q|} \approx \frac{\delta x}{|x|} + \frac{(\delta x + \delta y)}{|y|} \qquad \text{(Eq.3.11)}$$

Only certain conditions in the air column (low temperature, high RH, high NH_3 concentration) will ensure that the additional term δy is negligible. An average difference of 1‰ is assumed between nitrate and aerosol at the Marano lagoon. This assumption has been made not to lower too much the overall precision of the method, even if its accuracy might be affected.
Further studies are needed to know the MIF in HNO_3, to be able to increase the accuracy of the method in the summer and to use the tracer in systems where the gaseous nitrate is an important fraction of the total nitrate in the air column.
A graphical method is used to define the relative error of the method, based on the measured MIF x in receiving water, measured (or expected) MIF y in the atmosphere and their respective uncertainties.
The relative error presented in fig. 3.39 in calculated based on Eq. 3.11. Thus, δx in Eq. 3.11 is due to the IRMS precision only, while the uncertainty on y depends on both the IRMS precision and the presence of HNO_3.

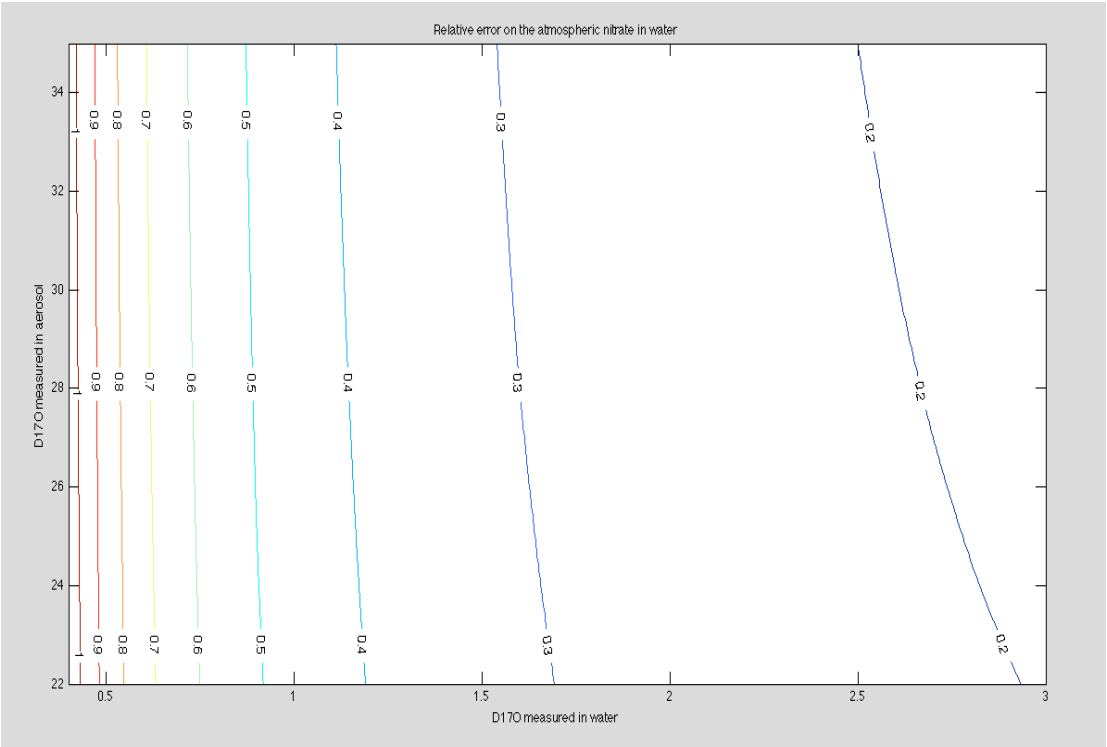

Fig. 3.39. *Relative error of the atmospheric nitrate in sample water as a function of x (nitrate MIF measured in sample water) and y (nitrate MIF measured in aerosol), assuming an uncertainty on x of 0.4‰ and an uncertainty on y of 1.4‰.*

Results shown in fig. 3.39 indicate that when the isotope anomaly in water is below 1‰, the relative error is roughly 46% (relative error 0.46) of the evaluation of atmospheric nitrate in sample water or greater.

When the isotope anomaly in the atmosphere is not measured, higher uncertainty δy should be expected.

Assuming an uncertainty of 1.8‰ due to the seasonal variation in May and September (Table 3.4) and an uncertainty of 2‰ to include the changes in the ratio fine/coarse mode and the partitioning between the gaseous and the aqueous phases, the relative error of atmospheric nitrate in sample water is shown in fig. 3.40.

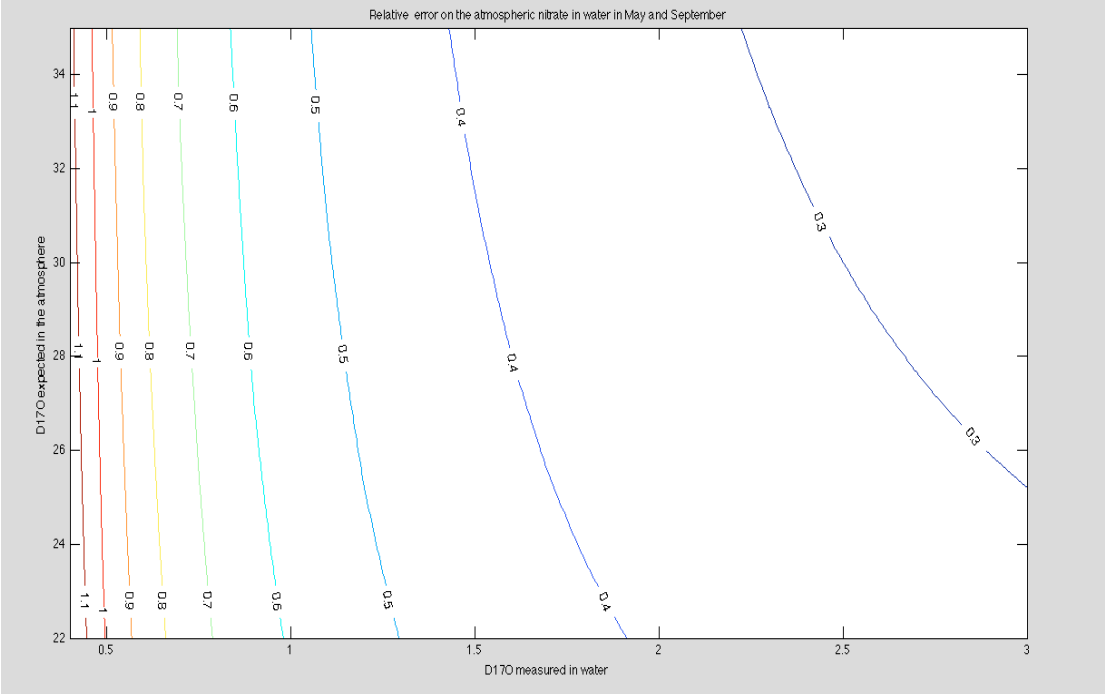

Fig. 3.40. *Relative error of the atmospheric nitrate in sample water as a function of x (nitrate MIF measured in sample water) and y (nitrate MIF expected in aerosol), assuming an uncertainty on x of 0.4‰ and an uncertainty on y of 3.8‰.*

According to the calculation presented in fig. 3.40, when the isotope anomaly in water in May and September is below 1‰ and the MIF signal in the atmosphere is assumed to be 24‰, the relative error on the atmospheric nitrate in sample water is the greater than or equal to 55% (relative error 0.55).
The relative error of x (the isotope anomaly in sample water) is not irrelevant in our case. As a consequence, Eq.3.3 might not be a suitable approximation of the overall uncertainty of the atmospheric nitrate in sample water.
The correct definition of q, when x and y are positive terms, is shown in Eq.3.12.

$$q = \left(\frac{x \pm \delta x}{y \pm \delta y} \right) \qquad \text{(Eq.3.12)}$$

The parameter q of Eq.3.12 ranges from a mininum value (when the minus sign is at the numerator and the plus sign is at the denominator of the fraction) to a maximum value (corresponding to the case when the minus sign is at the denominator and the plus sign is at the numerator).
If assuming that the best evaluation of q_{best} is the arithmetic average of the maximum and the minimum value, the relative error of q (calculated as the deviation of q_{best} from the maximum divided by q_{best}) does not change significantly from the results in fig. 3.39 and fig. 3.40 (data not shown).
Therefore the last two charts are considered a good approximation of the overall uncertainty on the evaluation of atmospheric nitrate in sample water.
Table 3.5 compare different ways of calculating the precision of the method and summarizes the major differences.

MIF measured in sample water	MIF measured or expected in the atmosphere	Atmospheric nitrate in sample water (q, according to Eq. 3.2)	Relative error δq/|q| according to Eq. 3.5 (%)	Error of q (±δq)
			dx=0.4 dy=0	
0.5	22	2.3	82	1.9
0.5	25	2.0	82	1.6
0.5	28	1.8	81	1.5
0.5	31	1.6	81	1.3
0.5	34	1.5	81	1.2
1	22	4.5	42	1.9
1	25	4.0	42	1.7
1	28	3.6	41	1.5
1	31	3.2	41	1.3
1	34	2.9	41	1.2
1.5	22	6.8	28	1.9
1.5	25	6.0	28	1.7
1.5	28	5.4	28	1.5
1.5	31	4.8	28	1.4
1.5	34	4.4	28	1.2
2	22	9.1	22	2.0
2	25	8.0	22	1.7
2	28	7.1	21	1.5
2	31	6.5	21	1.4
2	34	5.9	21	1.2
			dx=0.4 dy=1.4	
0.5	22	2.3	86	2.0
0.5	25	2.0	86	1.7
0.5	28	1.8	85	1.5
0.5	31	1.6	85	1.4
0.5	34	1.5	84	1.2
1	22	4.5	46	2.1
1	25	4.0	46	1.8
1	28	3.6	45	1.6
1	31	3.2	45	1.4
1	34	2.9	44	1.3
1.5	22	6.8	33	2.3
1.5	25	6.0	32	1.9
1.5	28	5.4	32	1.7
1.5	31	4.8	31	1.5
1.5	34	4.4	31	1.4
2	22	9.1	26	2.4
2	25	8.0	26	2.0
2	28	7.1	25	1.8

2	31	6.5	25	1.6
2	34	5.9	24	1.4
			dx=0.4 dy=3.8	
0.5	22	2.3	97	2.2
0.5	25	2.0	95	1.9
0.5	28	1.8	94	1.7
0.5	31	1.6	92	1.5
0.5	34	1.5	91	1.3
1	22	4.5	57	2.6
1	25	4.0	55	2.2
1	28	3.6	54	1.9
1	31	3.2	52	1.7
1	34	2.9	51	1.5
1.5	22	6.8	44	3.0
1.5	25	6.0	42	2.5
1.5	28	5.4	40	2.2
1.5	31	4.8	39	1.9
1.5	34	4.4	38	1.7
2	22	9.1	37	3.4
2	25	8.0	35	2.8
2	28	7.1	34	2.4
2	31	6.5	32	2.1
2	34	5.9	31	1.8

Table 3.5. *Summary of the overall precision of the method on samples collected in May and September, depending on whether the uncertainty on the nitrate MIF in aerosol is considered or not and, if it is, when the nitrate MIF in aerosol is measured or assumed.*

In most cases the average MIF signature in sample water from the Marano lagoon is below 0.6‰, corresponding to a relative error on q (the atmospheric nitrate in sample water) varying from 83% to 73%, depending on the method to calculate the precision.
Considering that in most sampling sites the water depth was limited (and therefore it can be assumed that the MIF at mid-depth water is close or equal to surface water) and that the signal showed no sensitivity to dry conditions and to more than 100mm of rainfall, it is questionable that the capital delta values could be used as a good tracer for atmospheric nitrate.
When considering only the data points for what the uncertainty is equal or below 50% of the measurement, the tracer proved to be good mainly at detecting a signal that seems to be correlated to sewage treatments with ozone.
This is because, excluding the MIF peaks from the populated areas of Lignano Sabbiadoro and Marano lagunare, the average isotope anomaly in the lagoon is 0.6‰ in May and 0.4‰ in September, the latter being equal to the uncertainty on x due to IRMS measurements. Hence, it is only possible to affirm that at the Marano lagoon the nitrate atmospheric input is below the precision of the method. The finding that atmospheric nitrate is usually a small source to coastal systems has already been discussed (Spokes and Jickells, 2005).

It is be possible that remote areas could be more suitable systems for using the tracer. Yet, the data from the Pacific Ocean (fig. 3.33) indicates that the signal is decreasing with increasing distance from the coast.
It is therefore vital to evaluate the accuracy of the method, before drawing any conclusion on the potential of the MIF signature as a tracer.
To do that, the focus should be on the discussion of the two basic assumptions behind the use of the tracer.
The first one is that only atmospheric nitrate has an isotope anomaly. This hypothesis implies that all the organisms involved in the local nitrogen cycle have a certain preference for the ^{17}O containing molecules of nitrate, which is depending on their preference for the nitrate molecules with an atom of ^{18}O, so that the process can be regarded as a mass dependent process (see chapter 1).
The tests on the denitrifier method when copper is present in solution would suggest that, at high level of stress, the organisms involved in the nitrogen cycle might generate an isotope anomaly.
Furthermore, the isotope anomaly in minerals where the atmospheric nitrate is an unlikely source, which is the topic of the next chapter, would indicate the chance that kinetic processes might generate a MIF signature that is well above 1‰.
The second general assumption is that a mass dependent process cannot change the isotope anomaly in a nitrate pool. Thus, the loss of nitrate due to assimilation or denitrification following a mass dependent fractionation will not alter the magnitude of the tracer (Kendall et al., 2007)(Morin et al., 2009).
As a result, the calculation of the percentage of atmospheric nitrate in sample water, due to the mixing with the other nitrate sources, is possible at any time.
If biological processes were able to change the capital delta of nitrate, the isotope anomaly in sample water should not be used as a tracer.
However, the capital delta values might be used to define the difference between atmospheric nitrate deposition rate and biological nitrate consumption.
However, the calculation will be complicated by the fact that, not only time series must be considered, with the evaluation of the fluxes of all the nitrate sources at any time, but also the biological preference for ^{17}O containing molecule due to each biological process involved in the local nitrate cycle.

4. The nitrate isotope anomaly in nitrate minerals: is the atmosphere the only source of a MIF signal?

4.1 Introduction

The aim of the present chapter is testing the general assumption that only the atmospheric processes can generate a nitrate isotope anomaly. In order to achieve the goal, the isotope anomaly in minerals where the atmospheric contribution can be regarded as minimal has been analyzed and compared with the isotope anomaly in minerals deriving from long-term atmospheric deposition.
It is widely accepted that an isotope anomaly can also be generated due to kinetic processes (Richter et al., 2009)(Miller et al., 2002)(Young et al., 2001) (Young et al. 1998), but that the magnitude of the measured anomaly is usually below 1‰.
However, the processes that have been considered for evaluating the magnitude of the isotope anomaly in samples of geochemical significance are mainly the ones associated with the formation of carbonates, oxides and silicates, and these are therefore minerals that contributed for the most to the definition of the TFL (the terrestrial fractionation line, see chapter 1).
Nitrate is the species with the highest isotope anomaly that can be also present as a geological record, being the atmospheric species with the second highest MIF signal ever reported, after ozone.
For this reason the MIF signature has been successfully used to identify the atmospheric source in Chilean nitrate ore deposits (Michalski et al., 2004). However, the MIF signature that has been measured (14–21 ‰) is well below the range of the isotope anomaly in nitrate aerosol at mid-latitude (22-35‰).
Recently, the isotope anomaly in the nitrate ore deposits of Turpan-Hami Basin (China) has been found to be in the range 12-17‰ (Li et al., 2010). According to the authors, the finding would suggest that the long-term atmospheric deposition is the source of the deposits.
The results from the Chilean and the Chinese nitrate ore deposit would pose a question: is the range of the nitrate isotope anomaly that has been found in nitrate minerals a proof of a different atmospheric oxidative capacity in the past, or it is rather that geochemical processes like evaporation and precipitation during brine evolution in a desert environment would change the magnitude of the signal?
It is possible that preindustrial MIF signal was lower than present day atmospheric nitrate anomaly, since the increase of troposheric ozone is associated with pollution (Fiore et al., 2002).
There is also some evidence that the MIF signature is not always retained in natural systems. As an example, the nitrate measurements on ice cores from Dome Concordia from two sampling campaigns (in 2004 and 2007) are compared and discussed (see fig. 4.1, from Frey et al., 2009). In the chart on the right side of fig. 4.1, the nitrogen delta values (in blue) and the nitrate concentration (in grey) profiles are shown. In 2004 there is a nitrate peak (see the base of the black arrow in fig. 4.1) at a depth (10 cm from the surface) that should be sufficient to rule out the chance of a further loss of nitrate due to photolysis. According to the authors, (see the first ordinate in fig.4.1) three years would correspond to a deposition of 20cm of snow. Thus, if no nitrate had been lost from 2004 to 2007, the same nitrate concentration should have been found in the 2007 sampling campaign at 30cm (see where the black arrow points). In fact

the nitrate concentration in 2007 at 30 cm from the surface (point circled in red) is five times smaller than the concentration in 2004 at a depth of 10 cm. This observation would suggest that a nitrate loss occurred. If there was no change in the isotope anomaly associated with the sink process, the measured MIF signal should be where the blue arrow in fig. 4.1 points.

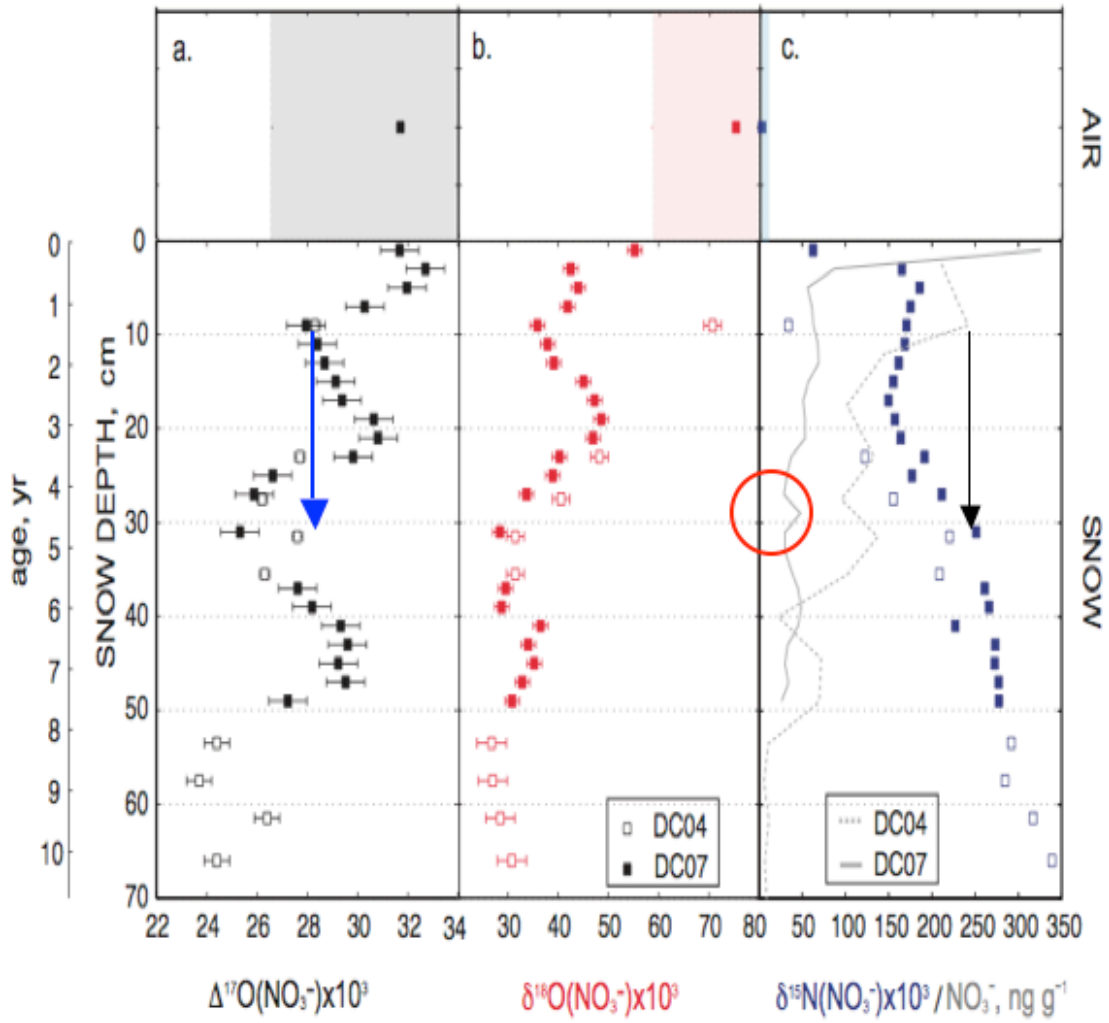

Fig 4.1. *$\Delta^{17}O$, $\delta 18O$, $\delta 15N$ and NO_3 concentration profiles at Dome Concordia, East Antarctica. From Frey et al., 2009.*

Since there is a change in the capital delta value of about 3‰, it is possible that the loss of nitrate caused the change in the isotope anomaly.
It is therefore necessary to understand in which circumstances the MIF signature can be regarded as a conservative tracer. Thus, tests on the occurrence of a change in the isotope anomaly during phase transitions have been carried out. The results are discussed in section 4.6.
Furthermore, to achieve the main goal of the chapter (testing the assumption that only atmospheric nitrate has a significant isotope anomaly), nitrate minerals of different origins have been analyzed for their N and O isotopic composition.
There are several advantages in considering nitrate minerals, to answer the primary question of the present chapter. First, there is a limited number of mineralogical

phases containing nitrate in the chemical formula, which makes possible undertaking a systematic study. Moreover, this strategy would allow an investigation of an isotope anomaly in nitrate minerals of different origins, since nitrate minerals could form due to chemical, physical and biological processes. Finally, due to the high solubility of most nitrate minerals, the very existence of nitrate minerals suggest that water-rock interactions can be regarded as minimal and the isotopic signature is likely to be the pristine signature related to sample formation.
Our specimens come from the collection of the Natural History Museum (with ID NHM), the Oxford University Museum (ID OUM), the National Museum of Wales (ID NMW), the National History Museum of Geneva (Switzerland) and from the personal collection of Prof. Murashko.
In the subsequent discussion the likely origin of the formation of each nitrate mineral analyzed is discussed. The complete XRF and XRD analyses are reported in Appendix 3, and are coupled, whenever possible, with major anion measurements with an Ion Chromatograph (Dionex ICS5000).

4.2. The evaporite series from the Atacama Desert.

Typical of a desert environment, the evaporite is a sediment that consists of water-soluble minerals and results from concentration and crystallization by evaporation of aqueous solutions (brine). Because of the high solubility, nitrate salts would usually precipitate after carbonates and sulphates, in association with halite (NaCl).
The exceptional dryness of the Atacama Desert (Chile), with annual rainfall less than 2mm, generated the largest nitrate ore deposits of the world.
The origin of the Chilean nitrate deposits had been considered controversial (Bohlke et al., 1997; Vega et al., 1996; Eriksen et al., 1981; Whitehead, 1920) until the isotope anomaly was measured (Michalski et al., 2004), demonstrating that the long-term atmospheric deposition is the main source of nitrate. The samples analyzed by the authors were heterogeneous mixtures of salts, with an isotope anomaly ranging from 14 to 21‰.
In the present work, minerals have been preferred to soils and mixtures of nitrate salts for the analyses of the MIF signature, because each phase would correspond to a specific stage of brine evolution. This is because it is important to understand whether the low isotope anomaly found in Michalski et al. (2004), compared to the MIF signature in present day aerosol, could be due to any geochemical process (like partial evaporation and/or fractional crystallization) that followed the deposition of atmospheric nitrate.
There are four different nitrate phases in the Chilean deposits (table 4.1).

Chlorides:	Halite	$NaCl$
Sulphates:	Anhydrite	$CaSO_4$
	Bloedite	$Na_2Mg(SO_4)_2.4H_2O$
	Glauberite	$Na_2Ca(SO_4)_2$
	Gypsum	$CaSO_4.2H_2O$
	Löweite	$Na_{12}Mg_7(SO_4)_{13}.15H_2O$
	Polyhalite	$Ca_2MgK_2(SO_4)_4.2H_2O$
	Starkeyite	$MgSO_4.4H_2O$
	Thenardite	Na_2SO_4
Carbonates:	Calcite	$CaCO_3$
Nitrates:	Nitratine	$NaNO_3$
	Niter	KNO_3
	Darapskite	$Na_3[NO_3SO_4].H_2O$
	Humberstonite	$K_3Na_7Mg_2[(NO_3)_2(SO_4)_6].6H_2O$
Borates:	Kaliborite	$KMg_2H[B_6O_8(OH)_5]_2.4H_2O$
	Probertite	$NaCa[(B_5O_7)(OH)_4].3H_2O$
Iodates:	Lautarite	$Ca(IO_3)_2$
	Hectorfloresite	$Na_9[(IO_3)(SO_4)_4]$
	Fuenzalidaite	$K_6(Na,K)_4Na_6Mg_{10}(SO_4)_{12}(IO_3)_{12}.12H_2O$
Chromates:	Dietzeite	$Ca_2[(IO_3)_2CrO_4]$
Oxides:	Hematites	Fe_2O_3
Silicates:	Quartz, heulandite, laumontite.	

Table 4.1. *Mineralogy in the Pedro de Valdivia deposits. From Vega et al., 1996*

According to Vega et al. (1996), it is possible to identify the stage of brine evolution in the Chilean nitrate deposits by studying the mineral association (Fig. 4.2)

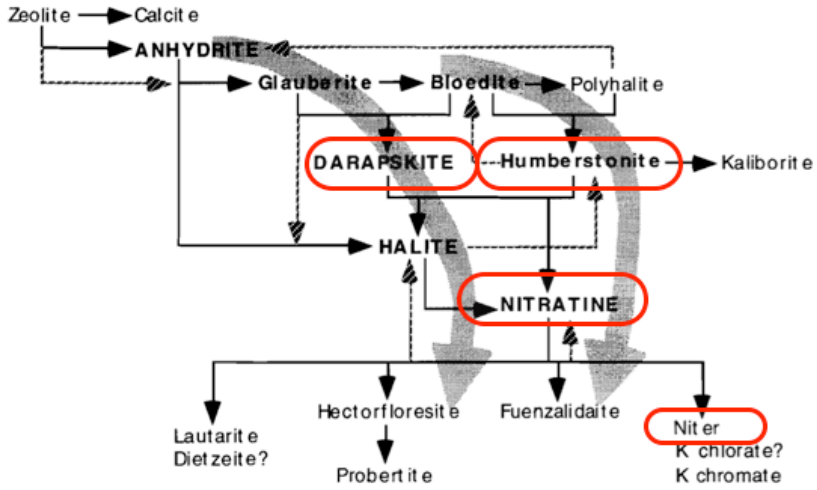

Fig. 4.2. *Synthetic diagram of parental brine evolution in the Pedro de Valdivia deposit. The main paragenetic relationships are indicated in solid lines, whereas the general trends are marked by thick hatched arrows. The minerals containing nitrate are marked in red (modified after Vega et al., 1996).*

The phase darapskite, with formula $Na_3(NO_3)(SO_4)\cdot H_2O$, is the first phase containing nitrate that precipitates after the sulphates (anhydrite and glauberite) in a Na-rich brine.

If Mg and K concentrations are sufficiently high, a second trend is possible, with the nitrate mineral humberstonite ($K_3Na_7Mg_2(SO_4)_6(NO_3)_2 \cdot 6H_2O$) following the precipitation of blödite ($Na_2Mg(SO_4)_2 \cdot 4H_2O$).
The most common nitrate phase of the Chilean ore deposits is nitratine ($NaNO_3$), which precipitates with halite (NaCl). The last stage of NO_3-rich brine evaporation correspond to niter formation (KNO_3, whose commercial name is saltpeter), often associated with chlorates and chromates.
Apart from niter, at least one sample of all the other nitrate phases that are present in the Chilean deposits has been analyzed for the isotope anomaly. This will allow testing of the hypothesis that the MIF signature might change due to fractional crystallization.
Investigating the occurrence of a change of the nitrate isotope anomaly during fractional crystallization could be certainly possible where the nitrate is present as superficial crusts and efflorescences in arid soils or lacustrine salt deposits. Because most of the nitrate at the Atacama Desert derives from salt deposition of circulating fluids, different phases from the same fluid could precipitate at a certain distance from each other.
Therefore only a proper sampling campaign would allow understanding thoroughly the genesis of a nitrate mineral and, possibly, the conditions at which the solid phase formed. This would help to fully explain any change of the nitrate isotope anomaly among different phases. Because undertaking a sampling campaign was not possible, specimens from museum collections were used.
This study on the MIF in nitrate from museum collections is therefore meant as an exploratory work. The results, coupled with laboratory tests (see section 4.6) would help to test if kinetic processes following the atmospheric nitrate deposition could alter the nitrate MIF signature.
It is important to point out that nitratine and darapskite are becoming ubiquitous, due to the increasing levels of pollutants in the atmosphere. The two phases, sometimes associated with nitromagnesite (with formula $Mg(NO_3)_2 \cdot 6H_2O$) are also found in natural building stones on old monuments, and are thought to be formed by chemical weathering (Grassegger, 1999)(Steiger and Zeunert,1996).
Franzen and Mirwald (2008) modeled their observed results of moisture sorption to determine the $Na–Mg–SO_4–NO_3–H_2O$ phase diagram (Fig 4.3)(the synonym nitronatrite is used instead of nitratine).

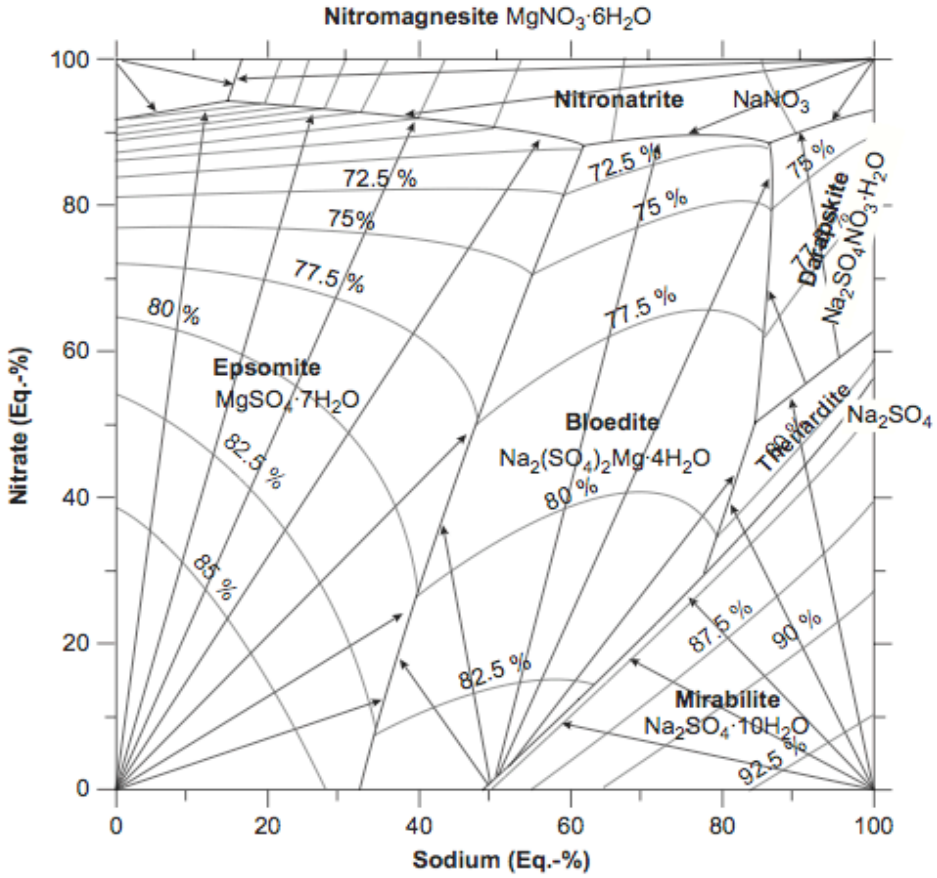

Fig. 4.3. *Na–Mg–SO_4–NO_3–H_2O phase diagram. From Franzen and Mirwald (2008).*

Laboratory tests (Franzen and Mirwald, 2008) suggested that theoretical considerations and computer simulations might not reproduce the real moisture behavior in porous materials in the presence of salt mixtures, underlying the complexity of the diffusive processes in multi-component systems. A comprehensive model for calculating thermodynamic properties of aqueous systems containing the Na^+, K^+, Mg^{2+}, Ca^{2+}, Cl^- and NO_3^- ions has been recently published (Gruszkiewicz et al., 2007).

It is important to point out that the mechanism of moisture sorption and desorption associated with the formation of nitrate salts arising from the attack of building materials by atmospheric nitric acid is probably similar to the formation of Chilean nitrate deriving from circulating groundwater filling voids in the bedrock.

A fifth rare nitrate mineral, the ungemachite ($K_3Na_8Fe^{3+}(SO_4)_6(NO_3)_2 \cdot 6H_2O$) is formed in oxidation zones of pyrite in an arid climate, and it is usually found in veins, associated with other iron sulphates. The nitrate isotope anomaly in the ungemachite from the Atacama Desert has never been measured.

Table 4.2 indicates the UEA ID, the original sample ID (OUM indicates the Oxford University Museum, NMW the National Museum of Wales and NHM the Natural History Museum) and the sample description in the museum catalogues.

UEA ID	Original ID	Locality	Locality details	Full description in museum catalogue
1OX	OUM 12903	Estaca Britannia, Antofagasta, Chile	Lat. 23°11', Long. 69°45' Depth 12 ?ft/m	Nitratine 19.5% Caliche achancacado
2OX	OUM 12903	Estaca Britannia, Antofagasta, Chile	Lat. 23°11', Long. 69°45' Depth 12 ?ft/m	Nitratine 19.5% Caliche achancacado
3OX	OUM 12906	Carmen Alto (Estaca D.) Antofagasta, Chile	Depth 8?ft/m	Nitratine 65%, flor de caliche azuprado (Flower of sulphur caliche).
4OX	OUM 12907	Estaca Victoria, Pampa Central, Antofagasta, Chile	Lat. 23°11', Long. 69°48' Depth 18? ft./m	Nitratine 38%. Caliche.
5OX	OUM 12907	Estaca Victoria, Pampa Central, Antofagasta, Chile	Lat. 23°11', Long. 69°48' Depth 18? ft./m	Nitratine 38%. Caliche.
6OX	OUM 12908	Carmen Alto, Antofagasta, Chile	Lat. 23°12', Long. 69°48' Depth 12? ft./m	Nitratine 60.3%. Caliche blanco azucar. White sugar caliche
7OX	OUM 12912	Carmen Alto, (Estaca 2a), Antofagasta, Chile	Depth 8?ft/m	Nitratine 26%. Caliche comun con pecas de cromato de potasa.
8OX	OUM 12913	Estaca Cienfuegos, Antofagasta, Chile	Lat. 23°10', Long. 69°45' Depth 4? ft./m	Nitratine 34%. Caliche colorado con piedra. Red nitrate.
9OX	OUM 12913	Estaca Cienfuegos, Antofagasta, Chile	Lat. 23°10', Long. 69°45' Depth 4? ft./m	Nitratine 34%. Caliche colorado con piedra. Red nitrate.
10OX	OUM 12914	Estaca VI or XI, Pampa Central, Antofagasta,	Lat. 23°10', Long. 69°45' Depth 8? ft./m	Nitratine 4.2%. Caliche conjelo.

		Chile		
11OX	OUM 12920	Aguas Blancas, Antofagasta, Chile		Common yellow nitrate.
12OX	OUM 12920	Aguas Blancas, Antofagasta, Chile		Common yellow nitrate.
13OX	OUM 12921	Antofagasta, Chile		Nitrate 96%. Refined.
14OX	OUM 19536	Darapskite		Nitratine 19.5% Caliche achancacado
1CA	NMW 67.154.GR.41	Tarapaca, Chile		Soda nitre
2CA	NMW 67.154.GR.41	Tarapaca, Chile		Soda nitre
3CA	NMW 67.154.GR.41	Tarapaca, Chile		Soda nitre
4CA	NMW 60.531.GR.3	Chile		Nitratine
5CA	NMW 60.531.GR.3	Chile		Nitratine
6CA	NMW 60.531.GR.3	Chile		Nitratine
7CA	NMW 60.531.GR.3	Chile		Nitratine
1LO	BM 1985 MI9293			Niter
2LO	BM 1985 MI9293			Niter
5LO	BM 77517			Darapskite
6LO	BM 77517			Darapskite

The term caliche refers to a sedimentary rock, usually a hardened deposit of calcium carbonate (Reeves, 1976). It forms when minerals are leached from the upper layer of the soil (the A horizon) and accumulate in the next layer (the B horizon), at depths of approximately 3 to 10 feet under the surface. In the Atacama Desert, the term is used for a mixture containing also gypsum, sodium chloride and sodium and potassium nitrate.

Table 4.3 summarizes the results obtained by combining the XRD and XRF measurements (see Appendix 3 for the complete data set) that have been carried out by Bertrand Leze (chief technician at the UEA Geotechnical Microanalysis Laboratory).

UEA ID	Full description	Sample description	Nitrate mineralogic phase
1OX	Nitratine 19.5% Caliche achancacado	Grey	Humberstonite
2OX	Nitratine 19.5% Caliche achancacado	Yellow	Humberstonite
3OX	Nitratine 65%, flor de caliche azuprado (Flower of sulphur caliche).	Powder	Nitratine
4OX	Nitratine 38%. Caliche.	Powder	Nitratine, humberstonite
5OX	Nitratine 38%. Caliche.		Nitratine, humberstonite
6OX	Nitratine 60.3%. Caliche blanco azucar. White sugar caliche		Nitratine
7OX	Nitratine 26%. Caliche comun con pecas de cromato de potasa.		
8OX		Pink, powder	
9OX	Nitratine 34%. Caliche coloroado con piedra. Red nitrate.	Red	
10OX	Nitratine 4.2%. Caliche conjelo.		Darapskite
11OX	Common yellow nitrate.	Yellow (possibly due to recrystallization?)	Nitratine
12OX	Common yellow	White crystal	Nitratine

	nitrate.		
13OX	Nitrate 96%. Refined.		Nitratine
14OX	Nitratine 19.5% Caliche achancacado		Darapskite
1CA		Black, powder	Nitratine
2CA		Black, Medium fragment	Nitratine
3CA		Black, large fragment	Nitratine
4CA		White, powder	Nitratine
5CA		Dark, medium fragment	Nitratine
6CA		Pink, medium fragment	Nitratine
7CA		White, large fragment	Nitratine
1LO		Looks very well crystallized	Nitratine
2LO		Looks very well crystallized	Nitratine
5LO		From the biggest fragment	Darapskite
6LO		From two medium fragments	Darapskite

Table 4.3. *Summary of XRD and XRF analyses on samples from the Chilean nitrate ore deposits.*

A mineral from the Natural History Museum (sample IDs 1LO and 2LO) that was previously classified as Chilean niter, proved to be nitratine.
Moreover, humberstonite has been found in some of the specimens of the Oxford University Museum, either as the only nitrate phase or in a mixture with nitratine.
This set of measurements has been undertaken at the UEA Geotechnical Microanalysis Laboratory mainly to rule out the chance that the nitrate in our samples is present as a mixture of salts. All the samples that contain more than one nitrate phase will not used when investigating the chance that the nitrate isotope anomaly could differ, depending on the mineralogical phase.
However, it is still possible that the analyzed specimens are a mixture of nitrate salts and that one of the components was not present in the powder used for XRD analyses, but was present in one of the solutions prepared for IRMS measurements.
No nitrate salt was detected with the XRD in 3 samples (with sample ID 7OX-8OX-9OX) but nitrate is present in the three solutions prepared for the denitrifier method.
Decomposition of several solid nitrates, including $NaNO_3$ and KNO_3 by X-ray has been reported (Cunningham et Heal, 1958). Due to the chance that partial photolysis

of nitrate could alter the sample pristine isotopic signature, the IRMS analyses of samples that had been previously used for XRD measurements is not recommended. However, a test showed that exposure to X-ray for up to six hours do not alter the isotope anomaly of well crystallized samples (see later discussion about the sample 4Ca extr).

In most cases, in order to assess the variability intra specimen, different solutions have been prepared by using small aliquots of samples from different parts of the same specimen.

To extract the nitrate from the salts, an aliquot of sample is finely crashed in a mortar and dissolved in 10ml of MQ. To prevent the chance of a partial dissolution, which might cause an isotope fractionation, the solutions are immersed for ten minutes in a sonicated bath and then on a shaker table overnight. This precaution has been made because of the presence of phases with a lower saturation point that could partially prevent the release of nitrate in solution.

Partial dissolution due to saturation is excluded, since the saturation point of sodium nitrate at 20°C is 9.2g of $NaNO_3$ in 10ml of water, which is well above the aliquot of sample used to prepare the solutions for the denitrifier method.

Samples are then filtered with cellulose acetate filters (0.4μm) and stored at -4ºC. All samples have been extracted the same day, apart from the ones with extr in the UEA sample ID (Table 4.4), which are discussed below.

Sample UEA ID	**Nitrate phase**	**Date of analyses**	**$\Delta^{17}O$‰(VSMOW)**	**$\delta^{15}N$‰(AIR)**
1 OX extr	Humberstonite	4/2/11	20.0±0.4	-0.25±0.3
3 OX	Nitratine	7/2/11	18.8±0.4	-1.8±0.3
5 OX	Nitratine, humberstonite	9/2/11	18.4±0.5	0.1±0.3
5 OX extr	Nitratine, humberstonite	7/2/11	17.8±0.4	-0.5±0.3
6 OX		9/2/11	19.7±0.5	1.3±0.3
7 OX		19/3/11	18.2±0.9	-0.6±0.3
8 OX		9/2/11	17.1±0.5	0.55±0.3
8 OX		19/3/11	16.9±0.9	-0.6±0.3
10 OX	Darapskite	7/2/11	15.4±0.4	1.9±0.3
11 OX	Nitratine	19/3/11	18.2±0.9	-0.55±0.3
12 OX	Nitratine	7/2/11	16.9±0.4	-0.6±0.3
13 OX	Nitratine	15/3/11	16.6±0.4	1.4±0.3
14 OX	Darapskite	4/2/11	15.9±0.4	2.0±0.3
1CA	Nitratine	7/2/11	18.1±0.4	-1.05±0.3
2CA	Nitratine	8/2/11	18.2±0.4	-0.7±0.3
2CA	Nitratine	15/3/11	18.8±0.4	-1.2±0.3
3CA	Nitratine	7/2/11	18.4±0.4	-1.3±0.3
4CA	Nitratine	8/2/11	19.6±0.4	-1.1±0.3
4CA extr	Nitratine	8/2/11	19.6±0.4	-1.2±0.3
4CA	Nitratine	15/3/11	20.2±0.4	-1.7±0.3
4CA extr	Nitratine	15/3/11	21.5±0.4	-1.7±0.3
5CA	Nitratine	8/2/11	19.1±0.4	-0.7±0.3
5CA	Nitratine	15/3/11	21.4±0.4	-1.7±0.3
6CA	Nitratine	9/2/11	20.6±0.5	-1.8±0.3

7CA	Nitratine	9/2/11	21.0±0.5	-1.7±0.3
1LO	Nitratine	19/3/11	16.2±0.9	-1.5±0.3
2LO	Nitratine	19/3/11	20.1±0.9	-1.6±0.3
5LO	Darapskite	19/3/11	17.4±0.9	5.4±0.3
6LO	Darapskite	19/3/11	18.1±0.9	5.4±0.3

Table 4.4. *Isotopic measurements of the samples from the Chilean nitrate ore deposits.*

The sample size ranges from 100-200nmol, depending on sample availability. Whenever possible, the higher sample size is preferred, to reduce any sample size effect and any memory effect (see section 2.3 and 2.6).
Apart from few cases (see the $\Delta^{17}O$‰ of 4CA extr and 5CA and the measured $\delta^{15}N$‰ of 5CA), when considering the isotopic composition of the same sample that has been measured in different batches, the variability due to different days of run proved to be within the uncertainty associated to IRMS measurements.
The variability intra specimen is usually quite limited in both $\Delta^{17}O$‰ and $\delta^{15}N$‰ (compare 5OX with 5OX extr, 11OX with 12 OX and 5LO with 6LO), being in the range of the uncertainty of IRMS measurements (±0.4-0.9‰ and 0.3‰ for nitrate O and N, respectively).
The higher variability in the capital delta in samples 1LO and 2LO could be due to the presence of niter with a different MIF signature compared to nitratine, the only nitrate phase that has been detected with the XRD (see Appendix 3). This hypothesis is related to the fact that both samples had been previously classified as niter.
The sample 4CA extr was extracted from a powder that had been used for XRD analyses. The results in Table 4.4 indicate that the nitrate isotope anomaly would not change after XRD analyses lasting up to six hours, at least in a well crystallized phase.
Overall, almost all measured nitrate N delta values fall in the range of atmospheric nitrate, which is approximately near to 0 ‰, according to Bohlke et al. (1997)(see also fig. 4.6). It is important to point out that the N isotopic composition of atmospheric nitrate could be quite variable. For instance, at Pretoria (South Africa), nitrate in rain has $\delta^{15}N$‰ values from -10 to +4, whilst nitrate due to dry deposition can have $\delta^{15}N$‰ up to 10‰ (Heaton, 1987). Due to the extreme dryness at the Atacama Desert, nitrate from dry deposition should be an important component of nitrate in chilean ore deposits. Thus, the nitrogen delta values of atmospheric nitrate could overlap the $\delta^{15}N$‰ range of nitrate of biological origin (see fig. 4.6).
Higher nitrate N delta values have been found in crystallites of nitratine, compared to poorly crystallized sodium nitrate (see section 4.6). The nitratine with the highest $\delta^{15}N$‰ in table 4.6 (sample 13OX) is from a specimen that was classified as refined nitratine. If temperature has been used to purify the nitrate sediments, partial crystallization might have changed the pristine $\delta^{15}N$ signature.
In this preliminary study, it is possible to consider if the isotopic anomaly varies as a function of mineral phase by assuming that there are no other effects giving rise to differences between samples from different locations.
If possible, field studies should be undertaken or dating analyses (like ^{14}C measurements of paragenetic carbonates) should be coupled with measurements of the nitrate isotope anomaly, to group and compare the nitrate phases of similar age

and test the hypothesis that no temporal variations are responsible for the differences among samples.
To test the chance that the isotope anomaly in Chilean nitrate depends also on the mineralogical phase, samples that proved to be mixtures of nitrate salts (sample 5OX), those whose mineralogical phase has not been identified with the XRD (samples 6OX, 7OX and 8OX) and the refined nitratine (sample 13OX, since purification procedures could have altered the pristine isotopic signature) are excluded from the statistical analyses. The isotope anomaly in this selected group of samples is restricted to a range spanning from 16.2 to 21.0‰.
The mineral darapskite seems to have a lower anomaly compared to nitratine (fig. 4.4).

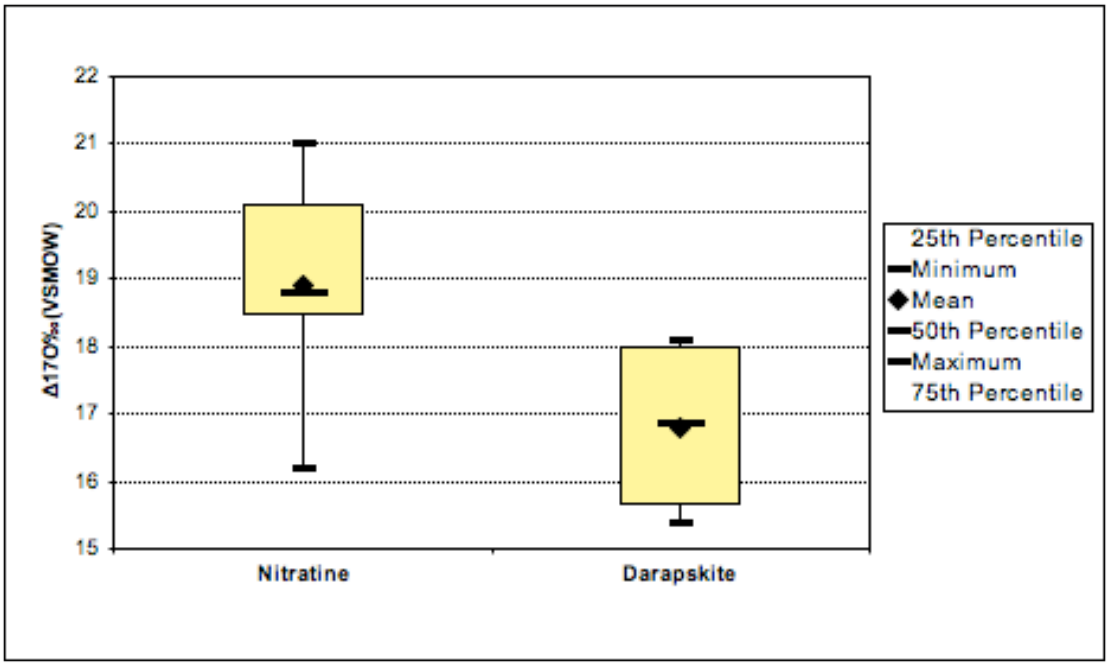

Fig. 4.4. *$\Delta^{17}O$‰(VSMOW) in three nitrate phases from the Chilean nitrate ore deposits.*

Results in fig. 4.4 indicate that some overlapping does exist in the nitrate isotope anomaly of the two groups, whereas nitrate N delta values in darapskite and nitratine seem to correspond to distinctive ranges (fig. 4.5).

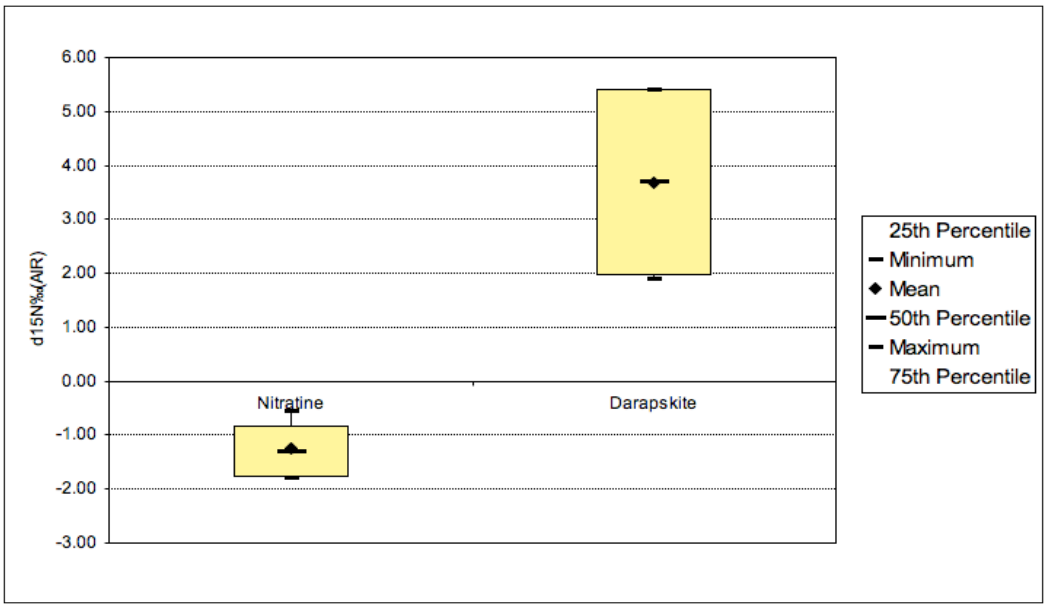

Fig. 4.5. *$\delta^{15}N$‰(AIR) in three nitrate phases from the Chilean nitrate ore deposits.*

After calculating the 2-mean t-test, both $\Delta^{17}O$‰ and $\delta^{15}N$‰ proved to be statistically different in nitratine and darapskite, since the null hypothesis (the two subsets are part of the same population) is rejected with 95% of confidence.
To sum up, only sparse measurements of the isotope anomaly in the Chilean nitrate ore deposits have been carried out. Statistical analyses of measured $\Delta^{17}O$‰ in samples of nitratine and darapskite would suggest that the nitrate isotope anomaly is not simply trapped during crystallization and might depend on the stage of brine evolution. Moreover, there is a significant difference between $\delta^{15}N$‰ in nitratine and darapskite, the latter approaching ^{15}N enrichments similar to the ones in nitrate deriving from bat guano (Mizutani et al.,1992).
Field sampling campaign are necessary to reconstruct any change in the MIF signal due to brine evolutions, by measuring spatial variations and mineral associations. Further studies on the occurrence of a change in the nitrate isotope anomaly due to fractional crystallization should be undertaken.
Because nitratine, darapskite and nitromagnesite in building stones are usually thought to be of atmospheric origin, it would be interesting to measure the isotope anomaly of this salts in monuments built in the industrial era, to verify how different is the MIF signature, compared to the signal of present day atmospheric nitrate.
Alternatively, similar tests to the ones described in Franzen and Mirwald (2008), generating different mineralogical associations, by using the standards USGS35 and USGS34 could be carried out.

4.3 The copper nitrate minerals

There are seven known solid phases in which nitrate is associated with copper. All of them are rare minerals, apart from the mineral gerhardtite, which is widespread as copper patinas in urban and polluted environments (Stoch et al., 2001).

The mineral gerhardtite (with formula $Cu_2(NO_3)(OH)_3$), the mineral likasite ($Cu_3(NO_3)(OH)_5 \cdot 2H_2O$) and the mineral buttgenbachite ($Cu_{36}(NO_3)_2Cl_8(OH)_{62} \cdot 4{-}10H_2O$) (Hibbs et al., 2002)(Hibbs et al., 2003a, b) are secondary minerals that can be found in oxidized zones of copper deposits. The mineral buttgenbachite forms a series with connellite ($Cu_{36}(SO_4)_2Cl_6(OH)_{62} \cdot 6{-}12H_2O$) and might be rarely found as patinas on bronzes (Frost et al., 2002).
The mineral rouaite, often confused with its dimorph gerhardtite (i.e. having the same formula, $Cu_2(NO_3)(OH)_3$), is a secondary mineral that has been found in cavities of the copper deposits of Roua (Alpes Maritimes, France, see Sarp et al., 2001).
The mineral mbobomkulite (Ni, Cu)$Al_4[(NO_3)_2, SO_4](OH)_{12} \cdot 3H_2O$), the mineral hydrombobomkulite (Ni, Cu)$Al_4[(NO_3)_2, SO_4](OH)_{12} \cdot 13{-}14H_2O$ and the mineral nickelaluminite (Ni, Cu)$Al_4[(NO_3)_2, SO_4](OH)_{12} \cdot 3H_2O$ are members of the group of chalcoalumite.
Only one study has been published on the N and O isotopic composition of copper nitrate minerals (Melchiorre et al., 2006), which demonstrated the biologic origin of the gerhardtite at the Great Australia Mine in Cloncurry by comparing the nitrate N delta values with local bulk termite-mound material.
The main author (Melchiorre) recently presented at the SGA conference (2011) some unpublished data on $\delta^{15}N$ from different copper nitrate minerals (fig. 4.6).

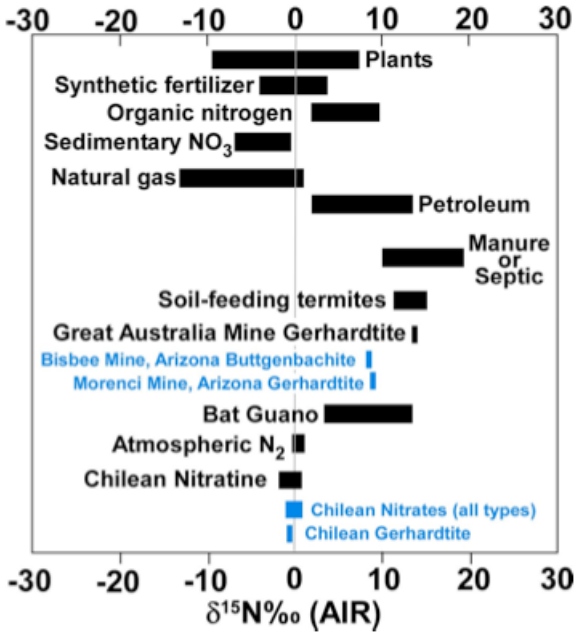

Fig. 4.6. *$\delta^{15}N$‰(AIR) in copper nitrate and its potential precursors. Presented at SGA2011 by Melchiorre (downloaded from https://sga.conference-services.net).*

According to the author, most nitrate in copper minerals is of biogenic origin, whereas the gerhardtite at the Atacama Desert and in the Pampa Bianca (first documented occurrence in Chile) is probably of atmospheric origin (abstract downloaded from https://sga.conference-services.net).
Gerhardtite is widespread as patinas due to the corrosion by atmospheric HNO_3 of copper (Samie et al., 2007). No attempt has been made to analyze the nitrate isotope

anomaly of such patinas because artificial patination was often made in the past by using a mixture containing also nitrate, to create a protective layer against natural corrosion (Hayez et al., 2006). Unless it is possible to rule out the chance of artificial patination, the analyses of the patinas in order to determine the transfer of the isotope anomaly from the atmosphere to the oxidized layer of copper is not recommended.
The description of the copper nitrate specimen is presented in Table 4.5.

UEA ID	Original ID	Locality	Nitrate phase
GERLO	BM 1985 MI33989	Congo	Gerhardtite
BUTLO	BM 1933 267	Likasi Mine, Congo	Buttgenbachite
BUTRU	//		Buttgenbachite
LIK	//	Dzhezkasgan Copper Deposit, Kazakhstan	Likasite
ROU	MHNG 477.100	Roua Mine, France	Rouaite

Table 4.5. *Sample IDs and description of the samples from the copper nitrate minerals.*

The mineral gerhardtite is soluble in dilute acids, whilst the buttgenbachite is soluble in acids and in ammonium hydroxide. It is usually not recommended to decrease the pH to extract the nitrate copper, since there could be an isotope exchange between nitrate and water (Bunton et al., 1952).
Due to the small amount of sample used (no more than few mg), it is assumed that samples that have been finely crushed in a mortar were completely dissolved in 10ml of MQ after staying 20 minutes in a sonicated bath and then on a shaker table in a incubator at 30°C overnight.
Because almost no nitrate was detected in the specimen of rouaite, a second attempt for extracting the nitrate has been made by decreasing the pH of the residual solution to 4 with the addition of diluted acetic acid. This strategy has been chosen because above a pH of 4 the isotope exchange between nitrate and water has been calculated to be low (Sigman et al., 2005).
Unfortunately the nitrate concentration in solution did not increase enough to get 50 nanomoles of nitrate in 10ml. A similar problem occurred with a specimen of buttgenbachite from the collection of Prof. Murashko (sample ID BUTRU, see Table 4.5). This sample was also extracted for a second time with acetic acid at a pH of 4 but the nitrate was insufficient for measuring the isotope anomaly.
The XRD patterns of connelite and buttgenbachite are similar and the two phases have been confused in the past (McLean and Anthony, 1972). It is therefore possible that the specimen was connellite ($Cu_{36}(SO_4)_2Cl_6(OH)_{62} \bullet 6{-}12H_2O$), or an intermediate phase (Hibbs et al., 2003), in which case the nitrate could be only a minor component.
Furthermore, comparison of the structure of different specimens of buttgenbachite from Likasi Mine (Fanfani et al. 1973)(Hibbs et al., 2003) revealed that nitrate is positioned along the zeolite-like channel where, it can be substituted by Cl^- or water.

This finding could suggest that buttgenbachite might transform to connellite, if storage conditions are not appropriate.
The isotopic composition of the specimens is presented in Table 4.6.

Sample UEA ID	**Nitrate phase**	**NO_3 injected (nmol)**	**$\Delta^{17}O$‰(VSMOW)**	**$\delta^{15}N$‰(AIR)**
GERLO	Gerhardtite	100	1.2 ±0.4	8.5 ±2?
BUTLO	Buttgenbachite	60	4.0 ±1.0	7.0 ±2?
LIK	Likasite	50	-1.5 ±1.0	1.6 ±2?

Table 4.6 *Isotopic composition of samples from the copper nitrate minerals. Due to artifacts in the nitrogen delta values during copper tests (see section 2.8) up to 1.8‰* (see table *2.16,) an approximate uncertainty of 2‰ is used*.

An isotope anomaly has been found in all copper nitrate samples. The most surprising finding is the magnitude of the isotope anomaly in the specimen of buttgenbachite.
It is unrealistic that the MIF signal in this sample is due to atmospheric nitrate, owing to the provenance of the specimen buttgenbachite from a copper mine. This is because it is expected that any atmospheric nitrate entering into the soils above or nearby the mine should undergo intense biological and chemical processes that include its consumption and regeneration, often resulting in nitrate with the isotopic signature of organic matter.
Similarly to the case of the gerhardtite from the Great Australian Mine (Melchiorre et al., 2006), nitrate could be transported to the copper deposit with groundwater. Also the nitrate in the buttgenbachite and gerhardtite from the copper mines in Arizona is associated to transport processes, since the mineral has been related to the oxidation of bat guano in limestone caves above the copper deposits (see fig. 4.6).
Table 4.6 shows also the measured $\delta^{15}N$‰. As discussed in section 2.8, there is the chance of an artifact on nitrate N delta values when using the protocol described in chapter 2. The artifact, which is below 2‰, could be due to either the presence of residual copper in solution during nitrate conversion with the denitrifier method or to the effect of the phosphatic reagent used for gross copper removal. However, such a shift, which is shown in table 2.16, seems to be below 2‰. Hence, some qualitative comments on the measured nitrogen delta values could be made.
First, the measured $\delta^{15}N$‰ of the specimen of gerhardtite and buttgenbachite are in the range of measured values of gerhardtite from the Great Australian Mine (ranging from 6.7 to 9.6‰, Melchiorre et al., 2006) as well as the copper nitrates from copper mines in Arizona, suggesting that nitrate could be of biological origin.
Because nitrate of biological origin is assumed to have no isotope anomaly, the measured capital delta could be associated to the stage of the mineral crystallization,
Another explanation could be that, due to the general low solubility of copper nitrate (especially the buttgenbachite, for which undiluted acid is usually necessary), the extraction procedure discussed in this section could have solubilized only a fraction of sample, generating a mass independent fractionation.

However, this hypothesis would imply that it could be possible to find an isotope anomaly of up to 4‰ in nitrate copper that underwent partial dissolution.
Surprisingly, the mineral likasite shows a distinctive low ^{15}N enrichment, associated to a negative isotope anomaly.
A negative anomaly has been found in stratospheric oxygen (Luz et al., 1999) and meteorites (Thiemens, 2006). To the best of our knowledge, no negative nitrate isotope anomaly has ever been reported so far (see fig. 4.10). Due to the limited availability, the specimen of likasite has been measured only once with a sample size of 50 nanomoles. Thus, there might be the chance of an artifact due to a memory effect (see section 2.3, the sample followed the analyses of 50nmol of the standard USGS34).
Further measurements of minerals should be necessary, to confirm the occurrence of negative capital delta values in nitrate minerals. Excluding the possibility that nitrate is of atmospheric origin, the analyses of sample $\delta^{15}N$‰ would suggest the presence of either nitrate from fertilizers (see fig. 4.6) or sedimentary nitrate, like the nitrate in fresh limestone and terra rossa soils (Sandler and Heaton, 1997). Only field studies and complementary data would allow distinguishing between these nitrate sources.
To sum up, the results presented in this section suggest the chance that kinetic effects could generate a mass independent fractionation of up to 4‰ during crystallization of copper nitrates.
So far, the terrestrial fractionation line (TFL, which is the line upon which data points from samples that are fractionated by mass-dependent processes lie in a three-oxygen isotopes plot, see chapter 1) has been defined mainly by using silicates and carbonates. The tendency of nitrate to fractionate in a mass independent way during atmospheric processes should not exclude that there could be a similar propensity to acquire an isotope anomaly during geochemical processes.
Isotopic measurements of niter (see section 4.4) and nitromagnesite from Pozalagua Cave samples (discussed in section 4.5) might corroborate this hypothesis.

4.4 The minerals niter and gwihabaite.

The minerals niter and gwihabaite are usually associated with biological processes. For instance, the mineral gwihabaite $(NH_4,K)NO_3$, which is the only natural solid phase that contains ammonium, is thought to form mainly in caves by bacterial action on bat guano (Martini, 1996).
Niter (KNO_3), sometimes associated with nitrocalcite ($Ca(NO_3)_2 \cdot 4H_2O$) and nitromagnesite ($Mg(NO_3)_2 \cdot 6H_2O$), is a typical cave deposit. The origin of nitrate in caves can be controversial (Barton and Northup, 2007 and reference therein). As an example, the case of the Mammoth cave is discussed. Some authors proposed a seeping groundwater mechanism whilst others suggest that nitrate is produced in situ by nitrifiers during degradation of bat guano or ammonium from urea. Fliermans and Schmidt (1977) reported the presence of the bacteria Nitrobacter in Mammoth Cave (USA) and indicated that the bacteria was responsible for the saltpeter deposit (saltpeter is the commercial name for niter, with formula KNO_3) in the cave.
Yet, Hill (1981, b), drilling cores up to 30cm in depth into wall limestone, demonstrated that at Mammoth Cave the limestone at the surface contains only few ppm of nitrate, whereas limestone protected from leaching rainfall can be enriched in nitrate (up to thousands of ppm). This finding could demonstrate that the entire cave could be impregnated of nitrate deriving from soil and transported with groundwater.

Recently, an article on the presence of aerosol containing nitrate at Mammoth Cave has been published (Zhao and Hopke, 2006) as well as gasoline, aged sea salt and saharian dust. The earliest measurements have been made in 1992, only 12 years after Hill's investigation. Thus, the nitrate isotope anomaly might be able to clarify how important is the atmosphere as a source of nitrate at Mammoth Cave.
The isotopic signature of nitrate N has been used to understand the origin of monomineralic KNO_3 stalactites (up to 90cm long, 20kg of total niter in Niter Cave has been calculated) in a limestone cave in Galilee, Israel (Sandler and Heaton, 1997). The range of $\delta^{15}N$ observed, (+7.1 to 9.7‰) overlaps the range reported for cave niter in three sites of South Africa (+7.9 to 13.5‰, Heaton 1987a). According to the authors, partial nitrification of ammonium derived from degradation of excreta could explain both nitrate and ammonium observed $\delta^{15}N$ in the cave.
The aim of the analyses of this small subset reported here is to investigate if nitrate of biological origin, which should have no isotope anomaly, could have acquired a MIF signature during the stage of crystallization.
The description of the samples that have been measured for the isotope anomaly is presented in Table 4.7.

UEA ID	**Original ID**	**Full description**	**Locality**
3LO	BM 1934 610	Niter from a river	USA
4LO	BM 1934 610	Niter from a river	USA
1RU	//	Niter	Bakla Mountains, Crimea, Ukraina
2RU	//	Niter	Bakla Mountains, Crimea, Ukraina
3RU	//	Niter	Bakla Mountains, Crimea, Ukraina
4RU	//	Gwihabaite	Kukhi-Malik, Tajikistan

Table 4.7. *Sample IDs and description of samples of niter and gwihabaite.*

The presence of niter in caves of the Bakla Mountains has been documented by Dvoichenko (1914) and Popov (1938)(both in Russian). The gwihabaite at Kukhi-Malik Gorge (formerly called Kan-Tag, or *Burning Mountain*) has already been investigated (Belakovski and Moskalev, 1988). According to the authors the mineral derives from coal burning due to the Ravat coal fire, which affected the region for more than 2000 years (Sharygin et al., 2009) (Belakovski and Moskalev, 1988).
The isotope anomaly of cave nitrate is presented in Table 4.8. The sample size is always 100nmol of nitrate; all samples have been measured in the same batch.

UEA ID	Nitrate phase	$\Delta^{17}O$‰(VSMOW)	$\delta^{15}N$‰(AIR)
3LO	Niter	-0.9±0.9	4.0±0.3
4LO	Niter	-2.0±0.9	5.0±0.3
1RU	Niter	0.7±0.4	13.2±0.3
3RU	Niter	-0.7±0.4	12.3±0.3
4RU	Gwihabaite	-0.4±0.4	-9.4±0.3

Table 4.8. *Isotopic composition of samples of niter and gwihabaite.*

The negative nitrogen delta value of the sample of gwihabaite might be related to the fact that the nitrate would derive from burnt wood, (see fig. 4.6). The most important information is that no measurable nitrate isotope anomaly is associated with gwihabaite formation.

The measured $\delta^{15}N$ values of the two samples from the Crimean cave (1RU and 3RU) fit the range of nitrate derived from bacterial degradation of excreta (Sandler and Heaton, 1997)(Heaton, 1984). No isotope anomaly is associated to the sample crystallization.

A clear assignement of the origin of niter from an American river (samples 3LO and 4LO) based on the N isotopic signature is difficult, due to both the limited ^{15}N enrichment and the lack of any complementary data.

The sample 3LO has been extracted from some powder, whilst the sample 4LO derived from a piece of a big fragment that looked well crystallized. Because the uncertainties associated to the isotopic measurements are high (±0.9‰), it is impossible to confirm whether there is a measurable difference in the isotope anomaly related to the degree of crystallization or not. The two samples data would suggest the presence of a small negative anomaly, similarly to the specimen of likasite (see table 4.6).

It is important to point out that there is probably no evidence for the development of a nitrate isotope anomaly due to biological processes because, to the best of our knowledge, no studies on the subject have been undertaken. Turro and Kraeutler (1980) found the magnetic fields generate isotopic effects in organic photochemical reactions. Later on, Buchachenko (1995) developed a theory on the MIE (magnetic isotope effects), whose main hypothesis is that any radical pair behaves as a spin-selective micro-reactor. The isotope ^{17}O has magnetic properties, which in fact could explain some anomalous ^{17}O enrichments as a function of the chain oxidation and the chain length of some organic compounds (Buchachenko et al., 1995). The same year a work on the magnetic effects in biology due to radical-pair mechanisms recombination was published (Grissom, 1995). Further studies suggested that the MIE could explain the kinetics of dislocations in diamagnetic crystals (Buchachenko, 2007) and, more importantly, that magnetic effects regulate the enzymatic activity (Buchachenko, 2008)(Buchachenko, 2007), which in fact proved to be responsible for anomalous enrichments in the isotopic composition of methylmercury (Buchachenko, 2010).

Thus, due to the known sensitivity of some enzymes to isotopes with magnetic properties, it is possible that some organisms involved in the nitrogen cycle could generate anomalous enrichment or depletion of ^{17}O. In order to investigate the occurrence of a negative nitrate isotope anomaly, further studies on the biological

preference for nitrate containing ^{17}O during denitrification and nitrification are necessary.

4.5 A MIF signature in the moonmilk deposits of Pozalagua Cave (Spain): a mass independent fractionation due to the effect of capillarity?

The dolomite cave called Pozalagua, in Karrantza Valley (57 km west of Bilbao, northern Spain, fig. 4.7) represents one of the most important karst systems of the region.

Fig. 4.7. *Karrantza Valley location (Google Maps, 2010).*

The cave was generated by hydrothermal fluid circulation that dissolved reef limestones of the Urgonian facies (Jurassic-Cretaceous transition). A paper on microclimate monitoring at the cave has been recently published (Lario and Soler, 2010). The reader is referred to the article and reference therein for a detailed description of the site.
The cave moonmilk deposits of Pozalagua Cave have been investigated in Martinez-Arkarazo et al. (2007). According to the authors, the salts formed owing to the water absorption from the floor through the speleothems. The term moonmilk refers to microcrystalline mineral aggregates in caves with a physical appearance ranging from a very soft paste to cottage cheese that dry to the consistency of talcum powder (Northup and Lavoie, 2001). It is usually associated with microbial activity on carbonatic substrates (Blyth and Frisia, 2008)(Canaveras et al., 2006, study of the deposits in Altamira Cave, Northern Spain).
Among the major component hydromagnesite (with formula $Mg_5(CO_3)_4(OH)_2 \cdot 4H_2O$), several nitrates phases (nitrocalcite, niter, nitromagnesite, nitratine and gwihabaite) have been detected.

Sampling of some nitrate deposits at the Pozalagua Cave has been carried out because it would represent a unique opportunity to measure the nitrate isotope anomaly in different mineralogical phases from the same site.
Five water samples and thirteen samples of moonmilk deposits from seven different zones of the cave have been collected (fig. 4.8).

Fig. 4.8. *Pozalagua Dolomite Cave with sampling sites, map adapted from Martinez-Arkarazo et al, 2007.*

Four water samples (sample IDs with an A) have been collected inside the cave, whilst the sample 5A is from Rio Seco, which flows nearby (Map 4.12, the sampling site location is circled in red, whilst the cave entrance is circled in blue).

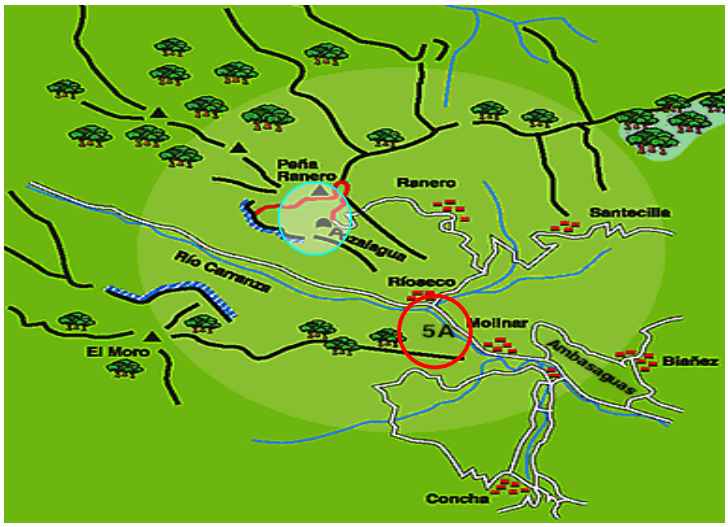

Fig. 4.9. *Rio seco and Pozalagua Dolomite Cave entrance.*

The samples 1A and 2A come from water dripping from the ceiling, whereas water samples 3A and 4A are collected from puddles in the cave.
All water samples have been filtered in situ with cellulose acetate filters (0.2μm) and frozen at -76°C within 12 hours from sampling.
The moonmilk deposits have been extracted with 5 ml of MQ in a sonicated bath for 20 minutes. The samples were then placed on a shaker table overnight, before being filtered with cellulose acetate filters (0.2μm). Sample major anion contents, measured with an ion chromatograph (Dionex ICS5000) with the help of the Laboratory Manager Liz Claxton, have been carried out. The ratios of major anions are presented in table 4.9.

Sample ID	**NO_3^-/ Cl^-**	**NO_3^-/ SO_4^{-2}**	**Cl^-/ SO_4^{-2}**
1-1	0.3	1.0	3.4
1-2	//	0.4	//
2-1	4.5	4.5	1.0
2-2	0.6	0.3	0.6
3	0.0	0.4	12.6
4-1	4.0	2.4	0.6
4-2	14.9	23.4	1.6
5-1	5.9	10.0	1.7
5-2	1.6	3.4	2.1
5-3	2.5	6.5	2.5
6	0.8	1.6	1.9
7-1	5.4	20.0	3.7
7-2	3.5	11.3	3.2
1A	0.1	0.1	0.7
2A	0.1	0.1	1.6
3A	0.0	0.1	4.2
4A	0.0	0.2	3.7
5A	1.1	1.3	1.2

Table 4.9. *Major anions ratio in moonmilk deposits and in water samples 1A-5A from Pozalagua Cave, Spain.*

The nitrate is the main component of the soluble fraction in the sediments of the zone 4 (the area called Organo Hall), 5 (the area called Versailles) and 7, which is consistent with the report in Martinez-Arkarazo et al. (2007). The nitrate, sulphate and chloride concentrations only have been analyzed. Yet, additional peaks in the chromatographs showed the presence of other ions (in table 4.10 the results of the chromatograph of sample 2-1 are presented).

No.	Retention Time min	Peak Name	Height µS	Area µS*min	Rel.Area %	Amount mg/l
1	5.32	Chloride	0.693	0.117	7.98	0.092
2	7.25	n.a. nitrite?	1.075	0.364	24.71	n.a.
3	10.90	n.a. Carbonate	0.812	0.548	37.27	n.a.
4	13.68	Sulphate	0.349	0.109	7.43	0.092
5	14.15	n.a. Phosphate?	0.298	0.118	7.99	n.a.
Total:			4.223	1.472	100.00	0.602

Table 4.10. *Chromatograph of sample 2-1.*

The peak at around 10.9 minutes, due to carbonates, is present in all samples, as expected in salts from a dolomite cave.
The peak after sulphate, with a retention time of 14 minutes, might be due to phosphate. A third peak, with a retention time of 6.15 minutes could be due to nitrite.
The XRD patterns obtained from all the samples are complex but similar to each other (results are presented in Appendix 3). Unlike the findings in Martinez-Arkarazo et al., (2007), no evidence of the presence of a mixture of nitrate phases has been found at Pozalagua Cave.
It is possible that the main nitrate phase could be nitromagnesite ($Mg(NO_3)_2*6H_2O$), since its major diffraction peak has been found in few samples, corresponding to a d space of 3.29Å.
The highest relative intensity (28%) of the diffraction peak of potential nitromagnesite has been found in sample 5-3, which is from an area where the presence of nitrate has been found to be important (see Table 4.9).
However, due to the complexity of the diffraction patterns, the general low intensity of the major diffraction peak of nitromagnesite and because of some overlapping between the minor diffraction peaks of nitromagnesite with other stronger signals, it was impossible to confirm that the main nitrate phase in the moonmilk deposits is nitromagnesite.
The lack of a definite diffraction pattern due to nitrate minerals, even when nitrate is the main component in the soluble fraction (see table 4.9), could indicate that the nitrate is not crystallized enough to be clearly detected with the XRD. Further analyses of our samples with the µRaman spectroscopy would be necessary, to increase the spatial resolution and being able to distinguish among different phases.
In table 4.11 the isotopic composition of three samples is shown.

Sample ID	$\Delta^{17}O$‰(VSMOW)	$\delta^{15}N$‰(AIR)
POZ 4-1	10.3±0.4	0.1±0.3
POZ 4-2	0.4±0.4	-1.25±0.3
POZ 7-1	0.2±0.4	-2.0±0.3

Table 4.11. *Isotopic composition of the moonmilk deposits at Pozalagua Cave, Spain.*

Unfortunately, no isotopic measurements of water samples inside the cave were obtained, due to their low nitrate content.

The most surprising result is the isotope anomaly in sample 4-1, which has been measured in duplicates in four different batches.
Previous less precise analyses, data not shown, suggested that the isotope anomaly was null in the whole sampling areas and that only the sample 4-1 had a measurable anomaly of 10‰. The isotopic anomaly in POZ 4-1 would be consistent with a sample deriving half its isotopic signature from atmospheric nitrate but, with only one sample showing this pattern, this seems unlikely. Furthermore, the sample POZ 4-2 has been collected from the same deposit but at its top (whilst POZ 4-1 is from the bottom of the same deposits, which was 7-8 cm wide and 15-20 cm long).
Consequently, assuming that the result is representative, it is more likely that a local process, probably associated to water adsorption, generated the mass independent fractionation.
The nitrate N delta values tend to negative values and are in the range of sedimentary nitrate (Melchiorre, 2011, see fig. 4.6)(Sandler and Heaton, 1997), which would be consistent with the nitrate deposit being due to geochemical processes rather than associated with in situ bacterial degradation of organic matter.
To the best of my knowledge, this is the highest nitrate isotope anomaly reported in non-atmospheric nitrate. The mass independent fractionation found at Pozalagua cave could reflect the occurrence of unusual kinetic processes.
Unfortunately, no attempts have been made to sample some material with a drill core and verifying what is the nitrate content impregnated in the speleothems. According to Hill (1981,b), the regeneration time of nitrate moonmilk could vary from a few months to 5-10 years. Assessing the regeneration time of the nitrate deposit at Pozalagua Cave might allow an understanding of the unique mechanism generating this isotope anomaly.
Further studies should be undertaken, to identify other potential sources of an isotope anomaly and to which extent they could affect the interpretations when the MIF signal is used as a tracer of atmospheric nitrate.

4.6 Laboratory tests on the change of the MIF signal during phase transitions

The results discussed in the present chapter suggest that the MIF signature may not be a conservative tracer.
Molecular dynamics simulations of sodium nitrate solutions (Thomas et al., 2007) indicate that nitrate resides primarily below the surface of the solutions over a wide range of concentrations. The molecules below the surface are significantly undercoordinated compared to in the bulk, and reactions involving solvent cage effects, like photochemical processes, could occur.
It is accepted that the photolysis of nitrate in snow could change the initial nitrate isotope anomaly (Frey et al., 2009). Similarly, due to the high nitrate surface tension, photolysis in brine slabs of the Atacama Desert could therefore be responsible for a change in the capital delta values of deposited nitrate. However, nitratine of the Chilean deposits is also thought to be due to water filling joints and cracks of rocks. It is therefore important to investigate the magnitude of the change of an isotope anomaly due to other common processes, like evaporation, dissolution and crystallization.
Three different types of tests have been undertaken to test if the MIF signature can change during such phase transitions. The first set of tests is on the evaporation of

nitrate solutions with an isotope anomaly that is similar to the one found in the nitratine from the Atacama Desert.
The nitrate used comes from the stock solution prepared for analyzing 13OX (refined chilean nitrate from Oxford University Museum, see Table 4.2). Each sample of this series of tests constitutes of an aliquot of 0.2 ml of 13OX diluted with 9.8ml of MQ. These samples were then subjected to varying degrees of evaporation in an oven.
The sample IDs of this subset constitutes of a number X, followed by a letter Y, a number W and a letter Z.
The number X can be either 35 or 45, which is the temperature (°C) at which the nitrate solution evaporated. The temperature of 35°C has been chosen has it is close to the average high temperature in the summer (30°C).
Intended as a first set of exploratory tests, a temperature of 35°C or higher has been chosen to amplify any change in the isotope anomaly due to kinetic effects that could be seen after a reasonable period of time and with a magnitude higher than the precision of the IRMS measurements (which can be, depending on days, up to 1‰).
The letter Y indicates the container used to place the nitrate solution in the oven. The letter Y is a B (if a beaker of 250ml is used), a T (a 50ml centrifuge tube) or a P (a Petri dish). Because the volume of sample is the same (10ml), the difference in the ratio surface/volume would cause different evaporation rates. Thus, for each temperature chosen (35°C and 45°C), three samples in different containers were placed in the oven.
The last combination WZ indicate the time after which 0.1ml of evaporating solution is transferred in a centrifuge tube and diluted with 9.9ml of MQ.
The letter Z could be H (hour) or D (day); as an example, the sample 45T1H has been extracted from the solution placed in a 50ml centrifuge tube after one hour since the start of the evaporation at 45°C.
After three days, both petri dishes were completely dried, with nitrate deposited as zoned white layers with a few prismatic crystallites at the edges of the dishes, where the last of the water evaporated.
It is assumed that partial evaporation as HNO_3 should be more important in the first few hours, whilst precipitation occured at a later stage of the experiments. Consequently, a change in the MIF signal in the first part of the experiment will be attributed to partial evaporation (and vice versa for nitrate precipitation).
Considering that water activity on $NaNO_3$ solutions with solute weight being less than 2% is approximately 1 (Tang and Munkelwitz, 1994) and assuming that also $[NO_3^-]$ activity is one (since the sample is refined nitratine, the ionic strength in water due to the presence of other ions can be safely regarded as insignificant), the partitioning between the liquid and the gas phase could be calculated based on the parameters used for the model ISORROPIA (Nenes et al., 1998), which takes into account the reaction ($HNO_{3(g)} \Leftrightarrow H^+_{aq} + NO_3^-{}_{aq}$).
Assuming that HNO_3 behaves as an ideal gas, it has been calculated that, due to the high solubility constant, no nitrate loss associated with evaporation can be measured. Yet, the chance that such a loss of nitrate can have a measurable effect in the nitrate isotope anomaly will be tested anyway.
Based on solubility curves and the initial nitrate concentration, it has been calculated that nitrate precipitation should occur when the volume of water is below 0.1ml.
A list of sample measurements from this subset, with their respective isotopic composition and nitrate concentration is presented in table 4.12. The nitrate concentration is deduced from the volume injection that is necessary to match the total beam areas of 100nmol of standards.

Sample ID	$\Delta^{17}O$‰ (VSMOW)	$\delta^{15}N$‰(AIR)	NO_3 (mM)
35T 1H	16.2	1.35	20.0
35T 1H	16.6	1.3	20.0
35T 24H	17.6	0.9	20.4
35T 24H	16.8	1.1	20.4
35T 24H	18.4	1.1	20.4
35T 3D	17.5	1.0	24.9
35T 3D	17.2	1.1	24.9
35T 3D	17.5	-0.7	24.9
35T 3D	17.2	0.9	24.9
35B 3D	16.5	1.1	78.5
35B 3D	17.4	1.0	78.5
35B 3D	17.1		78.5
35B 3D	17.5		78.5
35P 24H	16.0	1.1	61.7
35P24H	17.7	0.1	61.7
35P24H	16.7	1.0	61.7
45T 24H	18.2	1.2	22.1
45T24H	17.2	-0.4	22.1
45T24H	17.5	1.4	22.1
45B 24H	17.6	1.0	39.2
45B24H	17.2	1.2	39.2
45B24H	17.2	0.3	39.2
45P 24H	17.1	0.9	289.2
45P24H	17.3	0.8	289.2
45P24H	17.0	1.0	289.2

Table 4.12. *Results from the evaporation experiments of nitrate solution at 35°C and 45°C.*

Considering that the nitrate solution used for the evaporation experiments has an isotope anomaly of 16.3‰±0.4‰, the variability in the capital delta among the samples shown in table 4.12 proved to be within the precision of the method (see section 2.3). Consequently, these results would suggest that the nitrate isotope anomaly does not change during evaporation.

However, it is possible that the absence of a MIF shift during both evaporation and crystallization could be due to the high nitrate content of the original solution, which is unlikely to be found in brines of desert environments.

Nitratine and darapskite have been found in the caves of Cerna Valley (Romania) (Puscas et al., 2010)(Onac et al., 2011). The presence of phosphates associated with the mixture would prove the biological origin of nitrate. Based on $\delta^{34}S$ analyses, the authors suggested that hot ascending steam converted the guano in the sediments to a mixture of sulphates and nitrates. It would be interesting verifying the chance of an isotope anomaly in those nitrate deposits, which would confirm the potential of a hydrothermal system to generate an isotope anomaly.

A second type of tests was focused on comparing the isotope anomaly in the zoned layers and in the crystallites of nitratine found in the petri dishes of the first set of

experiments. Because the nitrate used for preparing the solutions derives from refined nitratine (specimen with sample ID 13OX), it is expected that only nitratine and amorphous sodium nitrate could form.
To enhance the nitrate separation between well-developed crystallites and zonated surrounding layers, which are due to the effect of capillarity, other experiments were carried out with the petri dishes in an oblique position.
Thus at the edge of the petri dish bigger crystallites with prismatic habit should form (since the water depth is higher and the last fraction of water evaporates later), whilst the surrounding layer should be more extended, owing to the decreased steepness of the wall.
Furthermore, other temperatures have been used, to increase the rate of evaporation and the effect of kinetic processes in the zoned layer.
The original solution has been made by dissolving in MQ the sample of the first set of experiments that stayed at 45°C in a petri dish, which completely evaporates within two days from the start of the evaporation.
The description of the samples from this second subset and their isotopic composition is presented in Table 4.13.

Description	**Temperature**	**Date analyses**	**$\Delta^{17}O$‰ (VSMOW)**	**$\delta^{15}N$‰ (AIR)**
Crystallite 1	45°C	24/3/11	17.0±0.8	0.4±0.3
Amorphous 1	45°C	24/3/11	17.0±0.8	-0.6±0.3
Crystallite 1	45°C	16/4/11	17.5±0.5	-1.3±0.3
Amorphous 1	45°C	16/4/11	18.1±0.5	1.0±0.3
Crystallite 2 (oblique position)	45°C	16/4/11	17.3±0.5	1.7±0.3
Amorphous 2 (oblique position)	45°C	16/4/11	//	-0.7±0.3
Crystallite 2 (oblique position)	45°C	19/4/11	17.5±0.6	2.1±0.3
Amorphous 2 (oblique position)	45°C	19/4/11	17.5±0.6	-0.2±0.3
Crystallite	60°C	24/3/11	18.0±0.8	0.1±0.3
Amorphous	60°C	19/4/11	17.5±0.6	-0.8±0.3
Crystallite	80°C	24/3/11	17.2±0.8	0.8±0.3
Crystallite	80°C	16/04/11	17.3±0.5	1.6±0.3
Amorphous	80°C	16/04/11	16.9±0.5	-0.7±0.3
Crystallite	80°C	19/4/11	17.0±0.6	2.1±0.3
Amorphous	80°C	19/4/11	16.8±0.6	-0.2±0.3

Table 4.13. *Isotopic measurements of crystallites of nitratine and solid sodium nitrate.*

No shift in the isotope anomaly has been found to depend on the degree of crystallization. This finding would suggest that no difference should be found in the isotope anomaly of the efflorescences and the crystals of nitratine of the same site.
On the other hand, there is a small nitrogen isotope fractionation between the crystallites and the evaporating solution that slightly increases with the temperature,

with a maximum difference in the delta values of 2.4‰ at 80°C (compare the results shown in the last four rows of table 4.13).
The last set of experiments was focused on the potential for a change in the nitrate isotope anomaly during the partial melt of ice containing nitrate.
The solution used is 8 ml of left over sample 45P24H (see table 4.12). The solution was frozen at in the -80°C freezer for an hour. The sample was then kept at room temperature for half an hour, so that the sample is only partially melted, and 1ml of melted solution is transferred to a centrifuge tube and diluted with 3ml of MQ (sample ID is ICE 1).
Once the sample is completely melted, it is placed again in the -80°C freezer for an hour. The procedure is repeated for 5 times (sample ID from ICE 1 to ICE 5), and the residual liquid is also analyzed (RES ICE).
Table 4.14 shows the description of the samples, with their isotopic composition and the nitrate concentration (based on sample volume injections necessary to match the total beam area of 100nmol of standard).

Sample ID	**(mg NO_3 /L)**	**$\Delta^{17}O$‰(VSMOW)**	**$\delta^{15}N$‰(AIR)**
RES ICE	294	18.6±0.6	1.1±0.3
ICE 1	87	18.2±0.6	1.1±0.3
ICE 2	114	17.6±0.6	1.1±0.3
ICE3	138	18.3±0.6	1.1±0.3
ICE4	158	17.5±0.6	1.2±0.3
ICE5	167	18.5±0.6	0.9±0.3

Table 4.14. *Results from the experiment on the partial melt of ice.*

No change has been found in the nitrate isotope anomaly due to partial melting of a nitrate solution. Similarly to the first subset of samples from the evaporation experiments, it is possible that high nitrate concentrations might make it difficult to see any changes that are possible in natural environments where concentrations are lower. In fact, the $\Delta^{17}O$ profiles in Antarctica (fig. 4.1, from Frey et al., 2009) and the isotope anomaly at the Marano lagoon as a function of nitrate concentration (fig. 3.6) would suggest that a change in the MIF signature could be possible at low nitrate concentrations (below 10mg/L).
Thus, due to the high nitrate content, never lower than 87mg/L, our samples might be not suitable to investigate the change of the nitrate isotope anomaly due to geochemical processes, if there is any.
There are several reasons behind the choice of not using solutions whose nitrate concentration is similar to water or brine in natural environments.
As discussed in Chapter 2, duplicates or triplicates are necessary to avoid artifacts due to the memory effect. Also, at least one attempt, but more often two, is necessary before knowing the right sample volume injection, to ensure that the sample total beam area is less than 10% different from the standards total beam area (to avoid any sample size effect). Moreover, in order to get a precision below 1‰, a sample size of 100 nmol or higher should be used. Finally, rinsing the syringe with sample water (see section 2.1) is necessary, to prevent contamination from previous samples. Consequently, the nitrate solution for the tests should be at least in the range 0.2-

0.4mM. Thus, further studies could be carried out when improvements in the nitrous oxide extraction and thermal decomposition are possible.
The high isotope anomaly discussed in the present chapter from the samples whose nitrate is unlikely to be of atmospheric origin, is shown and compared to previous published data (fig. 4.10 modified after Yanhe et al., 2010).

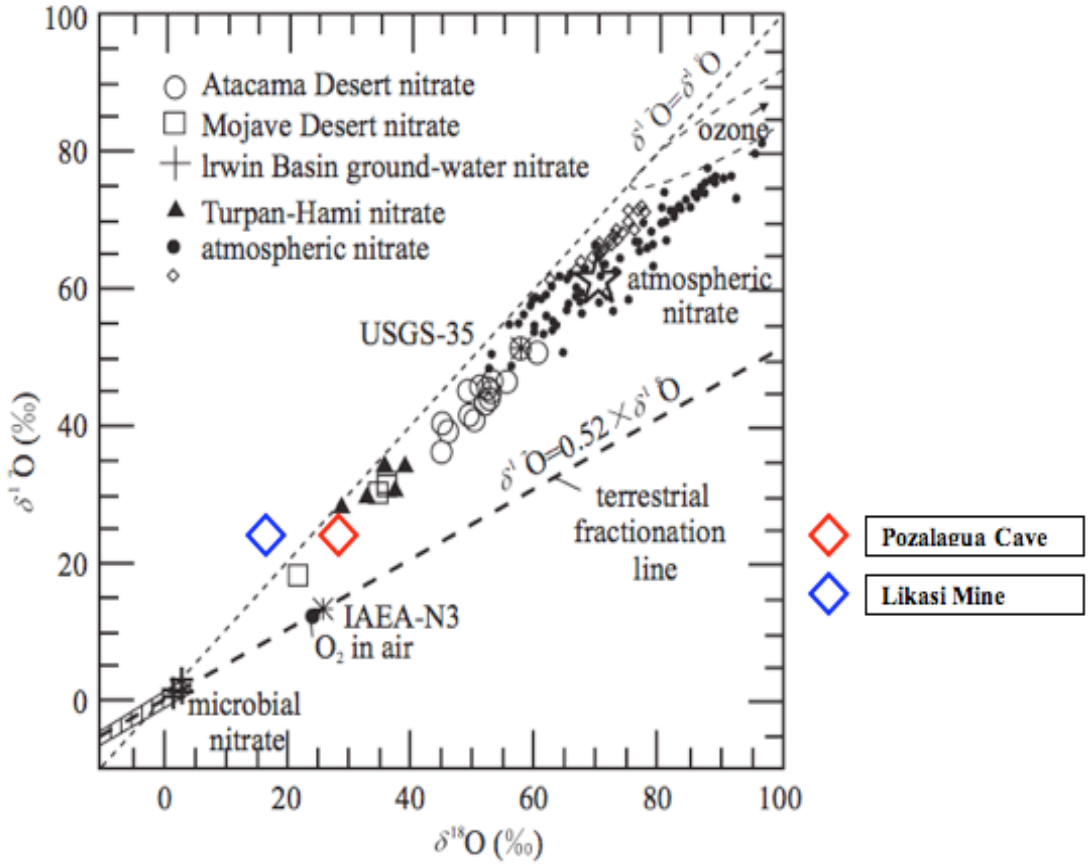

Fig. 4.10. *Published data on the isotope anomaly in nitrate with the addition of the data of the nitromagnesite found at Pozalagua Cave and the buttgenbachite from Likasi Mine (modified after Yanhe et al., 2010).*

Both measurements are rather unique since they suggest the chance of an isotope anomaly due to geochemical processes that is comparable to the mass independent fractionation generated in the atmosphere. Sometimes the term non-Rayleigh isotope fractionation is used as a synonym of a mass-independent fractionation (Young et al., 1998). It is important to point out that a Rayleigh isotope fractionation occurring in nature should be able to lead to a nitrate with high $\delta^{18}O$ values in certain circumstances (highly fractionation constant, high evaporation rates, low initial concentrations).
Yet, no nitrate samples with high $\delta^{18}O$ values and no isotope anomaly have been found so far. When nitrate has high $\delta^{18}O$ values, it is regarded as the proof that atmospheric nitrate is present. However, the nitrate at Pozalagua Cave and Likasi Mine is highly enriched in ^{18}O and ^{17}O but it is likely of terrestrial origin.
Due to fact that large uncertainties in measured $\delta^{18}O$ and $\delta^{17}O$ (up to 6‰, see section 2.3) are possible when using the thermal decomposition method with a gold furnace,

the isotope anomaly and the nitrogen delta values only have been presented in this thesis. The high uncertainty on the oxygen delta values is the main reason for not presenting the entire data set in the same way as in fig. 4.10.
However, the oxygen fractionation in both the samples showed in fig. 4.10 is high enough to be distinguished from the other measured oxygen delta values ($\delta^{18}O$ and $\delta^{17}O$ are 28‰ and 25‰ respectively for the cave specimen, whilst the other samples from Pozalagua Cave have oxygen delta values from -3 to +0.5‰, and 24‰ and 16.5‰ for the likasi buttgenbachite, whereas the other copper minerals have oxygen delta values lower than 10‰).
Recently, the nitrate N and O isotopic composition of niter deposits in Wuzongbulake (China) has been published (Qin et al., 2012). Interestingly, $\delta^{15}N$ are exceptionally high (from 15 to 27.6‰), suggesting that the nitrate should not be of atmospheric origin. Yet, measured $\delta^{18}O$ are also high (from 30.3 to 36.3‰) and almost comparable with the $\delta^{18}O$ of the samples from the Turpan-Hami deposit, whose $\Delta^{17}O$ is in the range 12.3-16.8‰.
It would be interesting to know what is the magnitude of the isotope anomaly in this niter deposit, which is highly fractionated in both the nitrate N and O isotopes.
To sum up, the results discussed in the present chapter would question the assumption that only the atmospheric nitrate has a significant isotope anomaly. Even if only two samples have a significant nitrate isotope anomaly, it is important to point out that the analyzed minerals whose nitrate is unlikely of atmospheric origin is a subset of data that excluded the results from the Chilean nitrates and constitutes 11 data points. Therefore an isotope anomaly has been found in 18% of this restricted population.
On two occasions a negative isotope anomaly has been found in a nitrate mineral. This occurrence, which has never been reported so far, would suggest that further analyses are needed, to understand its origin.
A positive MIF signature seems to be related to the degree of the oxygen isotopes fractionation (measured $\delta^{18}O$ of 28‰ and 24‰ for the cave sample and the mine sample respectively), suggesting that any geochemical process could generate, in certain circumstances, an isotope anomaly.
To verify the general assumption that the MIF signature can be regard as a conservative tracer, the effect of a mass dependent fractionation in the resulting capital delta value of a nitrate pool having an initial isotope anomaly ranging from null to 20‰ is explicitly calculated in the next chapter by considering the absolute isotope abundances.

5. Is the nitrate isotope anomaly a conservative tracer?

In this study results have been presented on N and O isotopic composition of nitrate from sample water collected at the Marano lagoon, to test the potential of the nitrate MIF signature as a tracer of local biogeochemical processes.
Based on the magnitude of the tracer, the atmospheric inputs proved to be low (the contribution of atmospheric input to nitrate in sample water usually below 3%) with the overall uncertainties in the range 30-50% of the estimated atmospheric nitrate content. Interestingly, no correlation was observed between the magnitude of the tracer and the meteorological conditions, even when comparing samples collected during periods of dryness with ones collected after important rain events (up to 100ml in 24 hours). This finding might suggest that at the Marano lagoon some biogeochemical processes involved in the local nitrate cycling could act as a buffer, maintaining the nitrate MIF signal in sample water in a restricted range.
There are some evidences that removal processes could change a sample capital delta (see fig. 3.6, and fig. 4.1, from Frey et al., 2009) and the isotope analyses of different mineralogical phases in samples from the nitrate ore deposits of the Atacama Desert (chapter 4) give support to the hypothesis that fractional crystallization could cause a shift in both nitrate $\Delta^{17}O$ and $\delta^{15}N$.
The results presented in the last two chapters also indicate the possibility that a nitrate isotope anomaly could be generated by processes in addition to reactions with ozone in the atmosphere, such as during crystallization from aqueous solutions or because of sewage treatments with ozone. Consequently, the atmosphere might not be the only source of a nitrate MIF signal.
During experiments for testing the suitability of the denitrifying method for analyzing copper nitrate minerals, an observed isotope anomaly of 1.5‰ during nitrate reduction by *Pseudomonas aureofaciens* in solutions with high copper concentration (20μM) could indicate that, under conditions of high levels of stress, some bacteria would generate a detectable MIF signature. Such a high copper content is unlikely to occur in natural environments and it would be important to assess what is the pollutant content threshold below which no mass independent fractionations associated to enzymatic processes will be detected.
Some observations on the theory of the isotope partitioning in systems at equilibrium conditions are made in this last chapter, to be able to reconcile some unexpected results of the present work. The choice of being focused on the theory of the mass dependent fractionation, rather than on the MIF, has been made for two reasons.
Firstly, the mass dependent fractionation is always associated with systems that reached equilibrium conditions and the occurrence of a MIF would indicate a departure from such conditions. Thus, if someone found that there would be the possibility of detecting an isotope anomaly as a consequence of a reversible process, such finding would have important implications, suggesting the need of reviewing the general theory of the isotope partitioning among phases.
When a strange phenomenon is observed, there are two possibilities: something new has been discovered or there is something incorrect in the existing theory. In my opinion, the increasing literature on anomalous isotope fractionations underlines the tendency towards choosing the first option.
It is important to point out that there is a reasonably wide literature on the theory of the MIF (see chapter 1 and reference therein), but very few published works focused on explaining the origin of the mass dependent fractionation (Urey, 1947; Bigeleisen

and Mayer, 1947; a review was made in Young et al., 2002). To the best of my knowledge, the theory of the mass dependent fractionation has been developed based on the work of Urey, Bigeleisen and Mayer and it has never been questioned. Thus, in most works on the MIF the existence of a MDF at equilibrium conditions is simply accepted and it is rarely explained. Nevertheless, many strange isotope anomalies have been observed so far and I would like to suggest that such effects could depend on our imperfect knowledge of how the isotopes distribute among phases, regardless of the reversibility of the process.

A second reason for my choice is that it should be legitimate trying at first to tests some hypotheses starting from the study cases that are simpler to describe. Defining theoretically the effect of irreversible processes is probably among the toughest challenges that scientists have to face. The rigorous application of the Onsager relationships (Onsager, 1931; Onsager 1953), which take into account electrical, gravitational and centrifugal fields to describe the exchange of matter and energy in a system, requires the use of a complex mathematical formalism and the knowledge of many parameters. Such theory has been used for the study of isotope diffusion in silicate melts (Richter, 1993).

Because the effects of irreversible processes are difficult to calculate, it is complicated designing an experiment to obtain a specific change of state in a system. On the other hand, by slowly changing one of the state variables of the system (like temperature and pressure), it should be easier to obtain the passage between two chosen equilibrium conditions during an experiment.

Finally, there is no work on testing the basic assumption that a mass dependent process cannot change the nitrate isotope anomaly in a sample (Morin et al., 2009; Thiemens, 2006; Kendall et al., 2007; Tsunogai et al., 2011), since no references are given when such an important property is mentioned. However, if this is only an assumption, it is important for the success of the use of the tracer that the validity of this hypothesis is proved.

A remarkable paper by Matsuhisa et al. (1978) on the oxygen isotope exchange between water and SiO_2 could question this hypothesis. The study is focused on the use of the three oxygen isotopes plot to establish when the quartz-water system reached equilibrium conditions. The authors made use of the fact that mixing two materials with no isotope anomaly but with a large difference in the isotopic composition generates a sample that is off the terrestrial fractionation line. Moreover, according to same authors, the isotope exchange between two phases, one of which had an isotope anomaly, causes both compounds to change their distance from the "primary fractionation line" (the TFL), until they lie on the straight line that is parallel to the TFL.

To the best of my knowledge, Matsuhisa et al. (1978) would represent the only published work where the effect of a MDF on the isotope anomaly of a sample is investigated. The surprising result is that both compounds involved in the isotope exchange would change their distance from the TFL. Therefore, based on this study, mass dependent processes could be able to change the isotope anomaly of certain species.

Fig. 5.1, from Matsuhisa et al. (1978), illustrates the principles of the mass dependent fractionation and the mechanism of the oxygen exchange in a three isotopes plot.

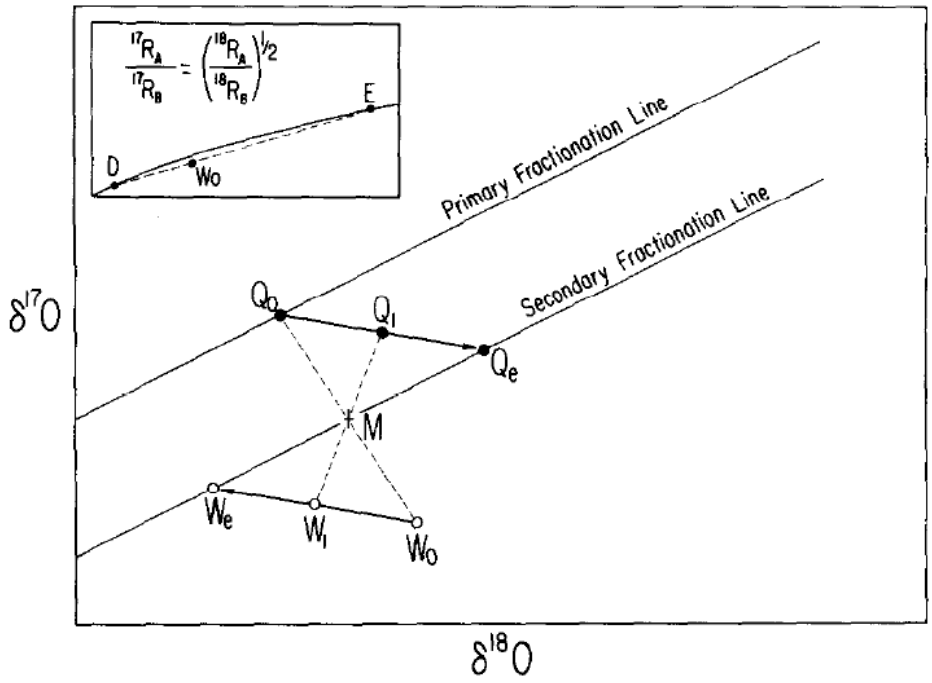

Table 5.1. **"***The principle of mass-dependent fractionation and three-isotope exchange of oxygen. The "Primary Fractionation Line" is the locus of data points of natural samples whose isotopic compositions are related to one another by mass-dependent fractionation. The inset shows the curvature of the Primary Fractionation Line over a wide range of isotope ratios. For ratios varying by only a few per cent, the straight line tangent to this curve is a good approximation. In the three-isotope exchange method, the two starting materials, denoted by Q_0 and W_0, are chosen so that their tie-line is not parallel to a fractionation line. After partial exchange, compositions have moved to Q_1 and W_1. At equilibrium, the compositions are Q_e, and W_e. Thus the classical criterion for demonstrating equilibrium is satisfied in a single experiment."(from Matsuhisa et al., 1978).*

According to the authors, at any stage of the isotope exchange the straight line connecting Q and W passes through the point M, which is the mean value of the system. Any Q_1 (or W_1) representing a certain stage of the isotope exchange lie on a straight line connecting the initial composition of Q_0 (or W_0) with the final composition Q_e (or W_e) only if two conditions are fulfilled. The first condition is a weight ratio of mineral to water of 1 and the second one is that there should be no intermediate metastable phases involved.

As a consequence, the faster synthesis of quartz in aqueous solutions from cristobalite showed the possibility of an "overshooting" of the equilibrium conditions, since the distance of quartz from the TFL is different from the distance of water from the same line (eq. 5.2).

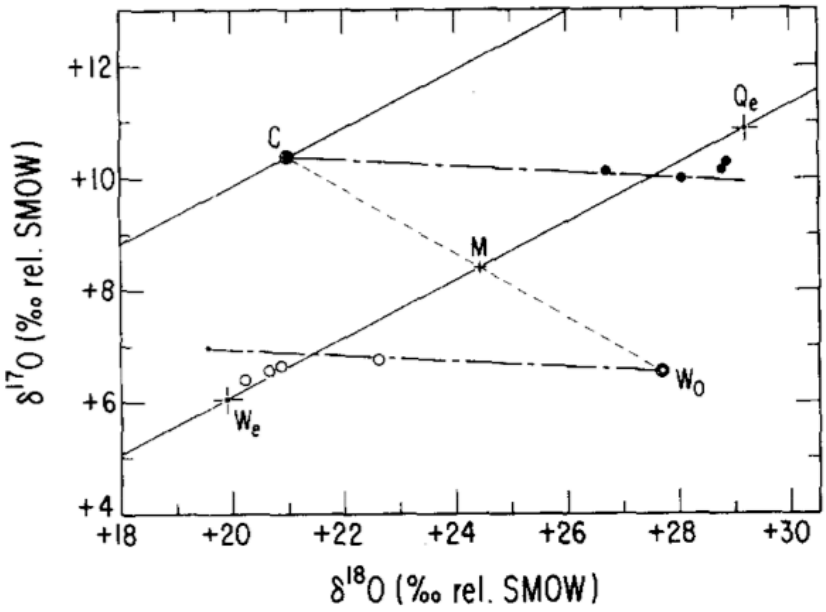

Table 5.2. *"Three isotopes plot for synthesis of quartz from cristobalite. C refers to starting cristobalite. Only in experiments longer than 1hr do data points leave the non-equilibrium line and show evidence of some exchange toward equilibrium."(from Matsuhisa et al., 1978).*

This phenomenon probably deterred the authors to investigate further the use of the three isotopes plot to understand whether equilibrium in a system of interest is reached or not. Consequently, no similar studies have been published on the change of an isotope anomaly due to common geochemical processes.
The last important question to answer is whether it is always possible to distribute the isotopes of a system among its phases so that the condition of a mass dependent fractionation is fulfilled.
A simple mathematical approach is used in section 5.1 to show that the condition of a mass dependent fractionation could not be always conceivable, since measuring a null capital delta would also depend on the initial isotopic absolute concentrations and on the chance that additional reversible processes would occur, once the system has become multiphasic. As a result, in certain circumstances, a mass dependent fractionation between two phases could generate a detectable $\Delta^{17}O‰$.

5.1 The mathematics behind the mass dependent fractionation

The occurrence of a mass dependent fractionation implies a strict condition in the distribution of three isotopes of an element between two phases A and B (eq. 5.1, see chapter 1).

$$\frac{\ln\left(\frac{\left(\frac{X_2}{X_1}\right)_a}{\left(\frac{X_2}{X_1}\right)_b}\right)}{\ln\left(\frac{\left(\frac{X_3}{X_1}\right)_a}{\left(\frac{X_3}{X_1}\right)_b}\right)} = \frac{\ln\left(\frac{^2R_a}{^2R_b}\right)}{\ln\left(\frac{^3R_a}{^3R_b}\right)} = \frac{\left(\frac{1}{m_1}-\frac{1}{m_2}\right)}{\left(\frac{1}{m_1}-\frac{1}{m_3}\right)} \qquad \text{Eq. 5.1}$$

It is worth questioning whether such a partitioning between phases is always possible, regardless of the initial conditions and the fractionating process.
It is useful visualizing the problem imagining a closed system containing three isotopes of an element as a box containing balls of three different colors. In most cases, studying the isotopic composition of samples involves measurements of isotopic ratios and element concentrations, with the approximation that the element concentration equals the concentration of the most abundant isotope.
In this section I imagine being able to count all the isotopes of a system so that I can calculate any sample delta values and its isotope anomaly using the absolute abundance of the species. Any deviation from the results obtained using the isotope ratios would give a measure of the difference between a real system and its representation with the isotopic measurements obtained with an IRMS.
The effect of mixing of sources A and B in sample delta values always follows eq. 5.2 (Miller and Tans, 2003).

$$\delta^{18}O_{measured} * C_{A+B} = \delta^{18}O_A * C_A + \delta^{18}O_B * C_B \qquad (\text{with } C_{A+B} = C_A + C_B) \qquad \text{Eq. 5.2}$$

(C_I indicates the element concentration in the phase I). An analogous relationship can be defined for $\delta^{17}O_{measured}$. Consequently, the observed isotopic composition of systems generated by mixing of two (or more) sources depends on both the isotopic composition of the sources and their relative importance.
It is usually assumed that two sources lying on the terrestrial fractionation line in a three isotopes plot can be mixed without generating any isotope anomaly. This assumption indicates that eq. 5.2 should apply also for any $\Delta^{17}O$. In fact, the equation used for calculating the content of atmospheric nitrate in the Marano lagoon samples (eq. 3.2), which can be found in Michalski and Thiemens (2006), makes implicitly use of eq. 5.2.
In order to verify this assumption, we represent a system as a closed box with a known absolute concentration of the three types of balls inside it. At first such system contains only the source A, which has no isotope anomaly (whose condition is imposed as eq. 5.1 with the phase b being the reference material VSMOW). At some point a source B with no isotope anomaly is added (mixed) to the source A in the closed box.
The chosen initial conditions of sources A and B before mixing are presented in Table 5.1. All the possible combinations of conditions in table 5.1 have been considered.

$\delta^{18}O(B)‰$	$\delta^{18}O(A)‰$	$^{16}O_B \approx C_B$ (number)	$^{16}O_A \approx C_A$ (number)
-100	$\delta^{18}O(B)‰$	1.00E+5	$0.01*^{16}O_B$
-25	$\delta^{18}O(B)‰+30$	1.00E+7	$0.1*^{16}O_B$
0	$\delta^{18}O(B)‰+60$	1.00E+9	$1*^{16}O_B$
30	$\delta^{18}O(B)‰+100$	1.00E+12	$10*^{16}O_B$
		1.00E+14	$100*^{16}O_B$

Table 5.1. *Initial conditions considered for testing the effect of mixing of two sources A and B on the isotope anomaly of the system (A+B).*

In order to evaluate the resulting isotope anomaly based on the absolute concentration, the number of ^{18}O in both sources is first obtained combining eq. 5.3 and eq. 5.4.

$$^{18}R_{A(orB)} = {}^{18}R_{VSMOW}(\delta^{18}_{A(orB)} + 1) \qquad \text{Eq. 5.3}$$

$$^{18}O_{A(orB)} = {}^{18}R_{A(orB)} * {}^{16}O_{A(orB)} \qquad \text{Eq. 5.4}$$

Because we impose that the sources have no isotope anomaly, the number ^{17}O for each phase is calculated extracting $^{17}R = {}^{17}O/{}^{16}O$ from eq. 5.5.

$$\left(\frac{^{17}R_{A(orB)}}{^{17}R_{VSMOW}}\right) = \left(\frac{^{18}R_{A(orB)}}{^{18}R_{VSMOW}}\right)^{\beta} \qquad \text{Eq. 5.5}$$

The resulting isotope anomaly when sources are mixed is therefore calculated with eq. 5.6, which makes use of the fact that we are able to count all the isotopes that are present in the system.

$$\Delta^{17}O(A+B) = \ln\frac{(^{17}R_{A+B})}{(^{17}R_{VSMOW})} - \beta\ln\frac{(^{18}R_{A+B})}{(^{18}R_{VSMOW})} = \ln\frac{\left(\frac{^{17}O_A + {}^{17}O_B}{^{16}O_A + {}^{16}O_B}\right)}{(^{17}R_{VSMOW})} - \beta\ln\frac{\left(\frac{^{18}O_A + {}^{18}O_B}{^{16}O_A + {}^{16}O_B}\right)}{(^{18}R_{VSMOW})}$$

Eq. 5.6

The set of conditions considered in table 5.1 that gave the highest isotope anomaly (in terms of absolute values) is presented in table 5.2.

$\Delta^{17}O(A+B)‰$	$\delta^{18}O(A+B)‰$	$\delta^{18}O(B)‰$	$\delta^{18}O(A)‰$	$^{16}O_B$ (number)	$^{16}O_A$ (number)
-0.35	-50.0	-100	$\delta^{18}O(B)‰+100$	all	$1*^{16}O_B$
-0.30	25	-25	$\delta^{18}O(B)‰+100$	all	$1*^{16}O_B$
-0.28	50	0	$\delta^{18}O(B)‰+100$	all	$1*^{16}O_B$
-0.27	80	30	$\delta^{18}O(B)‰+100$	all	$1*^{16}O_B$
-0.13	-70	-100	$\delta^{18}O(B)‰+60$	all	$1*^{16}O_B$

Table 5.2. *Effect of mixing of two sources A and B with no initial isotope anomaly on the resulting capital delta of the system (A+B)*

Interestingly, a measurable negative anomaly (first column of table 5.2) can be generated when mixing two sources with $\Delta^{17}O‰$ of zero, whilst the observed $\delta^{18}O$ in the system (A+B) is what is expected based on eq. 5.2. This finding would suggest that eq. 5.2 does not apply to capital delta values.
The calculations shown in table 5.2 would indicate that the size of the sources (i.e. the number of ^{16}O) gave irrelevant changes in the final capital delta of the system (A+B). By contrast, the difference in the size of the sources A and B seems to be the most important aspect for generating a negative isotope anomaly, with the highest magnitude obtained if the concentration of the two sources is the same. Furthermore, the chance of generating an isotope anomaly due to mixing is higher if sources have the greatest differences in their $\delta^{18}O$, with the highest magnitude when sources are depleted in the heavy isotopes (sources with negative delta values, see the first two rows of table 5.2).
The results presented in table 5.2 are in line with the experimental findings in Matsuhisa et al. (1978, see fig. 5.1) on the occurrence of a negative anomaly, since the authors generated samples with an isotope anomaly of -5‰ and -7‰ (versus SMOW) by mixing distilled water with an aliquot of water enriched in ^{18}O by 6100‰.
The negative anomaly found in the copper nitrate mineral likasite and in the niter (see chapter 4) might be potentially explained as evidence that the nitrate derives from the mixing of two sources with extremely different isotopic compositions.
It is important to point out that an important consequence of the results obtained in table 5.2 is that the effect of mixing of sources that have an initial isotope anomaly on the final $\Delta^{17}O(‰)$ would also depend on the isotopic composition of the sources. However, considering that the atmospheric deposition is a minor source in most systems and when assuming that the atmosphere is the only source of an isotope anomaly, the effect of mixing on the $\Delta^{17}O(NO_3)‰$ in sample water should be negligible.
The most important assumption behind the use of the MIF signal as a tracer is that any mass dependent fractionation occurring in a sample with an initial isotope anomaly will not change the magnitude of the anomaly (Morin et al., 2009; Thiemens, 2006, Kendall et al., 2007).
Let us now consider the partitioning between two phases A and B due to a mass dependent fractionation from the unusual perspective of studying such partitioning while being in a position to count all the isotopes that are present in both phases.
The initial condition is a system that has only one phase A (named A_0, to the able to distinguish the initial and the final condition of A), with an initial isotope anomaly ranging from 0 to 20 ‰.

At some point the system becomes biphasic (A+B) and a mass dependent fractionation is imposed to occur. We will not investigate the change over time of the isotope anomaly of both phases, since the calculation involves the use of the kinetic β ($\beta=\ln(m_1/m_2)/\ln(m_1/m_3)$, see chapter 1) but we assume that the count of the isotopes in the two phases start when the equilibrium conditions have been reached, so that the usual definition of β applies.
The conditions used for the calculations are shown in table 5.3; all the possible combinations have been considered. Two types of processes are simulated, both causing a $\delta^{18}O$ separation between the phases of 15 delta units, with the first (second) process causing an enrichment (depletion) of 10 delta units in A and a depletion (enrichment) of 5 delta units in B (see last column of table 5.3). It is simulated that the process ends (i.e. the equilibrium has been established) when B becomes 10%, 50% and 90% of the system (A+B) (fourth column of table 5.3).

$\Delta^{17}O(A_0)$‰	**$\delta^{18}O(A_0)$‰**	**$^{16}O_{A0}$ (number)**	**$^{16}O_B$ (number)**	**$\delta^{18}O(A)$‰ [$\delta^{18}O(B)$‰]**
0	30	1.00E+05	$0.1*^{16}O_{A0}$	$\delta^{18}O(A_0)$‰+10 [$\delta^{18}O(A_0)$‰-5]
2	10	1.00E+07	$0.5*^{16}O_{A0}$	$\delta^{18}O(A_0)$‰-10 [$\delta^{18}O(A_0)$‰+5]
5	0	1.00E+10	$0.9*^{16}O_{A0}$	
20	-20	1.00E+15		

Table 5.3. *Condition considered for calculating the capital delta in the phases A and B as a result of a mass dependent fractionation between the two phases.*

At first, the case of an initial isotope anomaly of zero is discussed. The number of ^{16}O, ^{17}O and ^{18}O at the initial condition is obtained using eq. 5.3, eq. 5.4 and eq. 5.5. The number of ^{16}O in A and in B is readily obtained using the condition of the third and the fourth column of table 5.3 and the assumption that $^{16}O_{A0}=^{16}O_A+^{16}O_B$.
The number of ^{18}O in A and B is computed by using eq. 5.3 and eq. 5.4 with the information of the last column of table 5.3.
Assuming that the process is fractionating in a mass dependent way, the ratio $^{17}R_A/^{17}R_B$ is obtained with eq. 5.7.

$$\frac{^{17}R_A}{^{17}R_B}=\left(\frac{^{18}R_A}{^{18}R_B}\right)^{\beta} \qquad \text{Eq. 5.7}$$

In our particular case, we are able to count all the isotopes that are present in a system, so that the conditions of eq. 5.8 always hold.

$$\begin{cases} ^{16}O_A+^{16}O_B=^{16}O_{A0} \\ ^{17}O_A+^{17}O_B=^{17}O_{A0} \\ ^{18}O_A+^{18}O_B=^{18}O_{A0} \end{cases} \qquad \text{Eq. 5.8}$$

Eq. 5.7 can be rewritten as eq. 5.9.

$$\frac{\frac{^{17}O_A}{^{16}O_A}}{\frac{^{17}O_B}{^{16}O_B}} = \left(\frac{^{18}R_A}{^{18}R_B}\right)^{\beta} \qquad \text{Eq. 5.9}$$

A parameter Y is defined in eq. 5.10.

$$Y = \left(\frac{^{18}R_A}{^{18}R_B}\right)^{\beta} \frac{^{16}O_A}{^{16}O_B} \qquad \text{Eq. 5.10}$$

The system of eq. 5.11 with the unknown values $^{17}O_A$ and $^{17}O_B$ has only one solution, which allows obtaining of the distribution of $^{17}O_{A0}$ between the two phases.

$$\begin{cases} ^{17}O_A = {}^{17}O_B Y \\ ^{17}O_A + {}^{17}O_B = {}^{17}O_{A0} \end{cases} \qquad \text{Eq. 5.11}$$

Knowing the absolute abundance of all isotopes in A and B, both $\delta^{17}O(A)‰$ and $\delta^{17}O(B)‰$ are calculated. The isotope anomaly in each phase is therefore obtained with eq. 5.12.

$$\Delta^{17}O_{A(orB)} = \ln(\delta^{17}O_{A(orB)} + 1) - \beta\ln(\delta^{18}O_{A(orB)} + 1) \qquad \text{Eq. 5.12}$$

Some relevant cases are presented in table 5.4.

$\Delta^{17}O(A)$ ‰	**$\Delta^{17}O(B)$ ‰**	**$\delta^{18}O(A_0)$ ‰**	**$^{16}O_{A0}$ (number)**	**$^{16}O_B$ (number)**	**$\delta^{18}O(A)‰$**	**$\delta^{18}O(B)‰$**
-4.6	-4.6	-20	1.00E+05	$0.1*^{16}O_{A0}$	$\delta^{18}O(A_0)‰+10$	$\delta^{18}O(A_0)‰-5$
-4.6	-4.6	-20	1.00E+10	$0.1*^{16}O_{A0}$	$\delta^{18}O(A_0)‰+10$	$\delta^{18}O(A_0)‰-5$
-4.5	-4.5	0	1.00E+07	$0.1*^{16}O_{A0}$	$\delta^{18}O(A_0)‰+10$	$\delta^{18}O(A_0)‰-5$
-4.3	-4.3	30	1.00E+05	$0.1*^{16}O_{A0}$	$\delta^{18}O(A_0)‰+10$	$\delta^{18}O(A_0)‰-5$
-1.3	-1.3	All	all	$0.5*^{16}O_{A0}$	$\delta^{18}O(A_0)‰+10$	$\delta^{18}O(A_0)‰-5$
1.8	1.8	10	1.00E+05	$0.9*^{16}O_{A0}$	$\delta^{18}O(A_0)‰+10$	$\delta^{18}O(A_0)‰-5$
1.8	1.8	10	1.00E+10	$0.9*^{16}O_{A0}$	$\delta^{18}O(A_0)‰+10$	$\delta^{18}O(A_0)‰-5$
1.9	1.9	0	1.00E+07	$0.9*^{16}O_{A0}$	$\delta^{18}O(A_0)‰+10$	$\delta^{18}O(A_0)‰-5$
1.9	1.9	-20	1.00E+07	$0.9*^{16}O_{A0}$	$\delta^{18}O(A_0)‰+10$	$\delta^{18}O(A_0)‰-5$
4.6	4.6	-20	1.00E+05	$0.1*^{16}O_{A0}$	$\delta^{18}O(A_0)‰-10$	$\delta^{18}O(A_0)‰+5$
4.6	4.6	-20	1.00E+07	$0.1*^{16}O_{A0}$	$\delta^{18}O(A_0)‰-10$	$\delta^{18}O(A_0)‰+5$
1.3	1.3	All	all	$0.5*^{16}O_{A0}$	$\delta^{18}O(A_0)‰-10$	$\delta^{18}O(A_0)‰+5$
-1.8	-1.8	10	1.00E+07	$0.9*^{16}O_{A0}$	$\delta^{18}O(A_0)‰-10$	$\delta^{18}O(A_0)‰+5$

Table 5.4. *Calculation of the isotope anomaly in phase A and B as a consequence of a mass dependent process fractionating the oxygen isotopes of a phase A_0 that has an initial $\Delta^{17}O(A_0)‰$ of zero.*

Surprisingly, the isotope anomaly in A and in B is always the same and differs from zero (see the first two columns in table 5.4). The magnitude of such MIF depends mainly on the relative importance of A and B. Interestingly, swapping the sign of the fractionation of ^{18}O in a phase causes a change of sign of the isotope anomaly (compare the isotope anomaly of the phase A when a ^{18}O enrichment of 10 delta units occurs with the results in case of similar initial conditions but with a ^{18}O depletion of 10 delta units in the same phase). The results in table 5.4 would suggest that it is possible to imagine that a measurable capital delta should be detected after a mass dependent fractionation in a system that had no initial isotope anomaly.

I will now consider the same system without using the notion of the absolute abundance of the isotopes of the system, but by using isotopic ratios, which is what you would get from sample measurements with an IRMS. The isotope ratio ^{18}R in both phases is calculated based on eq. 5.3 and using the condition imposed in the last column of table 5.3.

The second condition (the process fractionating the isotopes between A and B is mass dependent) is imposed as eq. 5.13, which allows the calculation of the isotope ratio $^{17}R_{A(orB)}$.

$$\frac{^{17}R_{A(orB)}}{^{17}R_{VSMOW}} = \left(\frac{^{18}R_{A(orB)}}{^{18}R_{VSMOW}} \right)^{\beta} \qquad \text{Eq. 5.13}$$

Once calculated the $\delta^{17}O$(vs. VSMOW) for both phases by using the isotope ratio ^{17}R obtained from eq. 5.13, the isotope anomaly in each phase is obtained by using eq. 5.12. Following this procedure, the final isotope anomaly in both phases is zero.

It is important to mention that the ratio $^{17}R_A/^{17}R_B$ obtained by calculating $^{17}R_X$ in both phases with eq. 5.13 is exactly the same as if eq. 5.7 is used instead, underlining that the reference material does not change the value of such ratio. However, $^{17}R_A$ and $^{17}R_B$ obtained with eq. 5.13 differs from the same parameters calculated solving the system of eq. 5.11, which is possible only when knowing the absolute abundance of all isotopes.

It is necessary to point out that, based on eq. 5.1, the condition of a mass dependent fractionation establishes a relationship between two isotopic ratios in two phases A and B (.i.e. it establishes a relationship among four isotopic ratios). The common substitution of one of the two phases with a reference material would therefore generate the difference. In other words, the occurrence of a MDF cannot be verified by measuring the oxygen isotope composition of only one phase, unless the initial absolute isotopic abundances before the partitioning are known.

A similar difference in the final capital delta values can be found when considering an initial anomaly of 20‰. The method using isotopic ratios indicates that the final isotope anomaly in phases A and B after a mass dependent fractionation is still 20‰ for both phases. By contrast, when imposing the condition of a mass dependent process fractionating the three oxygen isotopes between A and B and effectively counting all the isotopes of the system in the two phases, the isotope anomaly in A and B after equilibrium is not 20‰ anymore, as it becomes strictly dependent on the relative importance of phases A and B (see the deviations from the initial isotope anomaly of 20‰ in the first two columns of table 5.5).

$\Delta^{17}O(A)$ ‰	$\Delta^{17}O(B)$ ‰	$\delta^{18}O(A_0)$ ‰	$^{16}O_{A0}$ (number)	$^{16}O_B$ (number)	$\delta^{18}O(A)$‰	$\delta^{18}O(B)$‰
15.9	15.9	100	1.00E+05	$0.1*^{16}O_{A0}$	$\delta^{18}O(A_0)$‰+10	$\delta^{18}O(A_0)$‰-5
15.7	15.7	40	1.00E+05	$0.1*^{16}O_{A0}$	$\delta^{18}O(A_0)$‰+10	$\delta^{18}O(A_0)$‰-5
15.7	15.7	40	1.00E+15	$0.1*^{16}O_{A0}$	$\delta^{18}O(A_0)$‰+10	$\delta^{18}O(A_0)$‰-5
18.8	18.8	100	1.00E+05	$0.5*^{16}O_{A0}$	$\delta^{18}O(A_0)$‰+10	$\delta^{18}O(A_0)$‰-5
18.7	18.7	40	1.00E+07	$0.5*^{16}O_{A0}$	$\delta^{18}O(A_0)$‰+10	$\delta^{18}O(A_0)$‰-5
21.7	21.7	100	1.00E+05	$0.9*^{16}O_{A0}$	$\delta^{18}O(A_0)$‰+10	$\delta^{18}O(A_0)$‰-5
21.7	21.7	100	1.00E+07	$0.9*^{16}O_{A0}$	$\delta^{18}O(A_0)$‰+10	$\delta^{18}O(A_0)$‰-5
21.7	21.7	80	1.00E+10	$0.9*^{16}O_{A0}$	$\delta^{18}O(A_0)$‰+10	$\delta^{18}O(A_0)$‰-5
21.8	21.8	40	1.00E+07	$0.9*^{16}O_{A0}$	$\delta^{18}O(A_0)$‰+10	$\delta^{18}O(A_0)$‰-5
24.1	24.1	100	1.00E+05	$0.1*^{16}O_{A0}$	$\delta^{18}O(A_0)$‰-10	$\delta^{18}O(A_0)$‰+5
24.3	24.3	40	1.00E+05	$0.1*^{16}O_{A0}$	$\delta^{18}O(A_0)$‰-10	$\delta^{18}O(A_0)$‰+5
21.3	21.3	40	1.00E+05	$0.5*^{16}O_{A0}$	$\delta^{18}O(A_0)$‰-10	$\delta^{18}O(A_0)$‰+5
18.3	18.3	80	1.00E+10	$0.9*^{16}O_{A0}$	$\delta^{18}O(A_0)$‰-10	$\delta^{18}O(A_0)$‰+5

Table 5.5. *Calculation of the isotope anomaly in phase A and B as a consequence of a mass dependent process fractionating the oxygen isotopes of a phase A_0 that has an initial $\Delta^{17}O(A_0)$‰ of 20.*

The difference in the capital delta when the absolute isotopic abundances are known is not due to the choice of the reference used for defining the oxygen delta values. This is because, when considering a hypothetical second reference lying in the terrestrial fractionation line, the results (data not shown) on the final isotope anomaly are identical with the ones using the isotope ratios of VSMOW as a reference material.

It is important to point out that the final element concentration in phase A and B and the resulting $\delta^{18}O$‰ in both phases in a system at equilibrium is arbitrarily chosen for this type of calculation because variables that can be imposed during the experiments, such as temperature and pressure, would mainly determine the final element and isotopes distribution.

The calculations in table 5.5 would suggest that crystallization at equilibrium conditions from aqueous solutions with an initial nitrate isotope anomaly would result in a shift in the isotope anomaly in both the solution and the solid phase, until the capital delta values of the two substances is the same. This occurrence would be in line with Matsuhisa's experiments on the equilibrium exchange in the system water-quartz (fig. 5.1). This finding could suggest that the nitrate minerals from Atacama Desert might not have the same isotope anomaly as atmospheric nitrate because of the geological processes, both kinetic and reversible ones, subsequent to the atmospheric deposition.

These observations could also have important implications for the MIF signal in atmospheric nitrate. Let us imagine a point (or a layer) source of an isotope anomaly in an open system that is similar to a portion of the air column containing the height where the ozone profile reaches its maximum. Transport processes like diffusion, mechanical forces due to wind speed and convection would redistribute the isotope anomaly generated by the point (or the layer) source in the observed system. Such kinetic processes spreading the MIF signal would cause an isotope fractionation that can be assumed to be mass dependent (kinetic β is to be used).

As a result, spatial gradients and temporal trends could determine the circumstance that an observer in a position to count all the isotopes present in the system of interest will calculate an isotope anomaly that depends on the size of the system considered and the time that the observer takes to count all the isotopes, since space and lapses of time considered will both have an influence on the absolute isotopic abundance. Consequently, an observed MIF signature in atmospheric nitrate should not be considered as due to chemical reactions only, but rather potentially to a combination of physical and chemical processes.
It is worth mentioning that it has been recently demonstrated that a temperature gradient would cause a mass independent fractionation in both O_2 and in the sulphur isotopes of gaseous SF_6 (Sun and Bao, 2011). Thus, a review of the origin of the isotope anomaly due to atmospheric processes is expected in the future.
The last point to be discussed in this section is whether a mass dependent fractionation is always mathematically conceivable in a system that has more than two phases. In other words, is it possible to redistribute an initial set of oxygen isotopes among n distinct phases, so that any partitioning would reflect the fact that a mass dependent process has occurred?
I consider the case where the phase A of a monophasic system is subjected to two distinct reversible processes (A⇔B and A⇔C). In this case, a mathematical solution of how the isotopes distribute is always possible, once the fractionation of the ^{18}O in the three phases is known and the relative importance of A, B and C is established.
The unique solution for defining how many ^{17}O will be found in each of the three phases is given by solving the system of eq. 5.14.

$$\begin{cases} {}^{17}O_A = {}^{17}O_B Y_{AB} \\ {}^{17}O_A = {}^{17}O_C Y_{AC} \\ {}^{17}O_A + {}^{17}O_B + {}^{17}O_C = {}^{17}O_{A0} \end{cases} \qquad \text{Eq. 5.14}$$

The parameter Y_{XZ} is defined in eq. 5.15.

$$Y_{XZ} = \left(\frac{{}^{18}R_X}{{}^{18}R_Z} \right)^{\beta} \frac{{}^{16}O_X}{{}^{16}O_Z} \qquad \text{Eq. 5.15}$$

Possible examples are the crystallization of nitratine and darapskite from an aqueous solution or the fractionation of NO_2^- (A) to both NO_3^- (B) and NO (C).
Similarly, a mathematical solution to establish how an initial amount of ^{17}O will be partitioned from one to n+1 distinct phases due to n mass dependent processes (1⇔2, 1⇔3,… 1⇔n) is always possible to obtain, provided that the n processes have been identified and the relative importance of each phase of the system is measured, by solving the system of n+1 equations (eq. 5.16).

$$\begin{cases} {}^{17}O_1 = {}^{17}O_2 Y_{12} \\ {}^{17}O_1 = {}^{17}O_3 Y_{13} \\ \ldots\ldots\ldots \\ {}^{17}O_1 = {}^{17}O_n Y_{1n} \\ {}^{17}O_1 + {}^{17}O_2 + \ldots {}^{17}O_n = {}^{17}O_0 \end{cases} \qquad \text{Eq. 5.16}$$

However, if in the system (A+B+C) a new process fractionating the isotope between phase B and C occurred, a mathematical solution could be no longer guaranteed, since the system to be solved (eq. 5.17) has four equations but three variables ($^{17}O_A$, $^{17}O_B$ and $^{17}O_C$).

$$\begin{cases} {}^{17}O_A = {}^{17}O_B Y_{AB} \\ {}^{17}O_A = {}^{17}O_C Y_{AC} \\ {}^{17}O_B = {}^{17}O_C Y_{BC} \\ {}^{17}O_A + {}^{17}O_B + {}^{17}O_C = {}^{17}O_{A0} \end{cases} \qquad \text{Eq. 5.17}$$

As a result, if a process like an oxygen isotope exchange between B and C is established, it could not be possible to recognize that B and C formed from A due to a mass dependent process. This observation shows some similarities with the study case of quartz crystallizing from an aqueous solution due to the presence of cristobalite (Matsuhisa et al., 1978, see fig. 5.2), even if the findings are obtained from a completely different perspective.
The occurrence of an interaction between B and C in a triphasic system could happen if, for instance, an oxygen isotope exchange redistributed the oxygen isotope between two nitrate minerals like nitratine and darapskite that had been precipitated from the same aqueous solution. In this case, nitratine and darapskite should have the same nitrate isotope anomaly, which would differ from the isotope anomaly in the aqueous solutions in which they formed.
To sum up, there is the chance that a mass dependent fractionation between two phases of a multi-component system could not be retained due to subsequent mass dependent processes redistributing the isotopes among other phases.
Moreover, the use of $\Delta^{17}O$‰ time series does not necessarily provide information on whether a mass independent fractionation has occurred or not, since the volume of sample and the lapse of time after which the sample is considered collected would generate differences in the measured isotope ratios. In fact, the mass dependent fractionation establishes a mathematical relationship between the isotopes distribution in two phases, and a process cannot be investigated if the isotopic composition of only one phase is considered, unless the initial absolute isotopic abundances before the partitioning are known.
As a result, a decrease or an increase of the isotope anomaly in samples like the nitrate minerals from the Chilean ore deposits could be explained by any geochemical process following the nitrate deposition from the atmosphere.

5.2 Other sources of uncertainties associated to the use of the nitrate MIF signature as a tracer.

The results discussed in section 5.2 would suggest that a measurable shift in the initial nitrate isotope anomaly of a material could be theoretically generated in several circumstances.
Interestingly, most of the data on the nitrate MIF that have been published so far lie on a straight line with a slope of 1 (see fig. 4.10), which is interpreted as a mixing line (see fig. 1.10).

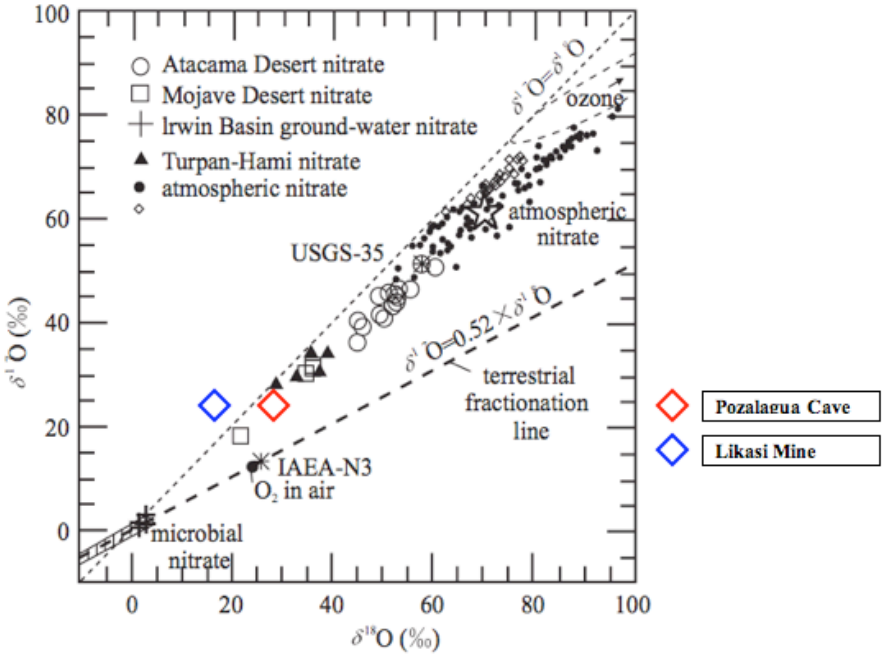

Fig. 4.10. *Published data on the isotope anomaly in nitrate with the addition of the data of the nitromagnesite found at Pozalagua Cave and the buttgenbachite from Likasi Mine (modified after Yanhe et al., 2010).*

As a consequence, the isotope anomaly (i.e. the distance of a data point in the three isotopes plot from the TFL) in all these measurements seems to be a function of $\delta^{18}O$, with the capital delta being higher when the sample is more enriched in ^{18}O.
It is difficult to reconcile this pattern with the calculations of the $\Delta^{17}O$ based on the initial absolute isotopic abundances in section 5.2. It is possible that this discrepancy arises owing to analytical problems. It is worth mentioning that comparison among methods does not always give satisfactory results. As an example, the samples of Chilean nitratine that have been reanalyzed by Michalski et al. (2004) with the bacterial method proved to give oxygen delta values systematically higher (up to 12 delta units) than previous analyses (Bohlke et al., 1997). The authors claim that the discrepancy is due to a reported $\delta^{18}O$ scale contraction in samples prepared by off-line combustion as $AgNO_3$ (Revesz and Bohlke, 2002), which is the method used in Bohlke et al. 1997. However, also the measurements with an on-line thermal decomposition method proved to give a contraction in the oxygen delta scales (see section 2.3).
Results in fig. 5.3, from Yahne et al. (2010), show that the same sample could have different delta values, depending on the procedure for extracting the oxygen.

Table 1 The values of $\delta^{17}O$ (‰) and $\delta^{18}O$ (‰) in the Kumutag nitrate deposit in the Turpan-Hami area of Xinjiang

Sample	Mineral	Method	$\delta^{17}O_{V\text{-}SMOW}(O_2)$	$\delta^{18}O_{V\text{-}SMOW}(O_2)$	$\delta^{17}O_{V\text{-}SMOW}(NO_3)$	$\delta^{18}O_{V\text{-}SMOW}(NO_3)$	$\Delta^{17}O$
KMTG-06	$AgNO_3$	Thermal decomposition	24.8	23.1	30.6	34.3	12.8
KMTG-09	$AgNO_3$	Thermal decomposition	25.5	25.4	31.3	36.6	12.3
KMTG-11	$AgNO_3$	Thermal decomposition	28.2	28.1	34.0	39.2	13.6
KMTG-01*	$AgNO_3$	Thermal decomposition			36.0	37.0	16.8
KMTG-03*	$AgNO_3$	Thermal decomposition			30.6	30.0	15.0
KMTG-02	$AgNO_3$	Fluorination	20.8	16.6			12.2
KMTG-04	$AgNO_3$	Fluorination	18.3	9.2			13.5
KMTG-05	$AgNO_3$	Fluorination	19.8	13.3			12.9

*American Louisiana State University measured.

Fig. 5.3. *The isotopic measurements of the nitrate deposits in the Turpan_Hami basin (from Yahne et al., 2010).*

The nitrate results reported in Yahne et al. (2010) were obtained by inducing precipitation of $AgNO_3$ (following the method in Silva et al., 2000). The oxygen for measuring the capital delta has been extracted by using two methods: the thermal decomposition (by inducing the reaction $AgNO_3 \Rightarrow 2Ag+2NO_2+O_2$) and the fluorination ($2AgNO_3+2BrF_5 \Rightarrow 2AgF+2BrF_3+ 2NO_2F+O_2$). In both methods, the oxygen is analyzed for assessing the sample isotope anomaly. The nitrate $\delta^{18}O$ is then calculated as $\delta^{18}O(NO_3)=0.98\delta^{18}O(O_2)+11.7$ (following Michalski et al., 2002).

Interestingly, unlike the samples measured with the first method, the samples analyzed with the fluorination method have $\delta^{17}O$ that are higher than $\delta^{18}O$. Thus, in a three isotopes plot those measurements should lie on straight lines with a slope higher than unity.

It is worth noting that the subset measured with the fluorination method has not been reported in the three isotopes plot presented in Yahne et al. (2010, see fig. 4.10), since no measurements lie above the line representing data points with a ratio $\delta^{17}O/\delta^{18}O$ of 1. Yet, such measurements will be similar to the data from the copper nitrate mineral of buttgenbachite from Likasi Mine, for what $\delta^{17}O$ is higher than $\delta^{18}O$ (see fig. 4.10).

Overall, these observations would underline that results from different laboratories are not necessarily comparable and, because isotopes can be easily fractionated at any step of sample purification and extraction, it seems that the chance of systematic errors is still a serious issue.

Another point is that for decades the discrepancies between theory and observations in the isotope fractionation constants were usually explained with the fact that equilibrium had not been reached during the experiments. Yet, it is possible that Urey's theory could not be always applied and that deviations from the mass-dependent rule are possible even in case of equilibrium conditions. In chapter 1 the existence of a temperature dependence of the pairs of isotopic ratios during an isotope exchange at equilibrium has been underlined (see fig. 1.4). Such findings in Urey's work would therefore indicate that the universality of the mass dependent fractionation is in fact an approximation.

The reason I made the calculations of section 5.2 is to demonstrate with a *reductio ad absurdum* that it is unlikely that a mass dependent fractionation would always be detected in a system that reached equilibrium. The calculation of the deviation from the expected result when counting all the isotopes of a system has been done also to emphasize that the systematic study of the relative isotopic abundance cannot always give a satisfactory explanation of the conditions leading to an isotope partitioning

between two or more phases. However, an explanation of the physics and the chemistry supporting such observation is needed.
To the best of my knowledge, the total number of isotopes fractionating between the phases A and B is never considered when calculating theoretically the isotope partitioning: it should be pointed out that in Urey's theory (1947) the molecular partition function q is used when describing the isotope fractionation constants.
It is attributed to Gibbs the statement that the partition function Q of a system equals $q^N/N!$, with N being the number of species present in the system (Lin, 1996). Such definition of Q is related to the so-called Gibbs paradox, which emphasized the existence of the entropy of mixing (see explanation below), and implies that entropy is an extensive property (i.e. entropy is a property that depends on the size of the system). Thus, the choice of using q instead of Q has the drawback that the contribution of the size of the system on the free energy available is never taken into account.
Pauli gave a solution to the Gibbs paradox with the scaling law only in 1973 (Pauli, 1973), which is curiously the same year of the publication of the first measurements of an isotope anomaly (Clayton, 1973). Pauli's scaling law, (i.e. S(T, qV, qN)=qS(T,V,N)) establishes that a system at a temperature T, volume qV and containing qN identical particles has an entropy that is q times higher than the system at the same temperature T containing N identical particles in a volume V.
It is important to point out that, when Urey, Bigeleisen and Mayer developed the theory of the isotope fractionation, they probably were not aware that the size of the systems would give a contribution to the free energy of the system.
During any chemical reaction, the final ratio products/reagents can be calculated as the equilibrium constant K, which is connected to the free energy F of the system as eq. 5.18 (R is the universal gas constant, T the temperature).

$$F=RT\ln K \qquad \text{Eq. 5.18}$$

The isotope fractionation constant α equals K when the system has reached equilibrium (Bigeleisen and Mayer, 1947; Young et al., 2002).
The free energy F depends on the enthalpy H of the system and its entropy S at the temperature T (eq. 5.19).

$$F=H-TS \qquad \text{Eq. 5.19}$$

Thus, if the correct entropy after equilibrium is reached is not identified, the proper isotope fractionation constant cannot be theoretically calculated.
Even if at a first sight it could seem beyond the scope of the present work discussing about these issues, I believe that the current debate on the Gibbs paradox (Lin, 2008; Ben-Naim, 2007; Dieks, 2010 and reference therein) would provide in the future a potential explanation to some observed isotope anomalies.
According to Gibbs's reasoning, we could imagine a system with **n** moles of an ideal gas of type 1 in a volume V and **n** moles of another non-interacting type 2 in another similar volume V, and that the two gasses are separated by a diaphragm. If the diaphragm is removed, once diffusive processes of the two gasses on the opposite sides of the system have terminated, a new equilibrium state is reached with 2**n** moles of a homogeneous gas mixture, occupying the total volume 2V with uniform composition, the temperature, pressure and total energy remaining unchanged.

If the gasses were of the same type, the system with no diaphragm has simply the double entropy (2S). It is important to mention that in such system it is possible at any time to insert the diaphragm again and reestablishing the initial condition of two identical systems with entropy S each.
However, if the gasses are of two different types, the initial condition will have been established, unless some work is made to the system (i.e. mixing distinguishable particles is not a reversible process). This means that the entropy of the system that reached equilibrium after a mixing process must have increased. The paradox is that the degree of similarity between the two particles will not change the magnitude of this additional entropy (i.e. we could theoretically compare systems with two large organic molecules or two small isotopes of the same element and getting the same entropy due to mixing distinguishable particles).
I now turn to quantifying such an increase of entropy due to mixing of distinguishable particles, making use of the definition of entropy S as a function of W by Boltzmann (eq. 5.20).

$S = k_B \ln W$ Eq. 5.20

W represents the number of possible microstates (the combination of positions and velocity of particles) giving the macrostate of the system. Configuration entropy is the portion of a system's entropy that is related to the position of its constituent particles rather than to their velocity. It is physically related to the number of ways of arranging all the particles of the system while maintaining the total energy.
To visualize why distinguishable particles produces higher entropy compared to undistinguishable particles, fig. 5.4 is presented.

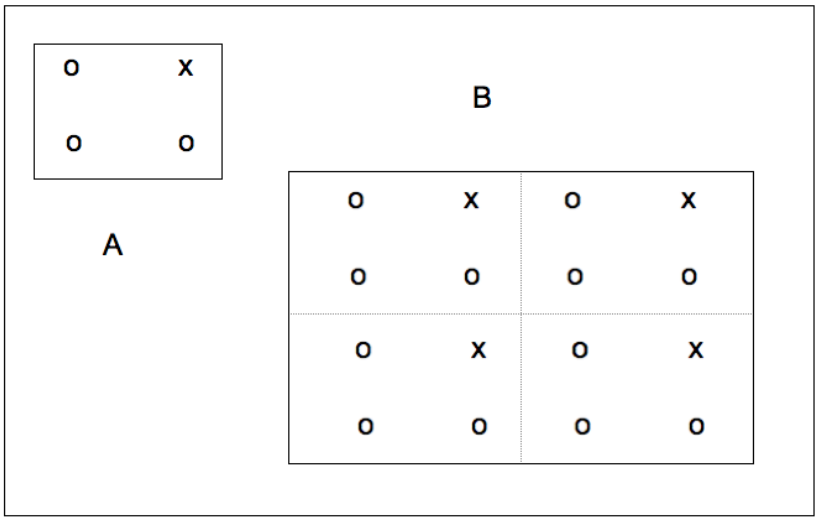

Fig. 5.4. *On the left the system A has four sites that could be filled with particles, whilst the system on the right B has sixteen sites. Two different types of particles, indicated with a circle and a cross respectively, are placed in the sites of the systems A and B with the same ratio 3:1.*

On the left of fig. 5.4, a portion of space (the system A) is depicted with fours sites to be filled by particles. If one of the particles is distinguishable from the other three, there are four distinguishable configurations. The system B on the right of fig. 5.4 is

simply four times the system A. Yet, the possible distinguishable configurations in B are more than four times higher than in A, as it can be understood when considering all the possible arrangements of the four crosses and the twelve circles in B.
The precise calculation of W, representing the number of possible distinguishable configurations based on the total number N of particles and the k types of distinguishable particles n_i, is shown as eq. 5.21.

$$W = \frac{N!}{\prod_{i=1}^{x} n_i!} \qquad \text{Eq. 5.21}$$

If there are N undistinguishable particles, the term of configuration entropy is zero because W in eq. 5.21 is one ($S_{configuration}=k_B \log 1=0$) and the total entropy of the system depends only on the distribution of velocities. In this case, the size of the system (i.e. the number of particles N) will increase the entropy of the system according to the scaling law given by Pauli (1973).
With the Stirling approximation ($N!\approx(2\pi N)^{1/2}*N^N exp^{-N}$), which can be found in most manuals of analytic combinatorics (Mortici, 2010), it is possible to calculate the change of entropy due to the size of the system of interest. Only when it is possible to approximate the limit $N\rightarrow\infty$, will the effect of the change of the size of the system on S will become negligible.
It is important to point out that the example shown in fig. 5.4 and eq. 5.21 would underline that the addition of one or more rare isotopes will have almost no effects on the macroscopic states of the systems (the velocity distribution of particles remains almost unchanged), but it could give a great contribution to the configuration entropy.
In 1996, Jaynes published an article on the finding that in fact Gibbs himself explained the paradox in *Heterogeneous Equilibrium (1875-8)*. Thus, according to Jaynes (1996), Gibbs's work was just misinterpreted for almost a century because "…the decipherment of this (*sentence)* into plain English required much effort, sustained only by faith in Gibbs".
The importance of such a discovery can be summarized in Jaynes's words: "For 60 years, all scientists have been taught that in the issue of extensivity of entropy we have a fundamental failure not just of classical statistics, but of classical mechanics, and a triumph of quantum mechanics. A consequence of the above observations (*there is no proper Gibbs paradox)* is that the question whether quantum theory really gave an extensive entropy function and determined the value of the chemical constant, also needs to be re-examined. Before a quantum theory analog of entropy has been defined, one must consider processes in which N change…This suggests that, contrary to common belief, the value of the chemical constant is not determined by quantum statistics as currently taught any better than it was by classical theory. It seems to be a fact of phenomenology that quantum statistics with k= 0 (*a constant to be added to the quantum partition function)* accounts fairly well for a number of measurements; but it gives no theoretical reason why k should be zero. Therefore we wonder how good is the experimental evidence that k is not needed, and for how many substances we have such evidence. For some 60 years this has not seemed an issue because one thought that it was all settled in favor of quantum theory; any small discrepancies were ascribed to experimental difficulties and held to be without significance. Now it appears that the issue is reopened; it may turn out that k is really zero for all systems; or it may be that giving it nonzero values may improve the

accuracy of our predictions. In either case, further theoretical work will be needed before we can claim to understand entropy".

The literature on the subject has recently increased, which underlines the importance of the issue (Shu-Kun Lin, 2008; Ben-Naim, 2007; Dieks, 2010 and reference therein). Only few months ago, a paper was published on a quantum solution to the Gibbs Paradox in the case of few particles (Dong et al., 2012). However, the observation of Jaynes should still remain: is the quantum mechanics a necessary theory?

As it was shown with the example of fig. 5.4, the issues of establishing the proper configuration entropy and calculating the entropy dependence on the size of the system of interest have immediate implications in the isotopic studies. Unfortunately, to the best of my knowledge, there is no trace of such debate in the work of the community focused on the theory of the isotope partitioning.

From Jaynes (1996): "In the thermodynamics of Gibbs, the variation of entropy with N is just the issue that is involved in the prediction of vapor pressures, equilibrium constants, or any conditions of equilibrium with respect to exchange of particles. His invention of the chemical potential has, according to all the evidence of physical chemistry, solved the problem of equilibrium with respect to exchange of particles, leading us to conclusion 2 (*the variation of entropy with N is not arbitrary*); chemical thermodynamics could not exist without it". "Indeed, for virtually all systems small deviations from exact extensivity are observable in the laboratory; the experimentalist calls them "surface effects" and we note that Gibbs' *Heterogeneous Equilibrium* gives beautiful treatments of surface tension and electrocapillarity, all following from his single variational principle".

Too many strange effects during the isotope partitioning at equilibrium conditions that have been observed in the 70's, like the effect of the grain size and a solute effect (from my discussions with Venturelli, Professor at the University of Parma) cannot be explained with the current theory of the isotope chemical equilibria.

Usually the observation of a dependence of the isotopic composition of a solid phase on the grain size (Meyer et al., 2008; Severinghaus and Battle, 2006) is explained with the influence of surface processes (Nakamura et al., 2005), kinetic processes (Muller and Watson, 2008; Giletti, 1986; Halas and Krouse, 1982), analytical techniques (Fouillac and Girard, 1996) and different equilibrium conditions mirroring different time of formations (Williams and Hervig, 2005).

However, configuration entropy should give a grain size effect also at equilibrium conditions when the size is below a critical diameter (below which the change of entropy with N cannot be neglected), especially if the rare isotopes of the element to partition are more abundant than as usual (since the number of distinguishable configurations W should increase, see eq. 5.20).

An example that is similar to the ones in section 5.2 is now made, in order to show how the condition of a MDF, based on the definition in Young et al. (2002), cannot be valid for the isotopes of sulphur and that the reason lies on the fact that configuration entropy is not taken into account.

Sulphur has four stable isotopes: we called them 1, 2, 3 and 4, with the last one being the most abundant species. We therefore define three isotopic ratios ${}^{i}R={}^{i}X/{}^{4}X$ (i=1, 2, 3). Starting from eq. 1.8 (Young et al., 2002, see below), we consider all the possible relationships that we could get with the four isotopes fractionating between phases A and B (eq. 5.22).

$$\begin{cases} \dfrac{\left(\dfrac{X_2}{X_1}\right)_a}{\left(\dfrac{X_2}{X_1}\right)_b} = \left(\dfrac{\left(\dfrac{X_3}{X_1}\right)_a}{\left(\dfrac{X_3}{X_1}\right)_b}\right)^{\beta} \\ \beta = \dfrac{\left(\dfrac{1}{m_1}-\dfrac{1}{m_2}\right)}{\left(\dfrac{1}{m_1}-\dfrac{1}{m_3}\right)} \end{cases} \qquad \text{Eq. 1.8}$$

$$\begin{cases} \dfrac{\left(\dfrac{X_1}{X_4}\right)_a}{\left(\dfrac{X_1}{X_4}\right)_b} = \left(\dfrac{\left(\dfrac{X_2}{X_4}\right)_a}{\left(\dfrac{X_2}{X_4}\right)_b}\right)^{\beta_{12}} \\ \dfrac{\left(\dfrac{X_2}{X_4}\right)_a}{\left(\dfrac{X_2}{X_4}\right)_b} = \left(\dfrac{\left(\dfrac{X_3}{X_4}\right)_a}{\left(\dfrac{X_3}{X_4}\right)_b}\right)^{\beta_{23}} \\ \dfrac{\left(\dfrac{X_1}{X_4}\right)_a}{\left(\dfrac{X_1}{X_4}\right)_b} = \left(\dfrac{\left(\dfrac{X_3}{X_4}\right)_a}{\left(\dfrac{X_3}{X_4}\right)_b}\right)^{\beta_{13}} \\ \beta_{xy} = \dfrac{\left(\dfrac{1}{m_4}-\dfrac{1}{m_x}\right)}{\left(\dfrac{1}{m_4}-\dfrac{1}{m_y}\right)} \end{cases} \qquad \text{Eq. 5.22}$$

Let's suppose that at a certain temperature, we measure the isotope ratio ${}^3R={}^3X/{}^4X$ in both A and B. The ratio ${}^3R_A/{}^3R_B$ should vary within a definite range, depending on the phases A and B chosen and other factors like temperature and pressure.
Thus, we can calculate the right hand side of the last two equations of the system 5.22 based on the measured ${}^3R_A/{}^3R_B$ and recall them Y_{23} and Y_{13}. As a result, the first equation of the system can be rewritten as eq. 5.23.

$$Y_{23} = \left(Y_{13}\right)^{\beta_{12}} \qquad \text{Eq.5.23}$$

Eq. 5.23 in terms of measured ${}^3R_A/{}^3R_B$ is shown as eq. 5.24.

$$\frac{{}^3R_A}{{}^3R_B} = \left(\left(\frac{{}^3R_A}{{}^3R_B}\right)^{\beta_{23}}\right)^{\beta_{12}} \qquad \text{Eq.5.24}$$

It is important to point out that eq. 5.24 is an identity (i.e. the equation is satisfied for any arbitrarily chosen ${}^3R_A/{}^3R_B$) only if $\beta_{23}*\beta_{12}=1$. Yet, such a condition is never met for sulphur, owing to the masses of its isotopes, with the consequence that it is impossible that the three equations of the system 5.22 are all satisfied. This means that it is impossible that all the four isotopes of sulphur partition in a way so that every pair of isotopic ratios in phases A and B meet the condition of a mass dependent fractionation. As a result, a system could have reached the equilibrium if we choose a pair of isotope ratios that meet the conditions of a MDF whilst, if we choose another pair of isotope ratios, the same system could have not reached the equilibrium because the condition of a MDF is not met.

This example would suggest that the condition of equilibrium should not be associated with the occurrence of a MDF in sulphur, since the MDF is defined only by using three isotopes and it does not contain any information of the distribution of the fourth one (i.e. the system (A+B) is never considered as a whole). Similarly, the condition of equilibrium for elements with three isotopes like oxygen should not be associated with the condition of a MDF, since the absolute abundances (and therefore the magnitude of configuration entropy) of the system are not necessary parameters.

To sum up, I believe that, unless configuration entropy and the partition function Q according to Gibbs are included in the theoretical treatments of the isotopes partitioning, it will not be possible to understand whether the isotope fractionation is a purely quantum phenomenon or not. Further studies on the isotope fractionation constants are needed, to verify with experiments whether it is possible to generate an isotope anomaly in a system moving slowly towards a different equilibrium state. This could be done by investigating the occurrence of any volume effect and by choosing some initial absolute isotope abundances and a final equilibrium state for what the resulting MDF condition would determine a substantial deviation from the condition of maximum entropy.

6 Conclusions

The results discussed in this thesis underline that there are still important assumptions to test and analytical problems to overcome before establishing whether the nitrate MIF signature could be successfully used in the future for describing the role of the nitrate atmospheric deposition on the nitrogen cycle.
Some evidences have been found showing that the atmosphere might not be the only source of a nitrate isotope anomaly. As an example, tests on the effects of copper in nitrate solutions on measured capital delta values would suggest the chance that an isotope anomaly could be associated to biological processes due to the presence of certain pollutants. Our data also indicate that a nitrate MIF signature might be generated due to geochemical processes and waste treatments with ozone.
The analyses of water samples from the Marano lagoon would suggest the presence of a process, possibly denitrification, buffering the MIF signal. Moreover, some simple examples in chapter 5 have been illustrated to show the effects of an isotope partitioning among phases in "real" systems (i.e. when considering absolute numbers instead of isotope ratios) on the initial isotope anomaly. It is therefore shown that it is not always possible to distribute any set consisting of three or more types of isotopes so that the initial isotope anomaly is retained in every phase of the system. As a consequence, both the measurements of the lagoon samples and the calculations of chapter 5 would indicate that the tracer could not always be a conservative parameter.
Overall, the study case of the Marano lagoon would indicate that the precision of the method is probably too low when considering a coastal environment, since the uncertainty is at least 75% of the measure when the atmospheric nitrate content in water sample is about 2%. The accuracy and the precision of the method can be both improved when also nitrate aerosol samples are collected and analysed. Yet, the nitrate partitioning between gaseous HNO_3 and aerosol in the air column will still have an effect on the accuracy of the method.
For all these reasons, the potential of understanding the effects of deposition events on the local nitrogen cycle by using the nitrate MIF signal as a tracer is probably limited.

6.1. Future work recommendation

The use of time series showing the change over time of the MIF signal in nitrate samples does have the potential of giving some information that could not be obtained otherwise. However, interpreting the measurements will not be an easy task, since there are no obvious simple relationships to apply and because the analyses of the MIF signature has to be coupled with several other key data. Consequently, at a first sight the apparent complexity of modeling the change of the nitrate isotope anomaly in a system could prevent using it as a tracer, since deviations due to analytical artifacts in the MIF measurements could lead to misinterpretations of the results.
A possible solution could be using an approach that certainly gives results of robust statistical significance. Neural networks (Haykin, 1999), being excellent problem solvers, could allow identification of the reason for the change of the variable of interest. So far not so many works have been undertaken on the use of artificial intelligence applied for isotopic studies, even if published results would suggest that it is a promising approach for understanding many natural environments.

A review on the applications of neural networks in earth sciences can be found in Valdes and Bonham-Carter (2006). When undertaking large training sets, artificial neural networks are able to predict the flux of species due to metabolic processes from isotopic data even without the knowledge of the pathway (Antoniewicz et al., 2006). Similar studies should be undertaken for modeling the resulting nitrate isotope anomaly after biological processes like denitrification and nitrification. Using the neural network could also be a potential approach to constrain the relative importance of chemical reaction vs. transport processes in generating the observed nitrate isotope anomaly in the air column, once the nitrate isotope fractionation constant dependence on temperature and pressure is defined, as well as the isotope effect of the partitioning between the gaseous and the liquid/solid phase present in aerosol.
It is worth mentioning a recent work (Skwarcec et al., 2009) using the artificial intelligence that could be an example to further interpret the large data set of the Marano lagoon obtained for the environmental program FONIMAR. The study considers temporal and spatial variability of three radioisotopes to interpret seasonal changes and the spatial variability in the catchment area of the Vistula River. If more detailed time series on the MIF signal in sample water and aerosol from the Marano lagoon were available (sample collected weekly or monthly), to be coupled with the existing key data like nutrients concentration in water (NH_4, PO_4 and NO_2) and the biomass distribution, the link between nitrate atmospheric deposition and the local biogeochemical processes in this lagoonal environment could be unraveled.

Acknowledgements

I wish to thank Bernard Leze, Liz Claxton and Emiliy Sears for their technical support.
Thanks to Prof. Tim Jickells, for the stimulating discussions during the stage of the writing of this thesis.
Thanks also to Dr. Alison Bateman and Dr. Alina Marca Bell for the training for the denitrifier method and the use of the mass spectrometer.

References:

Alexander, B., M. Hastings, et al. (2009). "Quantifying atmospheric nitrate formation pathways based on a global model of the oxygen isotopic composition ($\Delta^{17}O$) of atmospheric nitrate." Atmos. Chem. Phys **9**: 5043-5056.

Ansari, A. S. and S. N. Pandis (2000). "The effect of metastable equilibrium states on the partitioning of nitrate between the gas and aerosol phases." Atmospheric Environment **34**(1): 157-168.

Antoniewicz, M. R., G. Stephanopoulos, et al. (2006). "Evaluation of regression models in metabolic physiology: predicting fluxes from isotopic data without knowledge of the pathway." Metabolomics **2**(1): 41-52.

Atkinson, R. (2000). "Atmospheric chemistry of VOCs and NOx." Atmospheric Environment **34**(12-14): 2063-2101.

Atkinson, R., D. Baulch, et al. (1997). "Evaluated Kinetic and Photochemical Data for Atmospheric Chemistry: Supplement VI. IUPAC Subcommittee on Gas Kinetic Data Evaluation for Atmospheric Chemistry." Journal of Physical and Chemical Reference Data **26**: 1329.

Baker, A., K. Weston, et al. (2007). "Dry and wet deposition of nutrients from the tropical Atlantic atmosphere: Links to primary productivity and nitrogen fixation." Deep Sea Research Part I: Oceanographic Research Papers **54**(10): 1704-1720.

Baltensperger, U., N. Streit, et al. (2002). "Urban and rural aerosol characterization of summer smog events during the PIPAPO field campaign in Milan, Italy." J. Geophys. Res **107**(1-13): 8193.

Barrett, J. H., R. C. Parslow, et al. (1998). "Nitrate in drinking water and the incidence of gastric, esophageal, and brain cancer in Yorkshire, England." Cancer Causes and Control **9**(2): 153-159.

Barton, H. A. and D. E. Northup (2007). "Geomicrobiology in cave environments: past, current and future perspectives." Journal of Cave and Karst Studies **69**(1): 163-178.

Belakovskii, D. I., Moskalev, I.V . (1988). "Ammonium nitrate from products of coal fire in the Kukhi-Malik tract (central Tajikistan)." Novye Dannye o Mineralakh **35**: 191-194.

Ben-Naim, A. (2007). "On the so-called Gibbs paradox, and on the real paradox." Entropy **9**(3): 132-136.

Bigeleisen, J. (1949). "The relative reaction velocities of isotopic molecules." The Journal of Chemical Physics **17**: 675.

Bigeleisen, J. and M. G. Mayer (1947). "Calculation of equilibrium constants for isotopic exchange reactions." The Journal of Chemical Physics **15**: 261.

Blyth, A. J. and S. Frisia (2008). "Molecular evidence for bacterial mediation of calcite formation in cold high-altitude caves." Geomicrobiology Journal **25**(2): 101-111.

Bohlke, J., G. Ericksen, et al. (1997). "Stable isotope evidence for an atmospheric origin of desert nitrate deposits in northern Chile and southern California, USA." Chemical Geology **136**(1): 135-152.

Bohlke, J., S. Mroczkowski, et al. (2003). "Oxygen isotopes in nitrate: new reference materials for ^{18}O: ^{17}O: ^{16}O measurements and observations on nitrate-water equilibration." Rapid communications in mass spectrometry RCM **17**(16): 1835-1846.

Brimblecombe, P. and S. Clegg (1988). "The solubility and behaviour of acid gases in the marine aerosol." Journal of Atmospheric Chemistry **7**(1): 1-18.

Brost, R. A., A. C. Delany, et al. (1988). "Numerical Modeling of Concentrations and Fluxes of HNO_3, NH_3, and NH_4NO_3 near the Surface." Journal of Geophysical Research **93**(D6): 7137-7152.

Buchachenko, A. (2007). "The physical kinetics of magnetoplasticity of diamagnetic crystals." Journal of Experimental and Theoretical Physics **105**(4): 722-725.

Buchachenko, A. (2010). "Magnetic isotopy: New horizons." Herald of the Russian Academy of Sciences **80**(1): 22-28.

Buchachenko, A. L. (1995). "MIE versus CIE: comparative analysis of magnetic and classical isotope effects." Chemical reviews **95**(7): 2507-2528.

Buchachenko, A. L. and D. A. Kuznetsov (2008). "Magnetic field affects enzymatic ATP synthesis." Journal of the American Chemical Society **130**(39): 12868-12869.

Buchachenko, A. L., N. N. Lukzen, et al. (2007). "On the magnetic field and isotope effects in enzymatic phosphorylation." Chemical Physics Letters **434**(1): 139-143.

Buchachenko, A. L., L. V. Ruban, et al. (1995). "Spin catalysis of the radical recombination reaction." Chemical Physics Letters **233**(3): 315-318.

Bunton, C., E. Halevi, et al. (1952). "957. Oxygen exchange between nitric acid and water. Part I." J. Chem. Soc.(0): 4913-4916.

Canaveras, J. C., S. Cuezva, et al. (2006). "On the origin of fiber calcite crystals in moonmilk deposits." Naturwissenschaften **93**(1): 27-32.

Casciotti, K., D. Sigman, et al. (2002). "Measurement of the oxygen isotopic composition of nitrate in seawater and freshwater using the denitrifier method." Analytical Chemistry **74**(19): 4905-4912.

Casciotti, K. L. (2009). "Inverse kinetic isotope fractionation during bacterial nitrite oxidation." Geochimica et cosmochimica acta **73**(7): 2061-2076.

Chang, K., C. Lu, et al. (2002). "A theoretical evaluation on the HNO_3 artifact of the annular denuder system due to evaporation and diffusional deposition of NH_4NO_3-containing aerosols." Atmospheric Environment **36**(27): 4357-4366.

Cifuentes, L., J. Sharp, et al. (1988). "Stable carbon and nitrogen isotope biogeochemistry in the Delaware estuary." Limnology and Oceanography: 1102-1115.

Clayton, R. N. (1993). "Oxygen isotopes in meteorites." Annual Review of Earth and Planetary Sciences **21**: 115-149.

Clayton, R. N., L. Grossman, et al. (1973). "A component of primitive nuclear composition in carbonaceous meteorites." Science **182**(4111): 485-488.

Clayton, R. N., N. Onuma, et al. (1976). "A classification of meteorites based on oxygen isotopes." Earth and Planetary Science Letters **30**(1): 10-18.

Cloern, J. E., E. A. Canuel, et al. (2002). "Stable carbon and nitrogen isotope composition of aquatic and terrestrial plants of the San Francisco Bay estuarine system." Limnology and Oceanography: 713-729.

Corredor, J. E. and J. M. Morell (1994). "Nitrate depuration of secondary sewage effluents in mangrove sediments." Estuaries and Coasts **17**(1): 295-300.

Coss, A., K. P. Cantor, et al. (2004). "Pancreatic cancer and drinking water and dietary sources of nitrate and nitrite." American journal of epidemiology **159**(7): 693-701.

Covelli, S., A. Acquavita, et al. (2009). "Recent contamination of mercury in an estuarine environment (Marano lagoon, Northern Adriatic, Italy)." Estuarine, Coastal and Shelf Science **82**: 273-284.

Craig, H. (1957). "Isotopic standards for carbon and oxygen and correction factors for mass-spectrometric analysis of carbon dioxide." Geochimica et cosmochimica acta **12**(1-2): 133-149.

Cunningham, J. and H. Heal (1958). "The decomposition of solid nitrates by X-rays." Trans. Faraday Soc. **54**(0): 1355-1369.

Dasch, J. M., S. H. Cadle, et al. (1989). "Comparison of annular denuders and filter packs for atmospheric sampling." Atmospheric Environment (1967) **23**(12): 2775-2782.

Davis, B. L. (1984). "X-ray diffraction analysis and source apportionment of Denver aerosol." Atmospheric Environment (1967) **18**(10): 2197-2208.

De Groot, S. R. and P. Mazur (1962). Non-equilibrium thermodynamics, North-Holland, Amsterdam.

de Leeuw, G., L. Cohen, et al. (2001). "Atmospheric input of nitrogen into the North Sea: ANICE project overview." Continental Shelf Research **21**(18-19): 2073-2094.

De Pol, R. (2010). "Inquinamento da metalli pesanti in relazione ai processi metabolici: importanza delle metodiche di speciazione."

DeMore, W. B., S. Sander, et al. (1997). Chemical kinetics and photochemical data for use in stratospheric modeling, Jet Propulsion Lab., California Inst. of Tech., Pasadena, CA.

Dentener, F., J. Drevet, et al. (2006). "Nitrogen and sulfur deposition on regional and global scales: A multimodel evaluation." Global Biogeochemical Cycles **20**(4): -.

Dieks, D. (2011). "The Gibbs paradox revisited." Explanation, Prediction, and Confirmation: 367-377.

Doney, S. C., N. Mahowald, et al. (2007). "Impact of anthropogenic atmospheric nitrogen and sulfur deposition on ocean acidification and the inorganic carbon system." Proceedings of the National Academy of Sciences **104**(37): 14580.

Dong, H., C. Cai, et al. (2012). "A quantum solution to Gibbs Paradox with few particles." Arxiv preprint arXiv:1201.3395.

Duce, R., J. LaRoche, et al. (2008). "Impacts of atmospheric anthropogenic nitrogen on the open ocean." Science **320**(5878): 893-897.

Ehhalt, D., M. Prather, et al. (2001). Atmospheric chemistry and greenhouse gases, Pacific Northwest National Laboratory (PNNL), Richland, WA (US).

Emili, A., N. Koron, et al. (2011). "Does anoxia affect mercury cycling at the sediment-water interface in the Gulf of Trieste (northern Adriatic Sea)? Incubation experiments using benthic flux chambers." Applied Geochemistry **26**(2): 194-204.

Ericksen, G. E. (1981). "Geology and origin of the Chilean nitrate deposits."

Erisman, J. W., M. A. Sutton, et al. (2008). "How a century of ammonia synthesis changed the world." Nature Geoscience **1**(10): 636-639.

Esteve, V., J. Rius, et al. (1997). "Quantitative X-ray diffraction phase analysis of coarse airborne particulate collected by cascade impactor sampling." Atmospheric Environment **31**(23): 3963-3967.

Fanfani, L., A. Nunzi, et al. (1973). "The crystal structure of buttgenbachite." Mineralogical Magazine **39**(303): 264-270.

Ferrarin, C., G. Umgiesser, et al. (2010). "Hydraulic zonation of the lagoons of Marano and Grado, Italy. A modelling approach." Estuarine, Coastal and Shelf Science **87**(4): 561-572.

Fiore, A., F. Dentener, et al. (2009). "Multimodel estimates of intercontinental source-receptor relationships for ozone pollution." J. Geophys. Res **114**(D4): D04301.

Fliermans, C. and E. Schmidt (1977). "Nitrobacter in Mammoth Cave." International Journal of Speleology **9**(1): 1-19.

Force, N. S. T. and I. C. f. t. E. o. t. Sea (1993). North Sea quality status report 1993, Olsen & Olsen.

Forman, D. (1989). "Are nitrates a significant risk factor in human cancer?" Cancer surveys **8**(2): 443.

Fouillac, A. M. and J. P. Girard (1996). "Laser oxygen isotope analysis of silicate/oxide grain separates: Evidence for a grain size effect?" Chemical Geology **130**(1): 31-54.

Franklin, A. and A. Lidiard (1983). "Atomic transport via point defects in crystals. I. General kinetic theory of diffusion." Proceedings of the Royal Society of London. A. Mathematical and Physical Sciences **389**(1797): 405-431.

Franklin, A. and A. Lidiard (1984). "Atomic Transport via Point Defects in Crystals. II. Atomic Mobilities and Dielectric Relaxation." Proceedings of the Royal Society of London. A. Mathematical and Physical Sciences **392**(1803): 457-473.

Franzen, C. and P. W. Mirwald (2009). "Moisture sorption behaviour of salt mixtures in porous stone." Chemie der Erde-Geochemistry **69**(1): 91-98.

Frascari, F., M. Frignani, et al. (1988). "Sediments and Pollution in the Northern Adriatic Seaa." Annals of the New York Academy of Sciences **534**(1): 1000-1020.

Frey, M., J. Savarino, et al. (2009). "Photolysis imprint in the nitrate stable isotope signal in snow and atmosphere of East Antarctica and implications for reactive nitrogen cycling."

Frost, R. L., K. L. Erickson, et al. (2005). "Raman spectroscopy of likasite at 298 and 77K." Spectrochimica Acta Part A: Molecular and Biomolecular Spectroscopy **61**(4): 607-612.

Frost, R. L., P. Leverett, et al. (2004). "Raman spectroscopy of gerhardtite at 298 and 77 K." Journal of Raman Spectroscopy **35**(11): 991-996.

Frost, R. L., P. A. Williams, et al. (2002). "Raman spectroscopy of the polyanionic copper (II) minerals buttgenbachite and connellite: implications for studies of ancient copper objects and bronzes." Journal of Raman Spectroscopy **33**(9): 752-757.

Fung, K. and I. Tang (1992). "Analysis of aerosol particles by resonance Raman scattering technique." Applied spectroscopy **46**(1): 159-162.

Galloway, J., F. Dentener, et al. (2004). "Nitrogen cycles: past, present, and future." Biogeochemistry **70**: 153-226.

Galloway, J. N., A. R. Townsend, et al. (2008). "Transformation of the nitrogen cycle: recent trends, questions, and potential solutions." Science **320**(5878): 889-892.

Gao, Y. Q. and R. Marcus (2001). "Strange and unconventional isotope effects in ozone formation." Science **293**(5528): 259-263.

Gao, Y. Q. and R. Marcus (2002). "On the theory of the strange and unconventional isotopic effects in ozone formation." The Journal of chemical physics **116**: 137.

Gao, Y. Q. and R. Marcus (2007). "An approximate theory of the ozone isotopic effects: Rate constant ratios and pressure dependence." Journal Of Chemical Physics **127**(24): 244316-244500.

Gibbs, J. W. (1874). "On the equilibrium of heterogeneous substances."

Giletti, B. J. (1986). "Diffusion effects on oxygen isotope temperatures of slowly cooled igneous and metamorphic rocks." Earth and Planetary Science Letters **77**(2): 218-228.

Granger, J., D. M. Sigman, et al. (2008). "Nitrogen and oxygen isotope fractionation during dissimilatory nitrate reduction by denitrifying bacteria." Limnology and Oceanography: 2533-2545.

Granger, J., D. M. Sigman, et al. (2004). "Coupled nitrogen and oxygen isotope fractionation of nitrate during assimilation by cultures of marine phytoplankton." Limnology and Oceanography: 1763-1773.

Grassegger, G. (1999). "Decay mechanisms of natural building stones on monuments-A review of the latest theories." Werkstoffe und Werkstoffpr√ºfung im Bauwesen, Hamburgo, Libri BOD: 54-81.

Grissom, C. B. (1995). "Magnetic field effects in biology: A survey of possible mechanisms with emphasis on radical-pair recombination." Chemical reviews **95**(1): 3-24.

Groot, S. R. and P. Mazur (1984). Non-equilibrium thermodynamics, Dover Pubns.

Gruber, N. and J. N. Galloway (2008). "An Earth-system perspective of the global nitrogen cycle." Nature **451**(7176): 293-296.

Gruszkiewicz, M. S., D. A. Palmer, et al. (2007). "Phase Behavior of Aqueous Na, K, Mg, Ca, Cl,NO_3 Mixtures: Isopiestic Measurements and Thermodynamic Modeling." Journal of solution chemistry **36**(6): 723-765.

Hansell, D., D. Olson, et al. (2007). "Assessment of excess nitrate development in the subtropical North Atlantic." Marine Chemistry **106**(3-4): 562-579.

Harpale, V. M., S. D. Ralegankar, et al. (2006). "Chemical Identification of Urban Air Particulates in the Environment of Pune City(India) By Raman Spectroscopy." Aerosol and Air Quality Resarch **6**(3): 295-304.

Hayez, V., T. Segato, et al. (2006). "Study of copper nitrate,Äêbased patinas." Journal of Raman Spectroscopy **37**(10): 1211-1220.

Haykin, S. (1999). "Neural Networks: a Comprehensive Foundation." Prentice Hall.

Heaton, T. (1984). "Sources of the nitrate in phreatic groundwater in the western Kalahari." Journal of Hydrology **67**: 249-259.

Heaton, T. (1987). "15N 14N ratios of nitrate and ammonium in rain at Pretoria, South Africa." Atmospheric Environment (1967) **21**(4): 843-852.

Heaton, T. (1987). "Isotopic evidence for the diverse origins of nitrate minerals." South African journal of science **83**(2): 118-119.

Heidenreich III, J. E. and M. H. Thiemens (1986). "A non-mass dependent oxygen isotope effect in the production of ozone from molecular oxygen: The role of molecular symmetry in isotope chemistry." The Journal of chemical physics **84**: 2129.

Hibbs, D. E., P. Leverett, et al. (2002). "Buttgenbachite from Bisbee, Arizona, USA: a single-crystal X-ray study." Neues Jahrbuch fü r Mineralogie-Monatshefte **2002**(5): 225-240.

Hibbs, D. E., P. Leverett, et al. (2003). "A single crystal X-ray study of a sulphate-bearing buttgenbachite, $Cu_{36}Cl_{7.8}$ $(NO_3)_{1.3}$ $(SO4)_{0.35}$ $(OH)_{62.2}$. 5.2 H_2O, and a re-examination of the crystal chemistry of the buttgenbachite-connellite series." Mineralogical Magazine **67**(1): 47-60.

Hill, C. A. (1981). "Origin of cave saltpeter." The Journal of Geology: 252-259.

Holloway, J. A. M. and R. A. Dahlgren (2002). "Nitrogen in rock: Occurrences and biogeochemical implications." Global Biogeochemical Cycles **16**(4): 1118.

Hulston, J. and H. Thode (1965). "Variations in the S33, S34, and S36 contents of meteorites and their relation to chemical and nuclear effects." Journal of Geophysical Research **70**(14): 3475-3484.

Hutchinson, G. E. (1944). "Nitrogen in the biogeochemistry of the atmosphere." American Scientist **32**(3): 178-195.

Janssen, C., J. Guenther, et al. (2001). "Kinetic origin of the ozone isotope effect: a critical analysis of enrichments and rate coefficients." Phys. Chem. Chem. Phys. **3**(21): 4718-4721.

Jaynes, E. T. (1965). "Gibbs vs Boltzmann entropies." Am. J. Phys **33**(5): 391-398.

Jaynes, E. T. (1992). The Gibbs paradox, Kluwer Academic: Dordrecht.

Jensen, O. (1982). "Nitrate in drinking water and cancer in northern Jutland, Denmark, with special reference to stomach cancer." Ecotoxicology and environmental safety **6**(3): 258-267.

Jickells, T. (2006). "The role of air-sea exchange in the marine nitrogen cycle." Biogeosciences Discussions **3**(1): 183-210.

Jickells, T. D., Z. An, et al. (2005). "Global iron connections between desert dust, ocean biogeochemistry, and climate." Science **308**(5718): 67-71.

Joossens, J. V., M. Hill, et al. (1996). "Dietary salt, nitrate and stomach cancer mortality in 24 countries." International journal of epidemiology **25**(3): 494-504.

Kaiser, J., M. G. Hastings, et al. (2007). "Triple oxygen isotope analysis of nitrate using the denitrifier method and thermal decomposition of N_2O." Analytical Chemistry **79**(2): 599-607.

Kapteijn, F., J. Rodriguez-Mirasol, et al. (1996). "Heterogeneous catalytic decomposition of nitrous oxide." Applied Catalysis B: Environmental **9**(1): 25-64.

Kendall, C., E. M. Elliott, et al. (2007). "Tracing anthropogenic inputs of nitrogen to ecosystems." Stable isotopes in ecology and environmental science: 375-449.

Krishnamurthy, A., J. K. Moore, et al. (2010). "Impacts of atmospheric nutrient inputs on marine biogeochemistry." J. Geophys. Res **115**(10.1029).

Lamarque, J., J. Kiehl, et al. (2005). "Assessing future nitrogen deposition and carbon cycle feedback using a multimodel approach: Part 1. Analysis of nitrogen deposition." J. Geophys. Res **110**: D19303.

Lario, J. and V. Soler (2010). "Microclimate monitoring of Pozalagua Cave (Spain): application to management and protection of show caves." Journal of Cave and Karst Studies.

Lin, S. K. (1996). "Gibbs paradox of entropy of mixing: experimental facts, its rejection and the theoretical consequences." Electronic Journal of Theoretical Chemistry **1**(1): 135-151.

Lin, S. K. (2008). "Gibbs paradox and the concepts of information, symmetry, similarity and their relationship." Entropy **10**(1): 1-5.

Ling, T. Y. and C. K. Chan (2007). "Formation and Transformation of Metastable Double Salts from the Crystallization of Mixed Ammonium Nitrate and Ammonium Sulfate Particles." Environmental science & technology **41**(23): 8077-8083.

Luo, C., C. S. Zender, et al. (2007). "Role of ammonia chemistry and coarse mode aerosols in global climatological inorganic aerosol distributions." Atmospheric Environment **41**(12): 2510-2533.

Luz, B., E. Barkan, et al. (1999). "Triple-isotope composition of atmospheric oxygen as a tracer of biosphere productivity." Nature **400**(6744): 547-550.

Magalhaes, C., J. Costa, et al. (2007). "Impact of trace metals on denitrification in estuarine sediments of the Douro River estuary, Portugal." Marine Chemistry **107**(3): 332-341.

Marcus, R. (1952). "Unimolecular dissociations and free radical recombination reactions." The Journal of chemical physics **20**: 359.

Marcus, R. and O. Rice (1951). "The Kinetics of the Recombination of Methyl Radicals and Iodine Atoms." The Journal of Physical Chemistry **55**(6): 894-908.

Maria, S. F., L. M. Russell, et al. (2002). "FTIR measurements of functional groups and organic mass in aerosol samples over the Caribbean." Atmospheric Environment **36**(33): 5185-5196.

Martin, S. T. (2000). "Phase transitions of aqueous atmospheric particles." Chemical Reviews **100**(9): 3403-3453.

Martin, S. T., J. C. Schlenker, et al. (2003). "Crystallization of atmospheric sulfate-nitrate-ammonium particles." Geophys. Res. Lett **30**(21): 2102.

Martinez-Arkarazo, I., M. Angulo, et al. (2007). "Spectroscopic characterisation of moonmilk deposits in Pozalagua tourist cave (Karrantza, Basque Country, North of Spain)." Spectrochimica Acta Part A: Molecular and Biomolecular Spectroscopy **68**(4): 1058-1064.

Martini, J. E. J. (1996). "Gwihabaite - $(NH_4,K)NO_3$, orthorhombic, a new mineral from Gcwihaba Cave, Botswana." Bull. South African Speleological Assoc., **36**: 19-21.

Matsubara, T. and W. G. Zumft (1982). "Identification of a copper protein as part of the nitrous oxide-reducing system in nitrite-respiring (denitrifying) pseudomonads." Archives of Microbiology **132**(4): 322-328.

Matsuhisa, Y., J. R. Goldsmith, et al. (1978). "Mechanisms of hydrothermal crystallization of quartz at 250 C and 15 kbar." Geochimica et cosmochimica acta **42**(2): 173-182.

Mauersberger, K., B. Erbacher, et al. (1999). "Ozone isotope enrichment: Isotopomer-specific rate coefficients." Science **283**(5400): 370.

McLean, W. and J. Anthony (1972). "The disordered "zeolite-like" structure of connellite." American Mineralogist **57**: 426-438.

Melchiorre, E. B., P. A. Williams, et al. (2006). "Biogenic nitrogen from termite mounds and the origin of gerhardtite at the Great Australia mine, Cloncurry, Queensland, Australia." The Canadian Mineralogist **44**(6): 1447-1455.

Meng, Z. and J. H. Seinfeld (1996). "Time scales to achieve atmospheric gas-aerosol equilibrium for volatile species." Atmospheric Environment **30**(16): 2889-2900.

Meyer, C., B. Wunder, et al. (2008). "Boron-isotope fractionation between tourmaline and fluid: an experimental re-investigation." Contributions to Mineralogy and Petrology **156**(2): 259-267.

Michalski, G., J. Bohlke, et al. (2004). "Long term atmospheric deposition as the source of nitrate and other salts in the Atacama Desert, Chile: New evidence from mass-independent oxygen isotopic compositions." Geochimica et cosmochimica acta **68**(20): 4023-4038.

Michalski, G., Z. Scott, et al. (2003). "First measurements and modeling of Œî17O in atmospheric nitrate." Geophysical Research Letters **30**(16): 1870.

Michalski, G. and M. Thiemens (2006). "The Use of Multi-Isotope Ratio Measurements as a New and Unique Technique to Resolve NOx Transformation, Transport and Nitrate Deposition in the Lake Tahoe Basin."

Miller, M. F. (2002). "Isotopic fractionation and the quantification of 17O anomalies in the oxygen three-isotope system:: an appraisal and geochemical significance." Geochimica et cosmochimica acta **66**(11): 1881-1889.

Miller, M. F., I. A. Franchi, et al. (2002). "Mass-Independent Fractionation of Oxygen Isotopes during Thermal Decomposition of Carbonates." Proceedings of the National Academy of Sciences of the United States of America: 10988-10993.

Mizutani, H., D. A. McFarlane, et al. (1992). "Nitrogen and carbon isotope study of bat guano core from Eagle Creek Cave, Arizona, USA." Journal of the Mass Spectrometry Society of Japan **40**(1): 57-65.

Morin, S., J. Savarino, et al. (2009). "Comprehensive isotopic composition of atmospheric nitrate in the Atlantic Ocean boundary layer from 65 S to 79 N." Journal of Geophysical Research **114**(D5): D05303.

Morino, Y., Y. Kondo, et al. (2006). "Partitioning of HNO_3 and particulate nitrate over Tokyo: Effect of vertical mixing." JOURNAL OF GEOPHYSICAL RESEARCH-ALL SERIES- **111**(D15): 15215.

Mortici, C. (2010). "Best estimates of the generalized Stirling formula." Applied Mathematics and Computation **215**(11): 4044-4048.

Nakamura, M., H. Yurimoto, et al. (2005). "Grain growth control of isotope exchange between rocks and fluids." Geology **33**(10): 829.

Nakatsuka, T., N. Handa, et al. (1992). "The dynamic changes of stable isotopic ratios of carbon and nitrogen in suspended and sedimented particulate organic matter during a phytoplankton bloom." Journal of marine research **50**(2): 267-296.

Nenes, A., S. N. Pandis, et al. (1998). "ISORROPIA: A new thermodynamic equilibrium model for multiphase multicomponent inorganic aerosols." Aquatic geochemistry **4**(1): 123-152.

Nie, W., T. Wang, et al. (2010). "Comparison among filter-based, impactor-based and continuous techniques for measuring atmospheric fine sulfate and nitrate." Atmospheric Environment **44**(35): 4396-4403.

Northup, D. E. and K. H. Lavoie (2001). "Geomicrobiology of caves: a review." Geomicrobiology Journal **18**(3): 199-222.

Nowick, A. S. and J. J. Burton (1975). "Diffusion in solids: recent developments." Academic Press inc.

Onac, B. (2008). "Sulfur and oxygen isotope constraints on the genesis of gypsum in caves from Cerna Valley (Romania)."

Onac, B. P., J. G. Wynn, et al. (2011). "Tracing the sources of cave sulfates: a unique case from Cerna Valley, Romania." Chemical Geology.

Onsager, L. (1931). "Reciprocal Relations in Irreversible Processes. I." Physical Review **37**(4): 405.

Onsager, L. and S. Machlup (1953). "Fluctuations and irreversible processes." Physical Review **91**(6): 1505-1512.

Paerl, H. W. (1985). "Enhancement of marine primary production by nitrogen-enriched acid rain."

Paerl, H. W. (1988). "Nuisance phytoplankton blooms in coastal, estuarine, and inland waters." Limnology and Oceanography: 823-847.

Pakkanen, T. A., V. M. Kerminen, et al. (1996). "Distribution of nitrate over sea-salt and soil derived particles,Äîimplications from a field study." Journal of Atmospheric Chemistry **24**(2): 189-205.

Patris, N., S. Cliff, et al. (2007). "Isotopic analysis of aerosol sulfate and nitrate during ITCT-2k2: Determination of different formation pathways as a function of particle size." J. Geophys. Res **112**: D23301.

Pauli, W., C. P. Enz, et al. (1973). "Pauli lectures on physics." Physics Today **26**: 53.

Peterson, B. J. and R. W. Howarth (1987). "Sulfur, carbon, and nitrogen isotopes used to trace organic matter flow in the salt-marsh estuaries of Sapelo Island, Georgia." Limnology and Oceanography: 1195-1213.

Prodi, F., F. Belosi, et al. (2009). "Aerosol fine fraction in the Venice Lagoon: Particle composition and sources." Atmospheric Research **92**(2): 141-150.

Pueyo, J. J., G. Chong, et al. (1998). "Mineralogia y evolution de las salmueras madres en el yacimiento de nitratos Pedro de Valdivia, Antofagasta, Chile." Revista geologica de Chile **25**(1): 03-15.

Puscas, C. M., B. P. Onac, et al. (2010). "The mineral assemblage of caves within Salitrari Mountain (Cerna Valley, SW Romania): depositional environment and speleogenetic implications." Carbonates and Evaporites **25**(2): 107-115.

Qin, Y., Y. H. Li, et al. (2012). "N and O isotopes and the ore-forming mechanism of nitrate deposits in the Turpan-Hami Basin, Xinjiang, China." SCIENCE CHINA Earth Sciences **55**(2): 213-220.

Randall, C. and D. Buth (1984). "Nitrite build-up in activated sludge resulting from temperature effects." Journal (Water Pollution Control Federation): 1039-1044.

Rayleigh, L. (1939). "Nitrogen, argon and neon in the earth's crust with applications to cosmology." Proceedings of the Royal Society of London. Series A, Mathematical and Physical Sciences **170**(943): 451-464.

Revesz, K., J. Bohlke, et al. (1997). "Determination of oxygen-18 and nitrogen-15 isotopic ratios in nitrate."

Richter, F. M. (1993). "A method for determining activity-composition relations using chemical diffusion in silicate melts." Geochimica et cosmochimica acta **57**(9): 2019-2032.

Richter, F. M., N. Dauphas, et al. (2009). "Non-traditional fractionation of non-traditional isotopes: Evaporation, chemical diffusion and Soret diffusion." Chemical Geology **258**: 92-103.

Rodhe, H., F. Dentener, et al. (2002). "The global distribution of acidifying wet deposition." Environmental science & technology **36**(20): 4382-4388.

Rogers, K. M. (2003). "Stable carbon and nitrogen isotope signatures indicate recovery of marine biota from sewage pollution at Moa Point, New Zealand." Marine Pollution Bulletin **46**(7): 821-827.

Rumble, D., M. F. Miller, et al. (2007). "Oxygen three-isotope fractionation lines in terrestrial silicate minerals: An inter-laboratory comparison of hydrothermal quartz and eclogitic garnet." Geochimica et cosmochimica acta **71**(14): 3592-3600.

Sabine, C. L. and T. Tanhua (2010). "Estimation of anthropogenic CO2 inventories in the ocean." Annual Review of Marine Science **2**: 175-198.

Saccon, P., Leis, A., et al. (2011). "Individuazione e caratterizzazione delle potenziali fonti dei nitrati nella Laguna di Marano e messa a punto di un piano di monitoraggio

ambientale. Progetto FONIMAR. Parte II." Bollettino Soc. Naturalisti “Silvia Zenari” 35.

Samie, F., J. Tidblad, et al. (2007). "Atmospheric Corrosion Effects of HNO." Journal of the Electrochemical Society **154**: C249.

Sandler, A. and T. H. E. Heaton (1997). "Source of Nitrate and Hydrologic Origin of an Unusual Cave Niter Dripstone; Israel." The Journal of Geology **105**(6): 754-762.

Sandor, J., I. Kiss, et al. (2001). "Association between gastric cancer mortality and nitrate content of drinking water: ecological study on small area inequalities." European journal of epidemiology **17**(5): 443-447.

Sebilo, M., G. Billen, et al. (2003). "Isotopic composition of nitrate-nitrogen as a marker of riparian and benthic denitrification at the scale of the whole Seine River system." Biogeochemistry **63**(1): 35-51.

Severinghaus, J. P. and M. O. Battle (2006). "Fractionation of gases in polar ice during bubble close-off: New constraints from firn air Ne, Kr and Xe observations." Earth and Planetary Science Letters **244**(1): 474-500.

Sfriso, A., C. Facca, et al. (2009). "Validation of the Macrophyte Quality Index (MaQI) set up to assess the ecological status of Italian marine transitional environments." Hydrobiologia **617**(1): 117-141.

Sharygin, V., E. Sokol, et al. (2009). "Fayalite-sekaninaite paralava from the Ravat coal fire (central Tajikistan)." Russian Geology and Geophysics **50**(8): 703-721.

Sigman, D., K. Casciotti, et al. (2001). "A bacterial method for the nitrogen isotopic analysis of nitrate in seawater and freshwater." Analytical Chemistry **73**(17): 4145-4153.

Sigman, D., R. Robinson, et al. (2003). "Distinguishing between water column and sedimentary denitrification in the Santa Barbara Basin using the stable isotopes of nitrate." Geochemistry Geophysics Geosystems **4**(5): 1040.

Sigman, D. M., P. J. DiFiore, et al. (2009). "Sinking organic matter spreads the nitrogen isotope signal of pelagic denitrification in the North Pacific." Geophys. Res. Lett **36**: L08605.

Sigman, D. M., P. J. DiFiore, et al. (2009). "The dual isotopes of deep nitrate as a constraint on the cycle and budget of oceanic fixed nitrogen." Deep Sea Research Part I: Oceanographic Research Papers **56**(9): 1419-1439.

Sigman, D. M., J. Granger, et al. (2005). "Coupled nitrogen and oxygen isotope measurements of nitrate along the eastern North Pacific margin." Global Biogeochem. Cycles **19**(4).

Silva, S., C. Kendall, et al. (2000). "A new method for collection of nitrate from fresh water and the analysis of nitrogen and oxygen isotope ratios." Journal of Hydrology **228**(1): 22-36.

Skwarzec, B., K. Kabat, et al. (2009). "Seasonal and spatial variability of 210Po, 238U and 239+ 240Pu levels in the river catchment area assessed by application of neural-network based classification." Journal of environmental radioactivity **100**(2): 167-175.

Spokes, L. J. and T. D. Jickells (2005). "Is the atmosphere really an important source of reactive nitrogen to coastal waters?" Continental Shelf Research **25**(16): 2022-2035.

Spokes, L. J., S. G. Yeatman, et al. (2000). "Nitrogen deposition to the eastern Atlantic Ocean. The importance of south easterly flow." Tellus B **52**(1): 37-49.

Steiger, M. and A. Zeunert (1996). Crystallization properties of salt mixtures: comparison of experimental results and model calculations, SN.

Stoch, A., J. Stoch, et al. (2001). "FTIR study of copper patinas in the urban atmosphere." Journal of Molecular Structure **596**(1): 201-206.

Sturges, W. T. and R. M. Harrison (1989). "Semi-quantitative X-ray diffraction analysis of size fractionated atmospheric particles." Atmospheric Environment (1967) **23**(5): 1083-1098.

Sugimoto, R., A. Kasai, et al. (2008). "Nitrogen isotopic discrimination by water column nitrification in a shallow coastal environment." Journal of oceanography **64**(1): 39-48.

Sun, T. and H. Bao (2011). "Non-mass-dependent $\Delta^{17}O$ anomalies generated by a superimposed thermal gradient on a rarefied O_2 gas in a closed system." Rapid Communications in Mass Spectrometry **25**(1): 20-24.

Sun, T. and H. Bao (2011). "Thermal-gradient-induced non-mass-dependent isotope fractionation." Rapid Communications in Mass Spectrometry **25**(6): 765-773.

Swendsen, R. H. (2008). "Gibbs paradox and the definition of entropy." Entropy **10**(1): 15-18.

Tang, I. and H. Munkelwitz (1994). "Water activities, densities, and refractive indices of aqueous sulfates and sodium nitrate droplets of atmospheric importance." Journal of Geophysical Research **99**(D9): 18801-18808.

Tang, I. N. (1980). "On the equilibrium partial pressures of nitric acid and ammonia in the atmosphere." Atmospheric Environment (1967) **14**(7): 819-828.

Tedesco, L. P. and P. A. Jacinthe (2009). "Impact of elevated copper on the rate and gaseous products of denitrification in freshwater sediments." Journal of environmental quality **38**(3): 1183-1192.

Teitzel, G. M., A. Geddie, et al. (2006). "Survival and growth in the presence of elevated copper: transcriptional profiling of copper-stressed Pseudomonas aeruginosa." Journal of bacteriology **188**(20): 7242-7256.

Thiemens, M. H. (2006). "History and applications of mass-independent isotope effects." Annu. Rev. Earth Planet. Sci. **34**: 217-262.

Thiemens, M. H. and H. J.E. (1983). "The mass-independent fractionation of oxygen: A novel isotope effect and its possible cosmochemical implications." Science **219**(4588): 1073.

Thomas, J. L., M. Roeselov, et al. (2007). "Molecular dynamics simulations of the solution-air interface of aqueous sodium nitrate." The Journal of Physical Chemistry A **111**(16): 3091-3098.

Tolbert, M. A. and A. M. Middlebrook (1990). "Fourier transform infrared studies of model polar stratospheric cloud surfaces: Growth and evaporation of ice and nitric acid/ice." Journal of Geophysical Research **95**(D13): 22423-22,431.

Tsunogai, U., S. Daita, et al. (2011). "Quantifying nitrate dynamics in an oligotrophic lake using D17O." Biogeosciences **8**(3): 687-702.

Tucker, J., N. Sheats, et al. (1999). "Using stable isotopes to trace sewage-derived material through Boston Harbor and Massachusetts Bay." Marine Environmental Research **48**(4): 353-375.

Turk, O. and D. Mavinic (1989). "Stability of nitrite build-up in an activated sludge system." Journal (Water Pollution Control Federation): 1440-1448.

Turro, N. J. and B. Kraeutler (1980). "Magnetic field and magnetic isotope effects in organic photochemical reactions. A novel probe of reaction mechanisms and a method for enrichment of magnetic isotopes." Accounts of Chemical Research **13**(10): 369-377.

Twining, B. S., S. E. Mylon, et al. (2007). "Potential role of copper availability in nitrous oxide accumulation in a temperate lake." Limnology and Oceanography: 1354-1366.

Urey, H. C. (1947). "The thermodynamic properties of isotopic substances." J. Chem. Soc.(0): 562-581.

Valdes, J. J. and G. Bonham-Carter (2006). "Time dependent neural network models for detecting changes of state in complex processes: applications in earth sciences and astronomy." Neural Networks **19**(2): 196-207.

Watson, E. B. and T. M√ºller (2009). "Non-equilibrium isotopic and elemental fractionation during diffusion-controlled crystal growth under static and dynamic conditions." Chemical Geology **267**(3-4): 111-124.

Whitehead, W. L. (1920). "The Chilean nitrate deposits." Economic Geology **15**(3): 187-224.

Williams, L. B. and R. L. Hervig (2005). "Lithium and boron isotopes in illite-smectite: the importance of crystal size." Geochimica et cosmochimica acta **69**(24): 5705-5716.

Wombacher, F. and M. Rehkhamper (2003). "Investigation of the mass discrimination of multiple collector ICP-MS using neodymium isotopes and the generalised power law." J. Anal. At. Spectrom. **18**(11): 1371-1375.

Wu, H. B. and C. K. Chan (2008). "Effects of potassium nitrate on the solid phase transitions of ammonium nitrate particles." Atmospheric Environment **42**(2): 313-322.

Wu, H. B., M. N. Chan, et al. (2007). "FTIR characterization of polymorphic transformation of ammonium nitrate." Aerosol science and technology **41**(6): 581-588.

Yang, W. and W. Blasiak (2005). "Mathematical modelling of NO emissions from high-temperature air combustion with nitrous oxide mechanism." Fuel Processing Technology **86**(9): 943-957.

Yanhe, L., Q. Yan, et al. (2010). "Discovery of Mass Independent Oxygen Isotopic Compositions in Superscale Nitrate Mineral Deposits from Turpan-Hami Basin, Xinjiang, China and Its Significance." Acta Geologica Sinica, English Edition **84**(6): 1514-1519.

Yoder, C., E. Bushong, et al. (2010). "The synthesis and solubility of the copper hydroxyl nitrates: gerhardtite, rouaite and likasite." Mineralogical Magazine **74**(3): 433-440.

Young, E. D., A. Galy, et al. (2002). "Kinetic and equilibrium mass-dependent isotope fractionation laws in nature and their geochemical and cosmochemical significance." Geochimica et cosmochimica acta **66**(6): 1095-1104.

Young, E. D. and S. S. Russell (1998). "Oxygen reservoirs in the early solar nebula inferred from an Allende CAI." Science **282**(5388): 452-455.

Zhang, B. and F. M. Tao (2010). "Direct homogeneous nucleation of NO_2, H_2O, and NH3 for the production of ammonium nitrate particles and HONO gas." Chemical Physics Letters **489**(4-6): 143-147.

Zhang, Y. and A. Zindler (1993). "Distribution and evolution of carbon and nitrogen in Earth." Earth and Planetary Science Letters **117**(3): 331-345.

Zhao, W. and P. K. Hopke (2006). "Source identification for fine aerosols in Mammoth Cave National Park." Atmospheric Research **80**(4): 309-322.

Zumft, W. G. (2005). "Nitric oxide reductases of prokaryotes with emphasis on the respiratory, heme copper oxidase type." Journal of inorganic biochemistry **99**(1): 194-215.

Appendix 1: Marano Lagoon data set.

Map 1: Sampling area, from Saccon et al., (2011).

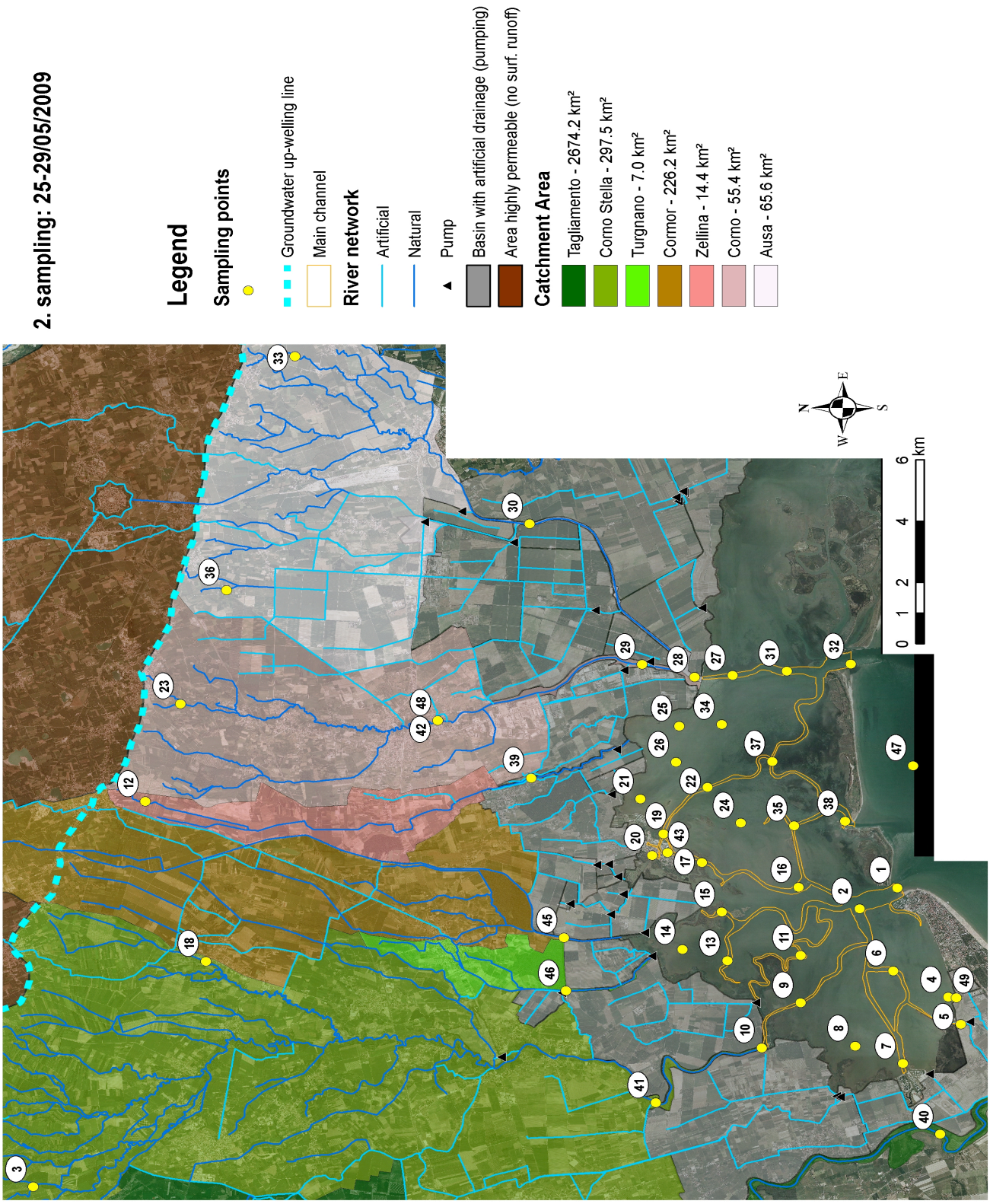

Map 2. Bathymetry Chart

Downloaded from http://www.abr.fvg.it/educazione-e-documentazione/cartografia, showing the water depth in meters at the Marano lagoon.

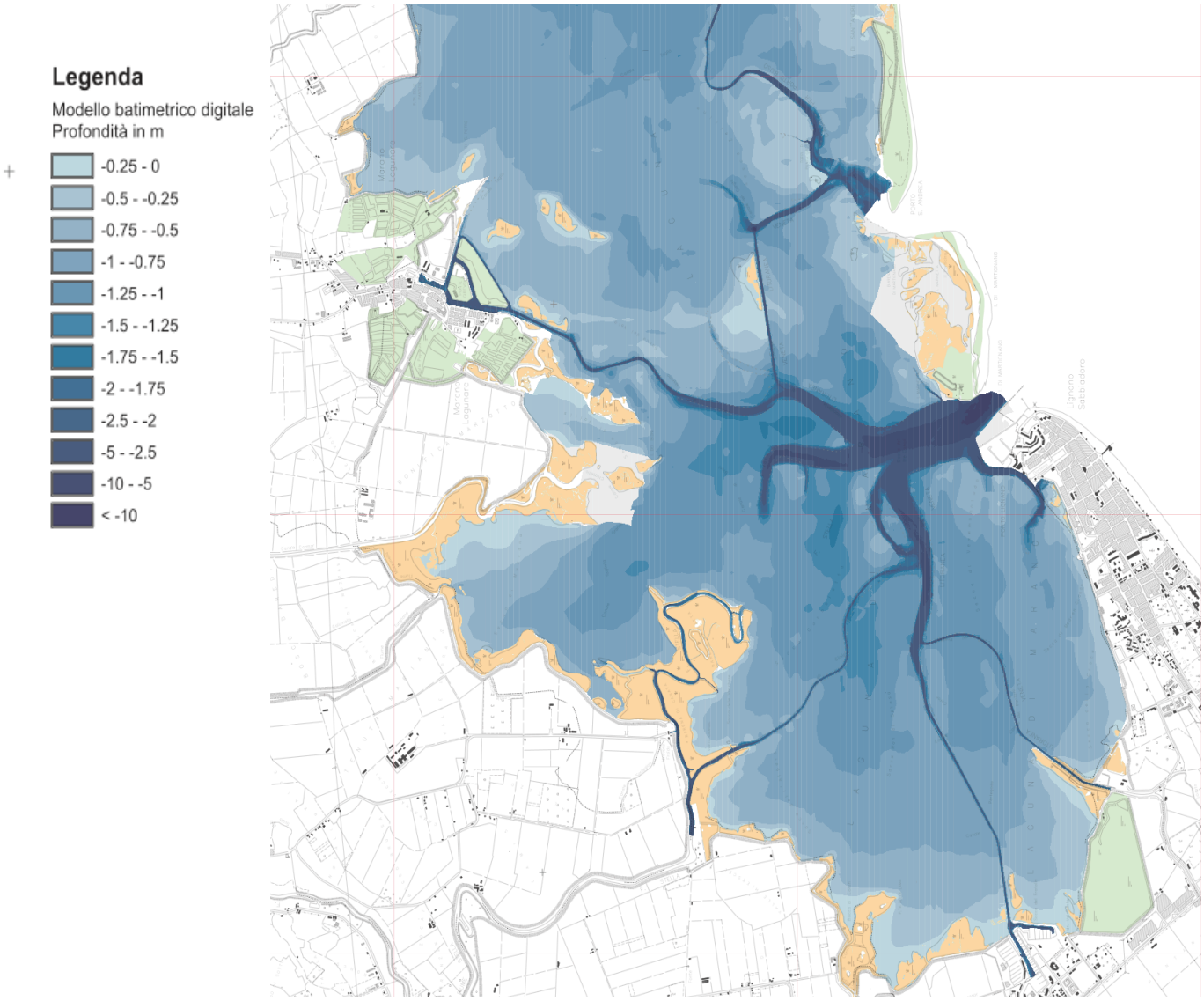

Map 3. Residual current with tide and NE wind. From Ferrarin et al., 2010.

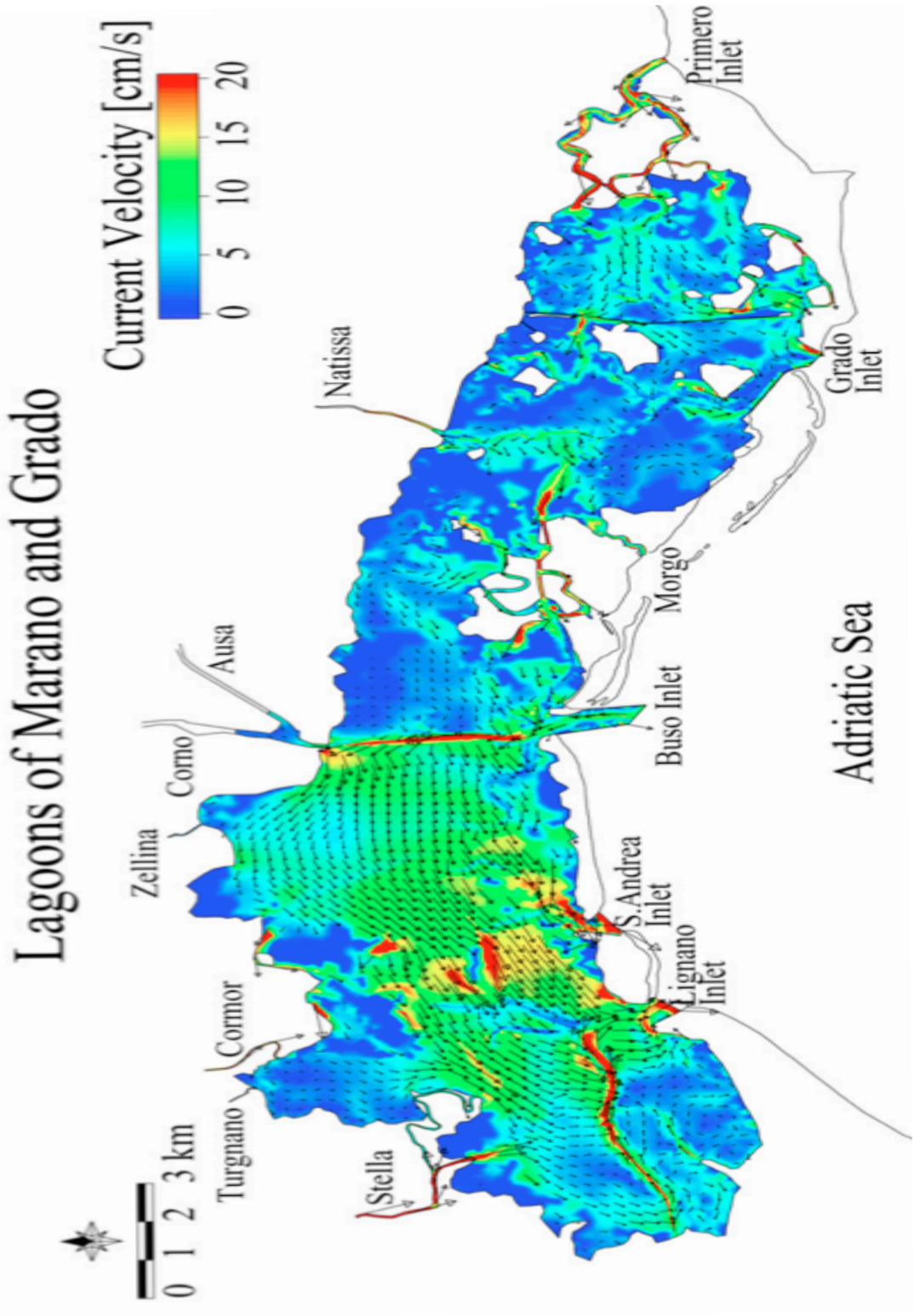

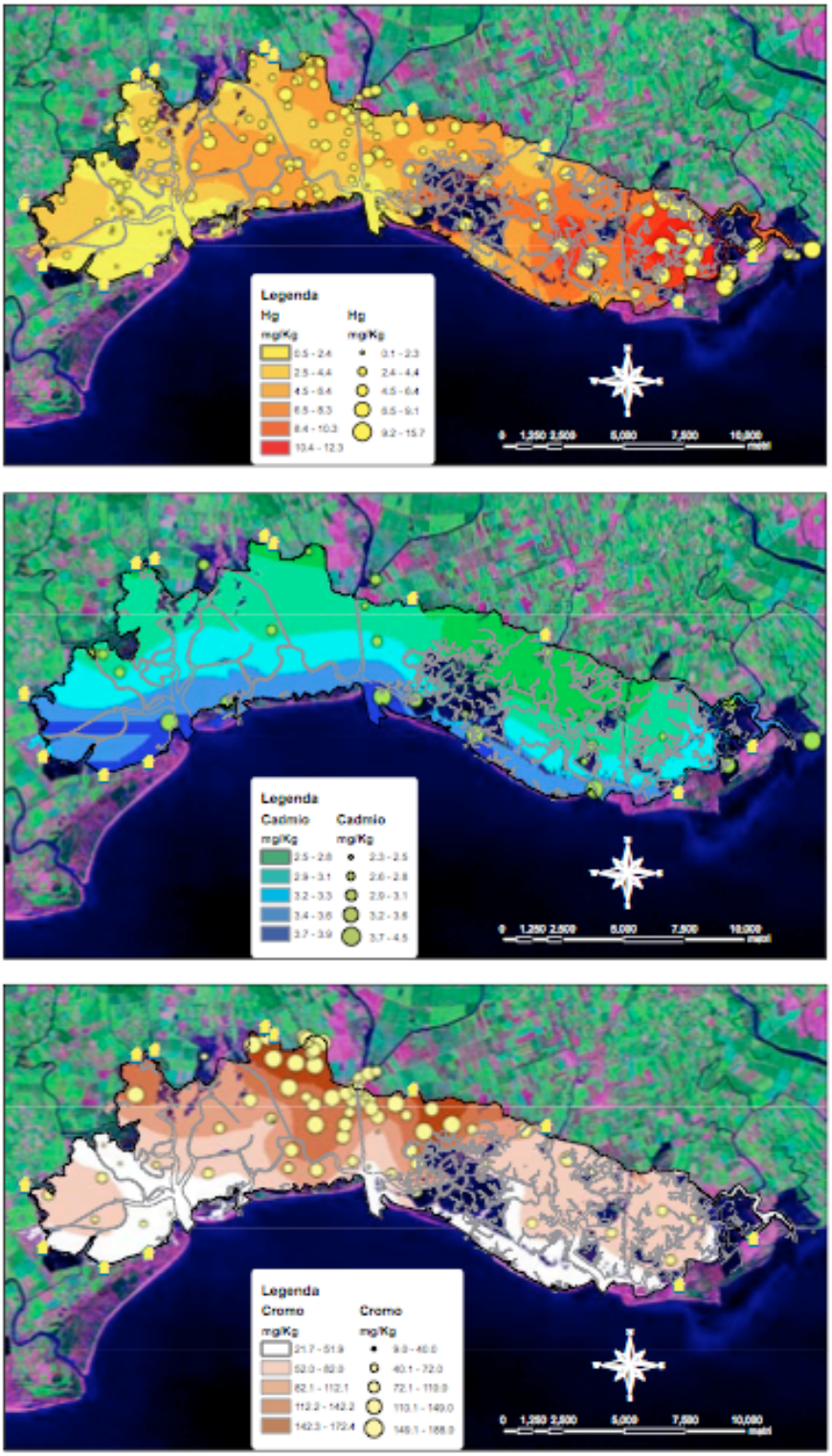

Map 4. Hg, Cd and Cr distribution (report presented in 2007 from the Regional Agency for the Environment Protection of Friuli Venezia Giulia).

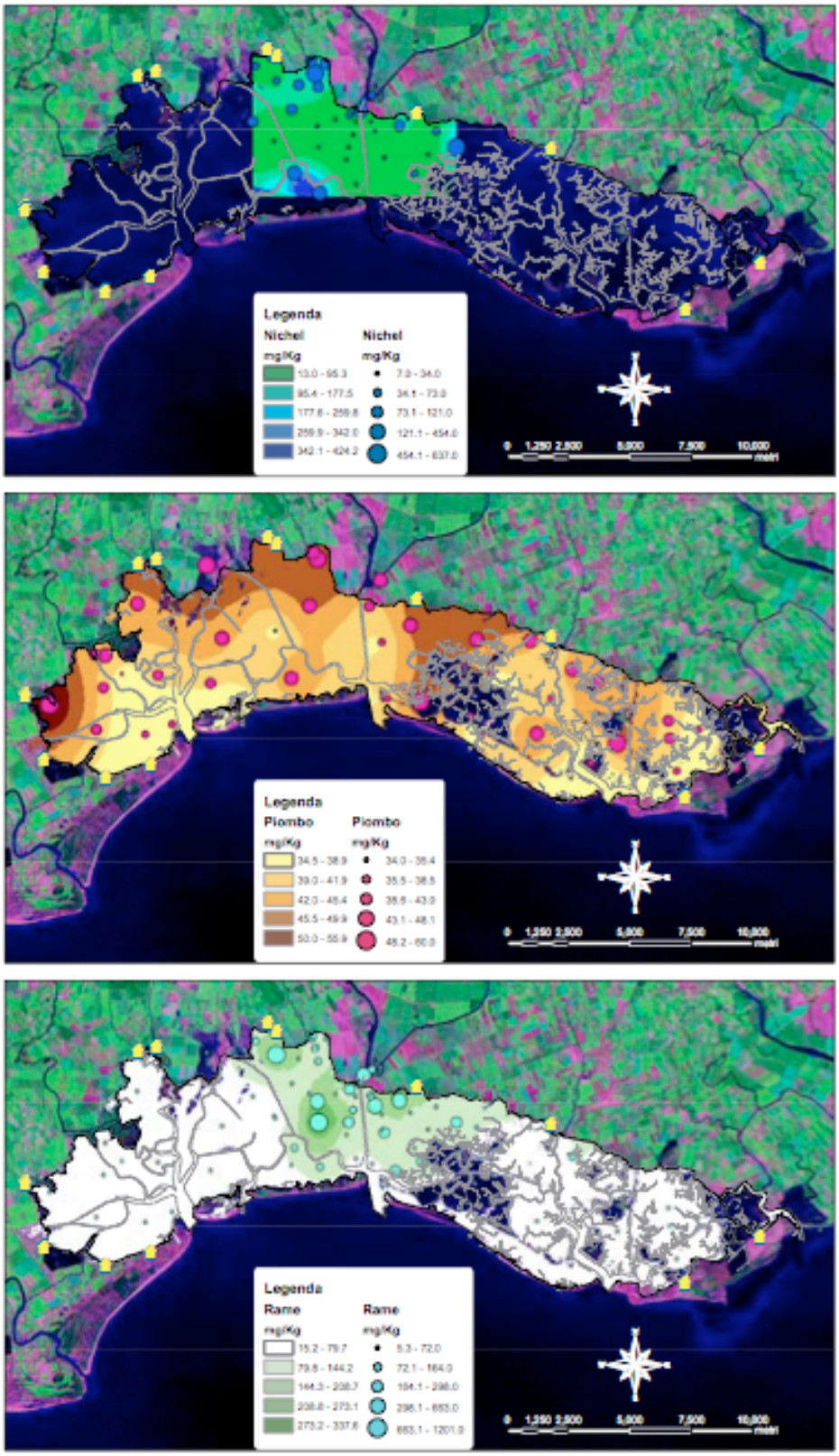

Map 5. Ni, Pb and Cu distribution (report presented in 2007 from the Regional Agency for the Environment Protection of Friuli Venezia Giulia).

Table 1: Samples decription.

Sample ID	Name of the sampling point	Category	Coordinate-EST	Coordinate-NORD
1	Lagoon inlet of Lignano	Lagoon inlet	2376252.303	5062556.282
2	Channel "Bocca dei tre Canali"	Channel	2375565	5063634
3	Roggia della Cartiera - Corno Stella	Groundwater up-welling line	2366496	5087172
4	Shallow water of the Croce	Shallow water	2372682.591	5061107.66
5	Channel of Bevazzana	Channel	2371796	5060752
6	Channel of the Pantani	Channel	2373544.376	5062675.494
7	Channel to Aprilia Marittima	Channel	2370517	5062401
8	Channel Coron	Shallow water	2371090.586	5063758.259
9	Channel Cialisia	Channel	2372502.177	5065319.032
10	River Stella	River	2371030.999	5066422.005
11	River Stella (in the lagoon)	Channel	2374049	5065320
12	Roggia Selva - Zellina	Groundwater up-welling line	2379066.989	5083982.793
13	Channel Tagliata Grande	Shallow water	2373873.321	5067401.522
14	Shallow water of Muzzana	Shallow water	2374244.458	5068685.037
15	Channel Chiasellis	Shallow water	2375460.962	5067561.317
16	Channel of Marano	Channel	2376270.246	5065370.579
17	Channel of Marano	Channel	2377074.414	5068130.655
18	River Torsa - Corno Stella	Groundwater up-welling line	2373854.67	5082258.527
19	Channel Taglio (Marano)	Channel	2378013.785	5069224.655
20	Channel of Marano (Marano)	Channel	2377310	5069547
21	Shallow water	Shallow water	2379158.039	5069874.097
22	Channel Taglio	Channel	2379528.003	5067963.382
23	Roggia Ronchi and Mulinazza - Corno	Groundwater up-welling line	2382254.416	5082976.561
24	Shallow water of Vela	Shallow water	2378367.263	5067015.524
25	Shallow water	Shallow water	2381531	5068777
26	Shallow water	Shallow water	2380347.597	5068865.45
27	River Ausa (in the lagoon)	Channel	2383182.21	5067251.47
28	Rivers Ausa/Corno	River	2383128.107	5068332.758
29	River Corno (Ausa/Corno)	River	2383538.342	5069829.375
30	River Ausa	River	2388126.8	5073032.713
31	River Ausa (in the lagoon)	Channel	2383327	5065710.788
32	Lagoon inlet of Porto Buso	Lagoon inlet	2383553	5063886
33	Roggia Brischis - Ausa	Groundwater	2393587	5079718

		up-welling line		
34	Shallow water	Shallow water	2381586.818	5067567.531
35	Channel S. Andrea/Channel of the Gorghi	Channel	2378275.416	5065494.291
36	Roggia Ciarmis - Ausa	Groundwater up-welling line	2385967	5081673
37	Channel S. Pietro/Channel Muro	Channel	2380379.273	5066122.486
38	Lagoon inlet S. Andrea island	Lagoon inlet	2378431	5064046
39	River Zellina	River	2379833.957	5072994.361
40	River Tagliamento	River	2368210.279	5061334.287
41	River Stella	River	2369238.462	5069444.704
42	River Corno (Ausa/Corno)	River	2381708.348	5075654.275
43	Channel of Marano (Marano)	Channel	2377396.145	5069104.622
45	Channel Cormor	River	2374621.737	5072055.551
46	River Turgnano	River	2372890	5071994
47	Open sea	Open sea	2380236.546	5062111.489
48	River Corno (Ausa/Corno)	Sewer pipe	2381717.8	5075659.2
49	Shallow water of the Croce	Shallow water	2372667.4	5060886.5
50	Mortegliano – road to Lestizza	River	2378231	5090049
51	Terenzano (Pozzuolo)	River	2380656	5096251
52	Roggia Ledra	River	2379970	5105227
54	Groundwater- well-Consortium of Ledra-Tagliamento	Groundwater	2377439	5093178
55-PO27	Groundwater- well-Consortium of Ledra-Tagliamento (Chiasellis)	Groundwater	2381441.17	5089219.37
56-PO30	Groundwater- well-Consortium of Ledra-Tagliamento (Gris)	Groundwater	2382421.22	5087214.71
57-PO101	Groundwater- well-Consortium of Ledra-Tagliamento (Mereto di Capitolo)	Groundwater	2386697.83	5086368.3

Table 2: Spring sampling campaign

Sample description	Sample ID	Sampling Date	Salinity (PSU)	Nitrate (mg/L)	$\Delta^{17}O$ ±0.4 (VSMOW)	$\delta^{15}N$ ±0.3 (AIR)
Lagoon inlet	1	27/05/2009	24.9	2.54	0.8	6.6
Channel	2	27/05/2009	27.3	2.94	0.4	7.3
Groundwater up-welling line	3	29/05/2009	0.3	20.82		
Shallow water	4	28/05/2009	16.99	1.93	1.6	4.2
Channel	5	28/05/2009	0.23	3.27		
Channel	6	28/05/2009	20.4	1.94	0.4	6.5
Channel	7	28/05/2009	18.06	0.50		
Shallow water	8	28/05/2009	13.65	4.61	0.2	6.3
Channel	9	28/05/2009	0.35	12.16		
River	10	28/05/2009	0.28	12.27		
Channel	11	28/05/2009	13.92	7.63	0.0	6.6
Groundwater up-welling line	12	29/05/2009	0.34	37.88		
Shallow water	13	27/05/2009	10.7	7.20	1.0	5.7
Shallow water	14	27/05/2009	4.66	6.41	0.2	7.7
Shallow water	15	27/05/2009	17.82	4.39	1.5	6.9
Channel	16	27/05/2009	23.5	1.51	0.4	6.4
Channel	17	26/05/2009	20.38	1.57	-0.2	7.3
Groundwater up-welling line	18	29/05/2009	0.3	22.96		
Channel	19	26/05/2009	19.79	4.70	2.1	6.9
Channel	20	26/05/2009	19.93	1.37	0.6	6.0
Shallow water	21	25/05/2009	18.66	<0.44		
Channel	22	26/05/2009	21.2	0.66		
Groundwater up-welling line	23	29/05/2009	0.37	51.74		
Shallow water	24	26/05/2009	22.7	1.65	0.9	6.5
Shallow water	25	25/05/2009	28.7	0.79		
Shallow water	26	25/05/2009	21.1	2.85	0.5	6.9
Channel	27	25/05/2009	30	0.55		
River	28	25/05/2009	22.3	8.30	0.6	7.4
River	29	25/05/2009	22.1	11.00	0.6	7.3
River	30	25/05/2009	2.39	16.28	0.4	6.0
Channel	31	25/05/2009	30.2	1.32	1.0	7.2
Lagoon inlet	32	25/05/2009	30	<0.44		
Groundwater up-welling line	33	29/01/1900	0.26	21.93		
Shallow water	34	25/05/2009	22.1	5.43	0.7	8.8
Channel	35	26/05/2009	26.3	4.30	0.7	9.1
Groundwater up-welling line	36	29/05/2009	0.34	39.76		
Channel	37	26/05/2009	29.9	10.93		
Lagoon inlet	38	26/05/2009	28.6	1.60	1.0	7.1
River	39	25/05/2009	0.29	20.61		
River	40	28/05/2009	0.21	3.06		
River	41	28/05/2009	0.27	12.46		

River	42	26/05/2009	0.3	31.73		
Channel	43	26/05/2009	20.02	3.28	0.8	6.2
River	45	27/05/2009	0.26	14.85		
River	46	27/05/2009	0.28	9.96		
Open sea	47	27/05/2009	29	0.68		
Sewer pipe	48	26/05/2009	0.26	25.11		
Shallow water	49	28/05/2009	21.37	1.89	2.4	4.6

Table 3: Summer sampling campaign

Sample description	**Sample ID**	**Sampling Date**	**Salinity (PSU)**	**Nitrate (mg/L)**	**$\Delta^{17}O$ ±0.4 (VSMOW)**	**$\delta^{15}N$ ±0.3 (AIR)**
Lagoon inlet	1	02/09/2009	33.1	0.44		
Channel	2	02/09/2009	33.3	<0.44		
Groundwater up-welling line	3	01/09/2009	0.3	21.83		
Shallow water	4	03/09/2009	22.6	6.47		
Channel	5	03/09/2009	23	1.23	1.2	4.6
Channel	6	03/09/2009	30.8	1.59		
Channel	7	03/09/2009	21.88	1.41	0.2	5.7
Shallow water	8	03/09/2009	19.33	2.18	0.1	5.1
Channel	9	02/09/2009	22.9	7.87	0.7	6.5
River	10	02/09/2009	0.73	11.11		
Channel	11	02/09/2009	31.2	1.47	0.9	6.5
Groundwater up-welling line	12	01/09/2009	0.34	40.86		
Shallow water	13	02/09/2009	27.5	3.39	0.4	6.4
Shallow water	14	02/09/2009	23.3	4.06	0.2	7.1
Shallow water	15	01/09/2009	23.5	6.17	0.4	6.3
Channel	16	02/09/2009	32.3	0.69		
Channel	17	01/09/2009	24.2	4.07	1.3	6.8
Groundwater up-welling line	18	01/09/2009	0.29	22.12		
Channel	19	01/09/2009	24.5	1.06		
Channel	20	01/09/2009	24.3	0.91		
Shallow water	21	31/08/2009	22.7	1.53	0.6	7.9
Channel	22	01/09/2009	24.9	3.29	0.4	7.2
Groundwater up-welling line	23	01/09/2009	0.38	52.70		
Shallow water	24	01/09/2009	26.3	1.65	0.2	7.3
Shallow water	25	31/08/2009	28.4	2.89	0.6	6.7
Shallow water	26	31/08/2009	24	4.54		
Channel	27	31/08/2009	34.1	3.35		
River	28	31/08/2009	30.4	4.63		
River	29	31/08/2009	23.7	8.75		
River	30	31/08/2009	26.5	5.90		
Channel	31	31/08/2009	34.3	<0.44		
Lagoon inlet	32	31/08/2009	34.2	<0.44		
Groundwater	33	31/08/2009	0.28	17.61		

up-welling line						
Shallow water	34	31/08/2009	28.2	3.01		
Channel	35	01/09/2009	28.3	2.01		
Groundwater up-welling line	36	31/08/2009	0.35	40.71		
Channel	37	01/09/2009	31.6	0.46		
Lagoon inlet	38	01/09/2009	32	0.86		
River	39	01/09/2009	2.25	18.30		
River	40	03/09/2009	18.8	1.83		
River	41	02/09/2009	0.28	11.47		
River	42	31/08/2009	0.3	30.34		
Channel	43	01/09/2009	24.4	1.00		
River	45	02/09/2009	0.27	15.29		
River	46	02/09/2009	0.27	10.30		
Open sea	47	02/09/2009	34.2	1.06		
Sewer pipe	48	31/08/2009	0.27	25.37		
Shallow water	49	03/09/2009	22.1	2.50		

Table 4: Autumn sampling campaign

Sample description	**Sample ID**	**Sampling Date**	**Salinity (PSU)**	**Nitrate (mg/L)**	**$\Delta^{17}O$ ±0.4 (VSMOW)**	**$\delta^{15}N$ ±0.3 (AIR)**
Lagoon inlet	1	04/11/2009	32.3	0.58		
Channel	2	04/11/2009	32.7	1.61		
Groundwater up-welling line	3	06/11/2009	0.31	23.19		
Shallow water	4	05/11/2009	17.12	9.05		8.1
Channel	5	05/11/2009	12.07	2.84	1.3	4.2
Channel	6	05/11/2009	24.8	3.78		
Channel	7	05/11/2009	18.27	9.67	0.5	6.3
Shallow water	8	05/11/2009	12.81	9.79	0.7	6.5
Channel	9	04/11/2009	1.09	13.93		
River	10	04/11/2009	0.28	17.74		
Channel	11	04/11/2009	28.7	5.40		
Groundwater up-welling line	12	06/11/2009	0.35	39.57		
Shallow water	13	04/11/2009	29.3	11.29		
Shallow water	14	04/11/2009	26.7	3.36		
Shallow water	15	04/11/2009	27.6	3.60		
Channel	16	03/11/2009	28.2	3.62		
Channel	17	03/11/2009	26.7	3.79		
Groundwater up-welling line	18	06/11/2009	0.31	24.03		
Channel	19	03/11/2009	25.8	2.61		
Channel	20	03/11/2009	9.65	29.79		
Shallow water	21	02/11/2009	24.9	1.98		
Channel	22	02/11/2009	24.2	3.91		
Groundwater up-welling line	23	06/11/2009	0.38	53.56		

Shallow water	24	03/11/2009	27.6	2.06		
Shallow water	25	02/11/2009	30.3	2.87		
Shallow water	26	02/11/2009	25.1	4.02		
Channel	27	02/11/2009	34.7	1.23		
River	28	02/11/2009	25.1	8.95		
River	29	02/11/2009	27.5	6.68		
River	30	02/11/2009	0.44	10.19		
Channel	31	02/11/2009	28.9	3.54		
Lagoon inlet	32	02/11/2009	29.4	5.59		
Groundwater up-welling line	33	06/11/2009	0.29	23.11		
Shallow water	34	02/11/2009	28.7	5.06		
Channel	35	03/11/2009	33.1	2.25		
Groundwater up-welling line	36	06/11/2009	0.36	42.67		
Channel	37	02/11/2009	27.1	6.61		
Lagoon inlet	38	03/11/2009	29.6	2.26		
River	39	03/11/2009	0.27	32.56		
River	40	05/11/2009	12.2	3.04		
River	41	04/11/2009	0.28	17.87		
River	42	04/11/2009	0.3	30.23		
Channel	43	03/11/2009	25.4	1.61		
River	45	03/11/2009	0.21	29.94		
River	46	05/11/2009	0.33	29.99		
Open sea	47	04/11/2009	34.9	<0.44		
Sewer pipe	48	02/11/2009	0.17	24.52		
Shallow water	49	05/11/2009	17.94	9.57		

Table 5: Winter sampling campaign

Sample description	**Sample ID**	**Sampling Date**	**Salinity (PSU)**	**Nitrate (mg/L)**	**$\Delta^{17}O$ ±0.4 (VSMOW)**	**$\delta^{15}N$ ±0.3 (AIR)**
Lagoon inlet	1	16/02/2010	32.3	0.74		
Channel	2	16/02/2010	33.8	0.38		
Groundwater up-welling line	3	18/02/2010	0.31	23.9	0.4	5.3
Shallow water	4	16/02/2010	19.16	4.08		
Channel	5	17/02/2010	26.9	2.76		
Channel	6	16/02/2010	27.3	2.31		
Channel	7	17/02/2010	12.97	5.75		
Shallow water	8	17/02/2010	21.05	5.77		
Channel	9	17/02/2010	24.6	5.46		
River	10	17/02/2010	1.35	10.9	0.9	5.1
Channel	11	17/02/2010	31	2.20		
Groundwater up-welling line	12	18/02/2010	0.35	53.6		6.4
Shallow water	13	17/02/2010	29.7	4.99		
Shallow water	14	17/02/2010	26.1	3.67		

Shallow water	15	17/02/2010	30.1	2.93		
Channel	16	16/02/2010	32.7	1.25		
Channel	17	16/02/2010	28	2.85		
Groundwater up-welling line	18	18/02/2010	0.3	25.3	0.1	5.2
Channel	19	16/02/2010	28.5	2.00		
Channel	20	18/02/2010	26.8	4.49		
Shallow water	21	15/02/2010	26.5	3.04		
Channel	22	16/02/2010	27.2	43.9		
Groundwater up-welling line	23	18/02/2010	0.37	53.2	-0.4	5.9
Shallow water	24	16/02/2010	29.1	5.47		
Shallow water	25	15/02/2010	30.5	7.55		
Shallow water	26	15/02/2010	26.9	17.4		
Channel	27	15/02/2010	33.8	1.87		
River	28	15/02/2010	28.1	11.6		
River	29	15/02/2010	29.8	11.50		
River	30	15/02/2010	5.6	11.0		
Channel	31	15/02/2010	32.1	4.38		
Lagoon inlet	32	15/02/2010	34	1.55		
Groundwater up-welling line	33	18/02/2010	0.26	21.3	0.7	4.7
Shallow water	34	15/02/2010	31.5	8.19		
Channel	35	16/02/2010	33.2	2.95		
Groundwater up-welling line	36	18/02/2010	0.34	38.7	0.2	6.2
Channel	37	16/02/2010	31.4	2.40		
Lagoon inlet	38	16/02/2010	33.9	3		
River	39	15/02/2010	0.48	22.1	0.2	6.3
River	40	17/02/2010	8.5	4.41		
River	41	17/02/2010	0.28	13.2	0.8	5.0
River	42	15/02/2010	0.31	31.7	0.7	6.1
Channel	43	16/02/2010	28.1	3.39		
River	45	16/02/2010	0.28	15.9	0.1	5.2
River	46	16/02/2010	1.35	7.37		
Open sea	47	15/02/2010	33.8	1.07		
Sewer pipe	48	15/02/2010	0.27	23.4		
Shallow water	49	16/02/2010	19.74	5.29		

Pierpaolo Saccon[a], Albrecht Leis[a], Alina Marca[b], Jan Kaiser[b], Laura Campisi[b], Joël Savarino[c], Michael E. Böttcher[d], Peter Escher[d], Anton Eisenhauer[e], Jürgen Sültenfuß[f], Joseph Erbland[c]

[a] JOANNEUM RESEARCH Forschungsgesellschaft mbH, Institute for Water, Energy and Sustainability, Graz, Austria

[b] School of Environmental Sciences, University of East Anglia, Norwich, United Kingdom

[c] UJF-Grenoble 1/CNRS-INSU, Laboratoire de Glaciologie et Géophysique de l'Environnement UMR 5183, St.-Martin-d'Hères, France

[d] Leibniz Institute for Baltic Sea Research (IOW), Geochemistry & Isotope Geochemistry Group, Marine Geology Section, Warnemünde, Germany

[e] IFM-GEOMAR, Kiel, Germany

[f] University of Bremen, Institute of Environmental Physics / Section of Oceanography, Bremen, Germany

Individuazione e caratterizzazione delle potenziali fonti dei nitrati nella Laguna di Marano e messa a punto di un piano di monitoraggio ambientale - progetto FONIMAR – Parte II.

Detection and characterisation of potential nitrate pollution sources in the Marano Lagoon and set-up of an environmental monitoring plan – FONIMAR project – Part II.

Riassunto

Come già anticipato nella prima parte pubblicata nel numero 34 del Bollettino della Società Naturalisti "Silvia Zenari" (Dicembre, 2010) questo progetto che ha avuto come obiettivo principale quello d'individuare oltrechè differenziare le potenziali fonti dei nitrati in soluzione presenti nella laguna di Marano e parte del suo bacino drenante è stato coordinato dallo Joanneum Research di Graz per conto dell'ERSA del Friuli-Venezia Giulia. In questa seconda parte vengono esposti i risultati finali del progetto **FONIMAR** (Individuazione e caratterizzazione delle potenziali **FO**nti dei **NI**trati nella Laguna di **MAR**ano) ottenuti nei due anni di monitoraggio e campionamento delle acque. Questo studio è da considerarsi un esempio di ricerca integrata dove sono state combinate assieme diverse discipline scientifiche quali: l'idrochimica, la geochimica isotopica, l'idrologia ed il telerilevamento. Va sottolineato che per poter individuare l'origine dei nitrati in un ambiente acquatico estremamente complesso come quello lagunare è stato necessario utilizzare gli ultimi ritrovati della tecnologia presenti attualmente in Europa. Il metodo multi-isotopico adottato in questo studio per indagare l'origine dei nitrati si basano sull'abbondanza degli isotopi stabili di azoto e ossigeno della molecola di nitrato ($\delta^{15}N$, $\delta^{18}O$ e $\Delta^{17}O$), idrogeno e ossigeno della molecola d'acqua ($\delta^{2}H$, $\delta^{18}O$), boro disciolto ($\delta^{11}B$), zolfo e ossigeno della molecola di solfato ($\delta^{34}S$, $\delta^{18}O$) mentre per la datazione delle acque di

falda è stato utilizzato il metodo isotopico del Trizio-Elio (^{3}H-^{3}He). L'analisi e l'interpretazione di questa serie d'isotopi rendono possibile l'individuazione e la differenziazione delle diverse fonti dei nitrati oltreché l'origine, provenienza e datazione delle acque così come segue: (i) nitrati presenti nell'acqua meteorica; (ii) nitrati di sintesi industriale (concimi sintetici); (iii) nitrati sintetizzati nel suolo dai processi microbici; (iv) nitrati provenienti dall'ossidazione della materia organica legata alle attività agricole (letame) o urbane (fosse settiche, fognature, etc.); (v) provenienza e miscibilità delle acque; (vi) datazione dell'acqua di falda. L'analisi delle acque campionate ha riguardato oltre all'analisi isotopica degli elementi e molecole sopracitate anche l'analisi della concentrazione dei seguenti ioni: nitrato, nitrito, ammonio, cloruro, bromuro, calcio, magnesio, potassio, sodio, solfato, orto-fosfato, fosfato totale, silicio totale, e boro totale oltreché i parametri chimico-fisici quali pH, conducibilità elettrica, ossigeno disciolto, salinità e temperatura. Per quest'ultima serie di parametri è stato eseguito, per ogni punto campionato, anche un profilo verticale ad intervalli di 0.5m che ha permesso d'individuare e caratterizzare la stratificazione della colonna d'acqua. La parte analitica del programma di monitoraggio è stata integrata con le tecniche del telerilevamento. L'analisi multi-temporale dei dati telerilevati dai satelliti Landsat-1 MSS, Landsat-5 TM, Landsat-7 ETM+ e ortofoto recenti ha permesso di ricostruire l'evoluzione spazio-temporale di: (i) flora algale; (ii) temperatura dell'acqua e (iii) dei principali cambiamenti morfologici della laguna a partire dagli anni '70 così come già ampliamente riportato nel numero 34 del Bollettino della Società Naturalisti "Silvia Zenari" (SACCON, 2010).
Va inoltre ricordato che, prima di questo studio, i nitrati presenti in laguna e nel bacino drenante della laguna di Marano stessa sono stati imputati ad un origine legate esclusivamente alle pratiche agricole escludendo a priori altre possibili fonti inquinanti. Nonostante questo sia stato uno dei primi studi condotti in Europa per l'individuazione e la caratterizzazione delle fonti dei nitrati in ambiente lagunare utilizzando la suddetta metodologia di ricerca integrata questo non vuole essere un punto d'arrivo ma bensì un punto di partenza per poter approfondire alcuni nuovi aspetti emersi da questa prima indagine scientifica.

Abstract

The aims of this study were mainly: (i) the identification and differentiation of the main anthropogenic nitrogen sources in the Marano Lagoon (Italy) and its catchment area; and (ii) the assessment of the intra-lagoonal water circulation, the morphological development of the lagoon and its anthropogenic pressure by applying a combined approach of hydrochemical, isotopic, hydrological and remote sensing techniques. To achieve the aforementioned targets analyses of stable isotope signatures of nitrate, boron, water and sulphate have been used. Moreover the residence times of groundwater were determined by the tritium-helium dating method. To characterize the chemical composition of the different water types the concentrations of the major ions and nutrients as well as the physicochemical parameters have been measured. Remote sensing techniques have been applied to assess the spatial distribution of most superficial algal flora, water temperature as well as the key environmental and morphological changes of the lagoon since the beginning of the 1970s as already

reported in the previous issue (N. 34, December 2010) of the "Bollettino della Società Naturalisti Silvia Zenari" (SACCON, 2010).

1 Introduction

Nitrate pollution is still a major concern in many European aqueous resources, which may originate from multiple sources: excess application of mineral nitrogen (N) fertilizers and animal manure in agriculture, discharges from urban or industrial N bearing waste water, septic leachate in unsewered areas, atmospheric deposition or decomposition of soil organic N. In addition to the existence of multiple potential nitrate sources, nitrate pollution may originate from present as well as from historical land use, which complicates the problem. In the framework of the Nitrates Directive (91/976/EEC) and the Urban Wastewater Directive (91/271/EEC), several policy measures with major socio-economic impact have been implemented to reduce nitrate inputs from agriculture or urban and industrial waste water. The Water Framework Directive (2000/60/EC) and Nitrates Directive require that the chemical water quality (concentration of nitrate and other ions) is monitored by the national environmental agencies to evaluate the effectiveness of the measures taken (EUR 23658 EN, 2008). The objectives of the directive are to ensure that the nitrate concentration in freshwater and groundwater supplies does not exceed the limit of 50 mg/l, and to control the incidence of eutrophication. European legislation on nitrate has been around for a long time; nonetheless nitrate pollution remains an issue. The development and implementation of effective remediation measures in nitrate polluted areas requires the identification of the main nitrate pollution sources and the estimation of their contribution is essential for environmental policy makers to implement effective, source-oriented as well as sustainable remediation measures. This information cannot be deducted from the application of a single investigation method like water quality monitoring alone (concentration measurements) without the introduction of an integrated and interdisciplinary water resources management approach. A multi-isotope method in combination with hydrochemical, hydrological and remote sensing investigations is a powerful, scientifically based tool to identify and characterize multiple nitrate pollution sources.

Nitrate (NO_3^-) is found naturally at moderate concentrations in many aquatic environments, but is often enriched to high levels by anthropogenic activities involving nitrogenous compounds such as mineral fertilizer and by-products of organic compounds from agriculture, septic systems and poultry, hog or cattle manure (BERGER ET AL., 1976; HEATON ET AL., 1983; MARIOTTI ET AL., 1988; OSTROM ET AL., 1998; WILLIAMS ET AL., 1998). In spite of the increasing efforts at national and European levels to reduce nitrate inputs from intensive agriculture (EC Directive 91/976/EEC), nitrate is still one of the major contaminants of aquatic systems (WIDORY ET AL., 2004). Traditional approach for environmental management and control of water quality regarding nitrate is merely based on the sole monitoring of pollutant concentrations. However, chemical data alone does not enable one to establish unambiguously the type, location and contribution of different nitrate pollution sources. In particular, differentiating urban and agricultural origin of nitrate is extremely difficult (even by increasing the number of monitoring stations or samples). The study area is located in the Marano lagoon in the Friuli-Venezia Giulia region (North-east Italy) where nitrates from intensive agricultural and anthropogenic activities are responsible for its pollution. In 2008, the entire catchment area of the Marano lagoon was designated as a nitrate vulnerable zone (NVZ) where an action

program on the reduction of nitrate leaching was initiated. Thus, to identify and characterize multiple-sources of nitrate pollution of agricultural and urban origin, a water monitoring network in the Marano lagoon and its catchment area was set-up. In the monitoring program water samples from the lagoon, its tributary rivers, the groundwater up-welling line, groundwater, sewer pipe and open sea on a quarterly interval from 2009 to 2010 were collected and analyzed.

The present study represents a novel approach on the identification and characterization of potential sources of nitrate pollution in a lagoon environment, which, beside the traditional hydrochemical analyses (main ions and nutrients), introduces the whole suite of stable isotopes of nitrate ($\delta^{15}N$, $\delta^{18}O$ and $\Delta^{17}O$), the isotopic signature of boron ($\delta^{11}B$), the stable isotopes of water ($\delta^{2}H$ and $\delta^{18}O$), the stable isotopes of sulphate ($\delta^{34}S$ and $\delta^{18}O$), the tritium-helium (^{3}H-^{3}He) isotopic method as well as hydrological, remote sensing and GIS techniques.

The project has been funded by the ERSA (Regional Agency for Rural Development) of the Friuli-Venezia Giulia region.

2 Study area

The Marano lagoon is located in the Northern Adriatic Sea (Northeast Italy) and it is entirely included in the Province of Udine of the Friuli-Venezia Giulia region as represented in Fig. 1. The lagoon has a surface of about 77 km^2, with a length of nearly 14 km and an average width of 5.5 km. To the east of the Marano lagoon, the Grado lagoon is situated, which is the second part of the Grado-Marano lagoon system. The area of the entire lagoon system is of approximately 160 km^2, with a length of almost 32 km and an average width of 5 km. The two lagoons are divided by the administrative border between the Udine and Gorizia provinces where the Ausa-Corno Channel is also located. In the south the Marano lagoon is connected to the Adriatic Sea through three lagoon inlets (Porto Lignano, Sant'Andrea and Porto Buso). A total mean water exchange rate between the lagoon and the Adriatic Sea through the Porto Lignano and Porto Buso inlets are respectively in the order of 1750 and 1500 m^3/s. The tide in the lagoon has a mean height of approximately 0.6 m with a maximum of about 1.0 m. The tide propagates along the major channels with a velocity of approximately 40-60 cm/s and then enters in the shallow areas where the velocity quickly decreases to below 10 cm/s (FERRARIN ET AL., 2010). The mean bathymetry in the shallow lagoon areas is roughly 0.8 m, while in the navigable channels it is about 3.2 m. The overall mean bathymetry of the lagoon is in the order of 1.95 m. In the southwest, the lagoon is characterized by the urban and touristic areas of Lignano Sabbiadoro city, which is one of the main summer resorts in northern Italy, and by the Aprilia Marittima resort. In this lagoon sector, the artificial channel of Bevazzana is located, which is responsible for the connection between the Tagliamento River and the lagoon.

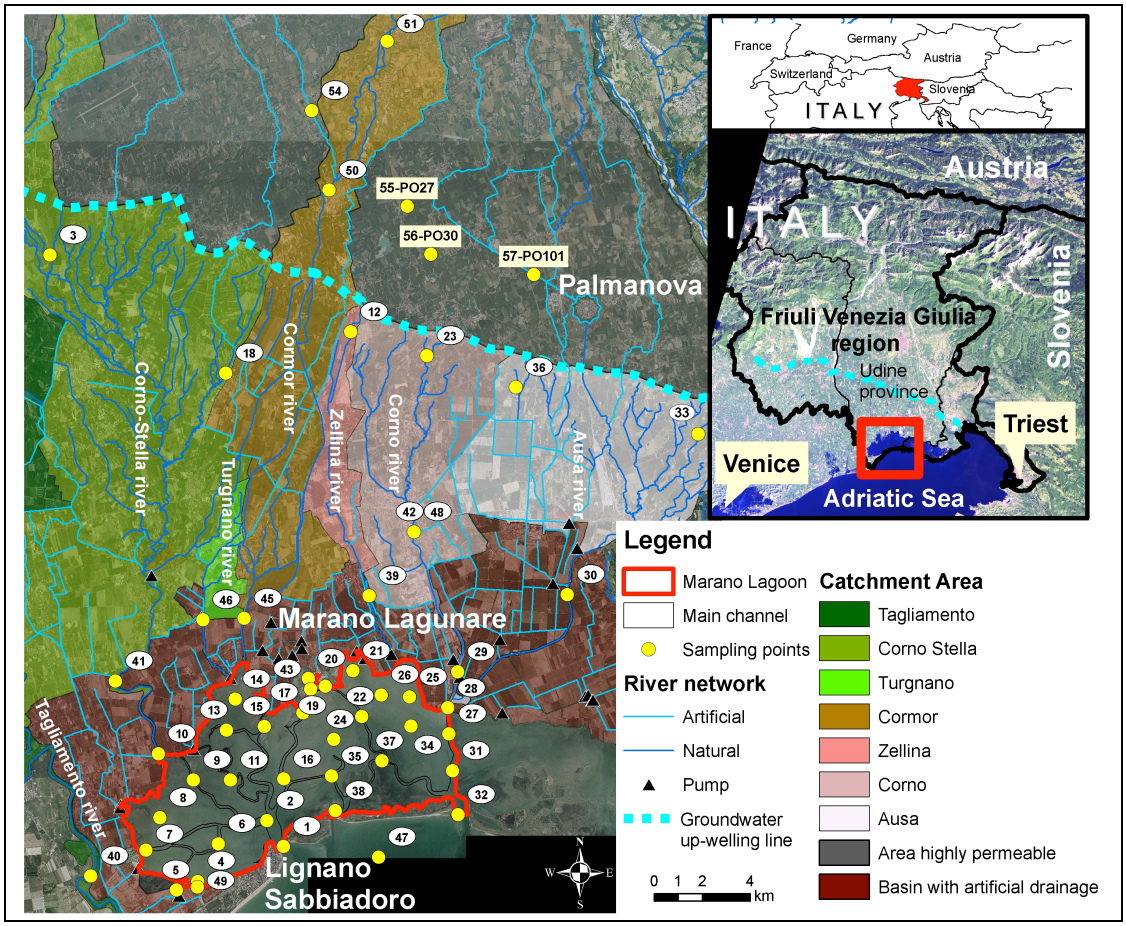

Fig. 1: Study area: Marano Lagoon (red line)

The Tagliamento River is a 7th order river that flows unimpeded by high dams for 172 km into the Northern Adriatic Sea. The Tagliamento River is the most important river of the Friuli-Venezia Giulia region with a catchment area of approximately 2674 km^2. The fishing community of Marano Lagunare is situated in the northern lagoon sector and with its 2007 inhabitants is the main urban centre within the lagoon perimeter. About 5 km east of Marano Lagunare city, the "Aussa-Corno" industrial site (ZIAC) is located. This important industrial area spans over 1000 ha and includes 87 factories comprising the following main categories: chemical, mechanical engineering, naval, iron and steel production, textile, food, wood, etc. The northern sector of the Marano lagoon is also characterized by the discharge of freshwater from its tributary rivers. The lagoon tributary rivers and their mean discharges are as follows: Corno-Stella (35.4 m^3/s), Turgnano (0.5 m^3/s), Cormor (9.3 m^3/s), Zellina (1.1 m^3/s), Corno (4.6 m^3/s) and Ausa with 10.0 m^3/s (RET, 2006). The springs of Stella River are located along the groundwater up-welling line. After the confluence with the Corno torrent, the Stella River becomes one of the main tributary rivers to the Marano lagoon. The catchment area of the Corno-Stella River is about 300 km^2, while those of the other rivers originating from the groundwater up-welling line like the Rivers Turgnano, Zellina, Corno and Ausa are respectively 7 km^2, 14.4 km^2, 55.4 km^2 and 65.6 km^2. The Cormor River's springs are located at an altitude of 250 m in the Mt San Lorenzo near Santo Stefano di Buia (UD) and after flowing for 51 km through the glacial moraines (Würmian), the Upper Friulian Plain and the groundwater up-welling line reach the Marano lagoon. The catchment area of the Cormor River is about 226 km^2. The groundwater up-welling line divides the Friuli-Venezia Giulia Plain into two

units, the Upper Friulian Plain and the Lower Friulian Plain. The mean discharge of the groundwater up-welling line in the left side of the Tagliamento River is about 80 m^3/s, which corresponds to a mean discharge of about 1.3 $m^3/s/km$. The Friuli-Venezia Giulia Plain groundwater systems are located in sediments that are underlain by an Eocene to Oligocene succession deposited above a 7 km thick Mesozoic carbonate platform (CATI ET AL., 1987; CARULLI, 2006). In the Marano lagoon, there are two nature reserves, the "Riserva delle foci del fiume Stella" (Reserve of the Stella River mouths) that takes the entire delta of the Corno-Stella River and the "Riserva della Valle Canal Novo" (Canal Novo Valley reserve) that covers a fishing area of around 35 hectares. They are protected by the Ramsar convention on wetlands of international interest. Also, according to the EU Birds Directive (2009/147/EC) on the conservation of wild birds and the EU Habitats Directive (92/43/EEC) on the conservation of natural habitats and of wild fauna and flora, the whole lagoon system is included in the Natura 2000 network.

3 Water sampling program

In the water sampling program the main climatic, environmental, and seasonal changes, as well as all relevant agricultural, livestock, anthropogenic and touristic activities that potentially influence the distribution, concentration and origin of nitrates have been taken into account. The 2009-2010 water sampling program was carried out on a quarterly basis, as indicated in Tab. 1:

Sampling campaign	Season	Date
1	Winter	02-06/02/2009
2	Spring	25-29/05/2009
3	Summer	31/08-03/09/2009
4	Autumn	02-06/11/2009
5	Winter	15-19/02/2010
6	Spring	25-29/05/2010; 15/06/2010

Tab. 1: Sampling program schedule

To achieve the project's goals and due to the necessity of doing extensive investigations on some particular and interesting areas the initial 47 sampling points were progressively increased to 55 points. The total sampling points were distributed as follows: 16 sampling points along the lagoon's navigation channels; 14 sampling points along the main tributary rivers of the lagoon; 6 sampling points along the groundwater up-welling line (linea delle risorgive); 11 sampling points in shallow water areas of the lagoon; 3 sampling points in the lagoon inlets to the Adriatic Sea; 1 sampling point in the open sea; 4 sampling points in groundwater.

4 Analytical methods

4.1 Hydrochemical analysis

For the chemical characterization of the different water types included in the monitoring program their chemical compositions have been determined using the following analytical methods:

1. In-situ chemical analysis and measurement of the physicochemical parameters;

2. Post-sampling analyses carried out in Graz at the Laboratory Centre for Isotope Hydrology and Environmental Analytics of Joanneum Research.

For this particular study, the water sampling depth has been fixed at approximately mid-water depth. By operating in this way, it was possible to minimize the unwanted contributions of: (i) rainfall in the upper layers of the water column; and (ii) various physicochemical as well as microbiological processes linked to the lagoon bottom.
Moreover, in determining the optimal sampling depth it was necessary, during each single sampling, to take into account the local tide condition, wind speed and direction, as well as the water current speed and its direction. Water samples were gathered using a Ruttner water sampler equipped with a drop messenger that could be closed at any desired depth.
The in-situ chemical analysis and measurement of the physicochemical parameters took place directly in the field including the following activities: (i) measurement of pH, water temperature, electrical conductivity, dissolved oxygen and salinity using a portable multi-parameter meter; (ii) measurement of nitrate, nitrite, and ammonium concentration using a portable spectrophotometer "WTW FC photoFlex/Turb 430 LED"; (iii) measurement of orthophosphate concentration using a second portable spectrophotometer "Merck SQ 118"; and (iv) storage of all collected water samples for the later analyses in the laboratories. In all cases water samples collected during the field campaigns were analyzed in Graz at the Laboratory Centre for Isotope Hydrology and Environmental Analytics of Joanneum Research. Dissolved cations (Ca^{2+}, Mg^{2+}, Na^{+}, K^{+}) and anions (Cl^{-}, Br^{-}, SO_4^{2-}) were analysed by ion chromatography (Dionex ICS-3000). Alkalinity was measured by titration and total phosphorus (P-total) was determined photometrically in the laboratory after digestion of deep frozen water samples.

4.2 Isotopic analysis and analytical techniques

Isotopes are atoms of the same element that have different numbers of neutrons. Differences in the number of neutrons among the various isotopes of an element mean that the various isotopes have different masses (KENDALL AND MCDONNELL, 1998). For example, among the hydrogen isotopes, deuterium (denoted as D or ^2H) has one neutron and one proton. The superscript number to the left of the element designation is called the mass number (A) and is the sum of the number of protons and neutrons in the isotope. Stable isotopes are analyzed either on gas- or solid-source mass spectrometers, depending on both the masses of the isotopes and the existence of appropriate gaseous compounds stable at room temperature. Radioisotopes can be analyzed by counting the number of disintegrations per unit time on gamma ray or beta particle counters, or analyzed on mass spectrometers (KENDALL AND CALDWELL, 1998).

The ratio between two isotopes is computed with the heavier isotope in the numerator (e.g. $R = n(^{15}N)/n(^{14}N)$, where n represents the amount of isotope). To avoid handling R

values with many decimals, a relative δ notation using the ratio between R_{sample} and $R_{standard}$ is used (see below). The main internationally accepted stable isotope standards for hydrogen, oxygen, nitrogen, boron and sulphur are as follows:

- Nitrogen: AIR (atmospheric N_2)
- Hydrogen and oxygen: VSMOW (Vienna Standard Mean Ocean Water)
- Boron: NBS-SRM 951 (boric acid)
- Sulphur: V-CDT (Vienna-Canyon Diablo Troilite)

Samples are either analyzed at the same time as this reference standard or with an internal laboratory standard that has been calibrated relative to the international standard.
δ values are computed as follows and expressed in parts per thousand (denoted as ‰, pronounced "per mil"):

$$\delta \text{ (in ‰)} = (R_{sample} / R_{standard} - 1) \times 10^3$$

where:

- R_{sample} is the ratio of the heavy isotope to the light isotope in the sample (e.g. $^{15}N/^{14}N_{sample}$);
- $R_{standard}$ is the ratio of the heavy isotope to light isotope in the international reference material;
- δ (pronounced delta) is the relative isotope ratio difference between sample and standard. δ will be positive if the measured sample is enriched in heavy isotopes relative to the standard ($R_{sample} > R_{standard}$) and will be negative in the reverse case ($R_{sample} < R_{standard}$).

The isotopic analyses of the water samples were carried out via the following phases:

1. The oxygen and hydrogen isotopic composition of water ($\delta^{18}O$ and $\delta^{2}H$) and the nitrogen isotopic composition ($\delta^{15}N$) of synthetic fertilizers, sewage and manure (collected in some farms of the Region Friuli-Venezia Giulia) were measured in Graz at the Laboratory Centre for Isotope Hydrology and Environmental Analytics of Joanneum Research.
2. The stable isotopes of nitrate ($\delta^{15}N$, $\delta^{18}O$ and $\Delta^{17}O$) from the first sampling campaign (February 2009) were analyzed in Grenoble (France) at UJF-Grenoble 1/CNRS-INSU, Laboratoire de Glaciologie et Géophysique de l'Environnement (LGGE) UMR 5183, St.-Martin-d'Hères, while for the other sampling campaigns the water samples were

analyzed in the United Kingdom at the Stable Isotope Laboratory of the School of Environmental Sciences, University of East Anglia, Norwich.

3. The analyses of the stable isotopes of boron ($\delta^{11}B$) were carried out in Kiel (Germany) at the Leibniz-Institute of Marine Sciences (Leibniz-Institut für Meereswissenschaften an der Christian-Albrechts Universität zu Kiel - IFM-GEOMAR).

4. The analyses of the stable isotopes of sulphate ($\delta^{34}S$) were conducted in Germany at the Leibniz-Institute for Baltic Sea Research, Geochemistry & Isotope Geochemistry Group, Marine Geology Section, Warnemünde (Leibniz-Institut für Ostseeforschung Warnemünde – IOW). $\delta^{18}O$ values were measured at the Max Planck Institute for Marine Microbiology (MPI Bremen).

5. Tritium and helium isotopes were analyzed in Germany, at the University of Bremen, Institute of Environmental Physics - Section of Oceanography (Universität Bremen, Institut für Umweltphysik – IUP).

4.2.1 Stable isotopes of water: oxygen-18 and deuterium

The oxygen-18 (^{18}O) and deuterium (^{2}H) isotopes are integrated parts of the water molecule and are, therefore well-suited for hydrological tracing and budget studies (SAETHER AND DE CARITAT, 1997). The ^{18}O and ^{2}H contents are expressed as $\delta^{18}O$ and $\delta^{2}H$, and reported relative to the VSMOW (Vienna Standard Mean Ocean Water) standard. Isotope hydrology provides complementary information on the type, origin and age of water. If the isotopic content does not change within the aquifer, it will reflect the origin of the water, particularly the location, period and processes of recharge. If the isotopic content changes along groundwater paths, this will reflect the history of the water, particularly the mixing, salinization and discharge processes. Analysis of water for $\delta^{18}O$ and $\delta^{2}H$ can also provide extremely useful information about the sources of the nitrate and other solutes in water (ARAVENA & ROBERTSON, 1998; MCMAHON & BÖHLKE, 2006). Very often, different sources of nitrate in rivers and groundwater are associated with different water $\delta^{18}O$ and $\delta^{2}H$ values because of evaporation or because the waters are derived from very different geographic areas (KENDALL ET AL., 2007). In this project deuterium ($\delta^{2}H$) was measured with a Finnigan DELTA^{plus} XP continuous flow stable isotope ratio mass spectrometer by chromium reduction using a ceramic reactor slightly modified from MORRISON ET AL. (2001). The oxygen isotopic composition ($\delta^{18}O$) of water was measured by the classic CO_2–H_2O equilibrium technique (EPSTEIN AND MAYEDA, 1953) with a fully automated device adapted from HORITA ET AL. (1989) coupled to a Finnigan DELTA^{plus} Mass Spectrometer.

4.2.2 Stable isotopes of nitrate: nitrogen-15, oxygen-18 and oxygen-17

The isotopic composition of the dissolved nitrogen (N) species has been used extensively to better constrain the sources and fate of N in groundwater (PANNO ET AL., 2001). The possibility of quantifying both the origin and the secondary processes affecting N concentrations by means of a single tracer appears more limited however.

Nitrogen cannot be considered conservative because it is biologically modified through nitrification and denitrification reactions, both during infiltration of the water and in the groundwater body, causing isotopic fractionation that modifies the $\delta^{15}N$ signatures of the dissolved N species (VOGEL ET AL., 1981; MARIOTTI ET AL., 1988; BÖTTCHER ET AL., 1990; SMITH ET AL., 1991; FEATS ET AL., 1998; ARAVENA AND ROBERTSON, 1998; PAUWELS ET AL., 2000, TORRENTÓ ET AL., 2010; ZHANG ET AL., 2010). In some cases, the interference between the isotopic fractionation (linked to denitrification) and the mixing processes (from the combination of multiple nitrate sources) might hamper the identification of nitrate sources, since the associated fractionation processes can alter the isotope composition of dissolved nitrate. Discriminating between multiple nitrate sources by their N isotopic composition alone becomes impossible wherever heterogenic or autogenic denitrification occurs, thus there is a need for establishing co-migrating discriminators of nitrate sources (WIDORY ET AL., 2004). Some of these limitations can be tackled by including the isotopic signature of tracers that migrate along with nitrate, e.g. boron, strontium, sulphate S and/or O (e.g. WIDORY ET AL., 2004; VITORIA ET AL., 2008; ZHANG ET AL., 2010). In the frame of this study the nitrate nitrogen and 18-oxygen isotopic compositions were analysed using the denitrifying bacteria procedures (denitrifier method) described in SIGMAN ET AL., 2001; CASCIOTTI ET AL., 2002; KAISER ET AL., 2007 and MORIN ET AL., 2009 and have been used to differentiate among nitrate coming from agriculture (synthetic and natural fertilizers), airborne nitrate and nitrate from nitrification processes in soils. For this analysis the *Pseudomonas aureofaciens* bacteria strain has been used, which was first grown on agar plates, from where single colonies were used to inoculate 500 ml media bottles containing tryptic soy broth with nutrients. Bottles were kept on a shaker table in the dark for minimum 5 days to maximum 10 days. After the growth period, bacteria were isolated from the nutrient media by centrifuging (Fig. 2, left), then re-suspended in a volume of nutrient free media (NFM) and a few drops of antifoaming agent. Aliquots of 2 ml of *Pseudomonas aureofaciens* in NFM were pipetted into 20ml volume glass vials, then crimp-sealed using butyl stoppers and aluminium caps. These vials were purged for 45 minutes using helium gas to remove traces of N_2O and the atmospheric gases (Fig. 2, right).

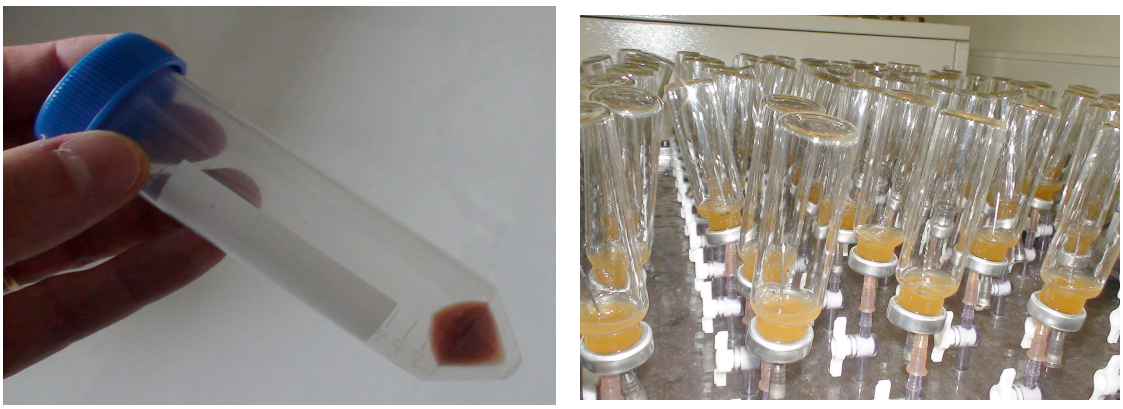

Fig. 2: Left: Isolated Pseudomonas aureofaciens bacterial; Right: Helium injection for degasification of the vials

The vials were kept overnight in the dark on a shaker table at room temperature. As bacteria were in NFM, any potential oxidised nitrogen contamination was consumed

by the bacteria overnight. The following day the vials were purged the second time with helium for 45 minutes to remove traces of residual N_2O that may have been produced overnight. After the second purge, a volume of water sample of known nitrate concentration was injected over the bacteria suspension, to produce 10 nmol of N_2O gas. After about two hours, 0.1 ml of 6 mol/l NaOH solution was added to each vial to kill the bacteria. The evolved N_2O was extracted, purified and measured using a Europa GEO 20-20 mass spectrometer on-line with a TGII prep system and Gilson auto-sampler. Water vapour was removed using three trapping systems: Nafion dryer, magnesium perchlorate trap and -80°C cryogenic trap. The remaining carbon dioxide was mostly removed using a carbosorb trap. Additionally, prior to the mass spectrometer, gases were passed through a GC column in order to separate carbon dioxide traces from the analyte N_2O, as these gases are isobaric. Samples were analyzed in triplicate, and together with them three international reference materials were analyzed in quadruplicate: IAEA N3, USGS 34 and USGS 35. The raw data was corrected for drift, blank, oxygen isotopic exchange with the parent water oxygen, isobaric interferences, scale conversion and stretch (SIGMAN ET AL., 2001; CASCIOTTI ET AL., 2002; BÖHLKE ET AL., 2003 and KAISER ET AL., 2007). Data was reported with respect to AIR (for $\delta^{15}N$) and with respect to VSMOW (for $\delta^{18}O$). The precision of the analyses was generally better than 0.3 ‰ for both ^{15}N and ^{18}O measurements, based on the quadruplicate analyses of the three international standard materials measured.
For the 17-oxygen analyses of nitrate the procedure used was identical to the one described above, but (i) the water sample volume injected over bacteria was five times higher, so the amount of N_2O produced from the bacterial denitrification was 50 nmol, and (ii) prior to the mass spectrometer the N_2O gas was passed through a gold tube heated at 800°C and converted to N_2 and O_2 gas, which were then passed through a molecular sieve GC column so that the N_2 gas was delayed with respect to the oxygen before going to the mass spectrometer. Using this protocol the ^{15}N, ^{17}O and ^{18}O isotopic compositions were measured using the nitrogen and oxygen gases, rather than the N_2O.

4.2.3 Stable isotopes of boron

Boron (B) has two naturally occurring stable isotopes, ^{10}B and ^{11}B. The large relative mass difference between the boron isotopes leads to a wide (ca. 90‰) natural range of $\delta^{11}B$ values (BARTH, 1993). Because B is widely used in industrial, agricultural, cosmetics, and household products, $\delta^{11}B$ is a useful tool for determining sources of pollutants including nitrate (EISENHUT ET AL., 1996; BARTH, 2000). The main industrial source of B to waters is sodium perborate ($NaBO_3$), which is used in laundry detergents (primarily as a bleaching agent) and in household cleaners; consequently, B is commonly found in household sewage. Purification of waters in sewage treatment plants generally removes little or no B (BARTH, 2000); hence, $\delta^{11}B$ is a conservative tracer of a wastewater source. While B isotopes are not affected by denitrification, they are fractionated through processes such as adsorption on clays.

Boron isotopes have been shown to be useful for identifying anthropogenic B sources in surface water and shallow groundwater systems: (i) municipal wastewater and sewage (BASSETT, 1990; VENGOSH ET AL., 1994, 1999; BASSETT ET AL., 1995; EISENHUT ET AL., 1996; BARTH, 1998; VENGOSH, 1998; SEILER, 2005); (ii) irrigation return flows (BASSETT ET AL., 1995); (iii) fertilizer-affected irrigation waters from

various agricultural settings (KOMOR, 1997); (iv) domestic solid waste deposit leachates from landfills (EISENHUT & HEUMANN, 1997; BARTH, 2000); (v) mixed agricultural sources dominated by animal waste (WIDORY ET AL., 2004); (vi) fly ash deposit leachates from a coal-fired power plant (DAVIDSON & BASSETT, 1993).

Use of $\delta^{11}B$ coupled with $\delta^{15}N$ has proved to be an effective means for tracing agricultural nitrate sources (e.g. hog manure, cattle feedlot runoff and synthetic fertilizers) in surface and groundwaters (BASSETT ET AL., 1995; KOMOR, 1997; WIDORY ET AL., 2004). In a recent study (WIDORY ET AL., 2004), $\delta^{11}B$ was used to distinguish between two types of sewage that were indistinguishable using $\delta^{15}N$ alone: a high-B/low-NO_3/low-$\delta^{11}B$ type that is derived from washing powders, and a moderate-B/moderate-NO_3 type with $\delta^{11}B$ values close to animal (probably human) manure. Some separation of different animal sources of B (e.g. sewage, cattle, hogs and poultry) is seen on plots of $\delta^{11}B$ vs. 1/B (WIDORY ET AL., 2004). The measurements of boron isotopes were performed on a Thermo Fisher AXIOM MC-ICP-MS (Multicollector-Inductively Coupled Plasma Mass Spectrometer) equipped with an ESI New Wave Research LFC (large format cell) (FIETZKE ET AL., 2010).

4.2.4 Stable isotopes of sulphate: sulphur-34 and oxygen-18

Sulphur and oxygen isotopes in sulphate can be used to trace natural and anthropogenic sources of sulphur. The dual isotope approach often provides a better separation of potential sulphur sources (BÖTTCHER, 1999). Moreover, this method provides information on the processes involved in sulphur cycling of the atmosphere, and terrestrial and marine ecosystems (VAN STEMPVOORT & KROUSE, 1994; BÖTTCHER ET AL., 1998; 2001). In this study isotope signatures of dissolved sulphate were used to distinguish between sulphate from geogenic, marine and anthropogenic origin in the catchment of the Marano lagoon. Dissolved sulphate was precipitated from acidified filtered samples by the addition of barium chloride solution. The precipitate was filtered, carefully washed and dried in a drying oven. For oxygen isotope measurements, the precipitate was additionally heated in an oven at 500°C to remove potential contaminations derived from DOC. Aliquots for sulphur isotope ration measurements were combusted by flash combustion in Sn cups together with p.a. grade V_2O_5 in a stream of He. Stable sulphur isotope measurements were carried out with a Thermo Finnigan MAT 253 gas mass spectrometer that was connected to via a Thermo Electron ConFlo IV split interface to a Thermo Scientific Flash 2000 elemental analyzer. Silver sulphide isotope reference materials (IAEA-S-1, IAEA-S-2 and IAEA-S-3) were used to link the mass spectrometric results ($^{34}S/^{32}S$) to the V-CDT scale (MANN ET AL., 2009). Replicate measurements agreed within better than ±0.3‰. Stable oxygen isotope measurements of sulphate were carried out with a Thermo Finnigan Delta$^+$ gas mass spectrometer after conversion in a Thermo Quest TCEA system. Samples were combusted in Ag cups and isotope results are given towards the V-SMOW standard using NBS127, IAEA-SO-5 and IAEA-SO-6 as reference materials.

4.2.5 Tritium-helium method for groundwater dating

The combined use of tritium (^3H) and its radioactive decay product helium (^3He) provides an excellent tool for groundwater dating. The tritium-helium (^3H-^3He) method is based on analysis of radioactive hydrogen (^3H) in the water molecule and

its decay product helium-3 (^{3}He) and it is one of the most frequently used dating techniques for shallow groundwater (SCHLOSSER ET AL., 1988; SOLOMON ET. AL., 1995). The advantage of the ^{3}H-^{3}He dating method over the use of tritium alone is that the ^{3}H-^{3}He dating is independent of the ^{3}H input function and the mean groundwater residence time (groundwater age) can be determined from an individual point within the aquifer. The major application of the non-atmospheric noble gas components in groundwater is dating; i.e. the determination of the mean residence time of the water in the subsurface. Dating applications fall into two major categories: (i) young groundwater with mean residence times between a few months to about 50 years can be studied with the ^{3}H-^{3}He technique as well as with the anthropogenic radioisotope ^{85}Kr. The natural radioisotope ^{222}Rn can be used to extend the age range to the study of very young groundwater (up to 20 days); and (ii) old groundwater with mean residence times of thousands to millions of years is studied by using the accumulation of stable radiogenic ^{4}He and ^{40}Ar, or by the long-lived radioisotope ^{81}Kr. Another radioisotope, ^{39}Ar, covers the time range between about 100 and 1000 years that otherwise is very difficult to access (KIPFER ET AL., 2002). Measurements of tritium (^{3}H) were carried out using the ^{3}He-ingrowth method at the noble gas laboratory of the Institute of Environmental Physics / Section of Oceanography, University of Bremen, Germany (SÜLTENFUß ET AL., 2009). Samples of 500g of water were degassed and stored for the accumulation of the ^{3}H decay product (^{3}He) in dedicated He-free glass bulbs. After a storage period of several months, ^{3}He was analyzed with the mass spectrometric system. This method achieves a detection limit of 0.01TU, which clearly allows the detection of the residue of pre-bomb ^{3}H tests. The uncertainty is typically less than 3% for samples of >1TU and 0.01TU for very low concentrations. For ideal samples, analytical conditions allow a time resolution of about 3 months for apparent ages less than 10 years. For the He and Ne isotope analysis, the gases were extracted from water. He and Ne were separated from other gases with a cryo-system, kept at 25 K and 14 K. ^{4}He, ^{20}Ne and ^{22}Ne were measured with a quadrupole mass spectrometer (Balzers QMG112A). Helium isotopes were analyzed with a high-resolution sector field mass spectrometer (MAP 215–50) (SÜLTENFUß ET AL., 2004). The system was calibrated with atmospheric air and controlled for stable conditions for the He and Ne concentrations and the ^{3}He/^{4}He ratio. The precision of the He and Ne concentrations is better than 1% and for the ^{3}He/^{4}He ratio is better than 0.5%. For most of the samples duplicate measurements have been conducted.

5 Results and Discussion

5.1 Hydrochemical charaterisation of waters

The results of the hydrochemical analyses have shown that the spatial distribution of nitrate concentration in the different lagoon sectors is very heterogeneous. To explain this phenomenon it has to be mentioned that the water circulation in the lagoon is very complex and influenced by many factors like, for example, the interaction and mixing processes between seawater, freshwater and rain water, tide, wave motion, water current direction, wind speed, discharge of the tributary rivers, lagoon bottom morphology, bathymetry as well as by the geometry and orientation of the intra-lagoon channels. Due to the reasons mentioned, in the eastern lagoon sector, the concentrations of nitrates coming from the Rivers Ausa and Corno were strongly

reduced by both dilution with seawater that flows into the lagoon through the Ausa-Corno Channel, which is directly connected to the Adriatic Sea and by the absorption of nutrients by the algal flora. Due to reduced dilution and mixing processes with seawater from the lagoon inlet of Porto Lignano, the spatial distribution of nitrate coming from the Corno-Stella, Turgnano and Cormor rivers was much more extended in the western lagoon sector, even though the concentrations of this ion were in general lower in comparison to those detected in the eastern lagoon sector. The mean annual nitrate concentration for 2009 is reported in Fig. 3. In order to quantify more precisely the mean annual nitrate concentration in each lagoon sector, five different concentration classes have been selected and then related to the lagoon surface as indicated in the diagram and Tab. 2.
From this statistical analysis it was possible to determine that: (i) 74.8% of the lagoon surface is characterized by a mean annual nitrate concentration lower than 5 mg/l (dark blue area); (ii) 98.9% of the lagoon surface has a concentration lower than 10 mg/l; and (iii) only 1.1% of the area in question has a mean annual nitrate concentration greater than 10 mg/l, whereby this area is located at the estuary area of the Ausa and Corno rivers. Generally, in 2009 the entire lagoon surface had a mean annual nitrate concentration of 3.95 mg/l.

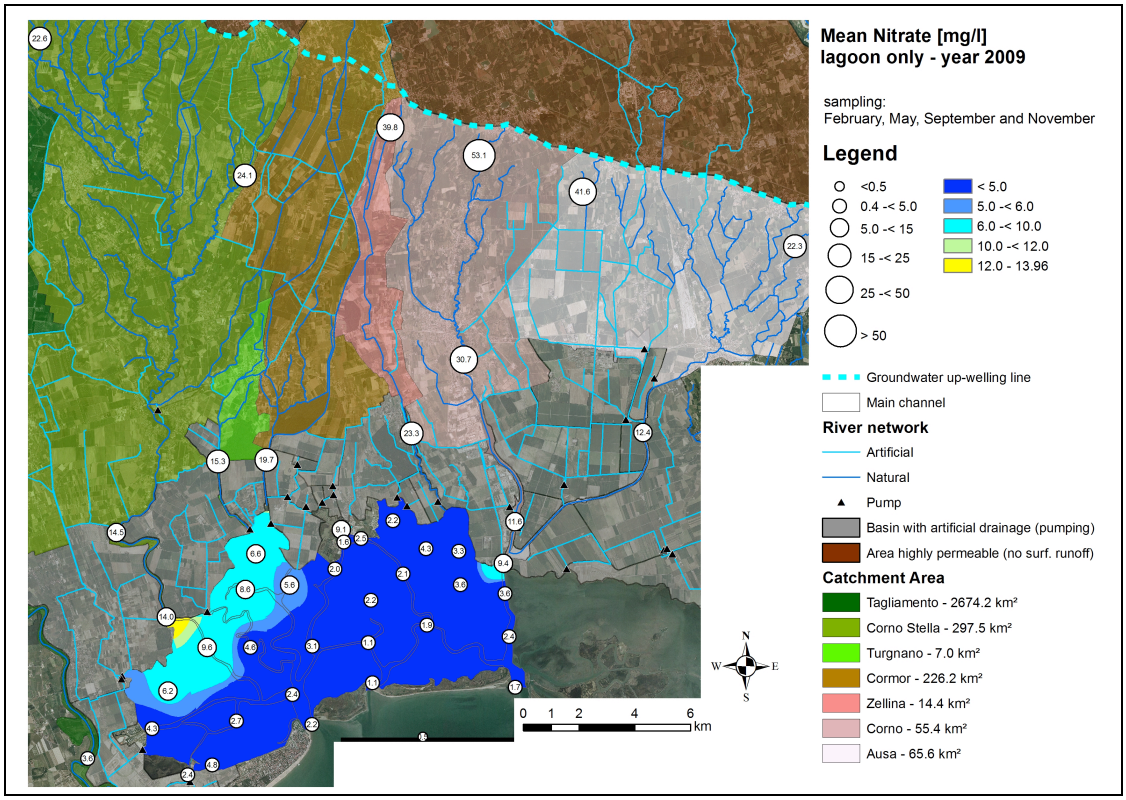

Fig. 3: Spatial distribution of the mean annual nitrate concentration for 2009

During the whole monitoring period 2009-2010, the highest nitrate concentrations in the lagoon and in its tributary rivers were observed in November 2009. In this period of the year all crops have already been harvested, therefore the combination of bare soils and high precipitation rates increases the soil nitrate leaching. However, the mean annual nitrate concentration within the lagoon perimeter was for 98.9% of its surface lower than 10 mg/l, while in the monitoring point located in the open sea the nitrate concentration was less than 1 mg/l (mean annual value = 0.5 mg/l). In contrast,

the nitrate concentrations in groundwater and along the groundwater up-welling line were always significantly higher and it sometimes exceeded the limit imposed by EU Directive for drinking water.
Relatively high ammonium and nitrite concentrations were detected in all the tributary rivers of the lagoon, while in groundwater and along the groundwater up-welling line their concentrations were below the detection limit. The presence of these two ions in the river system indicates that local pollution sources of anthropogenic origin (e.g. untreated urban and/or industrial wastewaters) have directly contaminated the surface waters. It is important to stress that nitrification processes involving these two nitrogen compounds will consequently increase the nitrate concentration in the lagoon. Additionally, phosphate was detected in all tributary rivers of the lagoon, while it has never been detected in groundwater and along the groundwater up-welling line. This clearly indicates that the only source of water contamination by phosphates comes from anthropogenic pollution, mainly from urban wastewaters. In the western lagoon sector, relatively high phosphate concentrations were detected. Due to the fact that this nutrient is the most important trigger of eutrophication in aquatic systems it has to be treated much more carefully than nitrate itself.

Conc. NO3 [mg/l]	Classes	Cells	%	Groups [%]	Area [m²]	Area [km²]	Area [ha]
< 5.0	1	575310	74.8	74.8	57531000	57.53	5753.10
5.0 -< 6.0	2	52372	6.8		5237200	5.24	523.72
6.0 -< 10.0	3	133087	17.3	98.9	13308700	13.31	1330.87
10.0 -< 12.0	4	4630	0.6		463000	0.46	46.30
12.0 - 13.96	5	3916	0.5	1.1	391600	0.39	39.16
Total		769315	100.00	100.00	76931500	76.93	7693.15

Conc. Nitrate [mg/l]		
Min	*Max*	*Mean*
1.13	13.96	3.95

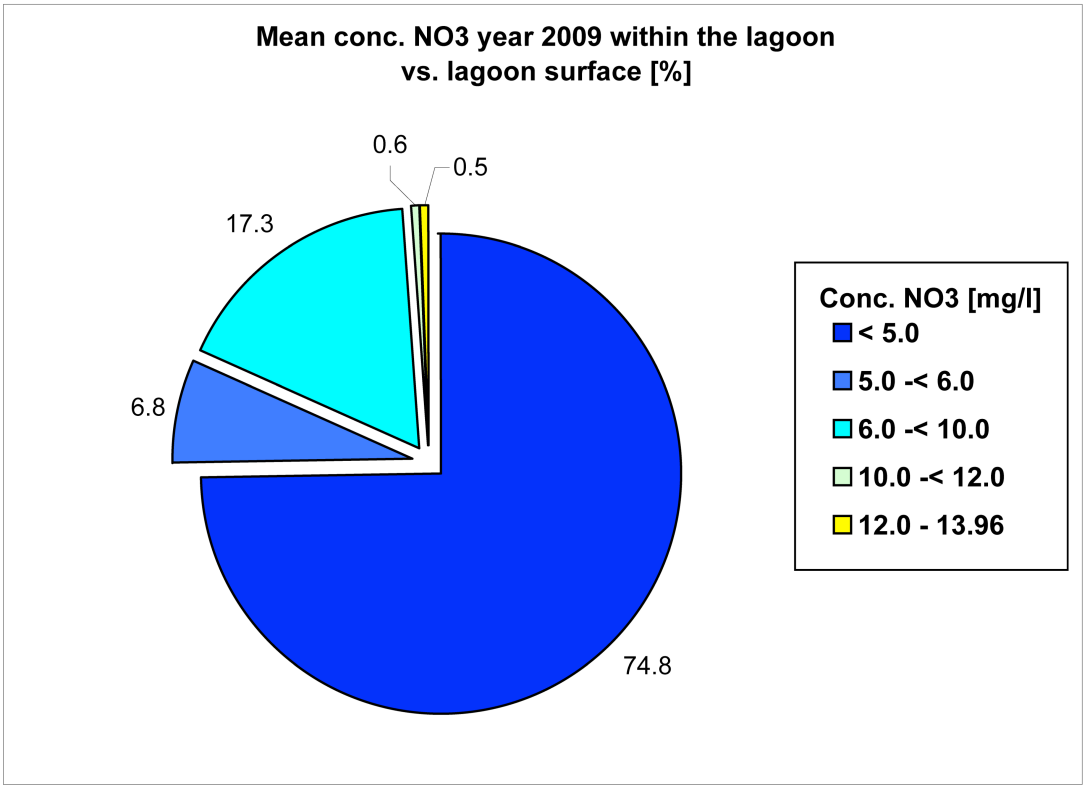

Tab. 2: Statistical analysis of the mean annual nitrate concentration for 2009

5.2 Nitrogen and oxygen isotopic composition of nitrate

The stable isotopes ($\delta^{15}N$, $\delta^{18}O$ and $\Delta^{17}O$) in nitrate from the first sampling campaign (February 2009) were analyzed at the Laboratoire de Glaciologie et Géophysique de l'Environnement in Grenoble (France), while the water samples from the other sampling campaigns were analyzed at the Stable Isotope Laboratory of the School of Environmental Sciences, University of East Anglia, Norwich (United Kingdom).
In order to better determine the potential origin of nitrate identified within the lagoon and its catchment area, the isotopic signatures of the main synthetic and organic fertilizers, typically used in the Region Friuli-Venezia Giulia (FVG), have been measured. The analyses on the isotopic composition of nitrogen ($\delta^{15}N$) in selected synthetic and organic fertilizers have been done at the Laboratory Centre for Isotope

Hydrology and Environmental Analytics of Joanneum Research in Graz (Austria). The $\delta^{15}N$ values in ‰ of these analyses are listed in Tab. 3.

$\delta^{15}N$ ‰	Organic and synthetic fertilizers
4.79	Manure (bovine) from Marianis farm
3.77	Liquid manure (bovine) from Marianis farm
8.52	Liquid manure (pigs)
0.59	Urea
0.30	Ammonium nitrate

Tab. 3: $\delta^{15}N$ values in ‰ of the main organic and synthetic fertilizers typically used in FVG

The isotopic compositions of different anthropogenic and natural nitrate sources as well as the values of measured samples are reported in Fig. 4. Both nitrogen compounds in mineral fertilizers (NO_3^- and NH_4^+) are usually synthesized through industrial fixation of atmospheric N_2. Therefore, the isotopic composition of nitrogen in nitrate derived from synthetic fertilizers is close to atmospheric N_2 ($\delta \approx 0$). These values were consistent with the measured $\delta^{15}N$ of ammonium nitrate and urea reported in Tab. 3. None of the measured lagoon samples fell into the isotopic range typically observed for nitrate originating from synthetic fertilizers. This result indicates that synthetic fertilizers have not entered the lagoon directly or, if present, must have undergone additional biological processing. Nitrogen in manure (both liquid and solid) is mainly in the form of urea, which is hydrolyzed to ammonium and converted to nitrate in the soil zone. The hydrolysis of urea produces a temporary rise in pH, which favours the formation of ammonia, easily lost to the atmosphere. These processes lead to an enrichment of $\delta^{15}N$ values of the remaining ammonium in liquid manure. The isotopic compositions of manure samples (both liquid and solid) collected in the study area were characterized by $\delta^{15}N$ values in the range of 3.7 – 8.5‰ (+/- 0.1‰) as shown in Fig. 4.

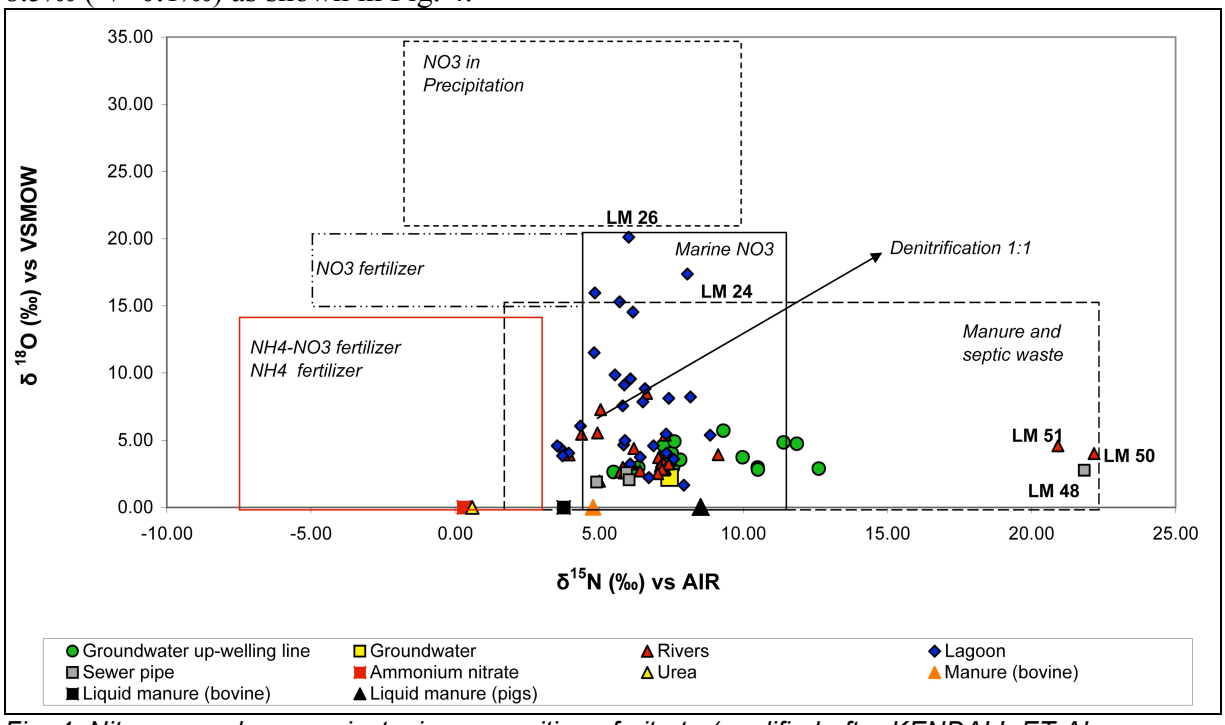

Fig. 4: Nitrogen and oxygen isotopic composition of nitrate (modified after KENDALL ET AL., 2007)

During the nitrification processes the nitrogen in manure (both liquid and solid) will be converted to nitrate where the isotopic values of this newly formed nitrate will be in a similar range or slightly more enriched as described above. Therefore, the isotopic compositions of the different local organic fertilizers have been used as main reference value for the isotopic characterization of the potential nitrate sources related to the agricultural activities. However, nitrate derived from urban sewage water is characterized by $\delta^{15}N$ values in the same range, and therefore it is not possible to distinguish it from agricultural nitrogen sources.
The isotopic composition of nitrate measured in the rivers was in the typical range of animal manure and urban sewage water but in the case that urban sewage water flows directly into the river system the $\delta^{15}N$ values can be much higher. This phenomenon has been detected in the Cormor River south of Udine city (sampling points: LM50 and LM51) and in the Corno river (sampling point LM48 at sewer pipe). Moreover, these isotopic values fit very well with the high concentrations of nitrate, nitrite, ammonium and phosphates measured at the same sampling points. Since nitrite, ammonium and phosphates are typical indicators of local and direct anthropogenic pollution it could be concluded that, in this case, the main nitrate sources come from urban wastewaters. Normally, one of the main difficulties in using N isotopic signature as a tracer of nitrate sources lies in the interference between two processes that can lead to an isotopic shift. These processes are dilution of the polluted surface water and natural denitrification. However, in our case the impact of the denitrification process is negligible due to the oxic conditions found in both the lagoon and river waters. The typical $\delta^{18}O$ values of nitrate from agriculture activities are in the range between 0 and 5‰ depending on the $\delta^{18}O$ value in soil water. If nitrate in the river system is formed from the nitrification of nitrogen compounds (i.e. ammonium) from urban sewage water the isotopic signature $\delta^{18}O$ will be more or less in the same range as described above. In the lagoon the characterization of origin and fate of nitrate is in general much more difficult to achieve because of complex mixing processes among different water types like seawater, river water and rain water. Since water circulation in the lagoon is strongly influenced by seawater (as confirmed by the analyses on the spatial distribution of bromide as well as by the isotopic composition of water) and since the $\delta^{18}O$ of seawater is higher than that of freshwater, the nitrate directly produced in the lagoon from nitrification of ammonium coming from both anthropogenic sources as well as from mineralisation of local dead biomass (remineralization process) will have a higher $\delta^{18}O$ value.
This may mean that nitrate with $\delta^{18}O$ greater than 8‰ mainly originated from nitrification processes within the lagoon itself, especially since the small $\Delta^{17}O$ values (mean 0.65‰, maximum 3‰) indicate an atmospheric nitrate contribution of no more than 3% on average (but up to 10% locally). $\Delta^{17}O$ values of atmospheric nitrate fall in the range of 22 to 35‰, with the corresponding $\delta^{18}O$ values between 50 and 90‰. A contribution of 3% atmospheric nitrate would therefore increase the $\delta^{18}O$ of lagoon nitrate by only about 2‰. Thus, the isotopic signatures of nitrates detected in the lagoon clearly showed that the nitrate load was not only derived from the agriculture activities but also from other sources like urban wastewaters, nitrification processes in the lagoon itself and from atmospheric deposition.

5.3 Boron isotopes

To assess the impact of different boron sources in a catchment area an “end-member mixing model” has to be used. The most important pollution end-members selected

for this study were: manure, urban wastewater and seawater. Manure has low boron concentrations (<0.1 mg/l) and big variations in $\delta^{11}B$ values from 15 to 30‰. Upwelling groundwater is influenced by agriculture and characterized by relatively low boron concentrations (0.11 to 0.23 mg/l). This is relatively close to natural background content (<0.1 mg/l) in Northern Italy (TARTARI & CAMUSSO, 1988). The $\delta^{11}B$ values of the upwelling groundwater samples analyzed in this study showed large variations from 4 to 22.7‰ (median value 17.7‰). In contrast, urban wastewater has higher boron concentrations (0.46 to 1.1 mg/l) and lower $\delta^{11}B$ values from 0 to 12.9‰ (VENGOSH ET AL., 1994). No significant differences in boron contents and isotopic compositions have been found between raw and treated sewage. Therefore, boron isotope variations can be applied for tracing contamination of groundwater by both raw and treated sewage effluents. The sampled seawater in the Adriatic Sea at sampling point 47 was characterized by a boron content of 4.2 mg/l and a $\delta^{11}B$ value of 40.5‰. Fig. 5 shows the different end-members and the theoretical mixing curves during admixing of seawater with manure and urban wastewater.

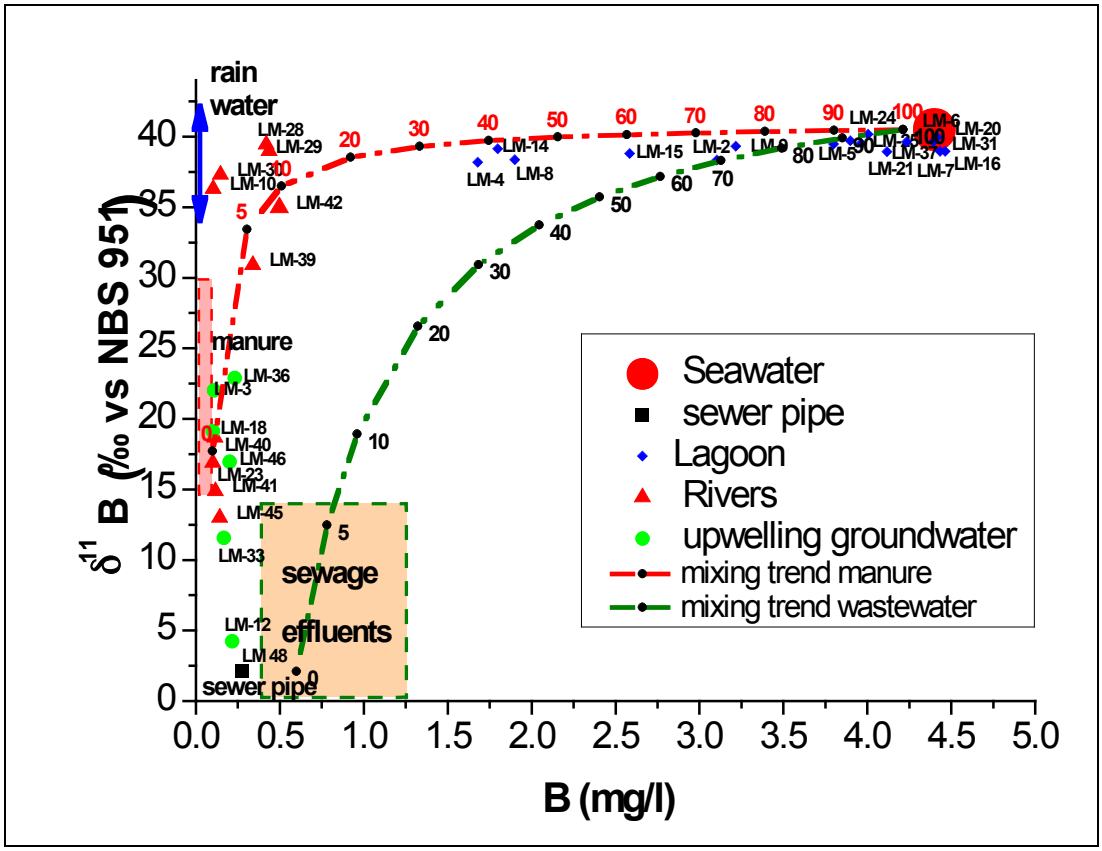

Fig. 5: $\delta^{11}B$ vs. B content and calculated mixing curves during admixing among the end-members (i.e. seawater, urban wastewater and manure)

Most of the samples plot within the range of these mixing curves can be explained by ternary mixing among the three end-members. However, some of the river water samples were above the mixing lines. This group of data is characterized by low to moderate boron contents (0.1 – 0.45 mg/l) and high $\delta^{11}B$ values (36.2 – 39.6‰). This may be the result of the direct mixing of local recharged groundwater with seawater. From this, it can be concluded that the mixing of river water boron with

anthropogenic boron from manure and wastewater as well as with boron from seawater is the major factor, which determines the distribution of $\delta^{11}B$ in the catchment of the lagoon and in the lagoon itself.
However, the higher boron concentrations in the seawater end-member result in non-linear (hyperbolic) boron concentration versus $\delta^{11}B$ mixing curves. That complicates the identification of the other pollution sources especially in the lagoon. Therefore, the $\delta^{11}B$ values have been normalized using bromide concentration in water as a second tracer for admixing of seawater as shown in Fig. 6. The data plotted below indicate that most of the samples were affected by both agriculture and urban wastewater pollution sources. Moreover, the data shows that in some areas of the lagoon the waters were less influenced by these pollution sources. This identifies rain water as an additional mixing end-member.

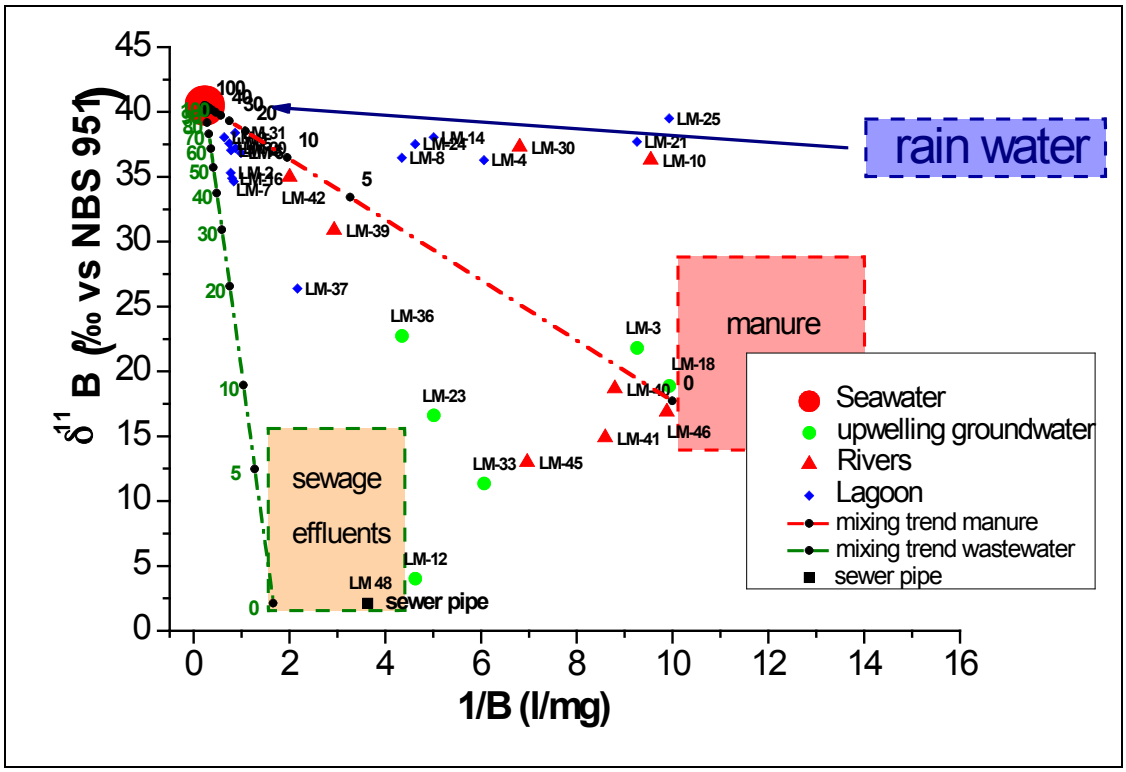

Fig. 6: $\delta^{11}B$ vs. 1/B diagram showing normalised boron concentrations and $\delta^{11}B$ values

5.4 Sulphur and oxygen isotopes

Dissolved sulphate in aquatic ecosystems may be derived from atmospheric (marine sea spray, anthropogenic sources), pedospheric (geogenic and fertilizers) and lithospheric (evaporates and oxidation of sulphide minerals) sources. Moreover, sulphur compounds in liquid industrial waste products are a potential additional source of sulphate. Fig. 7 shows the commonly observed fields of $\delta^{34}S$ and $\delta^{18}O$ values for sulphates depending on their geogenic or anthropogenic origin. The different sulphates are introduced to the aquatic ecosystem by groundwater discharge to rivers and direct mixing with seawater and to a smaller extend by precipitation (sea spray and atmospheric sulphate). Oxygen isotope values of dissolved sulphate are far from the isotope exchange equilibrium with water. Therefore, sulphur and oxygen isotopes can be used to trace natural and anthropogenic sources of sulphur in

agricultural watersheds as well as in coastal systems. Except for one sampling campaign at site LM40 (Tagliamento river), the sulphur isotope data indicate that seawater sulphur is the dominant sulphate source.

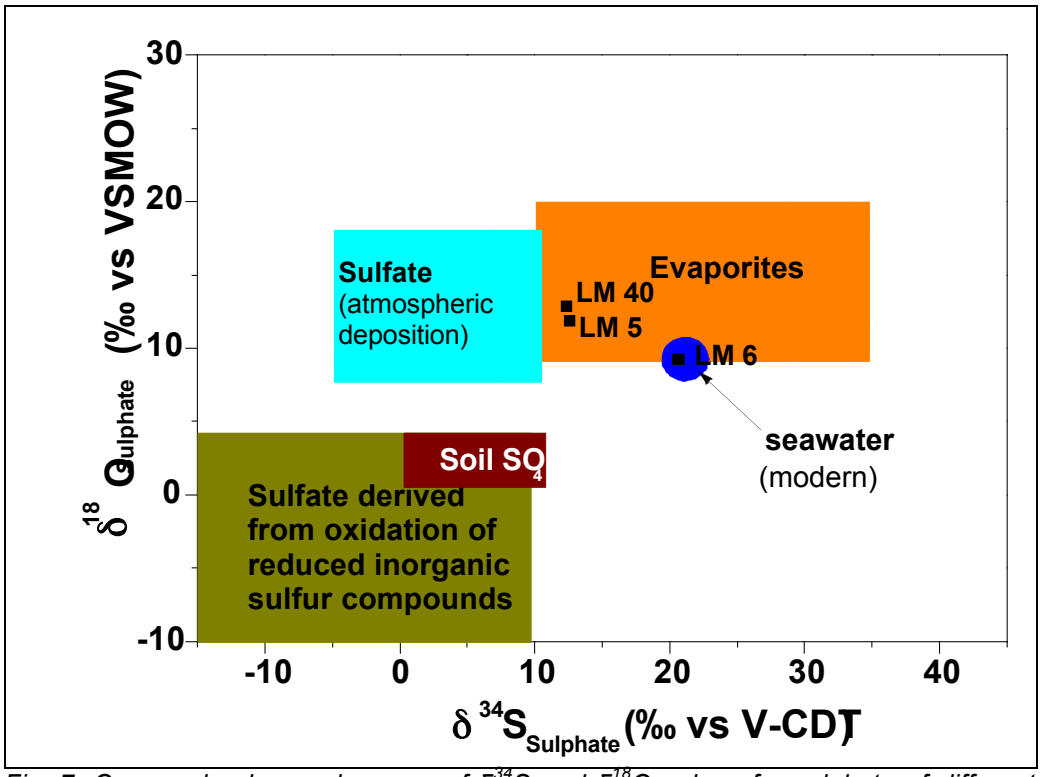

Fig. 7: Commonly observed ranges of $\delta^{34}S$ and $\delta^{18}O$ values for sulphate of different origin (after CLARK & FRITZ, 1997) and measured isotope values for dissolved sulphate in water samples at sites LM5, LM6 and LM40.

There is a sharp increase in sulphur isotope data with increasing chloride concentrations (Fig. 8) as expected for mixing between freshwater and seawater (e.g., FRY, 2002). The measured $\delta^{34}S$ and $\delta^{18}O$ values for sulphate at the sampling points LM40, on the other hand, were +12.3‰ and +12.9‰, respectively. This most likely indicates a lithogenic origin in the low-concentrated solutions, e.g. from the dissolution of Permian evaporites (BÖTTCHER, 1999). This is in agreement with the ion balance of the dissolved components found at these sites. Whereas pyrite oxidation induced by oxidants like, nitrate or oxygen, can be neglected as a significant sulphate source (ZHANG ET AL., 2010), mixing between different geogenic and anthropogenic sulphur sources, that may have partly been modified by microbially induced transformations, cannot completely ruled out and requires further investigations. Dissolved sulphate at the sampling point LM6 (lagoon) shows $\delta^{34}S$ and $\delta^{18}O$ values of +20.6‰ (vs V-CDT) and +9.3‰ (vs V-SMOW) respectively, that are typical for Mediterranean seawater (BÖTTCHER ET AL., 1998) without indication for significant net sulphate reduction or an intense reduction-oxidation cycle (BÖTTCHER ET AL., 2001). The stable isotope analyses of sulphate confirm that the water of the south-western lagoon sector is under influence of the Tagliamento river.

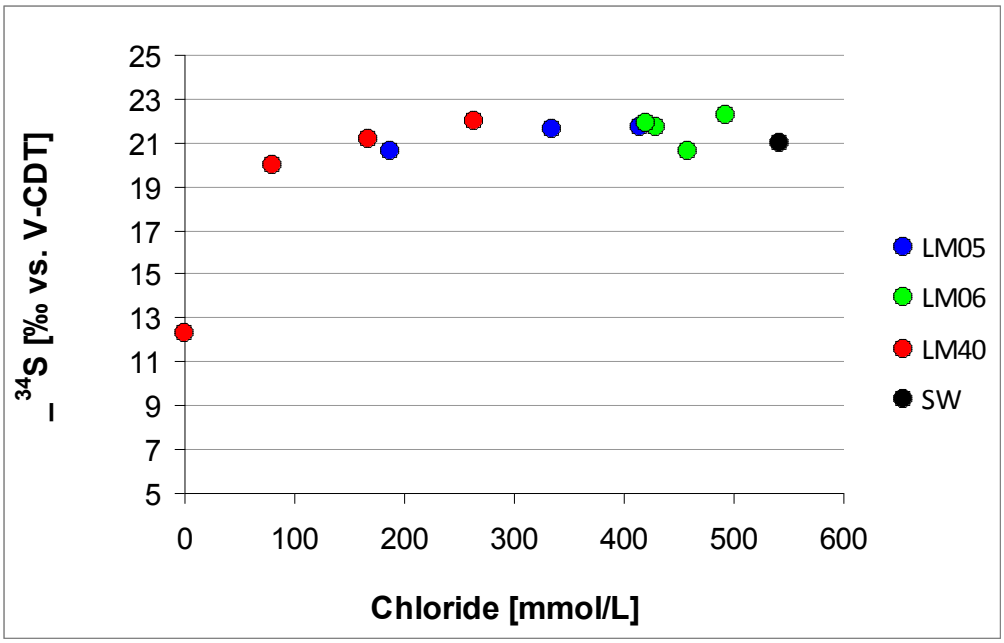

Fig. 8: Covariation of $\delta^{34}S$ data of dissolved sulphate with dissolved chloride concantrations, as a measure for the impact of seawater. Lighter Isotope data are found at low chloride concentrations.

5.5 Groundwater dating

Measurements of tritium (^3H) of the groundwater sampled in June 2010 were carried out using the helium-ingrowth (^3He) method at the noble gas laboratory of the Institute of Environmental Physics / Section of Oceanography, University of Bremen (Germany). The dating method utilized for these analyses is described e.g. by KIPFER ET AL. (2002). The groundwater in the Upper Friulian Plain was sampled at different irrigation wells where two samples of water for ^3H measurements were collected at each sampling point.
The characteristics of the selected wells as total well depth, groundwater table depth, groundwater sampling depth and depth of the installed pumps are described in Tab. 4, while the results of the analysis for tritium and helium isotopes for groundwater dating are reported in Tab. 5.

Sample ID	Sampling date	Total well depth [m]	Groundwater table depth [m]	Sampling depth [m]	Depth of pump 1 [m]	Depth of pump 2 [m]
55-PO27	15.06.10	26	16.12	18	21.35	22
56-PO30	15.06.10	33.6	10.61	13	15.5	17.5
57-PO101	15.06.10	35	14.35	17	21	35

Tab. 4: Characteristics of the selected groundwater sampling wells

Sample ID	^{3}H [TU]	Excess Ne [%]	^{4}He radiogenic [ccSTP/kg] Error: 0.2 E-6	^{3}He tritiogenic [TU]	Age [years] normalized to June 15. 2010
55-PO27	4.95±0.1	48	0.0 E-6	0.4	1.3±0.5
56-PO30	5.1±0.1	44	0.0 E-6	0.4	1.4±0.5
57-PO101	4.85±0.1	34	0.0 E-6	1.2	4.0±1.0

Tab. 5: Results of the analysis for tritium and helium isotopes for groundwater dating

The data reported in the table above were calculated with assumed infiltration temperature of 10°C, altitude 0m a.s.l. and scaled to the sampling date of June 15th 2010. Analytical errors of all data were negligible. For most of the samples double measurements have been conducted. Tritium concentrations and ages refer to 15th June 2010. Ages were calculated with the assumption of piston flow conditions in the aquifer. None of the samples show ^{4}He from radiogenic sources, which is used as an indicator for waters with ages much above 50 years. The concentrations of tritium and tritiogenic helium ($^3He_{tri}$) in the samples match the concentrations of tritium in precipitation quite well. The portion of excess Ne - compared to solubility equilibrium concentration - is rather high, namely in the order of 34 – 48% of the equilibrium value. This indicates that an equilibration of the dissolved gases in the water with the atmosphere after recharge could be excluded. Hence, the low concentration of $^3He_{tri}$ and the derived young ages are a reliable feature of the investigated aquifer. As shown in Fig. 9, the groundwater ages calculated at the three sampling points is reported. The calculated groundwater ages, normalized to June 15th 2010, are respectively 1.3 ± 0.5 years at the point 55-PO27 in Chiasellis and 1.4 ± 0.5 years at the point 56-PO30 in Gris, practically the groundwater age at these two points is the same. Instead, the calculated groundwater age at the point 57-PO101 in Mereto di Capitolo is 4 ± 1 years. The Upper Friulian Plain includes calcareous and dolomitic gravels with a well-developed phreatic aquifer, with an aquifer transmissivity of approximately 10^{-2} to 10^{-4} m^2/s in a southerly direction (MOSETTI, 1983; CARNIEL, 1999). To explain the groundwater age differences between the first two sampling points (55-PO27 and 56-PO30) and the point 57-PO101 it must be noted that shortly before sampling groundwater at point 57-PO101 the two pumps installed in the irrigation well were running. Therefore, mixed waters between upper groundwater and deeper groundwater layers (older groundwater) have been sampled. In the other two irrigation wells (55-PO27 and 56-PO30) the pumps were, for many days, out of service, therefore the sampled waters from these two wells were not mixed with deeper water as in the first case.

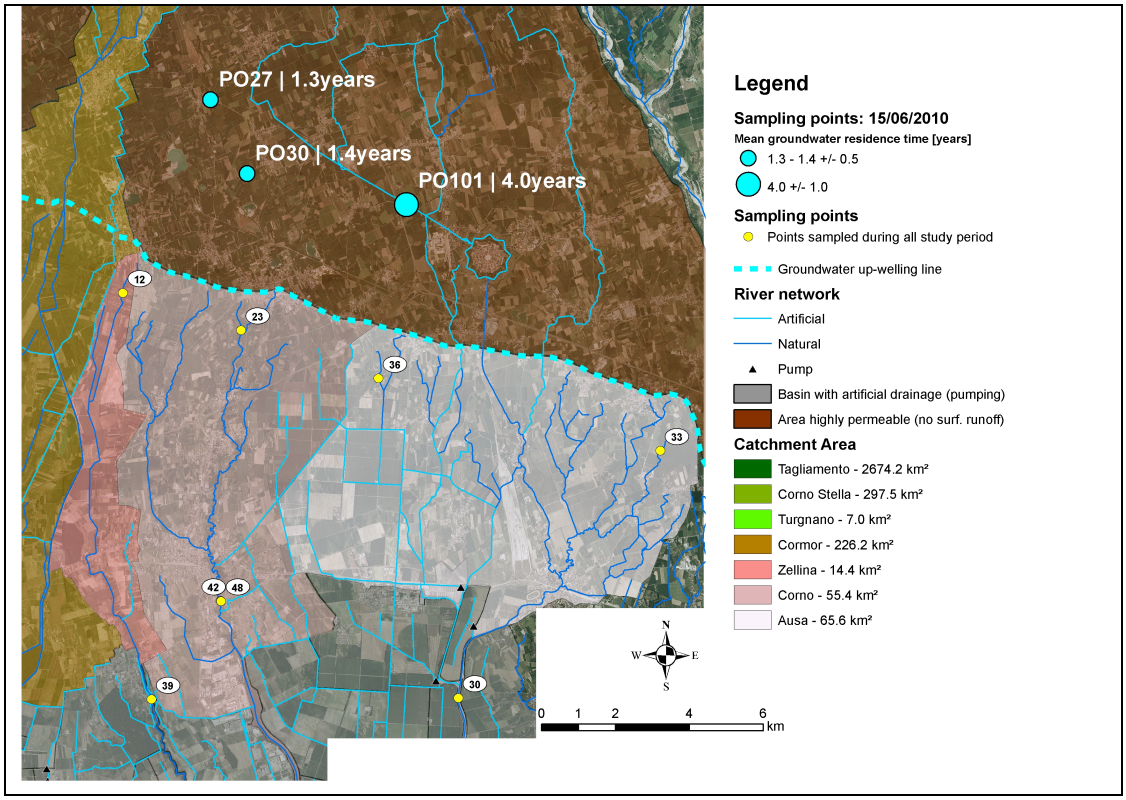

Fig. 9: Location of the groundwater sampling points and calculated mean groundwater residence time [years]

6 Conclusions

Nitrate pollution is still a major concern in many European aqueous resources, which may originate from multiple sources. The development and implementation of effective remediation measures in nitrate polluted areas requires identification of the main sources and estimation of their contribution is essential for environmental policy makers to implement effective, source-oriented remediation measures. For this reason the need of an integrated water resources management policy becomes fundamental in order to improve the management and the quality of water. Isotope data can help to identify nitrate pollution sources, to investigate the fate of nitrate in the environment and to come up with appropriate measures to reduce nitrate pollution. In 2008, in the Friuli-Venezia Giulia Region the entire catchment area of the Marano lagoon was designated as a nitrate vulnerable zone (NVZ) where an action program on the reduction of nitrate leaching was launched. Before this study all the remediation measures adopted within the NVZ were addressed to reduce pollution caused only by nitrates from agricultural activities excluding a priori other potential nitrate pollution sources.

This study represents a novel interdisciplinary research approach to the determination of potential nitrate sources in a lagoon environment, which, beside the traditional hydrochemical analyses (main ions and nutrients), introduces the isotope signature of nitrate ($\delta^{15}N$, $\delta^{18}O$ and $\Delta^{17}O$), boron ($\delta^{11}B$), water ($\delta^{2}H$ and $\delta^{18}O$), and sulphate ($\delta^{34}S$ and $\delta^{18}O$), the tritium-helium (^{3}H-^{3}He) isotopic method as well as hydrological, remote sensing and GIS techniques. The methodology adopted in this project represents also an example of integrated water resources management, where information and knowledge from different productive sectors have been combined

and implemented in the final interpretation of the project results. Moreover, this research study provides a new important scientific contribution in terms of identification of potential nitrate pollution sources that the water management authorities of the Friuli-Venezia Giulia Region have to implement in their future water policy in order to improve water quality of the Marano lagoon and its catchment area.

The stable isotopes in nitrate measured by the denitrifier method have been used to differentiate among nitrate coming from agriculture (synthetic and natural fertilizers), airborne nitrate and nitrate from nitrification processes in soils. Boron isotopes have been used to identify the impact of domestic wastewaters to the aquatic system. The stable isotopes in water have been used to calculate mixing ratios between sea and fresh water and to get information about the mean altitude of the recharge area of surface waters. The stable isotopes in sulphate have been adopted to determine both its origin and the marine and terrestrial contributions, while the tritium-helium isotopic method has been used for groundwater dating. Remote sensing and GIS techniques have been adopted to assess the spatial distribution of most superficial algal flora, surface water temperature as well as the key environmental and morphological changes of the lagoon since the beginning of the 1970s as already reported in the last "Bollettino della Società naturalisti Silvia Zenari", N.34, December 2010 (SACCON, 2010).
The isotopic compositions of different anthropogenic and natural nitrate sources as well as the isotopic signatures of nitrate in numerous water samples collected in the catchment area of the lagoon and in the lagoon itself were measured. None of the samples fell into the isotopic range typically observed for nitrate originating from synthetic fertilizers. Nitrates detected in groundwater and along the groundwater up-welling line are mainly related to the use of manure (both liquid and solid), while other nitrate sources come form urban wastewaters as detected in some rivers like, for instance, Cormor and Corno rivers. In the lagoon the characterization of the origins and fate of nitrate was in general much more difficult to achieve because of complex mixing processes among different water types like seawater, river water and rain water. However, it was possible to identify that nitrate can be formed in the lagoon by nitrification processes of ammonium coming from both anthropogenic sources as well as from remineralisation. Therefore, it can be concluded that the nitrate load in the lagoon, as detected during the monitoring period 2009-2010, was not only derived from agriculture activities but also from other sources like urban wastewaters, nitrification processes in the lagoon as well as from atmospheric deposition. Due to the fact that boron represents a co-migrant of nitrate in anthropogenic pollution sources, boron isotopes have been used as an additional tracer to identify different human impacts in aquatic ecosystems. Manure, urban wastewater and seawater were the three end-members used for this analysis. From the concentration values and from the isotopic signatures of boron found in the sampled waters, it can be concluded that the distribution of $\delta^{11}B$ in the lagoon and its catchment area was the result of mixing anthropogenic boron from urban wastewaters, manure (liquid and solid) and from boron in seawater. The measured data indicate that most of the samples were influenced by both pollution sources, i.e., agriculture and urban wastewaters. Moreover, the data shows that in some parts of the lagoon the water is less affected by these two pollution sources. Few samples along the groundwater up-welling line could not be explained by the use of the end-member mixing model. Therefore, these samples may be affected by the contamination of a different anthropogenic boron source such as landfill. The isotopic compositions of water have been used to

characterize the mean altitude of the recharge area of the freshwater samples as well as to identify the origin of groundwater along the groundwater up-welling line. Additionally, the water isotopes were used to identify mixing processes between freshwater and seawater within the lagoon. From these results it was possible to confirm that the sampled water along the groundwater up-welling line comes from local groundwater.
The isotopic signature of sulphate has been adopted to verify the possible connection between Tagliamento River and part of the western lagoon sector through the Bevazzana artificial channel. The $\delta^{34}S$ and $\delta^{18}O$ values of sulphate measured at the sampling points LM40 (Tagliamento River) and LM5 (Bevazzana channel) indicate that at both sites the sulphate may originate from the similar lithospheric sources (e.g., the dissolution of evaporites), whereas at the sampling point LM6 (lagoon) the sulphate originates from modern Mediterranean seawater. The sulphur and oxygen isotope analyses confirm that the waters of the southwestern lagoon sector are influenced by the Tagliamento River.
Moreover, the tritium-helium method was used for calculating the mean groundwater residence time (groundwater age). The results of this analysis conducted in three groundwater wells in the Upper Friulian Plain have shown that groundwater age is respectively 1.3 ± 0.5 years in the point 55-PO27 in Chiasellis and 1.4 ± 0.5 years in the point 56-PO30 in Gris. Instead, the calculated groundwater age in the point 57-PO101 in Mereto di Capitolo is 4 ± 1 years. At last, the multi temporal analysis of the remotely sensed data has shown that the main morphological changes of the lagoon and its surroundings mainland that occurred during the period of 1973-2007 were much more influenced by the numerous human activities (i.e. industrial, touristic and urban) in comparison to those related to the natural transformation processes (SACCON, 2010).

Acknowledgments

Many institutions and individuals have contributed to make this work possible.
First and foremost, we would like to thank the Regional Agency for Rural Development (ERSA) of the Friuli-Venezia Giulia region for funding the project and for the scientific support in all the project phases. We express our very sincere gratitude to the Regional Forestry Corps (Corpo forestale Regionale) and to the Regional agency for rural, agro-food and forest resources (Direzione centrale risorse rurali, agroalimentari e forestali) for providing logistical support in the fields and the very qualified personnel.
We are also thankful to the technical and scientific staff of all laboratories involved in the isotopic analyses and in particular to the colleagues Barbara Zirngast of the Laboratory Centre for Isotope Hydrology and Environmental Analytics of Joanneum Research, Ines Scherff (Leibniz-Institut für Ostseeforschung Warnemünde – IOW) and Thomas Max (Max Planck Institute for Marine Microbiology – MPI, Bremen). The research leading to the results carried out by the School of Environmental Sciences of the University of East Anglia have benefited from the research findings in the IntraMIF project in the European Community's Seventh Framework Programme (FP7/2007-1013) under grant agreement number n°237890. Moreover, the CNRS, the INSU and the LEFE-CHAT program are acknowledged for their scientific support of the present study mainly through the activities of Joël Savarino, and Joseph Erbland.

References

ARAVENA, R., ROBERTSON, W.D., 1998. Use of multiple isotope tracers to evaluate denitrification in ground water: study of nitrate from a large-flux septic system plume. Ground Water 36, 975– 982.

BARTH, S., 1993. Boron isotope variations in nature: a synthesis. Geologische Rundschau, 82, 640–651.

BARTH, S., 1998. Application of boron isotopes for tracing sources of anthropogenic contamination in groundwater. Water Res. 32, 685– 690.

BARTH, S., 1998. $^{11}B/^{10}B$ variations of dissolved boron in a freshwater–seawater mixing plume (Elbe Estuary, North Sea). Marine Chemistry 62, 1–14.

BARTH, S., 2000. Boron isotopic compositions of near-surface fluids: A tracer for identification of natural and anthropogenic contaminant sources. Water, Air and Soil Pollution, 127, 49–60.

BASSETT, R.L., 1990. A critical evaluation of the available measurements for the stable isotopes of boron. Appl. Geochem. 5, 541– 554.

BASSETT, R.L., BUSZKA, P.M., DAVIDSON, G.R., CHONG-DIAZ, D., 1995. Identification of groundwater solute sources using boron isotopic composition. Environ. Sci. Technol. 29, 2915–2922.

BERGER, G., BOSCH, B., LETOLLE, R., MARCE´, A., MARIOTTI, A., MEGNIEN, C., 1976. Recherches sur l'origine des nitrates dans les eaux souteraines de la Beauce. BRGM Report 76 SGN 444 BDP.

BÖHLKE, J.K., MROCZKOWSKI, S.J., AND COPLEN, T.B., 2003. Oxygen isotopes in nitrate: new reference materials for 18O:17O:16O measurements and observations on nitrate-water equilibration. Rapid Commun. Mass Spectrom, 17, 1835-1846.

BÖTTCHER, J., STREBEL, O., VOERKELIUS, S., SCHMIDT, H.L., 1990. Using stable isotope fractionation of nitrate – nitrogen and nitrate– oxygen for evaluation of microbial denitrification in a sandy aquifer. J. Hydrol. 114, 413– 424.

BÖTTCHER, M.E., 1999. The stable isotopic geochemistry of the sulfur and carbon cycles in a modern karst environment. Isotopes Environ. Health Stud. 35, 39-61.

BÖTTCHER M.E., BRUMSACK H.-J. & DE LANGE G.J., 1998. Sulfate reduction and related stable isotope (^{34}S, ^{18}O) variations in interstitial waters of the eastern Mediterranean. In: ROBERTSON A.H.F. et al. (eds.), *Proc. ODP, Sci. Res.* 160, 365-373.

BÖTTCHER M.E., THAMDRUP B. & VENNEMANN T.W., 2001. Oxygen and sulfur isotope fractionation during anaerobic bacterial disproportionation of elemental sulfur. *Geochim. Cosmochim. Acta* 65, 1601-1609.

CARNIEL, D., 1999. Idrodinamica della falda freatica in destra Tagliamento dalla stretta di Pinzano fino alla fascia delle Risorgive (Hydrogeological knowledge of phreatic aquifers between Pinzano and the Resurgence Belt in the Tagliamento Valley). Unpublished M. Sc thesis, University of Trieste, 124 pp.

CARULLI, GB., 2006. Carta geologica del Friuli Venezia Giulia, scale 1:150000 (Geological Map of Friuli Venezia Giulia, scale 1:150000). Ed. S.E.L.C.A. Firenze.

CASCIOTTI, K.L., SIGMAN, D.M., HASTINGS, M.G., ET AL., 2002. Measurement of the oxygen isotopic composition of nitrate in seawater and freshwater using the denitrifier method. Analytical Chemistry, 74, 4905–4912.

CATI A, FICHERA R, CAPELLI V., 1987. Interpretazione integrata dei dati geofisici e geologici (Geophysical and geological data interpretation of north-western Italy). AGIP San Donato Milanese, 121 pp.

CLARK, I. AND FRITZ, P., 1997. Environmental isotopes in Hydrogeology. Lewis Publishers, New York.

DAVIDSON, G.R., BASSET, R.L., 1993. Application of boron isotopes for identifying contaminants such as fly ash leachate in groundwater. Environ. Sci. Technol. 27, 172– 176.

EISENHUT, S., HEUMANN, K. & VENGOSH, A., 1996. Determination of boron isotopic variations in aquatic systems with negative thermal ionization mass spectrometry as a tracer for anthropogenic influences. Fresenius Journal of Analytical Chemistry, 345, 903–909.

EISENHUT, S. & HEUMANN, K., 1997. Identification of ground water contaminations by landfills using precise boron isotope ratio measurements with negative thermal ionization mass spectrometry. Fresenius Journal of Analytical Chemistry, 359, 375–377.

EPSTEIN, S., MAYEDA, T., 1953. Variation of O18 content of waters from natural sources. Geochimica et Cosmochimica Acta 4, 213–224.

EUR 23658 EN, 2008. The use of isotopes for improved management of nitrate pollution in aqueous resources. Joint Research Centre – Institute for Reference Materials and Measurements. EUR – Scientific and Technical Research series – ISSN 1018-5593.

FEATS, N.A., HISCOCK, K.M., DENNIS, P.F., ANDREWS, J.N., 1998. Nitrogen isotope hydrochemistry and denitrification within the Chalk aquifer system of north Norfolk. J. Hydrol., UK 211, 233–252.

FERRARIN, C., UMGIESSER, G., BAJO, M., BELLAFIORE, D., DE PASCALIS, F., GHEZZO, M., MATTASSI, G., SCROCCARO, I., 2010. Hydraulic zonation of the lagoons of Marano and Grado, Italy. A modelling approach, Estuarine Coastal and Shelf Sciences, 87(4), 561-572.

FIETZKE, J., HEINEMANN, A., TAUBNER I., BÖHM, F., EREZ, J. AND EISENHAUER, A., 2010.: Boron isotope ratio determination in carbonates via LAMC-ICP-MS using soda-lime glass standards as reference material - J. Anal. At. Spectrom. (in press).

FRY, B., 2002. Conservative mixing of stable isotopes across estuarine salinity gradients: A conceptual framework for monitoring watershed influences on downstream fisheries production. Estuaries 25, 264-271.

HEATON, T.H.E., TALMA, A.S., VOGEL, J.C., 1983. Origin and history of nitrate in confined groundwater in the western Kalahari. J. Hydrol. 62, 243– 262.

HORITA, J., UEDA, A., MIZUKAMI, K., TAKATORI, I., 1989. Automatic δD and $\delta^{18}O$ analyses of multi-water samples using H_2- and CO_2-water equilibration methods with a common equilibration set-up. Applied Radiation and Isotopes 40, 801–805.

KAISER, J. HASTINGS, M.G., HOULTON, B.Z., RÖCKMANN, T. AND SIGMAN, D.M., 2007. Triple Oxygen Isotope Analysis of Nitrate Using the Denitrifier Method and Thermal Decomposition of N_2O. Anal. Chem., 79, 599-607.

KENDALL, C. AND CALDWELL, E.A., 1998. Fundamentals of Isotope Geochemistry. In: Isotope Tracers in Catchment Hydrology, eds. Kendall, C., and J.J. McDonnell, 51-86. Elsevier, Amsterdam (http://wwwrcamnl.wr.usgs.gov/isoig/isopubs/itchch2.html).

KENDALL, C. AND MCDONNELL, J.J., 1998. Isotope Tracers in Catchment Hydrology. Eds. Kendall, C., and J.J. McDonnell. Elsevier, Amsterdam, 839p.

KENDALL, C., ELLIOTT, E.M., AND WANKEL, S.D., 2007. Tracing anthropogenic inputs of nitrogen to ecosystems, Chapter 12, In: R.H. Michener and K. Lajtha (Eds.), Stable Isotopes in Ecology and Environmental Science, 2nd edition, Blackwell Publishing, p. 375-449.

KIPFER, R., AESCHBACH-HERTIG, W., PEETERS, F., STUTE, M., 2002. Noble Gases in Lakes and Ground Waters 615 – 700 in Noble Gases in Geochemistry and Cosmochemistry (Eds. Porcelli D., Ballentine C.J., Wieler R.).

KOMOR, S.C., 1997. Boron contents and isotopic compositions of hog manure, selected fertilizers, and water in Minnesota. J. Environ. Qual. 26, 1212–1222.

MANN J.L., VOCKE R.D., and KELLY W.R., 2009. Revised delta S-34 reference values for IAEA sulfur isotope reference materials S-2 and S-3, *Rapid Commun. Mass Spectrom.*, **23**, 1116-1121.

MARIOTTI, A., LANDREAU, A., SIMON, B., 1988. ^{15}N isotope biogeochemistry and natural denitrification process in groundwater: application to the chalk aquifer of northern France. Geochim. Cosmochim. Acta 52, 1869– 1878.

MCMAHON, P.B. & BÖHLKE, J.K., 1996. Denitrification and mixing in a stream-aquifer system: effects on nitrate loading to surface water. Journal of Hydrology, 186, 105–128.

MORIN, S., SAVARINO, J., FREY, M.M., DOMINE, F., JACOBI, H.W., KALESCHKE, L., AND MARTINS, J.M.F., 2009. Comprehensive isotopic composition of atmospheric nitrate in the Atlantic Ocean boundary layer from 65_S to 79_N, J. Geophys. Res., 114, D05303, doi:10.1029/2008JD010696.

MORRISON, J., BROCKWELL, T., MERREN, T., FOUREL, F. & PHILLIPS A.M., 2001. On-line high-precision stable hydrogen isotopic analyses on nanoliter water samples. Analytical Chemistry 73: 3570–3575.

MOSETTI, F., 1983. Sintesi sull'idrologia del Friuli Venezia Giulia (Summary of the Friuli Venezia Giulia hydrology). Quaderni Ente Tutela Pesca 6:1–296.

OSTROM, N.E., KNOKE, K.E., HEDIN, L.O., ROBERTSON, G.P., SMUCKER, A.J.M., 1998. Temporal trends in nitrogen isotope values of nitrate leaching from an agricultural soil. Chem. Geol. 146, 219–227.

PANNO, S.V., HACKLEY, K.C., HWANG, H.H., KELLY, W.R., 2001. Determination of the sources of nitrate contamination in karst springs using isotopic and chemical indicators. Chem. Geol. 179, 113–128.

PAUWELS, H., FOUCHER, J.C., KLOPPMANN, W., 2000. Denitrification and mixing in a schist aquifer: influence on water chemistry and isotopes. Chem. Geol. 168, 307–324.

RET, M., 2006. Bilancio idrologico e circolazione idrica della Laguna di Marano e Grado. Master's thesis, Faculty of Engineering, University of Udine, Italy.

SACCON, P., 2010. Individuazione e caratterizzazione delle potenziali fonti dei nitrati nella Laguna di Marano e messa a punto di un piano di monitoraggio ambientale. Progetto FONIMAR. Parte I. (Detection and characterisation of potential nitrate pollution sources in the Marano Lagoon and set-up of an environmental monitoring plan – FONIMAR project – Part I.) Bollettino Soc. Naturalisti "Silvia Zenari", Pordenone (Italy), 34, 09-40.

SAETHER, O.M. UND DE CARITAT, P., 1997. Geochemical processes, weathering and groundwater recharge in catchments. Eds. Ola M. Saether, Patrice De Caritat. A.A. Balkema, Rotterdam, 400p.

SEILER, R.L., 2005. Combined use of ^{15}N and ^{18}O of nitrate and ^{11}B to evaluate nitrate contamination in ground water. Applied Geochemistry, 20(9), 1626–1636.

SCHLOSSER, P., STUTE, M., DÖRR, C., SONNTAG, C. AND MÜNNICH, K.O., 1988. Tritium/^{3}He-dating of shallow groundwater, Earth Planet Sci Lett., 89, 353-362.

SIGMAN, D.M., CASCIOTTI, K.L., ANDREANI, M., ET AL., 2001. A bacterial method for the nitrogen isotopic analysis of nitrate in seawater and freshwater. Analytical Chemistry, 73, 4145–4153.

SMITH, R.L., HOWES, B.L., DUFF, J.H., 1991. Denitrification in nitrate-contaminated groundwater: occurrence in steep vertical geochemical gradients. Geochim. Cosmochim. Acta 55, 1815– 1825.

SOLOMON, D.K., POREDA, R.J., COOK, P.G. AND HUNT, A., 1995. Site characterization using $^{3}H/^{3}He$ ground-water ages, Cape Cod, MA. Ground Water, 33, 988-996.

SÜLTENFUß, J. AND MASSMANN, G., 2004. Datierung mit der 3He-Tritium-Methode am Beispiel der Uferfiltration im Oderbruch. Grundwasser, 9(4), 221-234.

SÜLTENFUß, J., M. RHEIN, AND ROETHER, W., 2009. The Bremen Mass Spectrometric Facility for the measurement of helium isotopes, neon, and tritium in water. Isot. Environ. Health Stud., 45(2), 1–13.

TARTARI, G. AND CAMUSSO, M., 1988. Boron content in freshwaters of northern Italy. Water, Air, Soil Pollut., 38, 409-417.

TORRENTÓ, C., J. CAMA, J. URMENETA, N.OTERO, AND A. SOLER, 2010. Denitrification of groundwater with pyrite and *Thiobacillus denitrificans*, *Chemical Geology* 278, 80-91.

VAN STEMPVOORT, D. AND KROUSE, H., 1994. Controls of $\delta^{18}O$ in Sulfate: A review of experimental data and application to specific environments. Environmental Geochemistry of Sulfide Oxidation, 447-480.

VENGOSH, A., 1998. Boron isotopes and groundwater pollution. Water Environ. News 3, 15–16.

VENGOSH, A., HEUMANN, K.G., JURASKE, S., KASHER, R., 1994. Boron isotope application for tracing sources of contamination in groundwater. Environ. Sci. Technol. 28, 1968– 1974.

VENGOSH, A., BARTH, S., HEUMANN, K.G., EISENHUT, S., 1999. Boron isotopic composition of freshwater lakes from Central Europe and possible contamination sources. Acta Hydrochim. Hydrobiol., 27, 416– 421.

VITORIA L., SOLER A., CANALS A. AND OTERO N., 2008 Environmental isotopes (N, S, C, O, D) to determine natural attenuation processes in nitrate contaminated waters: example of Osona (NE Spain). Applied Geochemistry, 23(12), 3597-3611.

VOGEL, J.C., TALMA, A.S., HEATON, T.H.E., 1981. Gaseous nitrogen as evidence for denitrification in groundwater. J. Hydrol. 50, 191–200.

WIDORY, D., KLOPPMANN, W., CHERY, L., BONNIN, J., ROCHDI, H., GUINAMANT, JL., 2004. Nitrate in groundwater: an isotopic multi-tracer approach. Journal of Contaminant Hydrology, 72:165–188.

WILLIAMS, A.E., LUND, L.J., JOHNSON, J.A., KABALA, Z.J., 1998. Natural and anthropogenic nitrate contamination of groundwater in a rural community, California. Environ. Sci. Technol. 32, 32– 39.

ZHANG Y.-C., SLOMP C., van CAPPELLEN P., BOERS H.P., PASSIER H.F., BÖTTCHER M.E., OMOREGIE E.O., LLOYD J.R.,, POLYA D.A., 2010. Denitrification coupled to pyrite oxidation in a sandy aquifer: Stable isotope and microbiological evidence. In (BIRKLE & TORRES-ALVARADO, eds.) Water-Rock-Interactions XIII, Taylor & Francis, 975-978.

Appendix 3: Nitrate minerals data set.

Sample UEA ID	Sample museum ID	XRD data		XRF data	
1OX-2OX	OUM 12903	Dspace [Å]	Rel.Int. [%]	Formula	Concentration (%)
		8.71	16	O	42.70
		8.05	35	K	12.40
		4.52	27	S	12.13
		4.38	16	Na	11.10
		4.23	15	Si	9.68
		4.05	24	Ca	4.05
		3.71	22	Mg	3.94
		3.38	98	Al	2.45
		3.33	100	P	0.52
		3.27	31	Fe	0.49
		3.23	25	Cl	0.47
		3.17	26		
		3.12	15		
		2.89	24		
		2.80	58		
		2.72	51		
		2.58	31		
		2.56	15		
		2.48	19		
		2.20	22		
		1.86	43		
		1.82	17		
		1.56	16		
3OX	OUM 12906	Dspace [Å]	Rel.Int. [%]		
		3.04	48		
		2.82	50		
		2.31	13		
		2.12	60		
		1.99	32		
		1.90	17		
		1.88	100		
		1.63	10		
4OX-5OX	OUM 12907	Dspace [Å]	Rel.Int. [%]		

		5.44 23 5.10 17 4.40 100 4.28 15 4.04 26 3.89 13 3.61 16 3.46 23 3.38 14 3.20 14 3.04 52 2.94 24 2.90 30 2.82 61 2.68 16 2.31 13 1.99 27 1.90 21 1.88 14 1.80 30	
6OX	OUM 12908	Dspace [Å] Rel.Int. [%] 10.18 7 3.44 20 3.02 100 2.81 37 2.58 7 2.52 6 2.41 10 2.30 24 2.12 8 1.99 31 1.89 16 1.88 21 1.65 12 1.63 11	
7OX	OUM 12912	Dspace [Å] Rel.Int. [%] 7.59 10 4.27 6 3.26 6 3.06 8	

		2.94 4 2.87 4 2.82 100 1.99 32 1.63 12	
8OX-9OX	OUM 12913	Dspace [Å] Rel.Int. [%] 4.26 4 3.25 6 3.33 10 1.63 14 1.99 47 2.82 100	Formula Concentration (%) Cl 47.03 Na 29.40 O 5.07 Fe 2.46 Ca 2.07 Si 1.90 K 0.41 S 0.40 Al 0.34 P 0.33
10OX	OUM 12914	Dspace [Å] Rel.Int. [%] 9.91 28 3.98 67 3.70 34 3.42 23 3.30 74 3.17 70 3.15 100 2.79 27	Formula Concentration (%) O 44.40 Si 22.10 Na 7.53 Al 7.10 Ca 4.49 S 3.30 Fe 2.59 K 2.56 Mg 2.35 Cl 2.10 P 0.46 Ti 0.46 Mn 0.05
11OX-12OX	OUM 12920	Dspace [Å] Rel.Int. [%] 3.89 4 3.17 3 3.03 100 2.80 24 2.53 7 2.31 19 2.12 9 1.95 3 1.90 15 1.88 7	

		1.65 5 1.63 4	
13OX	OUM 12921	Dspace [Å] Rel.Int. [%] 3.88 2 3.17 3 3.03 100 2.81 12 2.53 13 2.30 25 2.12 7 1.94 2 1.89 14 1.88 6 1.65 4 1.63 3	
14OX	OUM 19536	Dspace [Å] Rel.Int. [%] 10.24 29 6.23 25 5.45 15 4.52 100 4.26 9 4.22 9 3.68 10 3.32 67 3.26 33 3.23 25 3.08 10 3.06 10 2.95 25 2.91 12 2.84 13 2.75 13 2.72 15 2.70 13	Formula Concentration (%) O 45.80 S 14.72 Na 13.50 Si 8.57 Cu 5.43 Al 4.34 Mg 3.91 K 2.01 Ca 0.89 P 0.43 Fe 0.30 Zn 0.14

		2.63 12 2.57 20 2.15 9 2.10 10 1.99 11 1.93 10 1.91 23 1.81 10 1.78 13 1.77 17 1.67 11	
2CA	NMW67 154 GR41	Dspace [Å] Rel.Int. [%] 3.86 3 3.47 6 3.32 5 3.23 4 3.01 100 2.92 4 2.80 88 2.52 15 2.50 4 2.30 17 2.11 8 1.99 22 1.89 24 1.87 9 1.65 6 1.62 11	XRF semi-quantitative analysis Formula Concentration (%) O 30.8 Na 24.6 Cl 13.2 Si 12.9 Al 5.41 Ca 3.64 Mg 2.30 Fe 2.26 S 0.69 K 0.56 P 0.36 Ti 0.23
3CA	NMW67 154 GR41	Dspace [Å] Rel.Int. [%] 4.24 11 3.49 15 3.34 48 3.25 8 3.03 74 2.82 100 2.53 9 2.31 36	XRF semi-quantitative analysis Formula Concentration (%) O 34.6 Si 17.7 Na 15.8 Cl 11.1 Ca 5.44 Al 5.21 Fe 3.48

		2.12	16	Mg	1.94
		1.99	31	K	0.92
		1.89	10	S	0.70
		1.63	18	Ti	0.32
				P	0.29
				Sr	0.02
4CA	NMW 60 531 GR3	Dspace [Å]	Rel.Int. [%]	XRF analysis Formula	semi-quantitative Concentration (%)
		3.85	3	Na	38.5
		3.23	3	Cl	33.6
		3.14	3	O	11.7
		3.01	100	Ca	4.24
		2.92	3	Si	1.89
		2.80	94	Al	0.69
		2.52	8	K	0.50
		2.29	8	S	0.37
		2.11	5	P	0.35
		1.98	33	Fe	0.31
		1.94	2	Mg	0.28
		1.89	29		
		1.87	5		
		1.65	2		
		1.62	9		
5CA	NMW 60 531 GR3	Dspace [Å]	Rel.Int. [%]	XRF analysis Formula	semi-quantitative Concentration (%)
		3.85	7	Na	33.8
		3.46	4	Cl	27.0
		3.31	11	O	17.1
		3.23	5	Ca	7.19
		3.14	3	Si	3.82
		3.01	99	Al	1.43
		2.80	100	K	0.94
		2.52	5	S	0.81
		2.30	19	P	0.68
		2.11	13	Fe	0.66
		1.98	54	Mg	0.49
		1.94	5		
		1.89	17		
		1.87	7		
		1.67	2		
		1.65	4		
		1.62	13		

6CA	NMW 60 531 GR3	Dspace [Å] / Rel.Int. [%] 3.14 4 3.01 100 2.79 19 2.52 4 2.39 3 2.30 63 2.11 5 1.98 13 1.94 2 1.89 7 1.87 6 1.64 4 1.62 3	XRF semi-quantitative analysis Formula / Concentration (%) Na 44.0 Cl 29.8 O 13.2 Ca 2.72 Si 1.41 P 0.64 Fe 0.47 K 0.35 S 0.25
7CA	NMW 60 531 GR3	Dspace [Å] / Rel.Int. [%] 3.87 2 3.34 1 3.24 3 3.16 4 3.02 100 2.81 21 2.79 21 2.53 3 2.30 10 2.12 5 1.99 7 1.94 2 1.89 6 1.88 11 1.65 3 1.63 5	XRF semi-quantitative analysis Formula / Concentration (%) Na 45.7 Cl 34.8 O 9.45 Ca 1.16 Si 0.31 P 0.22 K 0.19 Fe 0.14 S 0.14
1LO-2LO	BM 1985 MI9293	Dspace [Å] / Rel.Int. [%] 4.63 7 4.52 2 3.74 42 3.69 25 3.01 22	Formula / Concentration (%) Na 42.40 Cl 35.72 O 9.38 Ca 1.57 K 1.37

		2.74	13	S	0.65
		2.69	5	P	0.30
		2.64	27	Fe	0.27
		2.63	100	Si	0.25
		2.39	4		
		2.36	3		
		2.32	4		
		2.28	2		
		2.18	25		
		2.15	7		
		2.06	15		
		2.04	10		
		2.00	2		
		1.94	8		
		1.93	8		
		1.88	2		
		1.70	3		
		1.67	4		
		1.67	2		
3LO-4LO	BM 1934 610	Dspace [Å]	Rel.Int. [%]	Formula	Concentration (%)
		3.88	3	K	64.81
		3.25	4	O	21.20
		3.17	3	Ca	9.80
		3.03	100	Si	1.91
		2.93	3	Mg	1.00
		2.81	81	Fe	0.44
		2.79	60	P	0.34
		2.53	4	Al	0.26
		2.31	22	S	0.23
		2.12	4		
		1.99	26		
		1.95	3		
		1.89	13		
		1.88	8		
		1.65	3		
		1.63	8		
5LO-6LO	BM 77517	Dspace [Å]	Rel.Int. [%]	Formula	Concentration (%)
		10.09	100	O	39.90
		4.10	16	Na	38.50
		3.56	18	S	15.70

		3.50	61	Ca	1.90
		3.44	29	Cl	1.00
		3.25	14	P	0.93
		3.17	25	Si	0.84
		3.14	87	Fe	0.49
		2.86	42	K	0.47
		2.84	26		
		2.66	10		
		2.58	23		
		2.56	20		
		2.43	8		
		2.09	27		
		2.05	15		
		1.93	8		
		1.77	8		
		1.73	9		
		1.72	18		
LIK	BM 77517				
		Dspace [Å]	Rel.Int. [%]		
		10.72	100		
		5.70	44		
1RU		Dspace [Å]	Rel.Int. [%]	Formula	Concentration (%)
		4.61	9	K	74.89
		4.54	6	O	18.70
		3.74	61	Ca	5.09
		3.70	29	S	0.43
		3.01	36	Si	0.32
		2.75	27	Fe	0.28
		2.69	8	P	0.18
		2.63	32	Cu	0.08
		2.61	27		
		2.40	5		
		2.32	7		
		2.28	6		
		2.18	100		
		2.15	24		
		2.06	12		
		2.04	25		
		1.94	13		

		1.88 4 1.68 4 1.58 5	
POZ 1-1		Dspace [Å] Rel.Int. [%] 3.80 5 3.14 3 3.01 100 2.82 3 2.47 10 2.27 13 2.08 12 1.91 5 1.90 16 1.86 15 1.59 5	XRF semi-quantitative analysis Formula Concentration (%) Ca 66.0 O 30.2 P 2.17 Mg 1.08 Fe 0.41 Si 0.16
POZ 2		Dspace [Å] Rel.Int. [%] 3.81 8 3.14 3 3.01 100 2.81 4 2.48 16 2.27 15 2.08 17 1.91 5 1.90 30 1.86 19 1.81 10 1.80 6 1.60 7	XRF semi-quantitative analysis Formula Concentration (%) Ca 67.2 O 29.9 P 1.44 Si 0.59 Fe 0.39 Mg 0.27 Al 0.19
POZ 3		Dspace [Å] Rel.Int. [%] 3.83 14 3.38 5 3.15 4 3.02 100 2.69 4 2.48 19 2.36 4 2.32 4 2.28 25	XRF semi-quantitative analysis Formula Concentration (%) Ca 69.4 O 29.1 P 0.57 Mg 0.52 Si 0.18 Fe 0.17 Al 0.08 Zn 0.03

		2.08 15 1.97 4 1.91 30 1.87 21 1.60 7	
POZ 4-1		Dspace [Å] Rel.Int. [%] 9.01 46 6.34 35 5.74 66 4.15 19 3.32 22 3.29 25 3.13 24 2.88 100 2.68 35 2.49 20 2.46 19 2.29 41 2.20 20 2.18 19 2.15 29 1.98 21 1.97 17 1.62 22	XRF semi-quantitative analysis Formula Concentration (%) O 39.5 Mg 37.8 Ca 13.6 Si 4.58 P 1.84 Fe 1.27 Al 1.10 K 0.33
POZ 4-2		Dspace [Å] Rel.Int. [%] 9.06 51 6.35 44 5.76 91 4.16 28 4.06 16 3.30 31 3.19 17 3.14 24 3.02 60 2.89 100 2.68 32 2.50 26 2.29 39 2.20 24 2.18 17	XRF semi-quantitative analysis Formula Concentration (%) Mg 43.1 O 38.7 Ca 13.3 Si 2.76 P 0.75 Al 0.69 Fe 0.59 K 0.20

		2.15 38 1.99 30 1.97 24 1.93 16 1.62 22 1.56 19	
POZ5-1		Dspace [Å] Rel.Int. [%] 9.05 6 6.35 7 5.75 14 4.16 6 3.82 5 3.30 6 3.14 6 3.01 100 2.89 17 2.68 7 2.48 13 2.27 14 2.20 5 2.15 6 2.08 12 1.99 5 1.90 15 1.87 13 1.62 6 1.60 4	XRF semi-quantitative analysis Formula Concentration (%) Ca 43.0 O 33.6 Mg 21.1 P 0.94 Si 0.86 Fe 0.29 Al 0.18

POZ 7-1		Dspace [Å]	Rel.Int. [%]	XRF analysis Formula	semi-quantitative Concentration (%)
		9.05	45	Mg	44.4
		6.35	22	O	39.8
		5.76	39	Ca	8.76
		4.56	8	Si	3.93
		4.16	11	Al	1.40
		4.06	8	Fe	0.82
		3.33	40	P	0.72
		3.30	13	K	0.20
		3.19	8		
		3.14	13		
		2.89	46		
		2.68	15		
		2.50	10		
		2.47	7		
		2.29	30		
		2.20	9		
		2.18	8		
		2.15	11		
		2.11	57		
		2.10	100		
		1.98	10		
		1.62	11		
		1.56	8		

Corno inglese

Dalla collezione "Ossa di seppia" di Eugenio Montale (1896-1981).

Il vento che stasera suona attento
-ricorda un forte scotere di lame-
gli strumenti dei fitti alberi e spazza
l'orizzonte di rame
dove strisce di luce si protendono
come aquiloni al cielo che rimbomba
(Nuvole in viaggio, chiari reami di lassù!
D'alti Eldoradi malchiuse porte!)
e il mare che scaglia a scaglia,
livido, muta colore,
lancia a terra una tromba
di schiume intorte;
il vento che nasce e muore
nell'ora che lenta s'annera
suonasse te pure stasera
scordato strumento,
cuore.

English horn

From the collection "Cuttlefish bones" by Eugenio Montale (1896-1981)

The intent wind that plays tonight
-recalling a sharp clash of metal sheets-
the instruments of the thick trees and sweeps
the copper horizon
where streaks of light are trailing,
kites in the sky that roars
(traveling clouds, bright kingdoms up above,
High Eldorados' half-shut doors!)
and the livid sea
which, scale by scale,
turns color, hurls
a horn of contorted spume ashore;
the wind that's born and dies
in the hour that slowly goes dark
if only it could play you, too, tonight,
discordant instrument,
heart.